

STRUCTURAL AND FUNCTIONAL ANALYSIS
OF THE *SALMONELLA* PATHOGENICITY ISLAND 4
ENCODED TYPE-I SECRETION SYSTEM AND
ITS INTERACTION WITH A METHYL-ACCEPTING
CHEMOTAXIS PROTEIN

DISSERTATION

zur Erlangung des Grades

»**Doctor rerum naturalium**«

(Dr. rer. nat.)

Des Fachbereichs Biologie/Chemie
an der Universität Osnabrück
vorgelegt von

Stefanie Hoffmann

aus Blankenburg

Osnabrück, 2021

Hauptberichterstatter: Prof. Dr. Michael Hensel
2. Berichterstatter: Prof. Dr. Guntram Grassl

TABLE OF CONTENTS

I.	SUMMARY/ZUSAMMENFASSUNG	1
I.1.	Summary	1
I.2.	Zusammenfassung	2
II.	INTRODUCTION	5
II.1.	Historical perspective of <i>Salmonella</i>	5
II.2.	<i>Salmonella</i> Taxonomy	5
II.3.	<i>Salmonella</i> pathogenesis	6
II.4.	Bacterial protein secretion systems	9
II.5.	Pathogenicity Islands	13
II.6.	SPI-4	15
II.7.	Motility and Chemotaxis as virulence factors	19
II.8.	Homology between MotAB and SiiAB	22
II.9.	Methyl-accepting Chemotaxis Proteins	24
II.10.	Aims of the work	26
III.	RESULTS AND PUBLICATIONS	29
III.1.	High-Throughput Quantification of Bacterial-Cell Interactions Using Virtual Colony Counts	29
III.2.	Structural and functional characterization of SiiA, an auxiliary protein from the SPI-4-encoded type I secretion system from <i>Salmonella enterica</i>	43
III.3.	Scarless deletion of up to seven methyl-accepting chemotaxis genes with an optimized method highlights key function of CheM in <i>Salmonella Typhimurium</i>	75
III.4.	A chemotactic sensor controls <i>Salmonella</i> -host cell interaction	99
IV.	DISCUSSION	123
IV.1.	Virtual Colony Count	123
IV.2.	SiiAB functions as a proton channel and exhibits peptidoglycan-binding	125
IV.3.	Signal transduction from the chemotaxis system	127
IV.4.	Environmental control of SiiE retention	129
IV.5.	Mucus as a potential signal for CheM	132
IV.6.	Conclusion	133
V.	REFERENCES	135
VI.	LIST OF UNITS/PREFIXES/ABBREVIATIONS	143
VII.	CURRICULUM VITAE	145
VIII.	LIST OF PUBLICATIONS	149
IX.	DANKSAGUNG	151
X.	ERKLÄRUNG ÜBER DIE EIGENSTÄNDIGKEIT DER ERBRACHTEN WISSENSCHAFTLICHEN LEISTUNG	153
XI.	SUPPLEMENTS ON DVD	155

I. SUMMARY/ ZUSAMMENFASSUNG

I.1. Summary

Salmonella Typhimurium is a Gram-negative, facultative intracellular and anaerobic bacterium with high importance as an intestinal pathogen. For successful colonization and persistence within the host *S. Typhimurium* utilizes a set of virulence-associated secretion systems. One of these systems is the type I secretion system (T1SS) encoded by *Salmonella* pathogenicity island 4 (SPI-4). SPI-4 encodes for an adhesin which is necessary to establish initial contact between the bacteria and host cells. Subsequently, the type 3 secretion system encoded by SPI-1 (T3SS-1) injects its effector proteins into the host cell leading to the internalization of the bacteria.

SPI-4 harbors six genes, *siiAF*. SiiCDF form the canonical subunits of the T1SS, SiiE is the only known substrate and the two accessory proteins SiiAB probably form a proton channel. SiiE is an approximately 600 kDa large secreted adhesion. Interestingly, there is only a temporal stable retention of SiiE at the bacterial surface where it can exert its adhesin function. SiiAB is thought to play an important role in the switch between secretion and stable retention of SiiE as their deletion leads to reduced adhesion and invasion of polarized epithelial cells while secretion is only mildly affected. The aim of this thesis was to further characterize the role of SiiAB for SiiE-mediated adhesion and to identify possible environmental signals for the switch between retention and secretion of SiiE.

Invasion of polarized epithelial cells was used as a main readout to quantify SPI-4 function. For that the “Virtual Colony Count” method was established as an alternative analytical method and compared to the classical counting of colony-forming units (CFUs). With this automated evaluation method it was possible to increase the throughput of infection experiments and to minimize errors by manual CFU counting.

SiiAB has sequence and structural homologies to MotAB and other ion-conducting channels such as PomAB, ExbBD or TolQR, which is why a similar function is assumed. By ratiometric pH measurements in living *S. Typhimurium* cells it could be shown that overexpression of the supposed proton channel SiiAB actually leads to a drop in intracellular pH. The mutation of a conserved aspartate residue at position 13 of SiiA resulted in loss of proton-conducting

function of the SiiAB complex. The same holds true for aspartate 32 of MotB, which could confirm the hypothesis of the functionality of SiiAB.

In the present study, the methyl-accepting chemotaxis protein CheM was identified and characterized as an interaction partner of SiiAB. It could be shown that the perception of aspartate by CheM shifted the ratio of secreted and retained SiiE towards the retention of the adhesin. While this effect was independent of other motility or chemotaxis components, the transduction of this signal is probably mediated through the interaction with SiiAB. The stimulation of CheM thus has a direct influence on the SPI-4 mediated adhesion of the bacteria and thus represents an example of a noncanonical signal transduction of a MCP to a virulence factor.

It remains to be clarified whether this interaction is also important *in vivo* for a successful infection of *Salmonella*. Here, components of the mucus layer could provide the signals for the CheM sensor molecule resulting in precise triggering of SiiE-mediated adhesion in the enterocyte vicinity.

I.2. Zusammenfassung

Salmonella Typhimurium ist ein Gram-negatives, fakultatives intrazelluläres und anaerobes Bakterium mit hoher Bedeutung als Darmerreger. Für eine erfolgreiche Kolonisierung und Persistenz innerhalb des Wirtes verwendet *S. Typhimurium* eine Reihe von Virulenz-assoziierten Sekretionssystemen. Eines dieser Systeme ist das von der *Salmonella* Pathogenitätsinsel 4 (SPI-4) kodierte Typ 1 Sekretionssystem (T1SS). SPI-4 kodiert für ein Adhäsins, was für die initiale Bindung zwischen den Bakterien und den Wirtszellen notwendig ist. Anschließend injiziert das von SPI-1 kodierte Typ 3 Sekretionssystem (T3SS-1) seine Effektorproteine in die Wirtszelle, was zur Internalisierung der Bakterien führt.

SPI-4 umfasst sechs Gene, *siiAF*. SiiCDF bildet die kanonischen Untereinheiten des T1SS, SiiE ist das einzige bekannte Substrat und die beiden akzessorischen Proteine SiiAB bilden wahrscheinlich einen Protonenkanal. SiiE ist ein ca. 600 kDa großes sekretiertes Adhäsins. Interessanterweise beobachtet man nur eine zeitlich begrenzte stabile Retention von SiiE an der Bakterienoberfläche, währenddessen es seine Funktion als Adhäsins ausüben kann. Ziel dieser Arbeit war es, die Rolle von SiiAB für die SiiE-vermittelte Adhäsion weiter zu charakterisieren und mögliche Umweltsignale für den Wechsel zwischen Retention und Sekretion von SiiE zu identifizieren.

Die Invasion polarisierter Epithelzellen wurde als Hauptparameter zur Quantifizierung der SPI-4-Funktion verwendet. Dazu wurde die „Virtual Colony Count“ Methode als alternatives Analyseverfahren etabliert und mit der klassischen Zählung von Koloniebildenden Einheiten (KBE) verglichen. Mit dieser automatisierten Methode war es möglich, den Durchsatz von Infektionsexperimenten zu erhöhen und gleichzeitig den Fehler durch manuelle KBE-Zählung zu minimieren.

SiiAB hat Sequenz- und Strukturhomologien zu MotAB und anderen Protonenkanälen wie PomAB, ExbBD oder TolQR, weshalb eine ähnliche Funktion angenommen wird. Durch ratiometrische pH-Messungen in lebenden *S. Typhimurium*-Zellen konnte gezeigt werden, dass eine Überexpression des vermeintlichen Protonenkanals SiiAB tatsächlich zu einem Abfall des intrazellulären pH-Wertes führt. Die Mutation eines konservierten Aspartatrestes an Position 13 von SiiA führte zum Verlust der protonenleitenden Funktion des SiiAB-Komplexes. Dasselbe gilt für Aspartat 32 von MotB, womit die Hypothese zur Funktion von SiiAB bestätigt werden konnte.

In der vorliegenden Studie wurde das methylakzeptable Chemotaxis-Protein CheM als Interaktionspartner von SiiAB charakterisiert. Es konnte gezeigt werden, dass die Detektion von Aspartat durch CheM das Verhältnis von sekretiertem und oberflächenassoziiertem SiiE in Richtung der Retention des Adhäsins verschieben kann. Während dieser Effekt unabhängig von anderen Motilitäts- oder Chemotaxiskomponenten war, wird die Übertragung dieses Signals wahrscheinlich durch die Interaktion mit SiiAB vermittelt. Die Stimulation von CheM hat somit einen direkten Einfluss auf die SPI-4-vermittelte Adhäsion der Bakterien und stellt damit ein Beispiel für eine nicht-kanonische Signaltransduktion eines MCP zu einem Virulenzfaktor dar.

Es bleibt zu klären, ob diese Interaktion auch *in vivo* für eine erfolgreiche Salmonelleninfektion wichtig ist. Hier könnten Komponenten der Mukusschicht die Signale für das CheM-Sensormolekül liefern, was zu einer präzisen Auslösung der SiiE-vermittelten Adhäsion in der unmittelbaren Nähe der Enterozyten führen würde.

II. INTRODUCTION

Despite intensive research into the development of antibiotics and improved hygiene and nutrition conditions, infectious diseases remain one of the main reasons of death (WHO, 2018). Especially in developing countries these infections are a major health issue. The causes of these diseases are infections with pathogenic bacteria, viruses or fungi. Therefore, a thorough understanding of virulence mechanisms as well as pathogen-host interactions is needed to develop strategies to effectively combat these pathogens. Numerous in vitro and in vivo model systems for different pathogens have been established to characterize these processes. *Salmonella* is among the best studied pathogenic bacteria. Due to their broad host spectrum, the large number of infections caused, their easy handling in the laboratory and their good genetic accessibility, they are particularly suitable as model organisms. Sophisticated mechanisms enable *Salmonella* spp. to overcome the numerous physical and chemical barriers within the host, bypass the immune system and assert itself against the natural commensal microflora.

II.1. Historical perspective of *Salmonella*

In 1880 *Salmonella* (*S.*) *enterica* subsp. *enterica* serovar Typhi was first described by the German scientists Karl Joseph Eberth and Robert Koch as the causative agent of Typhus abdominalis in humans. Subsequently, in 1885, D. E. Salmon, together with his scientific assistant Theobald Smith, identified and isolated the pathogen of porcine cholera, now known as *S. enterica* subsp. *enterica* serovar Choleraesuis. The generic name *Salmonella* was finally given in 1900 by the French bacteriologist Joseph L. Lignières in honour of D. E. Salmon (Brands *et al.*, 2006).

II.2. *Salmonella* Taxonomy

Salmonella spp. belongs to the family of *Enterobacteriaceae*, which in turn is phylogenetically classified in the class of γ -proteobacteria. The genus *Salmonella* was formed by the acquisition of various genomic islands, which resulted in its separation from the joint development line with *Escherichia coli* (*E. coli*) about 140 million years ago (Desai *et al.*, 2013).

The genus *Salmonella* is divided into two species: *S. enterica* and *S. bongori*. *S. bongori* includes only the former subspecies V, which normally does not lead to a symptomatic disease. *S. enterica* is classified into six subspecies (*enterica*, *salamae*, *arizonae*, *diarizonae*, *houtenae* and *indica*) with meanwhile more than 2,600 serovars (Brenner *et al.*, 2000; Guibourdenche *et al.*, 2010). The systematic characterization of serovars is

done according to the White-Kauffmann-Le Minor scheme (Kauffmann F. The bacteriology of Enterobacteriaceae. Copenhagen, Denmark: Munksgaard; 1966) by typecasting lipopolysaccharide antigens (O antigens) and flagella antigens (H antigens) (Brenner *et al.*, 2000), and in some cases capsule antigens (Vi antigen of serovars Typhi, Paratyphi C and some strains of serovar Dublin) (Lim *et al.*, 2009).

II.3. *Salmonella* pathogenesis

Salmonella is able to infect a wide range of hosts, including both humans and various animals such as chickens, cattle and pigs. Depending on the serovar, host species and their immune status, either a rather harmless, self-limiting gastroenteritis or a life-threatening systemic infection is triggered. Virtually all serovars that can infect humans and other warm-blooded animals belong to the *S. enterica* subspecies *enterica*. The other subspecies, as well as *S. bongori*, preferably colonize cold-blooded animals while infections of humans occur only sporadically (Giammanco *et al.*, 2002).

In humans, the clinical picture can be roughly distinguished between typhoid and enteric salmonellosis. Typhoid salmonellosis is caused by the serovars *S. Typhi* and *S. Paratyphi* A, B and C, which are specifically adapted to humans and induce life-threatening systemic infections with an infection dose as low as 10^3 bacteria. These can be accompanied by high fever, headaches and a clouding of consciousness. In the case of paratyphoid infection the course is generally milder (Johnson *et al.*, 2018; Adam *et al.*, 2004).

Enteric salmonellosis is caused by all other serovars known as non-typhoid salmonellae (NTS). The infection dose for a clinically manifested disease in adults is significantly higher compared to typhoid salmonellosis with $>10^5$ bacteria (Adam *et al.*, 2004). The disease usually progresses as a rather harmless, self-limiting gastroenteritis. With 15,919 reported cases in 2019, salmonellosis is one of the most common bacterial infectious diseases in Germany (RKI www.survstat.rki.de). The actual number should be even higher due to the non-detection of mild courses. The total burden of *Salmonella* gastroenteritis worldwide is estimated with roughly 93.8 million cases with approximately 155,000 deaths (Majowicz *et al.*, 2010). Only in rare cases NTS serovars were shown to trigger systemic infections, whereby important factors are the immune status of the host and the infection dose (Adam *et al.*, 2004).

Salmonella infection is mainly caused by ingestion of contaminated food and to a lesser extent by direct human-to-human transmission. The orally ingested bacteria must first overcome the acidic milieu of the stomach. Therefore, the induction of *Salmonella* spp. acid tolerance response (ATR) takes place. As a result, various proton pumps are activated and certain proteins, known as acid shock proteins, are expressed. These proteins are involved in the repair or inhibition of acid-related macromolecular damage (Audia *et al.*, 2001; Foster, 1991).

After successfully passing the stomach, *Salmonella* spp. meets the intestinal barrier of the small intestine. This is formed by extracellular and cellular components, in particular

the mucus, the cellular epithelial barrier with the lymphatic tissue associated with the mucosa (MALT) and the gastrointestinal commensal microflora (Turner, 2009).

The small intestine is lined by mucus, consisting mainly of the gel-forming mucin MUC2. It has only a single layer on top of the epithelium which is easily detachable (Furter *et al.*, 2019). Mucins are secreted by goblet cells and can interact with bacterial cell surface polysaccharides or exposed protein structures such as flagella. It has a defensive function by capturing pathogenic bacteria that can be subsequently eliminated by intestinal peristalsis (Dharmani *et al.*, 2009; Lievin-Le Moal *et al.*, 2006). The mucus layer serves also as a nutrient source for the intestinal microbiota as well as for pathogenic bacteria. Therefore it is prone to degradation and must be constantly renewed. *Muc2*^{-/-} mice which are unable to produce a mucus layer are healthy when kept under germfree conditions. Seven weeks after colonization with a pathogen-free microbiota they develop colitis and have a predisposition for colon cancer (Hausmann and Hardt, 2019).

The cellular epithelial barrier itself consists of the intestinal epithelial cells and an apical connection complex, the tight junctions (TJ), which connect the epithelial cells to each other in a continuous layer. TJ regulate the transport of ions, water and immune cells via the paracellular route and at the same time block this path for pathogenic bacteria. *Salmonella* infections specifically cause disruption of tight junction structures to increase the permeability of this seal (Boyle *et al.*, 2006). This facilitates the translocation of the bacteria from the lumen to the subepithelial region (Ashida *et al.*, 2012).

Salmonella express different fimbrial and non-fimbrial adhesins (Gerlach *et al.*, 2007a) in order to adhere to different cell types and thereby avoiding of being shed from the intestine by peristalsis. After adhesion to non-phagocytic enterocytes, *Salmonellae* can actively induce their uptake via endocytosis by manipulating the host cell cytoskeleton. Alternatively, uptake takes place via so-called M-(microfold) cells. These are specialized intestinal epithelial cells that occur exclusively in the follicle-associated epithelium (FAE) of the Peyer plaques of MALT (Figure II.1). Their task is to transport antigens and microorganisms from the intestinal lumen via the epithelium to the basolateral side, where they are taken up by immune cells such as macrophages, polymorphonuclear leukocytes (PMN's) and dendritic cells (DC's) for antigen presentation and elimination (Kraehenbuhl *et al.*, 2000; Neutra *et al.*, 2001; Siebers *et al.*, 1996; Wolf *et al.*, 1984). M-cells express glycoprotein 2 on their apical plasma membrane which acts as a ligand for the fimbrial tip adhesin FimH, resulting in type I fimbriae-mediated *Salmonella* adhesion to these cells (Hase *et al.*, 2009).

Within the host cell, the bacterium is present in a membrane-enclosed compartment, the so-called *Salmonella*-containing vacuole (SCV). The SCV represents an intracellular niche for the pathogen in which it can escape elimination by the immune system and replicates in some cell types, such as macrophages. In this way, *Salmonella* gains access to the reticulohistiocytic system (RHS) within antigen-presenting phagocytes and, depending on the serovar, can spread systemically throughout the entire body, especially in the mesenteric lymph nodes (mLN), bone marrow, liver and spleen (Monack *et al.*, 2001).

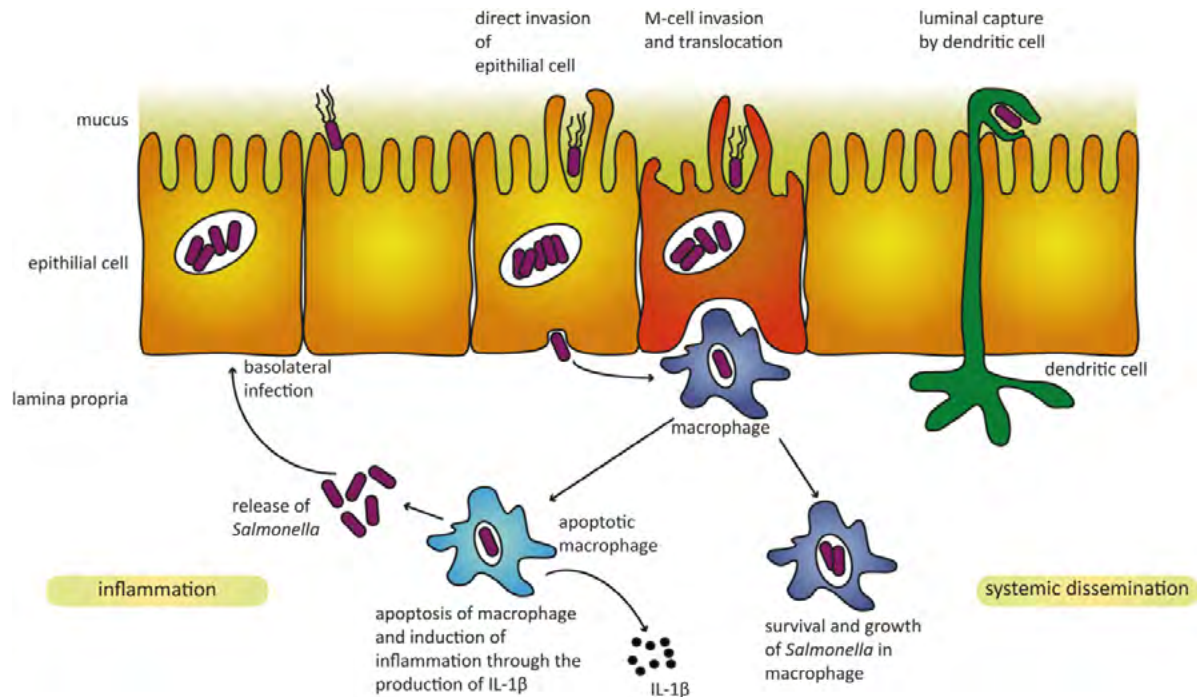


Figure II.1 Infection process of *Salmonella* spp.. *Salmonella* spp. has several options to overcome the intestinal epithelium. M-cells absorb bacteria via receptor-mediated endocytosis and pass it on the basolateral side to phagocytic cells of the immune system. However, *Salmonella* can also actively induce their uptake into both phagocytic and non-phagocytic cells via self-induced macropinocytosis. Furthermore, *Salmonella* can be captured from the intestinal lumen by DCs via phagocytosis. Bacteria released in the Peyer plaques are taken up by immune cells such as macrophages or neutrophilic granulocytes. Alternatively, the bacteria can also invade enterocytes again from the basolateral side. Protected intracellularly by SCV, *Salmonella* gains access to the RHS within antigen-presenting phagocytes and can spread locally or systemically throughout the body. It can also induce its release in phagocytes (such as macrophages or DCs) by induction of caspase1 dependent apoptosis. Invasion of the intestinal epithelium is associated with inflammation, destruction of TJ, stimulation of transepithelial migration of PMN, release of fluid into the intestinal lumen, and development of diarrhea. Modified after Sansonetti (2004)

By activating caspase1-dependent apoptosis, *Salmonella* can also initiate its release from phagocytic cells such as macrophages or DCs (Garai *et al.*, 2012; Monack *et al.*, 2000) and subsequently re-infect cells of the immune system or epithelial cells from the basolateral side (Sansonetti, 2004). Part of the *Salmonellae* is also phagocytosed directly via the pseudopodia of the DCs extending into the intestinal lumen (Rescigno *et al.*, 2001).

The infection of the intestinal epithelium is associated with the disruption of tight junctions (Bertelsen *et al.*, 2004; Boyle *et al.*, 2006; Finlay *et al.*, 1990; Gerlach *et al.*, 2008; Jepson *et al.*, 2001) and, as a consequence, a transepithelial migration of PMN's into the intestinal lumen occurs. This results in acute inflammation and necrosis of the uppermost layer of the small intestinal mucosa. The release of the proinflammatory cytokines interleukin (IL-) 8 and IL1 β by infected epithelial cells or macrophages is involved in this process (McCormick *et al.*, 1995). Injury of the intestinal epithelium is associated with increased vascular permeability leading to outflow of extravascular fluids from the bloodstream into the intestinal lumen, which finally causes diarrhea. The outflow of fluids is additionally supported by the secretion of chloride into the intestinal lumen (König *et al.*, 2016).

Salmonella is able to profit from the conditions in the inflamed gut. *Salmonella* is able to utilize hydrogen derived from the present microbiota during the initial phase of infection to establish itself in the gut (Maier *et al.*, 2013). Some serotypes can use alternative electron acceptors like nitrate or tetrathionate that are only present during colitis to promote their growth by anaerobic respiration. In the non-inflamed gut the microbiota produces butyrate, which inhibits the expression of NOS2 and therefore the synthesis of iNOS, leading ultimately to a diminished epithelial generation of nitrate (Byndloss *et al.*, 2017). To exploit these favorable niches bacteria have to be motile and chemotactically active (Rivera-Chávez *et al.*, 2013). Because of the diarrhea the gut is emptied and poor of nutrients which also increases the competition of *Salmonella* with the commensal microbiota. *Salmonella* adjusts to these conditions by utilizing mucus carbohydrates as high-energy source. It could be shown that acute intestinal inflammation caused by the bacterium leads to a reduction of the competing commensal microflora and thus has a beneficial effect on the spread of *Salmonella* (Stecher *et al.*, 2007). Infection with NTS is normally restricted to the intestine and the mLN.

In contrast, the epithelial layer remains largely unchanged when infected with typhoid serovars, as the inflammation is generally reduced (Raffatellu *et al.*, 2008; Raffatellu *et al.*, 2006; Zhang *et al.*, 2003). Responsible for this is the Vi antigen, a polysaccharide capsule that occurs exclusively in typhoid serovars. This Vi-capsule seems to be the reason for a reduced invasiveness of *S. Typhi* towards epithelial cells (Zhao *et al.*, 2001). It also prevents the production of IL8 and the recognition of the pathogen by the immune system via the toll-like receptors (TLR)4 and 5 and is involved in survival within phagocytes. This results in a systemic infection as no immune response is activated (Wilson *et al.*, 2010; Wilson *et al.*, 2007). NTS, on the other hand, are eliminated by the immune cells recruited during massive intestinal inflammation (Raffatellu *et al.*, 2006; Sabbagh *et al.*, 2010).

II.4. Bacterial protein secretion systems

Salmonella and other Gram-negative bacteria have developed a considerable number of different mechanisms for the transport of proteins across the cell membrane. Transport systems not only are essential for pathogenesis during interaction with eukaryotic host cells, but have also general cellular functions (Durand *et al.*, 2009). A schematic overview of most common secretion and translocation systems is given in Figure II.2.

Protein transport across the outer membrane can be divided into Sec-independent and Sec-dependent pathways. Protein transport over the inner membrane into the periplasmic space of Gram-negative bacteria takes place via the general secretory (Sec) or the twin arginine translocation (Tat) pathway. In a second step substrates are then secreted over the outer membrane by the “chaperone/usher” synthesis pathway of fimbrial adhesins, the autotransporter/type V secretion system (T5SS) pathway or the complex type II secretion system (T2SS) (Costa *et al.*, 2015; Tseng *et al.*, 2009). Sec-independent pathways

are the type I, type III, type IV and type VI secretion systems (T1SS, T3SS, T4SS, T6SS). In these cases no stable periplasmic intermediate occurs because in all four systems there is a protein-conducting channel that spans both bacterial membranes. In the case of T3SS, T4SS and T6SS an additional membrane of the host cell is spanned and effector proteins are directly translocated into the host cell cytoplasm.

Salmonella infection strongly depends on the function of two T3SSs encoded by SPI-1 (T3SS-1) and SPI-2 (T3SS-2). In general, T3SS are supramolecular complexes composed of at least 20 different subunits. From a structural and evolutionary point of view they are closely related to the flagellum system and are found in numerous Gram-negative bacteria such as *Salmonella* spp., *Yersinia* spp. or *Shigella* spp. Due to their shape and the ability to inject proteins directly into the host cell T3SS are also referred to as molecular needles (Cornelis, 2006).

Table II.1 Selection of effectors secreted by T3SS-1 and -2

Effector	Cellular function	Host-cell target
SopE*	Activates Cdc42, Rac1 and RhoG by its guanine nucleotide exchange factor (GEF) activity and disrupts tight junctions	Cdc42, Rac1, Rab5
SopE2*	Activates Cdc42, Rac1 and RhoG by its GEF activity and disrupts tight junctions	Cdc42, Rac1
SopB*	Activates Cdc42, RhoG, AktA and chloride secretion through its inositol phosphatase activity and disrupts tight junctions	Unknown
SopD*	Stimulates fluid accumulation in bovine ligated loops and contributes to diarrhea in calves and systemic disease in mice	Unknown
SopD2*	Contributes to sif-formation and inhibits the vesicular transport and tubule formation that extend outward from the SCV	Unknown
SopA*	Stimulates PMN transmigration by HECT-like E3 ubiquitin ligase activity	Unknown
AvrA*	Inhibits activation of NF- κ B transcription factor and apoptosis via the JNK pathway; promotes intestinal epithelial cell proliferation and tumorigenesis by blocking the degradation of I κ B α and β -catenin; activates the STAT3 signaling pathway	JNK pathway
SipA*	Decreases the critical concentration of G-actin and increases the stability of F-actin; induces PMN transepithelial migration and disrupts tight junctions; causes activation and release of caspase-3	F-actin, Tplatin, caspase-3
SipB*	Binds and activates caspase-1 and induces autophagy in macrophages; release of IL-18	Caspase-1, cholesterol, IL-18
SipC*	Nucleates and bundles actin; promotes <i>Salmonella</i> invasion	F-actin, cytokeratin-8, cytokeratin18
SptP*	Inhibits Cdc42 and Rac1 by its GAP activity and MAPK signaling and IL-8 secretion through its tyrosine phosphatase activity	Rac1
SifA**	Induces Sif (<i>Salmonella</i> induced filaments) formation, maintains integrity of the SCV and downregulates kinesin recruitment to the SCV	SKIP, Rab7
SseJ**	Maintains integrity of the SCV and has deacylase activity	Unknown
SseF**	Contributes to Sif formation and microtubule bundling, inhibit Rab1Amediated autophagy, interact with the mammalian Golgi network-associated protein ACBD3 to anchor the SCV at the Golgi network	Rab1A, ACBD3
SseG**	Contributes to Sif formation and microtubule bundling, inhibit Rab1Amediated autophagy, interact with the mammalian Golgi network-associated protein ACBD3 to anchor the SCV at the Golgi network	Rab1A, ACBD3
SspH2#	Inhibits the rate of actin polymerization and contributes to virulence in calves	Filamin, profilin

* T3SS-1 secreted effectors

** T3SS-2 secreted effectors

secreted by both T3SS

Many effectors involved in the uptake of bacteria also have a function in later processes such as early SCV formation, membrane transport, cell division, apoptosis and cytokine and chemokine production or antigen presentation (summarized in Santos *et al.*, 2009). An overview of the function of the individual SPI effectors can be found in Velge *et al.* (2012) or Haraga *et al.* (2008). Some of the most important effectors secreted by T3SS-1 and -2 are shown in Table II.1.

II.4.1. Type I Secretion Systems

Type I secretion systems are widespread among Gram-negative bacteria and mediate the transport of a wide variety of proteins from the cytoplasm across the outer membrane into the extracellular space (Gerlach *et al.*, 2007a).

Type I secretion systems are three partite complexes consisting of an IM (inner membrane) ABC (ATP-binding cassette) exporter, a PAP (periplasmic adaptor protein) and a pore-forming OMP (outer membrane protein) (Figure 2). ABC transporters minimally contain two transmembrane (TM) domains and two nucleotide binding domains (NBDs) that is why ABC proteins of T1SS likely form homodimers (Smith *et al.*, 2018). They are responsible for substrate recognition and specificity, as well as for the energization of secretion by ATP hydrolysis (Deleplaire *et al.*, 2004; Moussatova *et al.*, 2008). The PAP is anchored by its N-terminal region in the IM, the short cytoplasmic part of which is probably involved in substrate recognition together with the ABC protein. It probably exists as a hexamer (Trepout *et al.*, 2010; Xu *et al.*, 2011; Janganan *et al.*, 2011) and spans the periplasm with its long C-terminal region, connecting the ABC protein with the trimeric OMP in the outer membrane (Thomas *et al.*, 2013).

Most type I-secreted proteins described so far have a C-terminal signal peptide, which is usually not processed (Holland *et al.*, 2005). Substrates of T1SS in *Salmonella* include the SPI-4-encoded adhesin SiiE and the SPI9-encoded protein BapA, which is involved in biofilm formation (Latasa *et al.*, 2005). The translocation of type I-secreted proteins happens in a single step without a periplasmic intermediate. Typically, T1SS substrates bind Ca^{2+} ions through glycine-rich repeat sequences (e.g. GGXGXDXXX). Those motifs are thought to prevent premature folding inside the cell due to low intracellular calcium concentrations. The higher extracellular calcium concentration drives the ratchet-like folding process, triggered by Ca^{2+} -binding (Bumba *et al.*, 2016). T1SS is also widespread in other pathogenic Gram-negative bacteria. Well-known substrates are for example the hemolysin HlyA (*E. coli*), the CyaA hemolysin/adenylate cyclase (*Bordetella pertussis*) or the toxin RtxA (*Vibrio cholerae*). All three examples are RTX (repeats-in-toxin) toxins (Thomas *et al.*, 2013). However, proteases, phosphatases or glucanases are also secreted via T1SSs (Deleplaire, 2004).

Another interesting example of a type I-secreted adhesion is LapA of *Pseudomonas fluorescens*. LapA is an outer membrane adhesin involved in biofilm formation. Its loss

from the bacterial surface is controlled by cyclic dimeric GMP (c-di-GMP) through an inside-out signaling process. The IM protein LapD binds to c-di-GMP in the cytoplasm which leads to the inhibition of the periplasmic protease LapG that targets the N-terminus of LapA. This results in the maintenance of adhesion. In low P_i conditions on the other hand, c-di-GMP is depleted causing loss of LapA and therefore the detachment of biofilm (Newell *et al.*, 2011; Martínez-Gil *et al.*, 2014). A similar secretion mechanism has been described for a few other adhesins, e.g. for BpfA (*Shewanella* spp.), BrtA (*B. bronchiseptica*) and RtxA (*L. pneumophila*) (Smith *et al.*, 2018).

Another type I-secreted adhesin is FrhA of *Vibrio cholerae*. It has nine RTX repeats and four to nine cadherin-like domains in its central portion. The function of FrhA is similar to that of eukaryotic cadherins in mediating surface interactions. It is involved in hemagglutination, adherence to epithelial cells, biofilm formation, and chitin binding. Its C-terminus shares sequence similarities with BpfA, indicating a type I secretion mechanism (Satchell, 2011).

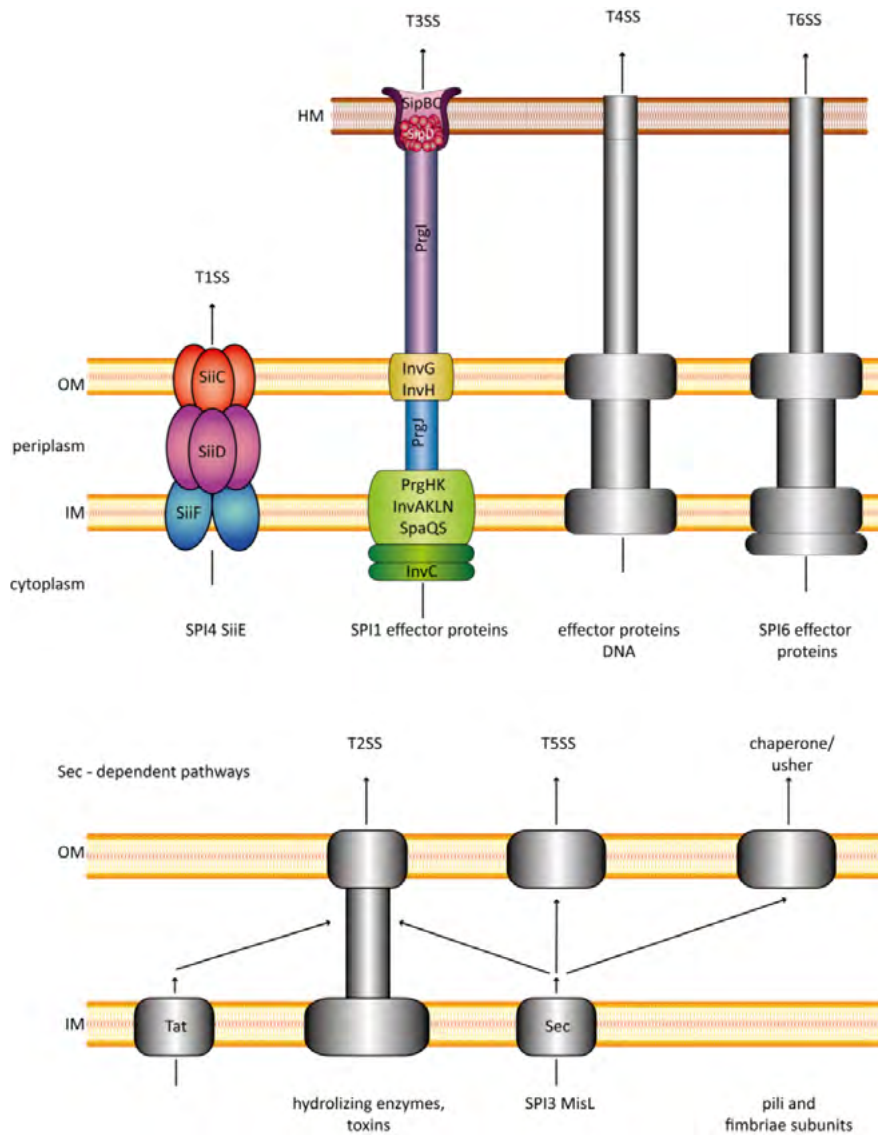


Figure II.2 Overview of the secretion systems in Gram-negative bacteria. See text for details. Modified after Gerlach *et al.*, 2007a

II.5. Pathogenicity Islands

Considering the complex interactions of *Salmonella* with its host it becomes apparent that the bacteria need multiple genes for full virulence. In *Salmonella*, several virulence genes are often found clustered together in pathogenicity islands (PAI). The presence of a set of genes distinguishes pathogenic bacteria from their non-pathogenic close relatives. These genes are called virulence genes and contribute to an organism's ability to cause disease (Schmidt and Hensel, 2004). The general structure of a PAI is shown in Figure II.3.

The majority of PAIs is 10 to 200 kb in size and can constitute a relatively high proportion of the genome. They can differ from the core genome with respect to base composition (different G/C content) and codon usage. PAIs are often adjacent to tRNA genes, which are highly conserved between different bacterial species. They could therefore serve as anchor points for the chromosomal recombination of foreign DNA, which was e.g. taken up by conjugation or transduction. Transducing bacteriophages are able to transfer bacterial DNA and associated virulence genes between different bacterial species. In addition to tRNA genes, phage-specific integration sites also serve as anchor points for the integration of foreign DNA into the host genome. DNA acquired by horizontal gene transfer is often associated with mobile elements, like insertion elements (IS elements) and flanked by direct repeats (DR) which are defined as DNA sequences of 16 to 20 bp (up to 130 bp) with a perfect or almost perfect sequence repetition. In addition, they act as recognition sequences for enzymes involved in the liberation of mobile elements such as integrases or transposases. PAI often carry cryptic or functional genes encoding for these enzymes. In this way, DR contribute to the instability of the embedded PAI. In lysogenic bacteriophages, integrases mediate both the integration of the phage genome into a host genome and its release, which is necessary for the entry into the lytic cycle. However, the exact mechanism that promotes the deletion of PAI is not known yet. The loss of a PAI results in reduced genome size, which in turn leads to a faster generation time and thus to a growth advantage in competition with other microbes.

PAIs in *Salmonella* are called *Salmonella* Pathogenicity Islands (SPI). Currently there are 22 SPIs reported but not all of them are present in every species, subspecies or serovar. Although the function of many of them is still unclear it is thought that the acquisition of different SPIs led to the evolution of various species and subspecies and their diversification with respect to host specificity (Fookes *et al.*, 2011; Gerlach *et al.*, 2007b).

The best characterized SPIs are SPI-1 and SPI-2. Both are encoding the structural and functional components of T3SSs, as well as for their respective effector proteins. The T3SS-1 enables *Salmonella* to actively invade non-phagocytic cells and plays an important role in the stimulation of intestinal inflammation and the induction of apoptosis of phagocytic cells (Hapfelmeier *et al.*, 2004; Hersh *et al.*, 1999; Ochman *et al.*, 1996). After adhesion to the host cell membrane, T3SS-1 translocates at least 15 effector proteins in a coordinated sequence into the host cell (Lara-Tejero *et al.*, 2011, McGhie *et al.*, 2009). The translocated effectors cause a temporary massive rearrangement of the actin cytoskeleton resulting in the formation of membrane ruffles and the internalization of

the bacterium via macropinocytosis (summarized in McGhie *et al.* 2009). The T3SS-2 on the other hand is important for the intracellular survival of *Salmonella* and its systemic infections (Gerlach *et al.*, 2007b; Marcus *et al.*, 2000). Currently more than 20 effector proteins are known to be translocated via T3SS-2 across the bacterial membrane into the host cytosol. There they are mainly involved in the formation and maintenance of the SCV and the acquisition of nutrients (Ibarra *et al.*, 2009; Ramsden *et al.*, 2007).

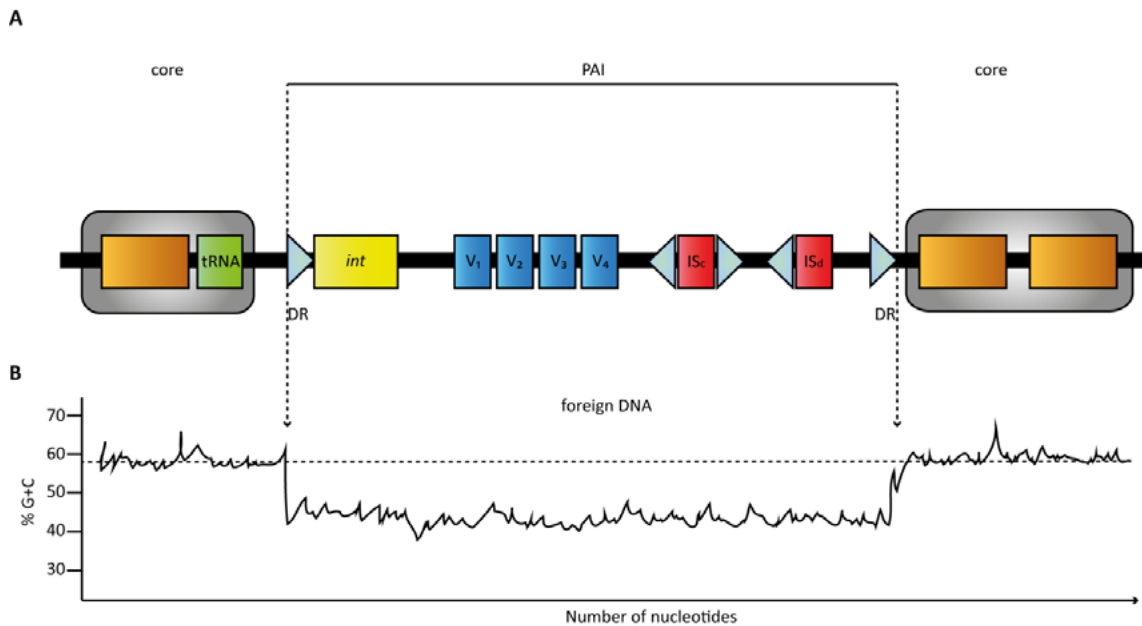


Figure II.3 General structure of a PAI. (A) PAIs are typically distinct regions of DNA found only in the genome of pathogenic bacteria and absent in non-pathogenic strains of the same or related species. They are often inserted at specific sites in the host genome (grey bars) adjacent to tRNA or tRNA-like genes (green bar). In a typical PAI mobile genes, such as integrases (*int*), are located at the beginning of the island, near the tRNA locus or the respective attachment site. PAIs contain one or more virulence genes (V1-V4) and are mostly associated with other mobile elements such as IS elements (IS_c , complete insertion element) or cryptic remainders thereof (IS_d , defective insertion element). The boundaries of PAIs are frequently determined by DRs (triangles), which are utilized for insertion and deletion processes. (B) A characteristic of PAI is a G/C content that differs from the rest of the genome. Modified after Schmidt, H. and Hensel, M. (2004)

II.6. SPI-4

The SPI-4 was identified in 1998 in a comparative genome hybridization of the *S. Typhimurium* LT2 genome with that of the *E. coli* K12 strain (Wong *et al.*, 1998). It covers a range of ~24.7 kb which is conserved among different *Salmonella* serovars and has been detected in all sequenced subspecies of *S. enterica* and *S. bongori* (Figure II.4) (Desai *et al.*, 2013; Edwards *et al.*, 2002, Main-Hester *et al.*, 2008).

First indications of a contribution of the SPI-4 to the pathogenicity of *Salmonella* were provided by the experiments carried out by Morgan *et al.* (2004). They showed the involvement of SPI-4 in the colonization of the intestinal epithelium in the bovine- but not in the chicken-infection model. As a result of this observation, the six open reading frames (ORFs) of the SPI-4 (*stm425762*) were renamed in *siiAF* (*Salmonella* intestinal infection) (McClelland *et al.*, 2001). Furthermore, SPI-4 in conjunction with SPI-1 contributes to the development of intestinal local inflammation in oral application in the murine colitis model (Gerlach *et al.*, 2007d). In the same study it could be shown for the first time that SPI-4 is essential for the adhesion to and invasion into polarized epithelial cells.

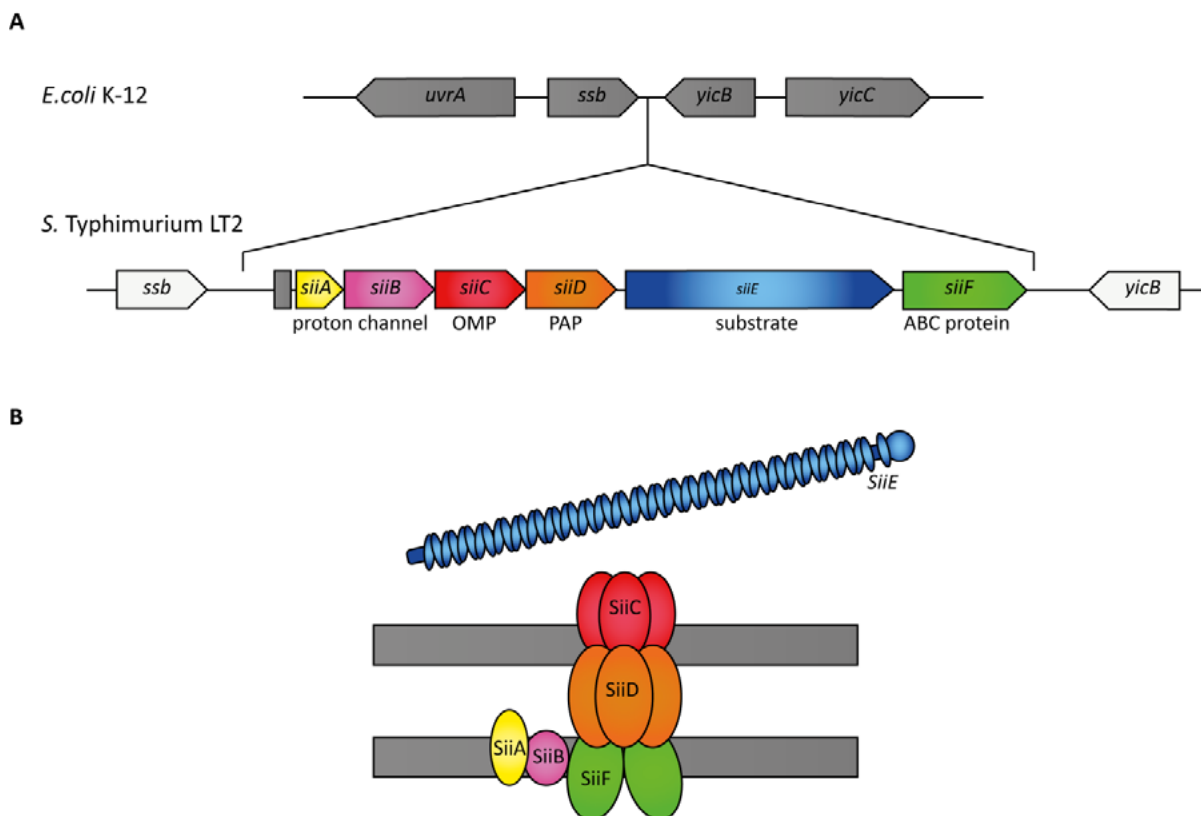


Figure II.4 Structure of the SPI-4. SPI-4 comprises a region of ~24.7 kb that occurs in *Salmonella* but not in *E. coli*. In total, the SPI-4 encodes six ORFs that form an operon and whose expression is regulated by a promoter upstream of *siiA*. SPI-4 has a mosaic-like structure with an average G/C content of 37.44% (the G/C content of the core genome is about 52%). While the first four genes have overlapping reading frames, *siiD* and *siiE* as well as *siiE* and *siiF* are separated by intergenic regions. Both the separation by the intergenic regions and the different GC contents indicate an independent acquisition of *siiABCD*, *siiE* and *siiF* (Gerlach *et al.*, 2007b, Kiss *et al.*, 2007).

The SPI-4 genes *siiA-F* constitute an operon (Gerlach *et al.*, 2007b), where the genes *siiCDF* encode the components of a T1SS. SiiC is the pore-forming OMP, SiiD the PAP and SiiF the inner membrane ABC exporter. The only known substrate is SiiE, a large, non-fimbrial adhesin (Gerlach *et al.*, 2007d; Morgan *et al.*, 2007; Griessl *et al.*, 2013; Peters *et al.*, 2017). In addition to the function of the T3SS-1, the secretion of SiiE is essential for the invasion of polarized intestinal epithelial cells. During the first steps of invasion it is temporarily located on the bacterial surface and probably establishes initial contact with the microvilli of the apical membrane (Gerlach *et al.*, 2008). SiiE binds to host cells in a lectinlike manner using N-acetylglucosamin and α 2,3-linked sialic acid-containing structures as ligands (Wagner *et al.*, 2014). Its activity is important for maximal bacterial entry into polarized cells as it enables clusters of *Salmonella* that are close to the site of invasion to be pulled into the membrane ruffle (Lorkowski *et al.*, 2014).

Fattinger *et al.* (2020) showed that the invasion of absorptive epithelial cells in the mouse gut takes place by discreet-invasion. This process is facilitated by the adhesion of *Salmonella* via SiiE and results in invasion of mainly epithelial cell neighbouring goblet-cells.

There are also two accessory proteins encoded by *siiAB* which form a proton-conducting channel in the IM and seem to play a crucial role in the regulation of SiiE secretion and retention (Wille *et al.*, 2014). Deletion of *siiA* and /or *siiB* results in decreased virulence of mutants in the oral infection in the mouse model (Kiss *et al.*, 2007) as well as in the MDCK infection model (Wille *et al.*, 2014).

II.6.1. Regulation of SPI-4 expression

The expression of SPI-4 is regulated by a promoter region upstream of *siiA*. Within the promoter region, a jump-start region was identified containing an operon polarity suppressor (*ops*) element (Morgan *et al.*, 2004). *Ops* elements are rare sequence motifs found in the promoter regions of large operons (Nieto *et al.*, 1996; Bailey *et al.*, 1997). These elements can be bound by the antiterminator protein RfaH, which stabilizes the elongation of long transcripts. Accordingly, the deletion of *rfaH* or the mutation of the *ops* element in the case of SPI-4 had only a minor effect on the expression of *siiA*, but a significant effect on the distal *siiE*. In contrast, no influence of RfaH on the expression of *siiF* could be detected (Gerlach *et al.*, 2007c, Main-Hester *et al.*, 2008). This observation supported the assumption that the expression of SPI-4 results in a long transcript (*siiA-F*) and a short transcriptional unit of *siiF* (Main-Hester *et al.*, 2008). However, recent results from RNA deep sequencing experiments did not provide any indication of a further transcriptional start within the SPI-4 (Ramachandran *et al.*, 2012).

The first indications for a co-regulation of the SPI-4 and SPI-1 were provided by the results of Ahmer *et al.* (1999), who showed that the SPI-4 is regulated by the transcription factors HilA and SirA analogous to SPI-1. Further work demonstrated that the deletion of *sirA* leads to a significant reduction of SiiE secretion and SPI-4 mediated adhesion to polarized epithelial cells (Gerlach *et al.*, 2007c). With respect to the regulation of SPI-4 by HilA, a HilA-box could be identified within the *siiE* locus and downstream of *siiA* above the SPI-4 promoter region (De Keersmaecker *et al.*, 2005, Thijs *et al.*, 2007). The binding of HilA within the SPI-4 probably counteracts silencing by the nucleotide-associated protein HNS (Main-Hester *et al.*, 2008). It is known that HNS binds to the AT-rich sequences typical for horizontally acquired DNA which results in transcriptional silencing (Navarre *et al.*, 2006, Lucchini *et al.*, 2006). Furthermore, Saini *et al.* (2010) recently demonstrated that the SPI-1 encoded transcription factor SprB can bind directly to the SPI-4 promoter (P_{siiA}) and induce SPI-4 gene expression. In their proposed model HilA activates the expression of SprB. SprB in turn not only induces the expression of SPI-4, but also acts as a weak repressor of SPI-1 gene expression and establishes the molecular link between SPI-1 and SPI-4 gene expression (Saini *et al.*, 2010).

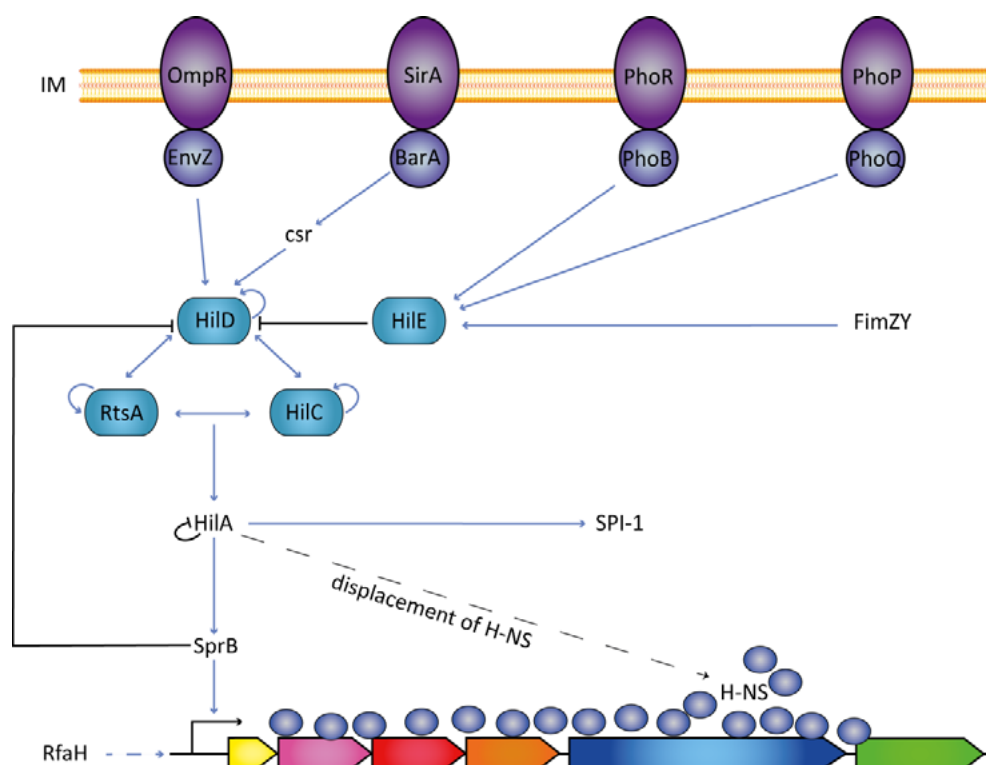


Figure II.5 Regulation of SPI-4 HilA is the key regulator of SPI-1 and SPI-4. Its activity is mainly regulated at the transcriptional level depending on a complex network of transcription factors and two component systems in response to certain environmental cues. The blue arrows show the induction of gene expression, whereas the black lines with a bar at the end indicate repression of transcription. Figure was modified according to Ellermeier *et al.*, 2007; Main-Hester *et al.*, 2008; Saini *et al.*, 2010.

II.6.2. Structure of SiiE

SiiE is a very large, non-fimbrial adhesin necessary for the adhesion of *Salmonella* to polarized epithelial cells. It has a molecular weight of 595 kDa and is the largest protein of the entire *S. Typhimurium* proteome. The structure of SiiE is highly repetitive and consists mainly of 53 bacterial immunoglobulin-like (Blg) domains. Each Blg domain consists of about 100 amino acids (aa). The C-terminal Blg domain 53 is surrounded by two sequence segments comprising about 50 aa (Figure II.6). The crystal structure of a SiiE fragment spanning Blg domains 50-52 shows two SiiE-specific Ca^{2+} binding sites (Figure II.7). Due to homologies to other parts of the SiiE sequence it can be assumed that SiiE can interact in full length with more than 100 Ca^{2+} ions (Griebl *et al.*, 2013). According to the classical characteristics of a type I-secreted protein, the secretion signal could be localized in the second sequence segment at the C-terminus of SiiE (Gerlach *et al.*, 2007c; Wagner *et al.*, 2011). The N-terminus, however, is formed by a coiled-coil region with eight heptad repeats flanked by B-sheet structures. The function of the N-terminal region is associated with the retention and release of the adhesin on the bacterial surface (Wagner *et al.*, 2011). Ultrastructural analyses using electron microscopy showed that SiiE is a linear filamentous molecule with a length of about 200 nm. The extreme length is most likely due to the fact that SiiE must reach through the lipopolysaccharide (LPS) layer. This could enable binding to a specific receptor on the host cell surface (Gerlach *et al.*, 2008).

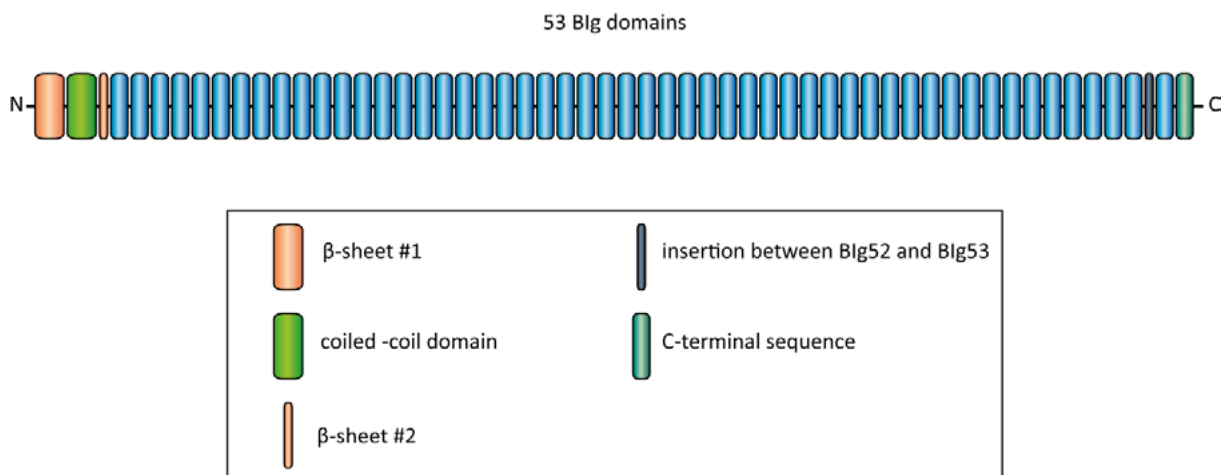


Figure II.6 Schematic representation of the domain structure of SiiE. SiiE is highly repetitive and consists mainly of 53 bacterial immunoglobulin-like (Blg) domains. The N-terminus consists of a coiled-coil region with eight heptad repeats flanked by B-sheet structures. The C-terminus contains undefined structural elements, like the insertion between Blg52 and Blg53. Figure modified after Wagner *et al.* (2011)

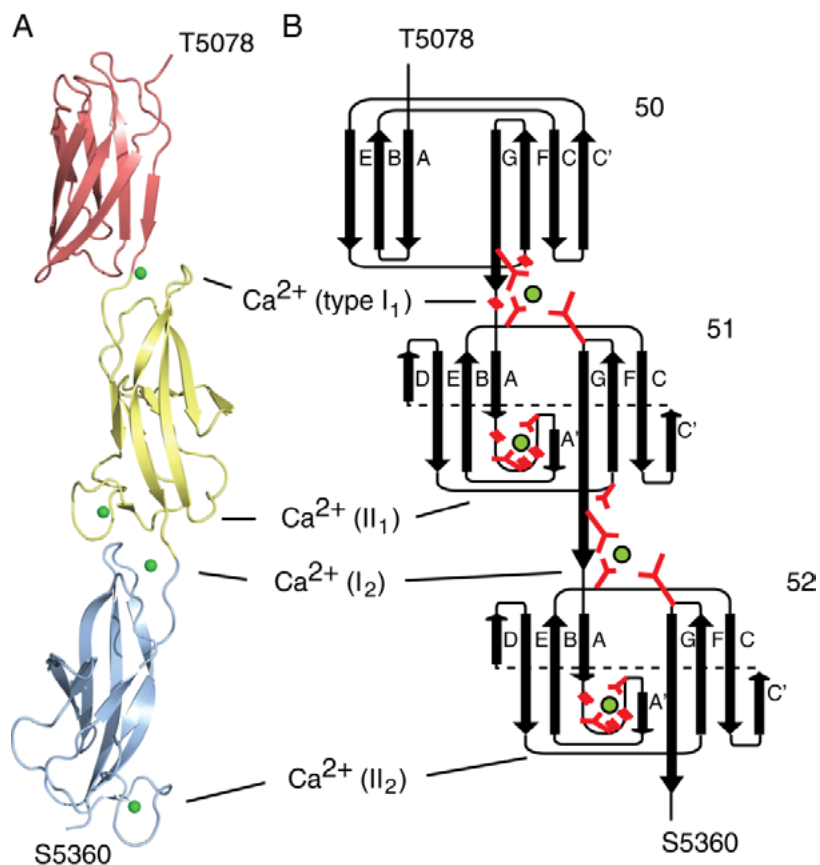


Figure II.7 Crystal structure of the Blg Domains 50-52 of SiiE (A) Ribbon model of the crystal structure, Blg50 in red, Blg51 in yellow and Blg52 in blue. Calcium ions are shown as green spheres. (B) The topology plot shows the connections between the B-sheets (arrows), preserved aspartates are highlighted in red. Source: Griebl *et al.*, 2013

II.7. Motility and Chemotaxis as virulence factors

Motility in combination with the ability to react upon chemical gradients (Figure II.8), chemotaxis for short, is one of the evolutionary oldest abilities of bacteria. Chemotaxis enables bacteria to find new nutrient sources as well as to avoid detrimental chemicals such as toxic metal ions. Bacteria have a broad spectrum of different specialized proteins localized in the inner membrane, so called methyl-accepting chemotaxis proteins (MCPs) that are able to sense certain molecules. After sensing the reaction is triggered via a phosphorylation cascade (phosphorelay). CheA gets phosphorylated and in turn phosphorylates the response regulator CheY. Phosphorylated CheY interacts with the flagellar switch protein FliM which leads to the clockwise (CW) rotation (default state) of the flagellum and therefore to tumbling of the bacterium. Upon dephosphorylation of CheY through CheZ the flagellar rotation is switched to counterclockwise (CCW) and results in a smooth swimming phenotype. This enables the bacteria to move in the direction of nutrients (attractants) and away from harmful chemicals (repellants).

Chemotactically active bacteria are propelled by the rotation of flagella. Flagella are long helical structures consisting of hundreds of subunits of flagellin (FliC) and are anchored in the bacterial cell membrane via a rotor-stator complex. There are also *Salmonella enterica* subspecies (I, II, IIIb and VI) that have two genes encoding for flagellin, namely *fliC* and *fliB*, respectively (Liu *et al.*, 2017). A schematic structure is shown in Figure II.9. A flagellum consists of three main parts: the basal body, the hook and the filament. The basal body comprises of a rotary motor and a protein export apparatus which translocates flagellar components. It consists of the rod and three coaxially mounted rings (MS, P and L ring). The MS ring is located in the inner membrane whereas the P and L rings are embedded in the peptidoglycan layer and outer membrane, respectively. The rod is composed of the proximal (FlgBCF) and the distal rod (FlgG) and spans the entire periplasmic space (Terashima *et al.*, 2008). The so called Cring is localized on the MS ring facing the cytoplasm. It is composed mostly of FliM and FliN which form, together with FliG, the switch complex. The export apparatus is located inside the MS ring structure and is composed of six integral TM proteins (FlhAB and FliOPQR) (Terashima *et al.*, 2008). The hook functions as universal joint and the filament as propeller (Duan *et al.*, 2011).

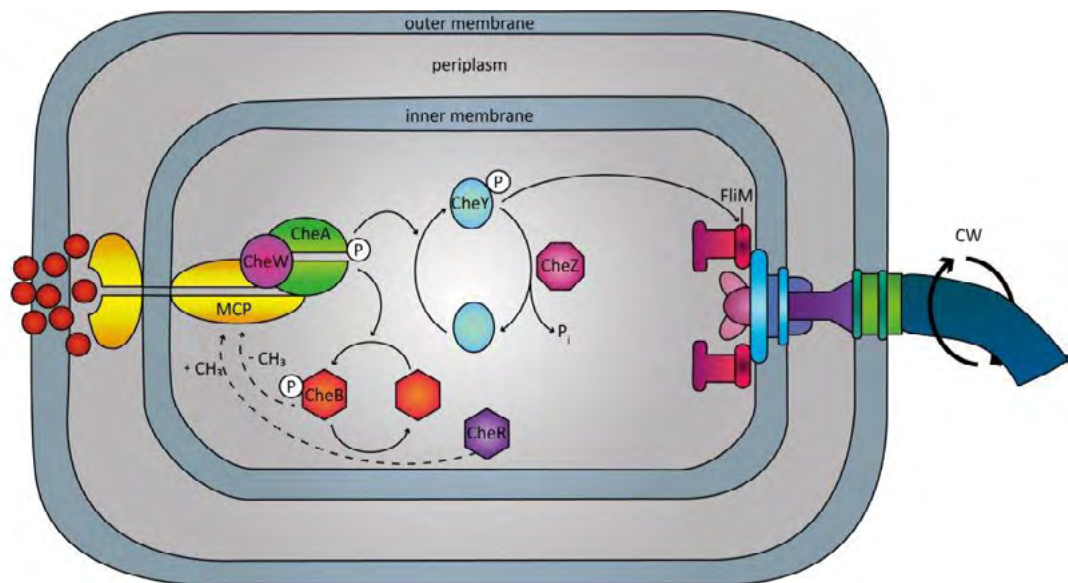


Figure II.8 Scheme of chemotaxis in *E. coli* Upon sensing certain chemicals e.g. amino acids by a MCP, CheA gets phosphorylated and in turn phosphorylates the response regulator CheY. CheY interacts with the flagellar switch protein FliM which leads to the clockwise (CW) rotation of the flagellum and therefore to tumbling of the bacterium. When CheY gets dephosphorylated by CheZ or is missing, the flagellar rotation is switched to counterclockwise (CCW) and leads to a smooth swimming phenotype.

The rotation of the flagella is powered by the proton motive force (PMF). The stator of the flagellum consisting of MotA and MotB anchors the complex in the peptidoglycan layer and forms a protonconducting channel through the inner membrane (Zhu *et al.*, 2013). MotA consists of 4 TM domains, where domains TM1 and 2 as well as TM3 and 4 are connected in the periplasm by two short loops. MotA also has two relatively large

cytoplasmic domains, one between TM2 and 3 and one behind TM4. Certain amino acids of the cytoplasmic loop between TM2 and 3 interact via electrostatic interactions with the C-terminal motility domain of FlhG in the rotor, which is crucial for flagella rotation. MotB consists of a short N-terminal domain in the cytoplasm, a TM domain and a large periplasmic domain. There is also a peptidoglycan binding motif, which is why MotB serves as an anchor for the MotA₄B₂ complex (Kojima and Blair, 2004). The proton channel is formed by the TM domain of MotB and TM3 and 4 of MotA (Braun *et al.*, 2004).

Flagella are also involved in surface sensing and therefore in the transition from the planktonic lifestyle to biofilm formation. It is believed that bacteria recognize surfaces by mechanosensation which leads to different cellular processes including the expression of adhesive structures. The downstream signaling is mediated by the second messenger c-di-GMP (O'Toole and Wong, 2016; Hughes and Berg, 2017).

An additional function of the flagella is the adhesion of the bacteria to host cells during the initial phase of infection (summarized in Rossez *et al.*, 2015), which makes them an important virulence factor. Reversible binding to host involves also additional factors such as Fim fimbriae while irreversible docking is achieved by binding through the T3SS-1 (Misselwitz *et al.*, 2010). The tight functional interaction between flagella and the T3SS-1 is reflected in a coregulation of gene expression via the RtsAB transcriptional factors (Ellermeier and Slauch, 2007).

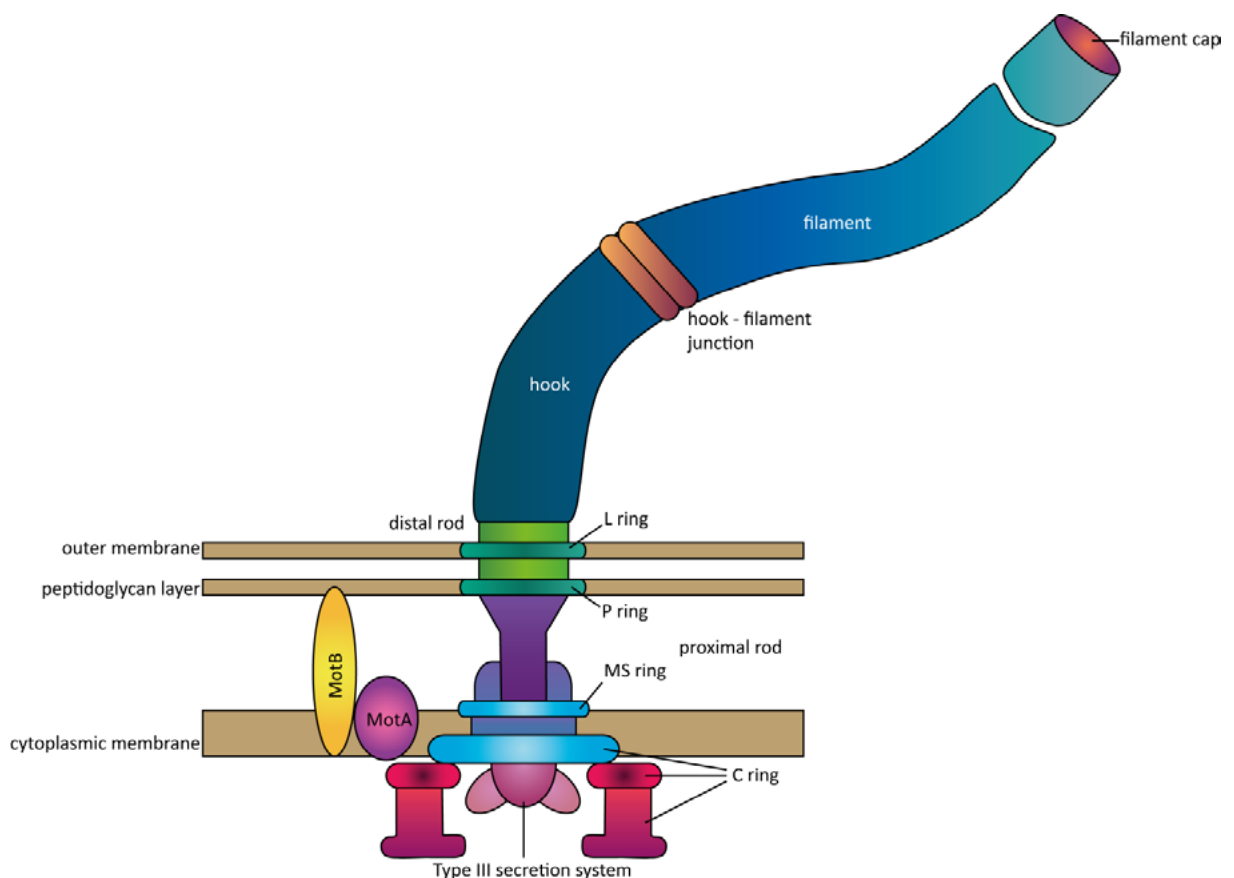


Figure II.9 Schematic structure of the flagellum of *E. coli* K12. Shown are the filament and the rotor stator complex with accessory proteins, such as MotAB, and regulators (FlhM, FlhCD...). The figure was modified after the KEGG database.

II.8. Homology between MotAB and SiiAB

The MotAB complex forms the stator of the bacterial flagellum. It is a heterohexameric complex with a MotA₄B₂ stoichiometry that forms a protonconducting channel through the inner membrane (Zhu *et al.*, 2013; Takekawa *et al.*, 2016). PMF-driven proton flux through the channel powers the flagellar rotation.

Up to a dozen stator complexes are associated with one motor complex (Terashima *et al.*, 2017; Baker and O'Toole, 2017). There are fluctuations in torque depending on the number of MotAB complexes leading to different rotational speeds of the flagellum (Baker and O'Toole, 2017). The number of stator complexes depends on many external factors e.g. the viscosities of the environment and therefore different loads the flagellum is exposed to (Lele *et al.*, 2013; Tipping *et al.*, 2013).

As described in section II.7 MotA and MotB are located in the IM with several TM domains per molecule.

For MotB, a TM domain, a periplasmic C-terminus and a cytoplasmic N-terminus were predicted and the same holds true for SiiA. SiiB on the other hand shows similarities to MotA. Here three TM domains were predicted, which are connected by short links in both, cytoplasm (TM1 and TM2) and periplasm (TM2 and TM3). A special feature of SiiB is a relatively long C-terminus in the cytoplasm. SiiA has a highly conserved aspartate at position 13 which corresponds to a similarly conserved Asp at MotB position 32 (Wille *et al.*, 2014). This conserved Asp is crucial for proton conduction of MotAB and other proton channel complexes. In MotAB protonation and deprotonation of Asp32 leads to conformational changes in the cytoplasmic region of MotA that interacts with FliG and is decisive for the rotation of the flagellum (Berg, 2003). A similar function for the SiiAB complex was shown by inactivation of SiiAB function in a SiiA[D13N] mutant (Wille *et al.*, 2014). The putative membrane topology of the SiiAB proton channel based on homology to the MotAB complex is shown in Figure II.10.

The question that arises from the possible function of SiiAB as a proton channel is the type of activation. MotAB, for example, is only activated by assembly with the motor complex. A domain of MotB is serving as a plug to prevent premature leaking of protons through the channel. This plug is located in the periplasm just C-terminal from the MotB TM. Deletion of this domain leads to a massive proton flux and acidification of the cytoplasm which finally arrests cell growth (Hosking *et al.*, 2006). In *Salmonella* it could be shown that the proton-conductivity of a MotAB complex not incorporated in the motor is two orders of magnitude lower than that of an incorporated and activated channel (Morimoto *et al.*, 2010).

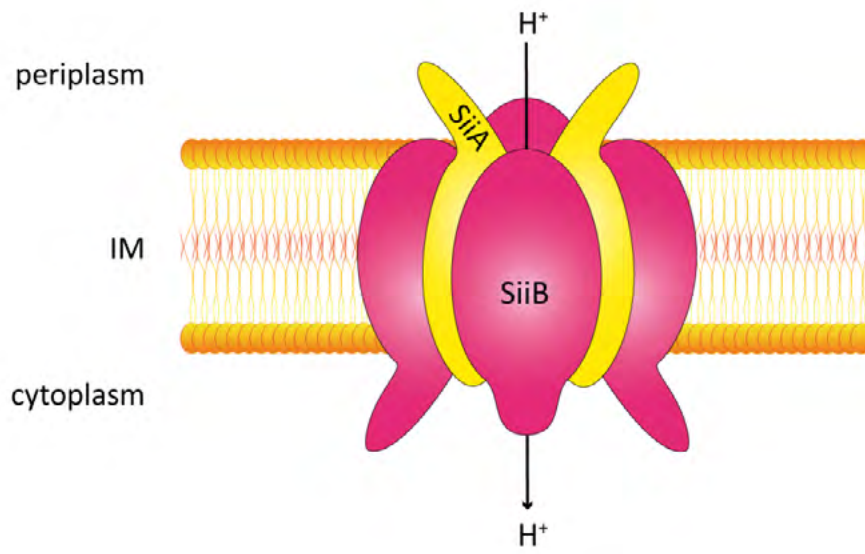
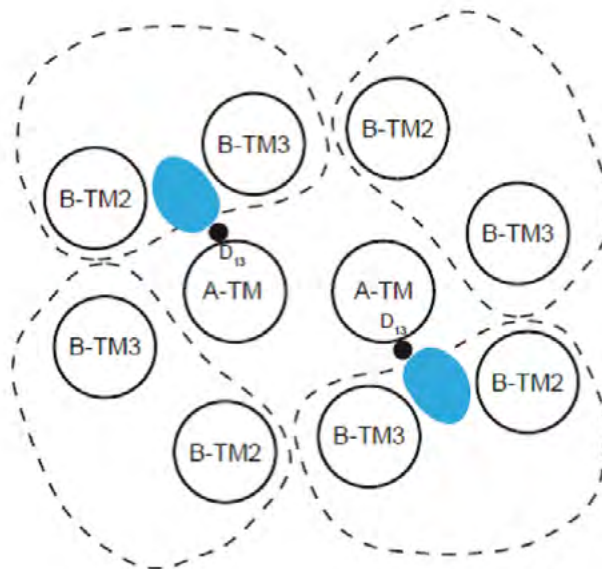
A**B**

Figure II.10 **A**) Possible SiiAB complex formed in the inner membrane (IM) **B**) Depiction of the putative SiiAB proton channel complex. mod. from Wille *et al.*, 2014

II.9. Methyl-accepting Chemotaxis Proteins

Methyl-accepting chemotaxis proteins (MCPs) are receptors that allow bacteria to react to the presence and absence of different chemicals via phosphorylation or dephosphorylation. They are stable homodimers and consist of four domains. Certain substances can bind to the periplasmic binding domain making it unique for each MCP. The transmembrane domain consists of two helices and spans the IM. Furthermore, there are one or more HAMP (histidine kinases, adenyl cyclases, methyl-binding proteins and phosphatases) domains and a highly conserved cytosolic C-terminal domain that interacts with the subsequent signal transduction cascade (Falke and Hazelbauer, 2001). Figure II.11 schematically shows the structure of an MCP dimer. Upon ligand binding at the periplasmic ligand binding domain these helices are shifted in a piston-like motion to transmit the signal across the IM to the cytoplasmic helices and therefore to the HAMP domain. All these events necessary for signaling are based on asymmetric interactions/motions (Park *et al.*, 2011). The HAMP domain connects the output methylation helices that comprise part of the receptor kinase control module (Parkinson, 2010). Through the piston-like displacement of the HAMP domain the signal is passed on to the kinase interaction domain and the phosphorylation of the signaling cascade proteins leads to clockwise (CW) or counterclockwise (CCW) rotation of the flagellum.

MCPs are coupled to the histidine autokinase CheA via the scaffold protein CheW. There are two conformations of these signaling complexes, the “kinase-on” and “kinase-off” states that are in equilibrium. Motor response is elicited by shifting this equilibrium to one of the two states due to chemical stimuli. A higher attractant concentration provides for more complexes in the “kinase-off” state whereas a higher repellent concentration shifts receptors to the “kinase-on” conformation. This regulates the flux of CheA phosphoryl groups to the response regulators CheY and CheB. Phospho-CheY binds to the flagellar switch protein FliM, enhancing the probability of CW rotation, which leads to the tumbling of the bacterium (Welch *et al.*, 1993; Toker *et al.*, 1997). The adaptation system records chemical conditions by reversible receptor methylation at four to six glutamyl residues in the adaptation domain. Here phospho-CheB deaminates glutamates whereas CheR methylates them. So in the “kinase-off” conformation chemoreceptors have high attractant affinity and low demethylation propensity (Sourjik *et al.*, 2002; Sourjik *et al.*, 2004).

In *Salmonella* there are seven MCPs known (Table II.2) which contribute to its virulence by helping finding favorable niches.

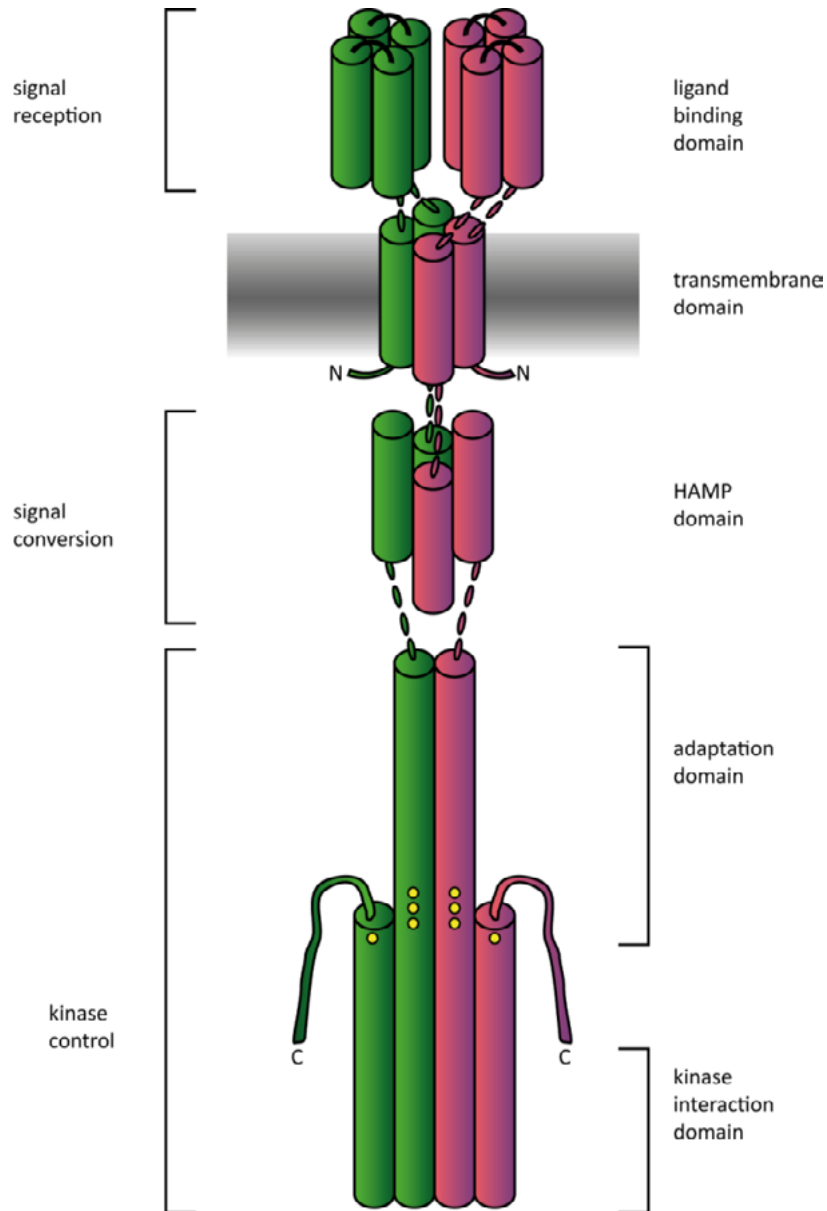


Figure II.11 structure of a methyl-accepting chemotaxis protein consisting of two monomers (red, green). Methylation takes place at the adaptation domain after converting of the sensed signal via conformational changes of the HAMP domain. Modified after Falke and Hazelbauer, 2001

Table II.2 Methyl-accepting chemotaxis proteins of *Salmonella*

MCP	stimulus	source/reference
Aer	redox potential	Bibikov <i>et al.</i> , 2004
Tsr	nitrate, serine	Rivera-Chávez <i>et al.</i> , 2016
Trg	glucose, galactose, ribose	Kondoh <i>et al.</i> , 1979
CheM	aspartate	Blat <i>et al.</i> , 1995
Tcp	citrate, phenol	Yamamoto <i>et al.</i> , 1993
McpB	L-cysteine	Lazova <i>et al.</i> , 2012
McpC	L-cysteine	Lazova <i>et al.</i> , 2012

II.10. Aims of the work

The major objective of this work was to unravel the molecular mechanism of how the giant nonfimbrial adhesin SiiE is secreted or retained on the bacterial cell surface by the T1SS encoded on SPI-4. Previous work suggested the involvement of the two accessory proteins SiiA and SiiB in this process, which are believed to form a proton-conducting channel. We wanted to proof this hypothesis experimentally and understand the functional link to the T1SS-4 and SiiE. The current working model is shown in Figure II.12. The activation of the SiiAB proton channel and the resulting ion flux leads to conformational changes of SiiF, SiiD and / or SiiC, causing the retention of SiiE. A question arising from this hypothesis is how the activity of SiiAB is controlled.

The receptor responsible for the reaction of *Salmonella* to aspartate, CheM, was identified as a potential interaction partner of SiiAB in an immunoprecipitation experiment followed by mass spectrometry analysis. The interaction of CheM with the components of the T1SS-4 as well as the possible role as signal generator for the activity of SiiAB and therefore the retention of SiiE should be tested in the course of this work.

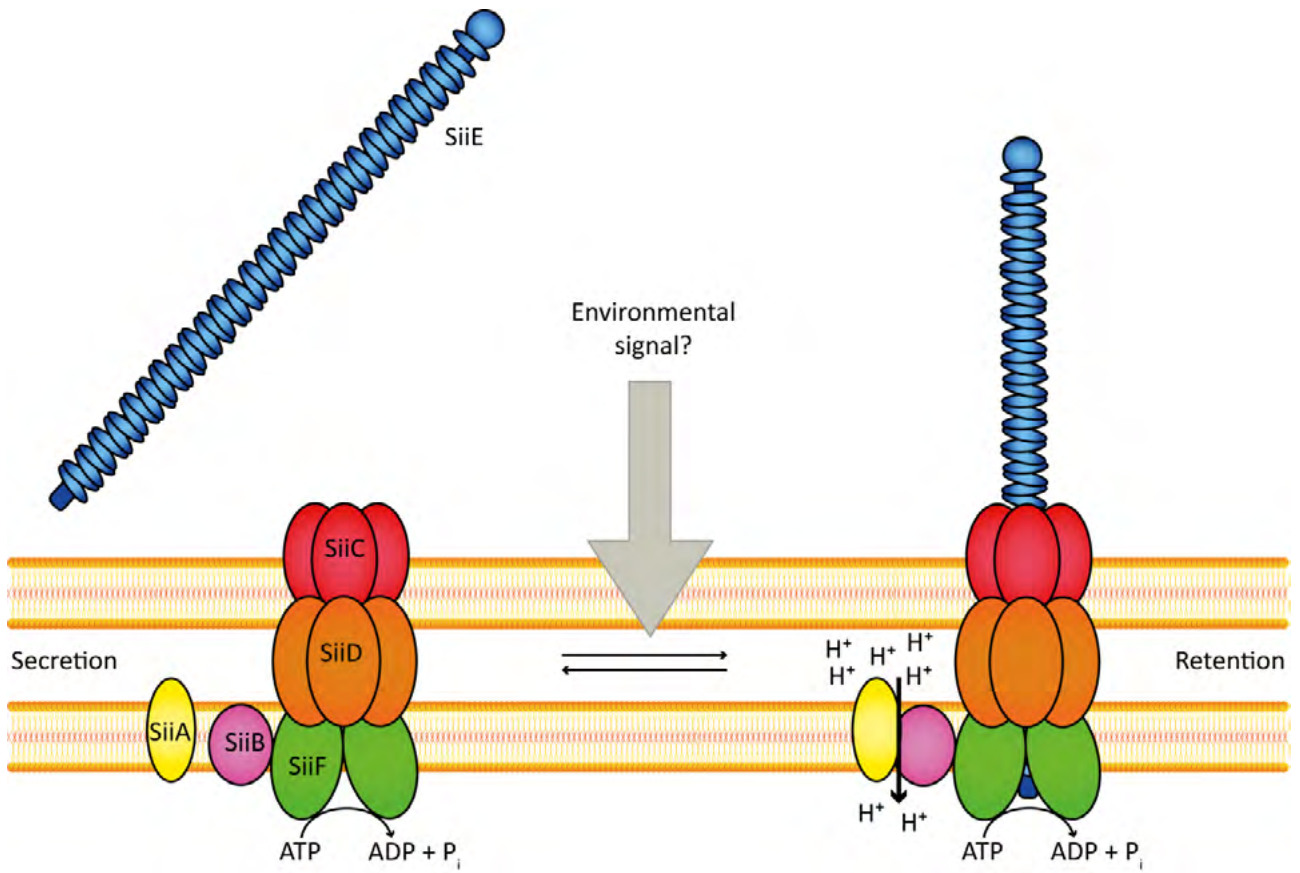


Figure II.12 Working model Secretion and retention of SiiE through the T1SS4. Upon activation of the SiiAB proton channel due to an unknown signal there is an influx of ions which lead to conformational changes of SiiF, SiiD and 7 or SiiC resulting in the retention of SiiE.

III. RESULTS AND PUBLICATIONS

III.1. High-Throughput Quantification of Bacterial-Cell Interactions Using Virtual Colony Counts

Stefanie Hoffmann^{1‡}, Steffi Walter^{1‡}, Anne-Kathrin Blume², Stephan Fuchs³, Christiane Schmidt¹, Annemarie Scholz^{1†} and Roman G. Gerlach¹

¹ Project Group 5, Robert Koch Institute, Wernigerode, Germany

² Department of Bioorganic Chemistry, Leibniz Institute of Plant Biochemistry, Halle, Germany

³ Division 13: Nosocomial Pathogens and Antibiotic Resistances, Robert Koch Institute, Wernigerode, Germany

‡ These authors have contributed equally to this work.

High-Throughput Quantification of Bacterial-Cell Interactions Using Virtual Colony Counts

Stefanie Hoffmann^{1†}, Steffi Walter^{1†}, Anne-Kathrin Blume², Stephan Fuchs³, Christiane Schmidt¹, Annemarie Scholz^{1†} and Roman G. Gerlach^{1*}

¹ Project Group 5, Robert Koch Institute, Wernigerode, Germany, ² Department of Bioorganic Chemistry, Leibniz Institute of Plant Biochemistry, Halle, Germany, ³ Division 13: Nosocomial Pathogens and Antibiotic Resistances, Robert Koch Institute, Wernigerode, Germany

OPEN ACCESS

Edited by:

Yousef Abu Kwaik,
University of Louisville, United States

Reviewed by:

Leigh A. Knodler,
Washington State University,
United States

Stephanie M. Seveau,
The Ohio State University,
United States

*Correspondence:

Roman G. Gerlach
GerlachR@rki.de

† Present Address:

Annemarie Scholz,
Department of Food Chemistry and
Toxicology, Berlin Institute of
Technology, Berlin, Germany

† These authors have contributed
equally to this work.

Received: 24 October 2017

Accepted: 31 January 2018

Published: 15 February 2018

Citation:

Hoffmann S, Walter S, Blume A-K,
Fuchs S, Schmidt C, Scholz A and
Gerlach RG (2018) High-Throughput
Quantification of Bacterial-Cell
Interactions Using Virtual Colony
Counts.
Front. Cell. Infect. Microbiol. 8:43.
doi: 10.3389/fcimb.2018.00043

The quantification of bacteria in cell culture infection models is of paramount importance for the characterization of host-pathogen interactions and pathogenicity factors involved. The standard to enumerate bacteria in these assays is plating of a dilution series on solid agar and counting of the resulting colony forming units (CFU). In contrast, the virtual colony count (VCC) method is a high-throughput compatible alternative with minimized manual input. Based on the recording of quantitative growth kinetics, VCC relates the time to reach a given absorbance threshold to the initial cell count using a series of calibration curves. Here, we adapted the VCC method using the model organism *Salmonella enterica* sv. Typhimurium (S. Typhimurium) in combination with established cell culture-based infection models. For HeLa infections, a direct side-by-side comparison showed a good correlation of VCC with CFU counting after plating. For MDCK cells and RAW macrophages we found that VCC reproduced the expected phenotypes of different S. Typhimurium mutants. Furthermore, we demonstrated the use of VCC to test the inhibition of *Salmonella* invasion by the probiotic *E. coli* strain Nissle 1917. Taken together, VCC provides a flexible, label-free, automation-compatible methodology to quantify bacteria in *in vitro* infection assays.

Keywords: *Salmonella*, invasion, adhesion, intracellular replication, gentamicin protection assay, virtual colony count, bacterial quantification, cell culture infection model

INTRODUCTION

The ability of pathogenic bacteria to interact with eukaryotic cells depends on a complex interplay of bacteria- and host-derived factors. At the bacterial side the presence of virulence factors such as adhesins and secretion systems significantly contributes to this interaction (Gerlach and Hensel, 2007a). Cell culture based infection models have been used with great success to identify and characterize virulence factors important for the interaction with defined cell types. As a main readout these analyses rely on the enumeration of bacteria bound to or internalized within these cells. The gold standard to quantify bacteria in these assays is still plating of a dilution series on solid agar and counting of the resulting colony forming units (CFU). This method is laborious and inherits many manual steps making it hard to establish a standardized or automated procedure required for high-throughput analyses. Therefore, alternative methods based on radioactive, fluorescence, luminescence, or chromogenic labeling of bacteria have been developed

(Acord et al., 2005; Vesterlund et al., 2005; Martens-Habben and Sass, 2006). Labeling is achieved through either genetic modification or preparatory staining of the bacteria. Depending on the bacterial species or strain such manipulations or processing steps might not be possible or could exert unpredictable effects on cell physiology. Furthermore, specialized and sensitive detection equipment is required.

As a label-free alternative to CFU counting a method called “Virtual Colony Count” (VCC) has been developed (Brewster, 2003). The principle of VCC shows many similarities to quantitative polymerase chain reaction (qPCR). While in qPCR assays the increase in fluorescence intensity is monitored over time, VCC monitors quantitative growth kinetics based on absorbance measurements. Instead of cycles required to meet a certain fluorescence threshold (C_t) in qPCR, VCC relies on the time to reach a given absorbance threshold (T_t). Correlation of T_t to the initial cell count is achieved with the help of a series of calibration curves (Brewster, 2003). So far, use of VCC was limited to enumerate cells in pure bacterial cultures, e.g., to quantify the bactericidal effect of antimicrobial peptides (Ericksen et al., 2005; Xie et al., 2005; Zou et al., 2008; Rajabi et al., 2012; Zhao et al., 2012; Pazgier et al., 2013), but was not applied to infection models.

Pathogenicity of *Salmonella enterica* serovar Typhimurium (*S. Typhimurium*) has been characterized in detail with the help of cell culture-based infection models. In conjunction with animal models it could be demonstrated that virulence of *S. Typhimurium* is largely determined by a set of genes encoded on genomic loci called *Salmonella* pathogenicity islands (SPI) (Gerlach and Hensel, 2007b). The type three secretion systems (T3SS) encoded by SPI-1 and SPI-2 (T3SS-1/2) are *inter alia* required for trigger-like invasion of non-phagocytic cells and intracellular survival and replication, respectively (Fàbrega and Vila, 2013). For invasive pathogens such as *S. Typhimurium*, the gentamicin protection assay is an established *in vitro* methodology to distinguish intracellular from extracellular bacterial cells. While the latter ones are killed by antibiotic treatment, intracellular organisms are protected and survive. After subsequent lysis of host cells, bacteria are quantified to determine the invasiveness or their ability for intracellular replication (Devenish and Schiemann, 1981). Here we demonstrate a workflow, including automated data analysis, to apply VCC for bacterial quantification in gentamicin protection assays using three different *Salmonella* infection models.

MATERIALS AND METHODS

Bacterial Strains and Growth Conditions

All bacterial strains used are listed in Table 1. *Salmonella* mutants are all isogenic to the wild-type strain *S. Typhimurium* NCTC 12023. Bacteria were grown aerated overnight (O/N) at 37°C in LB medium without or with the addition of 50 µg ml⁻¹ kanamycin, where appropriate. For calibration curves, bacterial cultures were inoculated 1:100 in fresh LB and continued to grow aerated in a roller drum (TC-7, New Brunswick, Edison, NJ, USA) for 2 h 30 min at 37°C until an OD₆₀₀ of 1.4–1.8 was

TABLE 1 | Bacterial strains used in this study.

Strain	Relevant characteristic(s)	Source or reference
<i>S. enterica</i> serovar Typhimurium strains		
NCTC12023	Wild type (WT)	NCTC, Colindale, UK
MvP818	<i>invC</i> FRT (T3SS-1 ⁻)	Gerlach et al., 2008
WRG226	<i>sseJ::3xFlag</i> FRT, <i>ssaV</i> FRT (T3SS-2 ⁻)	Lab collection
WRG238	SiiF _{E627Q} (Walker B mutant, SPI-4 ⁻)	Lab collection
WRG300	<i>malYX::PEM7</i> I-Scel <i>aph</i> , Kan ^r	Lab collection
<i>E. coli</i> strain Ec ^{Nissle}	Nissle 1917 wild-type strain	Bärbel Stecher, Munich

reached. For invasion assays (HeLa, MDCK), bacterial cultures were inoculated 1:31 in fresh LB and continued to grow aerated in a roller drum for 3 h 30 min at 37°C.

Cell Culture

MDCK cells were cultured in MEM medium (Biowest, Nuaille, France) supplemented with 10% FCS, 2 mM Glutamax (Thermo, Karlsruhe, Germany), non-essential amino acids (Biowest), 100 U ml⁻¹ penicillin and 100 µg ml⁻¹ streptomycin (Biowest). For invasion assays, cells were seeded at a density of 8 × 10⁴ per well in 96-well plates (Cellstar #655180, Greiner Bio-One, Germany) using the four inner rows. Cells were allowed to differentiate for 10–11 days. The growth medium was replaced by fresh medium every other day and was changed at least 4 h before infection after one washing step with PBS to complete cell culture medium without antibiotics. HeLa and RAW264.7 cells (LGC Standards, Wesel, Germany) were cultured in DMEM medium (high glucose, stable glutamine, sodium pyruvate) (Biowest) supplemented with 10% FCS. HeLa and RAW264.7 were seeded in 96-well plates (Greiner Bio-One) 24 h before infection using the four inner rows at a density of 6 × 10³ per well or 5 × 10⁴ per well, respectively. All cell lines were kept under a humidified atmosphere of 5% CO₂ at 37°C.

Infection and Virtual Colony Count (VCC) Assay

Overnight (RAW264.7) or sub-cultured (HeLa, MDCK) bacteria were adjusted to an OD₆₀₀ of 0.2 (~2 × 10⁸ CFU ml⁻¹) in sterile PBS. Bacteria were then diluted in complete cell culture medium without antibiotics to get the desired MOI and cells were infected with 100 µl of bacterial suspension per well. Infection was allowed for 25 min (MDCK, HeLa) or 60 min (RAW264.7) at 37°C. Non-adherent bacteria were removed by one washing step with pre-warmed PBS and cells were further incubated for 1 h with complete cell culture medium containing 100 µg ml⁻¹ gentamicin to kill non-invaded, extracellular bacteria. For infection of RAW264.7 cells two plates were infected in parallel and cell culture medium containing 10 µg ml⁻¹

gentamicin was used for the remainder of the experiment. After the indicated incubation period host cells were washed twice with PBS and lysed by the addition of 100 μ l pre-warmed lysis buffer containing 2.0% (v/v) Elugent (#324707, Merck, Darmstadt, Germany), 0.0625% (v/v) Antifoam B emulsion (#A5757, Sigma-Aldrich, Steinheim, Germany) in PBS for 30 min shaking at 37°C. VCC was used to quantify intracellular bacteria. After complete lysis the four outer rows of the 96-well plate were filled with 100 μ l per well of the inoculi, 10-fold diluted in lysis buffer. Microbial growth was initiated with the addition of 100 μ l pre-warmed, 2-fold concentrated BHI medium to each well. The microtiter plate was incubated with lid under constant shaking at 37°C in a microplate reader (Infinite M1000, Tecan, Grödig, Austria) and absorbance at 600 nm was measured every 5 min. In case of HeLa infections additional serial dilutions of the lysates and inoculi were made in PBS and spot-plated on LB agar for CFU enumeration.

Data Analysis

The complete analysis pipeline was implemented in the statistical programming language “R” (R Core Team, 2017). A 5-parameter log-logistic fit (formula 1) implemented in the “R” package “drc” (Ritz et al., 2015) was applied to an analysis window of the raw data which range was defined by a fixed first data point and the position of the maximum slope or of the first local maximum minus a predefined fixed number of data points.

$$y = c + \frac{d - c}{(1 + e^{b*(x-e)})^f} \quad (1)$$

Subsequently, T_t was defined as intersection point between the fitted 5-parameter log-logistic function and a line following this formula:

$$y = 0.02 + c \quad (2)$$

Here, c represents the lower asymptote of the fitted log-logistic function. We provide two “R” scripts (Supplementary Data) including sample data files which share the methodology to determine T_t from growth curves and allow for further correlation to $\log(\text{CFU})$ on the basis of calibration curves or calculation of VCC and invasion rates, respectively. Alternatively, the R package “chipPCR” (Rödiger et al., 2015) was used to analyze the raw data. With “chipPCR” a linear background function was calculated using the “least” method from a data window within the lag phase and subsequently subtracted from the raw data. The normalized growth curves were fit using the moving average (mova) function. For calculation of the time to reach the threshold of 0.02, the intersection with a linear regression of four data points near the threshold was used. Data was visualized using either the “R” package “ggplot2” (Wickham, 2016) or Prism v7.03 (GraphPad Software, San Diego, CA, USA).

RESULTS

Curve Fit and Calculation of Threshold Times (T_t)

A challenging aspect of VCC is the determination of the time to reach a certain absorbance threshold (T_t). Previously, T_t was calculated from data normalized by subtracting the first (Ericksen et al., 2005) or the second (Rajabi et al., 2012; Zhao et al., 2012, 2013) data value from raw data or from a linear fit including five data points around an absorbance threshold (Brewster, 2003). In another approach growth curves with significant differences in the baseline and maximal absorbance were background-subtracted and similarly scaled based on the detection of their maximum slope (Brewster, 2003). Our goal was to establish a more reliable and empiric methodology for automatic calculation of T_t from relatively noisy data originating from host cell debris-containing samples. For that, robust background detection and fitting of the individual growth curves is required. We tested two different curve fitting and normalization methods using the statistical programming language “R” (R Core Team, 2017).

The first approach is based on the package “chipPCR” (Rödiger et al., 2015) for “R”. Although “chipPCR” is primarily designed for the analysis of qPCR data, we utilized it successfully for the analysis of bacterial growth curves. ChipPCR is capable of calculating a linear background function from a data window within the lag phase. For the two example data sets shown in **Figure 1A** data points 10–30 were used for this purpose. The moving average (“mova”) curve fitting method was applied to the background-subtracted raw data. The threshold times T_t were calculated based on an absorbance threshold of 0.02 which was previously shown to be optimal for VCC (Ericksen et al., 2005). For that the intersection points of the absorbance threshold (**Figure 1A**, dashed green line) with a linear regression from four data points (**Figure 1A**, blue) derived from the “chipPCR” curve fit and surrounding $A_{600} = 0.02$ were calculated. Subsequently, T_t of 10,874 s and 19,243 s (**Figure 1A**, dotted black lines) were determined for the exemplary dataset.

For the second approach the “R” package “drc” (Ritz et al., 2015) was used which provides a set of model functions for dose-response analyses. We decided to use the 5-parameter log-logistic function included in “drc” because this model has been shown to fit bacterial growth curves very well (Zwietering et al., 1990) and was especially robust in background (lag phase) determination even with noisy data which is essential for exact T_t calculation (data not shown). Unfortunately, we frequently observed low quality fits in cases where stationary growth phase followed an inhomogeneous trend. As a consequence, a method for automatic determination of an analysis window only including the lag- and the logarithmic growth phases was implemented in our “R” script. While a fixed number of initial data points can be excluded to account for noise due to the possible presence of incompletely solubilized debris or air bubbles at the beginning of the kinetic, the end of the analysis window is individually determined for each growth curve. Depending on the analyzed data two methods can be accessed in the script to define the last data point to be included in the curve fit: by detecting (i) the maximum slope or (ii) the first local maximum. After

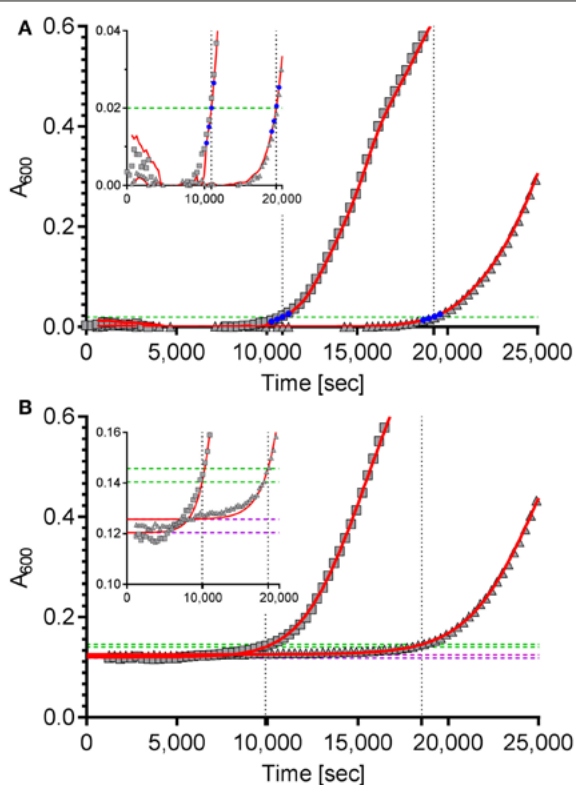


FIGURE 1 | Calculation of the time to reach the threshold of $\Delta A_{600} = 0.02$ of two example growth curves using two different curve fitting and normalization methods. **(A)** The “R” package “chipPCR” was used to analyze the raw data (gray squares and triangles). After subtraction of a background function, the curves were fit using the moving average (mova) function (red lines). To calculate the time to reach the threshold of 0.02 (dashed green line), the point of intersection with a linear regression of four data points (blue) near the threshold was used. Here, threshold times of 10,874 s and 19,243 s (dotted black lines) were determined. **(B)** The same raw data sets shown in **(A)** were fit to a 5-parameter log-logistic function implemented in the “R” package “drc” (red lines). The thresholds of $\Delta A_{600} = 0.02$ were calculated individually for each data set (dashed green lines) by adding up 0.02 to the lower asymptotes (dashed purple lines) of the log-logistic functions. Threshold times of 9,890 s and 18,534 s were calculated from the intersection points (dotted black lines). Insets: zoomed views of the data ranges showing the transition to logarithmic growth.

the curve fit the lower asymptote of the log-logistic function was used as individual background reference (**Figure 1B**, dashed purple lines). Subsequently, an absorbance threshold of $\Delta A_{600} = 0.02$ was set based on these references (**Figure 1B**, dashed green lines). Threshold times (T_t) were calculated from the intersection points with the fitted logistic function (**Figure 1B**, dashed black lines). Using this method, T_t of 9,890 s and 18,534 s were determined for the two exemplary growth curves shown in **Figure 1B**, respectively.

The quality of curve fits produced by “chipPCR” was highly depending on the careful window selection for background calculation. Although “chipPCR” has the potential for superior curve fitting results (see **Figure 1** insets) it required manual

adjustments of parameters for each data set. In contrast, the log-logistic fit based on an analysis window calculated individually for each growth curve did not require any further adjustments. After establishing global parameters depending on the bacterial strain, growth medium and microplate reader used, we found the log-logistic fitting of growth data to be more consistent and robust for background estimation of rather noisy data. Therefore, the log-logistic fitting methodology was used in all further analyses.

Optimization of Host Cell Lysis

Efficient host cell lysis is of critical importance for the turbidimetric detection of bacterial growth. In classical gentamicin protection assays the detergent Triton X-100 is often used for cell lysis (Small et al., 1987). We observed that addition of Triton X-100 resulted in clumping of host cells (data not shown) that would have required further mechanical treatment (e.g., pipetting). These additional processing steps should be circumvented as a source of errors and to streamline batch processing. We found the detergent Elugent, a mixture of alkyl glycosides and inexpensive substitute for octyl glycoside, very effective to lyse host cells. With this detergent we were able to obtain efficient lysis of HeLa and RAW264.7 cells at concentrations of 0.5% (v/v) whereas for confluent MDCK cell layers a final concentration of 2.0% (v/v) was required (data not shown). The addition of the detergent introduced foaming which heavily interfered with optical detection of bacterial growth. To prevent foam formation of the lysis buffer the silicone-based emulsion “Antifoam B” was added. We tested different concentrations of Antifoam B and Elugent for their potential inhibition of bacterial growth which should be visible through a delay of T_t compared to controls. For Antifoam B, no significant impact on bacterial growth was observed for 1:200 or higher dilutions (Supplementary Figure 1A). Elugent concentrations of 0.125% (v/v) and above slightly attenuated bacterial growth (Supplementary Figure 1B). To ensure efficient lysis of all host cells a buffer containing 2.0% (v/v) Elugent in the presence of 0.0625% (v/v; 1:1,600 dilution) Antifoam B was used in all subsequent experiments. A control experiment revealed no significant difference in CFU counts comparing bacteria treated with 2% (v/v) Elugent or left untreated (Supplementary Figure 1C).

Generation of Calibration Curves

VCC requires a set of calibration curves with known amounts of bacteria for absolute quantification of bacterial numbers. In an exemplary analysis a ten-fold dilution series was prepared from logarithmically growing *S. Typhimurium* in lysis buffer starting at 10^7 bacteria per 100 μ l down to 10^{-3} bacteria per 100 μ l. By applying 100 μ l to each well, a complete column of a 96-well plate was used for every dilution step. After addition of 100 μ l 2-fold concentrated brain-heart infusion (BHI) broth, quantitative growth curves were recorded in a temperature-controlled microplate reader (Supplementary Figure 2A). In parallel, aliquots of the 10^2 and 10^3 dilutions were spotted onto LB agar plates for CFU counting. We provide a customized “R” script (“VCC_calibration.R,” Supplementary Data) which

automates the calculation of T_t as described above and correlation of T_t against the logarithm of CFU counts. Growth was detected for seven out of eight wells at a concentration of 10 bacteria/well which can be defined as the detection limit of the method. After excluding the single data point for ~ 1 bacteria per well (10^0 , column 8) from the data set shown in Supplementary Figure 2A, linear regression could be calculated with a coefficient of determination (R^2) of 0.99612 (Supplementary Figure 2B). Furthermore, the script output contains a residuals vs. fitted plot (not shown) and additional graphical representations of T_t and the residual standard error of the non-linear fit (S) in a 96-well plate layout (Supplementary Figure 2C) as well as graphs of the log-logistic fit of each growth curve and a summary in text format (data not shown). Notably, the parameters of the calibration curves will vary depending on the bacterial strain and the incubation conditions (medium, microplate reader, temperature, shaking etc.) used and need to be determined individually. Moreover, for exact calculation of bacterial numbers in cell culture infection models the generation of separate calibration curves in the presence of host cells is required.

Comparative Analysis of *Salmonella* Invasion in HeLa Cells

HeLa cells are widely used as a well-characterized infection model to investigate invasion of *Salmonella* in non-phagocytic cells. *S. enterica* can trigger its own uptake in these cells with the help of effector proteins translocated by the T3SS encoded on SPI-1 (Cain et al., 2008). *Salmonella* invasion of HeLa cells was used to evaluate VCC against CFU counting on solid agar in a direct side-by-side comparison. Besides wild-type (WT) bacteria the invasion-deficient *S. Typhimurium* mutant MvP818, which lacks the T3SS-1 ATPase InvC, was used in this infection model. For the two quantification methods two 96-well plates with HeLa cells were infected in parallel from the same inoculi at a multiplicity of infection (MOI) of 100. Serial dilutions of the inoculi were made in PBS and spotted onto LB agar plates for CFU counting. For VCC the inoculi were diluted 1:10 in lysis buffer, stored at 4°C and warmed to 37°C 10 min before bacterial growth was initiated with the addition of 2x BHI. After a standard gentamicin protection assay, lysis buffer was added to liberate intracellular bacteria from the host cells. In case of VCC, bacterial growth was started by adding 100 μ l of 2x BHI. For CFU counting serial dilutions of the lysed host cell samples were spotted onto LB agar plates. To calculate VCC from T_t we used two different calibration curves generated in the absence (inoculi) or in the presence (intracellular bacteria) of HeLa cells. A customized “R” script is provided (“VCC_invasion.R,” Supplementary Data) where the parameters of both calibrations curves can be entered as variables and which can automate the determination of T_t with subsequent conversion to VCC and calculation of invasion rates (normalized to the respective inoculi). In **Figure 2A** the bacterial numbers in the inoculum and of intracellular bacteria recovered 1 h after infection are depicted. As expected, the mutant MvP818 is highly attenuated for invasion compared to WT using both quantification methods. Although both methods yielded very comparable results in terms of absolute numbers, VCC showed

lower variances for intracellular bacteria. There was an adequate correlation ($R^2 = 0.9821$) of both detection methods in four independent experiments (**Figure 2B**). A Bland-Altman diagram of the same data revealed an almost unbiased ~ 2 -fold variation from the average of both methods (**Figure 2C**). In conclusion, our comparative analysis of HeLa infections showed that VCC and the standard CFU counting produced very similar results.

Infection of Polarized MDCK Cells

For efficient invasion of polarized epithelial cells such as Madin-Darby Canine Kidney (MDCK) cells, the functional cooperation of two *Salmonella* secretion systems is required. The *Salmonella* pathogenicity island 4 (SPI-4) encoded giant adhesin SiiE and cognate type 1 secretion system (T1SS) are needed to mediate efficient binding to the apical cell side. This intimate bacterial contact enables subsequent invasion using the T3SS-1 (Gerlach et al., 2008). MDCK cells were grown as a dense monolayer and hereinafter infected with *S. Typhimurium* WT as well as isogenic mutants deficient for a functional T3SS-1 (MvP818) or a SPI-4 T1SS (WRG238) at an MOI of 25. In WRG238 a chromosomal point mutation within the Walker B box of the ABC protein SiiF (E627Q) renders the T1SS non-functional. While VCC of the inoculi showed equal amounts for all strains, MvP818 and WRG238 were both attenuated for invasion. As expected, lower counts of intracellular bacteria were observed for MvP818 compared to the SPI-4 deficient WRG238 (**Figure 3A**). From these data the invasion rate in percent of the inoculum was calculated for each strain which confirmed our initial observations (**Figure 3B**). Although confluent MDCK cell layers are challenging to lyse our results showed that VCC can be successfully used for bacterial quantification in infection models based on polarized cells.

Quantification of Probiotic Activity

We speculated that VCC could be also useful to analyze co-infection experiments when antibiotic markers are utilized to differentiate between the individual strains. As a proof of principle we chose to quantify probiotic activity. The probiotic *E. coli* strain Nissle 1917 (E_c^{Nissle}) (Grozdanov et al., 2004) was shown to inhibit *Salmonella* invasion of INT407 (Altenhoefer et al., 2004). We wanted to test whether E_c^{Nissle} can exert its protective effect also in combination with polarized MDCK cells. MDCK were pre-incubated for 4 h with different amounts of E_c^{Nissle} corresponding to MOIs of 25 to 500. The numbers of *E. coli* cells used for this incubation step were confirmed by VCC (**Figure 3C**, orange dots). After removing unbound *E. coli*, the MDCK cells were infected with a kanamycin-resistant *S. Typhimurium* at an MOI of 25 as described above. Host cells were lysed and growth of intracellular *S. Typhimurium* was selectively started with addition of 2x BHI containing 50 μ g ml^{-1} kanamycin. We did not observe growth of E_c^{Nissle} under these conditions (data not shown). Compared to untreated controls a significant reduction of intracellular *Salmonella* was evident with E_c^{Nissle} pre-incubation at MOI of 500 (**Figure 3D**). The observed dose-dependent probiotic activity of E_c^{Nissle} demonstrates that VCC can be used to analyze individual bacterial strains of a

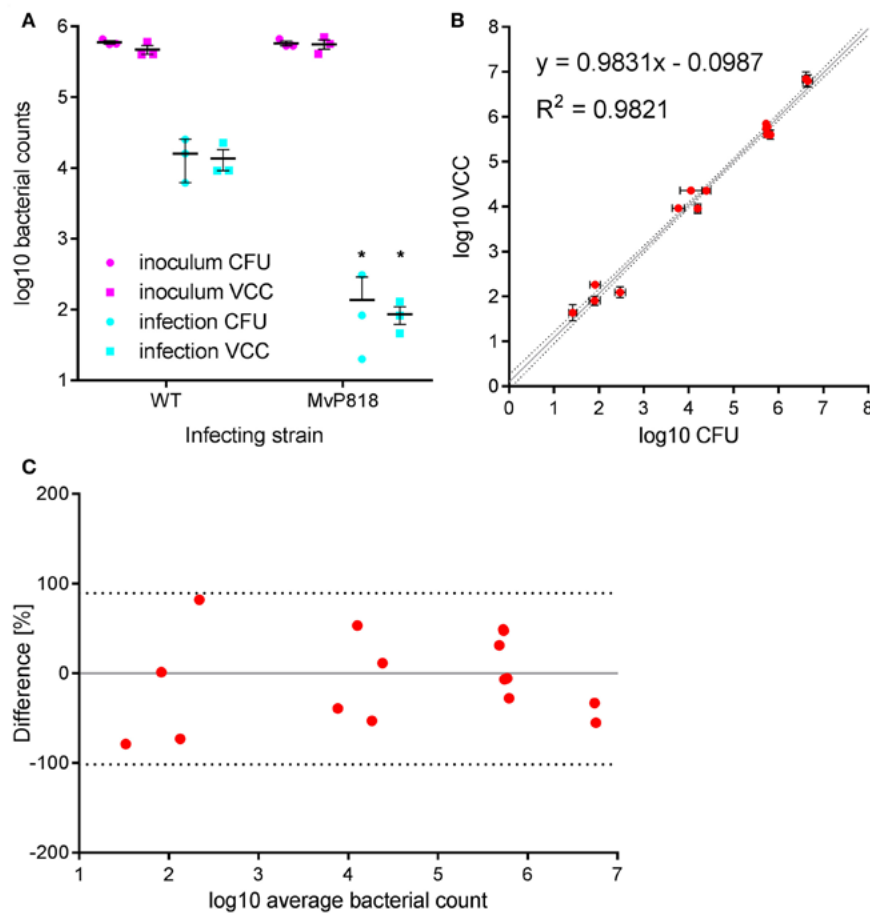


FIGURE 2 | *Salmonella* invasion of HeLa cells was used to evaluate VCC against CFU counting on solid agar in a direct side-by-side comparison. **(A)** Bacterial numbers in the inoculum (magenta) and intracellular bacteria recovered after 1 h of infection (cyan) with wild-type (WT) or a T3SS-1 deficient *Salmonella* strain (MvP818) at an MOI of 100 from three independent experiments done in triplicates including means and SD are depicted. Statistical analysis by Student's *t*-test demonstrates that mutant MvP818 is highly attenuated compared to WT using both enumeration methods. **P* < 0.05 **(B)** Samples from four independent experiments enumerated with both methods are shown with SD indicated separately for VCC and CFU counting. The coefficient of determination (R^2) is given for the correlation of both methods. Dotted black lines indicate the 95% confidence interval of the linear regression (gray line). **(C)** The data shown in **(B)** were plotted in a Bland-Altman diagram. Here, the mean of the corresponding bacterial counts determined with both methods was used as reference (0, gray line). The red dots represent the relative difference of the CFU counts compared to VCC by calculating $100 \cdot (\text{CFU} - \text{VCC}) / \text{average}$. The 95% limits of agreement (dashed black lines) are at -101.6 and 89.4%, respectively.

mixed population utilizing differences in antibiotic resistance phenotypes.

Intracellular Replication in Macrophages

Intracellular survival and replication are key virulence capabilities of *S. Typhimurium* which can be assessed *in vitro* using RAW264.7 macrophages (Govoni et al., 1999). RAW264.7 cells were infected with *S. Typhimurium* WT and the isogenic mutant strain WRG226 which harbors a non-functional T3SS-2 as a negative control. Effectors of the T3SS-2 are essential for intracellular survival and replication of *Salmonella* (Hensel et al., 1998; Figueira and Holden, 2012). Two 96-well plates were infected in parallel with both strains using the MOIs as indicated in **Figure 4**. Bacteria in the inoculum and intracellular bacteria after 2 h of infection were determined by VCC using

the first plate. The second plate was used for quantification of intracellular bacteria after 24 h of infection (**Figure 4A**). As intended, an increasing amount of bacteria in the inoculum could be detected with the increase in MOI. After 2 h the amount of intracellular bacteria increased with the MOI for WRG226 whereas uptake of WT bacteria reached a plateau with MOI of 15. After 24 h of infection, an increase of intracellular bacteria could be observed in case of WT where the maximum total amount was reached with an MOI of 5. In contrast, the T3SS-2 deficient strain WRG226 showed no increase in intracellular bacteria after 24 h (**Figure 4A**). By normalizing the 24 h time points with the 2 h values, the replication capability of the strains could be evaluated. WT bacteria exhibited a ~35-fold replication at a MOI of 1 which decreased to ~3-fold at a MOI of 25 (**Figure 4B**). In agreement with the pivotal role of T3SS-2

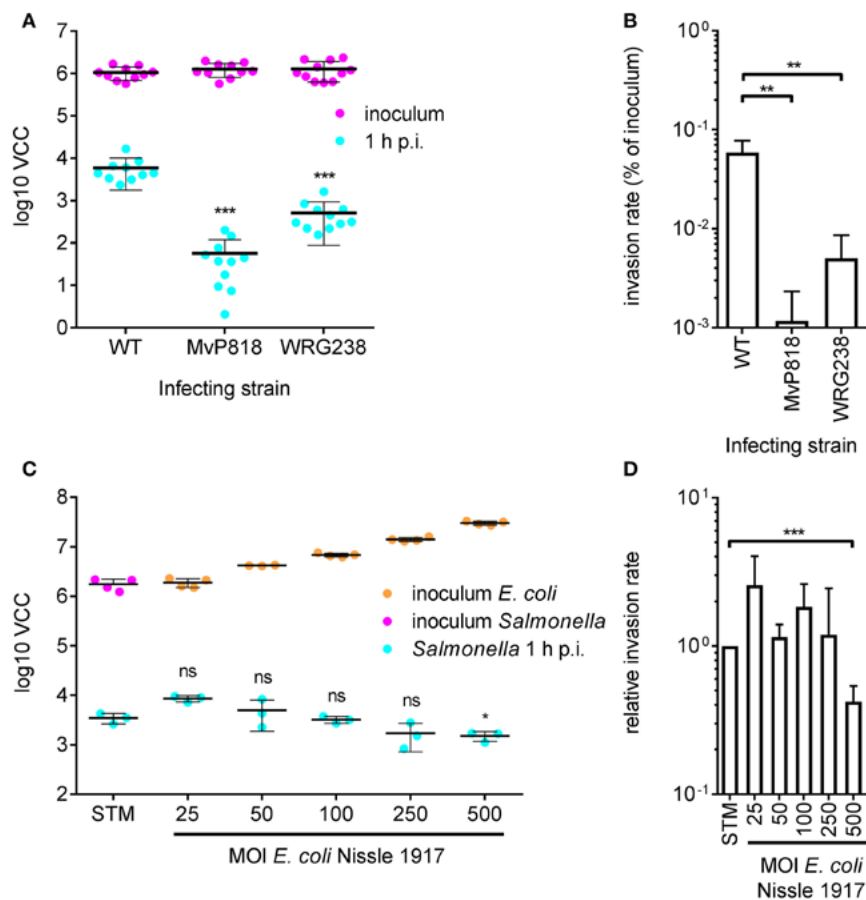


FIGURE 3 | Quantification of invasion of polarized MDCK cells with VCC. **(A)** Bacterial numbers in the inoculum (magenta) and intracellular bacteria recovered from MDCK infected with the indicated *Salmonella* strains at an MOI of 25 1 h post-infection (p.i.) (cyan) from three independent experiments done in 4-fold replicates are depicted. **(B)** From the data shown in **(A)** the invasion rates of the strains were calculated. Both mutants showed a significantly reduced invasiveness compared to the WT. **(C)** Cells were incubated for 4 h before infection using different MOIs of the probiotic *E. coli* strain Nissle 1917 (*Ec*^{Nissle}) as indicated. The amounts of *Ec*^{Nissle} cells were determined for each MOI using VCC (orange dots). MDCK were subsequently infected with a kanamycin resistant *S. Typhimurium* WT strain (STM) at an MOI of 25 (magenta) as described in **(A)**. Intracellular *Salmonella* (cyan) were significantly reduced when cells were pre-incubated with *Ec*^{Nissle} at an MOI of 500. Means and standard deviations from one representative out of three similar experiments done in 4-fold replicates (dots) are depicted. **(D)** The relative invasion rates of STM depending on the MOI of *Ec*^{Nissle}, normalized to controls without *Ec*^{Nissle} (STM), were calculated from data of three independent biological replicates. Statistical analysis by Student's *t*-test was done by comparing to WT or individual strains as depicted: ****P* < 0.001 ***P* < 0.01; **P* < 0.05.

for intracellular replication in macrophages (Hensel et al., 1998), WRG226 showed no net increase of bacterial cells after 24 h (Figure 4B).

DISCUSSION

We could establish VCC as a robust method for bacterial enumeration in three different cell culture infection models using the bacterial pathogen *S. Typhimurium*. A hallmark of *Salmonella* virulence is its ability for trigger-like invasion of non-phagocytic cells through T3SS-1 activity. Although T3SS-1 independent, zipper-like invasion mechanisms are described for *S. enterica* (Rosselin et al., 2011), its pivotal role is exemplified by highly reduced numbers of intracellular bacteria *in vitro*

with non-functional T3SS-1 (Finlay et al., 1988; Galán and Curtiss, 1989). We reproduced this expected phenotype in HeLa and MDCK cells using VCC where a T3SS-1 deficient strain showed ~100-fold reduced invasion rates compared to WT controls. Efficient adhesion of *S. Typhimurium* to MDCK and other polarized cells is mediated by the SPI-4 encoded giant adhesin SiiE (Gerlach et al., 2007). As a consequence, invasion through T3SS-1 in these host cells is highly attenuated for SPI-4 deficient strains (Gerlach et al., 2008). In this regard our VCC data showed ~30-fold less SPI-4 negative bacteria compared to WT controls. A functional T3SS-2, however, is required to establish a replicative niche for intracellular *Salmonella* (Hensel et al., 1998; Fàbrega and Vila, 2013). Its crucial role was reproduced with VCC in RAW264.7 macrophage-like cells where the T3SS-2 mutant showed almost no net replication after 24 h

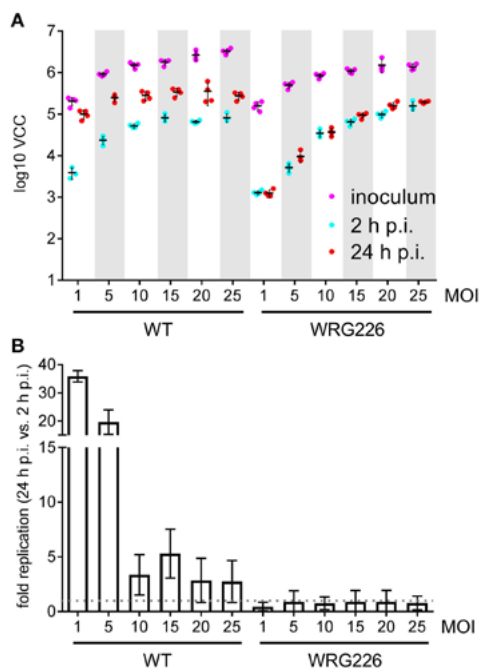


FIGURE 4 | Replication of *Salmonella* within RAW264.7 macrophages. **(A)** Two 96-well plates with RAW 264.7 macrophages were infected in parallel with the strains and MOIs as indicated. In the first plate, bacteria in the inoculum (magenta) and intracellular bacteria after 2 h post-infection (p.i.) (cyan) were determined by VCC. The second plate was used for enumeration of intracellular bacteria after 24 h of infection (red). Means and standard deviations from one representative out of three similar experiments done in 4-fold replicates (dots) are depicted. **(B)** From the data of three independent biological replicates the fold replication of the strains were calculated. The maximum capacity of intracellular WT bacteria to replicate is reached after 24 h with an MOI of 1. The T3SS-2 deficient strain WRG226 showed no net replication (dashed gray line).

of infection. These results are in good agreement with data from J774.1 macrophages using CFU counting (Hensel et al., 1998). Interestingly, the maximum uptake of WT bacteria was reached after 2 h at an MOI of 15. After 24 h the maximal number of intracellular bacteria was already reached with an MOI of 5. These results likely illustrate the limits of RAW264.7 cells in their capacity to take up and to support growth of intracellular bacteria under these experimental conditions.

In a further approach we tested the suitability of VCC to analyze co-infection experiments with an antibiotic marker to differentiate between probiotic *Ec*^{Nissle} and *Salmonella*. Supplementation of the growth medium with kanamycin allowed for selective growth of *S. Typhimurium* while no replication of *Ec*^{Nissle} was observed. Although only one bacterial strain can be quantified by VCC from one well, analysis of several replicate wells with the addition of strain-specific antibiotics would allow for high throughput competitive index assays (Segura et al., 2004).

Label free detection methods, such as thermography (Salaimeh et al., 2011) rely solely on bacterial growth. Here, the

logarithmic signal amplification enables high sensitivity together with a huge detection range. In case of VCC we could quantify bacteria over six orders of magnitude with a detection limit of about 10 *S. Typhimurium* cells per well. In a direct comparison between CFU counting and VCC, bacterial numbers were within a 2-fold difference from the mean of both methods. Although this is a good correlation, it is known that quantification via CFU on agar plates has a certain inaccuracy (Naghili et al., 2013). In that light it is not optimal that VCC calibration curves are correlated to actual “colony counts” using CFU counting.

With optimized protocols classical CFU counting can be scaled up to medium-high throughput by doing serial dilutions in 96-well plates and multichannel pipetting on solid agar (Steele-Mortimer, 2008). With VCC similar or higher throughput is possible with the advantage that no dilution steps are required and data collection and analysis can be easily automated requiring only absorbance detection equipment and a freely available open source software. Given the benefits of VCC over CFU counting also some limitations of the technique should be considered. First, on agar plates differences in growth rates have an impact on colony size, but not on actual counts. However, the same differences very strongly affect the duration of the lag phase thereby leading to incorrect VCCs. Mutations or environmental changes (e.g., from intracellular to extracellular) might result in altered growth rates of bacteria. Based on these observations it is of utmost importance, that growth rates of test strains are comparable to those used in calibration curves. If this cannot be guaranteed separate calibration curves need to be recorded for the strains in question. Second, alterations in bacterial physiology with impact on absorbance measurements (e.g., apparent or real cell size, light scattering or biofilm formation) will interfere with VCC. These problems might not be easy to address but optimizations should include review of growth conditions (e.g., shaking speed, plate material) and careful correlation of T_t to log(CFU) in calibration curves.

The reliable, reproducible and batch-processing compatible calculation of T_t from raw absorbance data had to be established before VCC could be applied in infection models. This was especially challenging because initially incomplete lysis of host cells followed by the occurrence of debris results in relatively noisy raw data. Improved host cell lysis and homogenization might be achieved with alternative well geometries (Funke et al., 2009). However, to our knowledge no cell culture treated microtiter plates with other than round wells are available. As a solution we established a workflow based on a curve fit to the log-logistic distribution which is a robust and proven model of microbial growth (Zwietering et al., 1990) and enables largely automatic calculation of T_t from raw absorbance data using our customized “R” script.

In conclusion, VCC is a label-free, automation-compatible methodology suitable for enumeration of intracellular bacteria in *in vitro* infection models. This approach should be also coextensive with studying other types of bacterial-cell interactions such as adhesion. VCC is flexible and can be adapted to be used together with bacteria other than *Salmonella* and any type of temperature-controlled, shaking microplate reader after a few optimizations. With its high reproducibility and

throughput, the method is especially qualified to foster the further characterization of the host-pathogen interface.

AUTHOR CONTRIBUTIONS

SH, SW, CS, and AS performed experiments. SH, RG, A-KB, and SF analyzed the data. RG conceived the study and wrote the paper.

FUNDING

SH and SW were supported by grants GE 2533/2-2 and GE 2533/1-1 of the Deutsche Forschungsgemeinschaft (DFG),

REFERENCES

- Acord, J., Maskell, J., and Sefton, A. (2005). A rapid microplate method for quantifying inhibition of bacterial adhesion to eukaryotic cells. *J. Microbiol. Methods* 60, 55–62. doi: 10.1016/j.mimet.2004.08.011
- Altenhofer, A., Oswald, S., Sonnenborn, U., Enders, C., Schulze, J., Hacker, J., et al. (2004). The probiotic *Escherichia coli* strain Nissle 1917 interferes with invasion of human intestinal epithelial cells by different enteroinvasive bacterial pathogens. *FEMS Immunol. Med. Microbiol.* 40, 223–229. doi: 10.1016/S0928-8244(03)00368-7
- Brewster, J. D. (2003). A simple micro-growth assay for enumerating bacteria. *J. Microbiol. Methods* 53, 77–86. doi: 10.1016/S0167-7012(02)00226-9
- Cain, R. J., Hayward, R. D., and Koronakis, V. (2008). Deciphering interplay between *Salmonella* invasion effectors. *PLoS Pathog.* 4:e1000037. doi: 10.1371/journal.ppat.1000037
- Devenish, J. A., and Schiemann, D. A. (1981). HeLa cell infection by *Yersinia enterocolitica*: evidence for lack of intracellular multiplication and development of a new procedure for quantitative expression of infectivity. *Infect. Immun.* 32, 48–55.
- Ericksen, B., Wu, Z., Lu, W., and Lehrer, R. I. (2005). Antibacterial activity and specificity of the six human α -defensins. *Antimicrob. Agents Chemother.* 49, 269–275. doi: 10.1128/AAC.49.1.269-275.2005
- Fàbrega, A., and Vila, J. (2013). *Salmonella enterica* serovar Typhimurium skills to succeed in the host: virulence and regulation. *Clin. Microbiol. Rev.* 26, 308–341. doi: 10.1128/CMR.00066-12
- Figueira, R., and Holden, D. W. (2012). Functions of the *Salmonella* pathogenicity island 2 (SPI-2) type III secretion system effectors. *Microbiology* 158(Pt 5), 1147–1161. doi: 10.1099/mic.0.058115-0
- Finlay, B. B., Starnbach, M. N., Francis, C. L., Stocker, B. A., Chatfield, S., Dougan, G., et al. (1988). Identification and characterization of TnphoA mutants of *Salmonella* that are unable to pass through a polarized MDCK epithelial cell monolayer. *Mol. Microbiol.* 2, 757–766. doi: 10.1111/j.1365-2958.1988.tb00087.x
- Funke, M., Diederichs, S., Kensy, F., Müller, C., and Büchs, J. (2009). The baffled microtiter plate: increased oxygen transfer and improved online monitoring in small scale fermentations. *Biotechnol. Bioeng.* 103, 1118–1128. doi: 10.1002/bit.22341
- Galán, J. E., and Curtiss, R. III. (1989). Cloning and molecular characterization of genes whose products allow *Salmonella typhimurium* to penetrate tissue culture cells. *Proc. Natl. Acad. Sci. U.S.A.* 86, 6383–6387. doi: 10.1073/pnas.86.16.6383
- Gerlach, R. G., Cláudio, N., Rohde, M., Jäckel, D., Wagner, C., and Hensel, M. (2008). Cooperation of *Salmonella* pathogenicity islands 1 and 4 is required to breach epithelial barriers. *Cell. Microbiol.* 10, 2364–2376. doi: 10.1111/j.1462-5822.2008.01218.x
- Gerlach, R. G., and Hensel, M. (2007a). Protein secretion systems and adhesins: the molecular armory of Gram-negative pathogens. *Int. J. Med. Microbiol.* 297, 401–415. doi: 10.1016/j.ijmm.2007.03.017
- Gerlach, R. G., and Hensel, M. (2007b). *Salmonella* pathogenicity islands in host specificity, host pathogen-interactions and antibiotics resistance respectively. Work of Project Group 5 is supported by the Robert Koch Institute.

ACKNOWLEDGMENTS

We thank Bärbel Stecher, Max von Pettenkofer-Institute, Munich for providing the *E. coli* strain Nissle 1917.

SUPPLEMENTARY MATERIAL

The Supplementary Material for this article can be found online at: <https://www.frontiersin.org/articles/10.3389/fcimb.2018.00043/full#supplementary-material>

- of *Salmonella enterica*. *Berl. Munch. Tierarztl. Wochenschr.* 120, 317–327. doi: 10.2376/0005-9366-120-317
- Gerlach, R. G., Jäckel, D., Stecher, B., Wagner, C., Lupas, A., Hardt, W. D., et al. (2007). *Salmonella* Pathogenicity Island 4 encodes a giant non-fimbrial adhesin and the cognate type 1 secretion system. *Cell. Microbiol.* 9, 1834–1850. doi: 10.1111/j.1462-5822.2007.00919.x
- Govoni, G., Canonne-Hergaux, F., Pfeifer, C. G., Marcus, S. L., Mills, S. D., Hackam, D. J., et al. (1999). Functional expression of Nramp1 *in vitro* in the murine macrophage line RAW264.7. *Infect. Immun.* 67, 2225–2232. doi: 10.1128/JB.186.16.5432-5441.2004
- Grozdanov, L., Raasch, C., Schulze, J., Sonnenborn, U., Gottschalk, G., Hacker, J., et al. (2004). Analysis of the genome structure of the nonpathogenic probiotic *Escherichia coli* strain Nissle 1917. *J. Bacteriol.* 186, 5432–5441. doi: 10.1128/JB.186.16.5432-5441.2004
- Hensel, M., Shea, J. E., Waterman, S. R., Mundy, R., Nikolaus, T., Banks, G., et al. (1998). Genes encoding putative effector proteins of the type III secretion system of *Salmonella* pathogenicity island 2 are required for bacterial virulence and proliferation in macrophages. *Mol. Microbiol.* 30, 163–174. doi: 10.1046/j.1365-2958.1998.01047.x
- Martens-Habbena, W., and Sass, H. (2006). Sensitive determination of microbial growth by nucleic acid staining in aqueous suspension. *Appl. Environ. Microbiol.* 72, 87–95. doi: 10.1128/AEM.72.1.87-95.2006
- Naghili, H., Tajik, H., Mardani, K., Razavi Rouhani, S. M., Ehsani, A., and Zare, P. (2013). Validation of drop plate technique for bacterial enumeration by parametric and nonparametric tests. *Vet Res Forum* 4, 179–183.
- Pazgier, M., Ericksen, B., Ling, M., Toth, E., Shi, J., Li, X., et al. (2013). Structural and functional analysis of the pro-domain of human cathelicidin, LL-37. *Biochemistry* 52, 1547–1558. doi: 10.1021/bi301008r
- R Core Team (2017). *R: A Language and Environment for Statistical Computing*. Vienna: R Foundation for Statistical Computing. Available online at: <https://www.R-project.org/>
- Rajabi, M., Ericksen, B., Wu, X., de Leeuw, E., Zhao, L., Pazgier, M., et al. (2012). Functional determinants of human enteric α -defensin HD5: crucial role for hydrophobicity at dimer interface. *J. Biol. Chem.* 287, 21615–21627. doi: 10.1074/jbc.M112.367995
- Ritz, C., Baty, F., Streibig, J. C., and Gerhard, D. (2015). Dose-response analysis using R. *PLoS ONE* 10:e0146021. doi: 10.1371/journal.pone.0146021
- Rödiger, S., Burdukiewicz, M., and Schierack, P. (2015). chipPCR: an R package to pre-process raw data of amplification curves. *Bioinformatics* 31, 2900–2902. doi: 10.1093/bioinformatics/btv205
- Rosselin, M., Abed, N., Virlogeux-Payant, I., Bottreau, E., Sizaret, P. Y., Velge, P., et al. (2011). Heterogeneity of type III secretion system (T3SS)-1-independent entry mechanisms used by *Salmonella* Enteritidis to invade different cell types. *Microbiology* 157(Pt 3), 839–847. doi: 10.1099/mic.0.044941-0
- Salaimeh, A. A., Champion, J. J., Gharaibeh, B. Y., Evans, M. E., and Saito, K. (2011). Real-time quantification of viable bacteria in liquid medium using infrared thermography. *Infrared Phys. Technol.* 54, 517–524. doi: 10.1016/j.infrared.2011.08.004
- Segura, I., Casadesús, J., and Ramos-Morales, F. (2004). Use of mixed infections to study cell invasion and intracellular proliferation of *Salmonella*

- enterica* in eukaryotic cell cultures. *J. Microbiol. Methods* 56, 83–91. doi: 10.1016/j.mimet.2003.09.004
- Small, P. L., Isberg, R. R., and Falkow, S. (1987). Comparison of the ability of enteroinvasive *Escherichia coli*, *Salmonella typhimurium*, *Yersinia pseudotuberculosis*, and *Yersinia enterocolitica* to enter and replicate within HEp-2 cells. *Infect. Immun.* 55, 1674–1679.
- Steele-Mortimer, O. (2008). "Infection of epithelial cells with *Salmonella enterica*," in *Bacterial Pathogenesis. Methods in Molecular Biology, Vol. 431*, eds F. R. DeLeo and M. Otto (Totowa, NJ: Humana Press), 201–211. doi: 10.1007/978-1-60327-032-8_16
- Vesterlund, S., Paltta, J., Karp, M., and Ouwehand, A. C. (2005). Measurement of bacterial adhesion-*in vitro* evaluation of different methods. *J. Microbiol. Methods* 60, 225–233. doi: 10.1016/j.mimet.2004.09.013
- Wickham, H. (2016). *ggplot2: Elegant Graphics for Data Analysis*. New York, NY: Springer.
- Xie, C., Prah, A., Ericksen, B., Wu, Z., Zeng, P., Li, X., et al. (2005). Reconstruction of the conserved β -bulge in mammalian defensins using D-amino acids. *J. Biol. Chem.* 280, 32921–32929. doi: 10.1074/jbc.M503084200
- Zhao, L., Ericksen, B., Wu, X., Zhan, C., Yuan, W., Li, X., et al. (2012). Invariant gly residue is important for α -defensin folding, dimerization, and function: a case study of the human neutrophil α -defensin HNP1. *J. Biol. Chem.* 287, 18900–18912. doi: 10.1074/jbc.M112.355255
- Zhao, L., Tolbert, W. D., Ericksen, B., Zhan, C., Wu, X., Yuan, W., et al. (2013). Single, double and quadruple alanine substitutions at oligomeric interfaces identify hydrophobicity as the key determinant of human neutrophil alpha defensin HNP1 function. *PLoS ONE* 8:e78937. doi: 10.1371/journal.pone.0078937
- Zou, G., de Leeuw, E., Lubkowski, J., and Lu, W. (2008). Molecular determinants for the interaction of human neutrophil α defensin 1 with its propeptide. *J. Mol. Biol.* 381, 1281–1291. doi: 10.1016/j.jmb.2008.06.066
- Zwietering, M. H., Jongenburger, I., Rombouts, F. M., and van 't Riet, K. (1990). Modeling of the bacterial growth curve. *Appl. Environ. Microbiol.* 56, 1875–1881.

Conflict of Interest Statement: The authors declare that the research was conducted in the absence of any commercial or financial relationships that could be construed as a potential conflict of interest.

Copyright © 2018 Hoffmann, Walter, Blume, Fuchs, Schmidt, Scholz and Gerlach. This is an open-access article distributed under the terms of the Creative Commons Attribution License (CC BY). The use, distribution or reproduction in other forums is permitted, provided the original author(s) and the copyright owner are credited and that the original publication in this journal is cited, in accordance with accepted academic practice. No use, distribution or reproduction is permitted which does not comply with these terms.

Supplementary Material

High-throughput quantification of bacterial-cell interactions using virtual colony counts

Stefanie Hoffmann[†], Steffi Walter[†], Anne-Kathrin Blume, Stephan Fuchs, Christiane Schmidt, Annemarie Scholz and Roman G. Gerlach^{*}

^{*} Correspondence: Corresponding Author: GerlachR@rki.de
[†] These authors have contributed equally to this work.

1 Supplementary Data

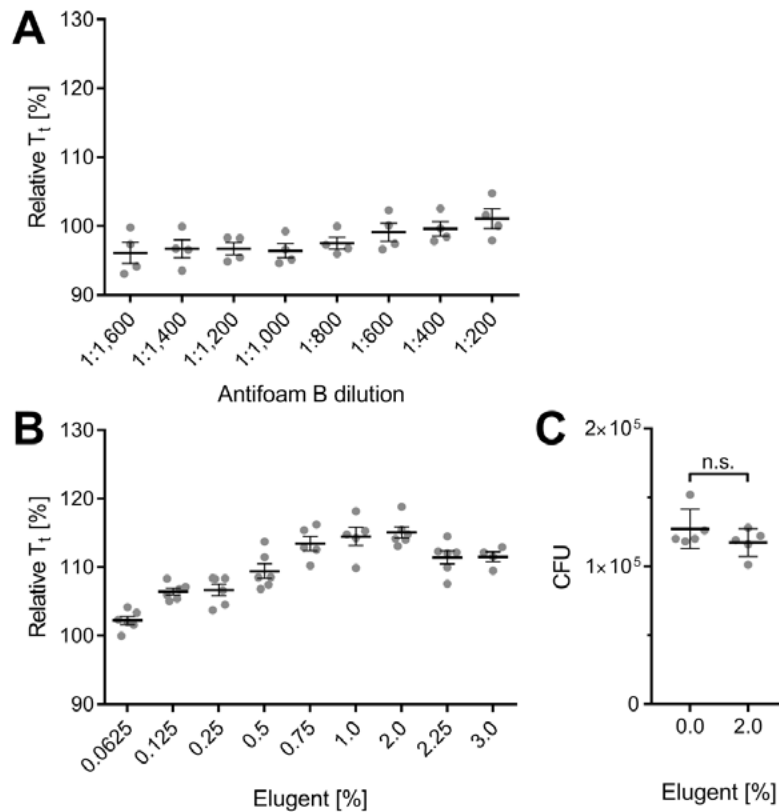
Two 'R' scripts are provided as supplementary data:

'VCC_calibration.R' – allows for correlation to log (CFU) on the basis of calibration curves, corresponding example data set: 'example_calibration_curves.xlsx'

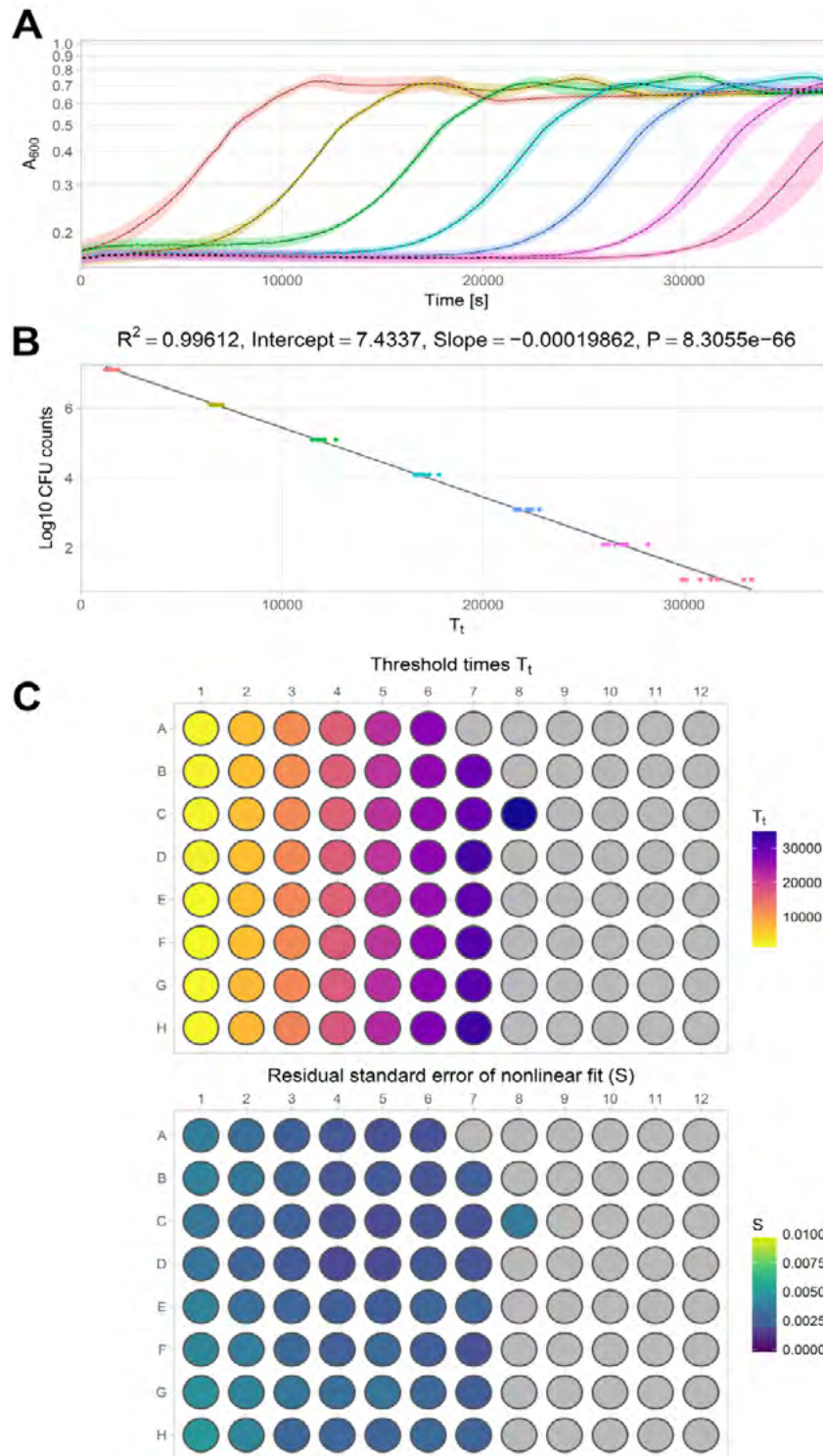
'VCC_invasion.R' – allows for calculation of VCC and invasion rates, corresponding example data set: 'example_invasion.txt'

2 Supplementary Figures and Tables

2.1 Supplementary Figures



Supplementary Figure 1. The impact of different concentrations of Antifoam B and the detergent Elugent on the time to reach the threshold (T_1). (A) Equal numbers of bacteria were added to BHI medium containing 0.5x PBS and the indicated dilutions of Antifoam B. Growth curves were fit using a 5-parameter log-logistic function in 'R'. T_1 was calculated and subsequently normalized to controls without Antifoam B (=100%). No significant influence on bacterial growth was observed for 1:200 or higher dilutions. (B) Using the same experimental setup as described in (A), relative T_1 were determined for growth in medium containing different amounts of Elugent as indicated. To prevent foaming Antifoam B was added at a concentration of 0.0625% (1:1,600) to all samples. A slight attenuation in bacterial growth was observed for concentrations of 0.125% (v/v) Elugent and above. (C) An equal number ($\sim 1.2 \times 10^5$) of bacteria was incubated with 2% (v/v) Elugent or left untreated. Subsequent CFU counting revealed no significant detrimental effect of Elugent on CFU counts.



Supplementary Figure 2. Calibration curve to correlate the time to reach the threshold of $\Delta A_{600} = 0.02$ (T_t) to $\log(\text{CFU})$. In (A), mean (black lines) and SD (shaded areas) of growth curves of a dilution series of 10^7 to 10^1 CFU well^{-1} *S. Typhimurium* in lysis buffer/BHI done in 8-fold replicates are shown. (B) Parallel determination of colony-forming units (CFU) on agar plates allowed for correlation with threshold times (T_t , dots) which were calculated as described in the text from the data shown in (a). The coefficient of determination (R^2) and the 95 % confidence interval (grey area) is given for the linear regression (black line). (C) Schematic 96-well plate layout of the threshold times T_t (upper panel) and the residual standard errors of the nonlinear fit S (lower panel) calculated for each individual growth curve of the data set shown in (A).

III.2. Structural and functional characterization of SiiA, an auxiliary protein from the SPI-4-encoded type I secretion system from *Salmonella enterica*

Peter Kirchweger¹, Sigrid Weiler¹, Claudia Egerer-Sieber¹, Anna-Theresa Blasl¹, Stefanie Hoffmann², Christiane Schmidt², Nathalie Sander³, Dorothee Merker³, Roman G. Gerlach², Michael Hensel³ and Yves A. Muller¹

¹ Division of Biotechnology, Department of Biology, Friedrich-Alexander-University Erlangen-Nürnberg, Henkestr. 91, D-91052, Erlangen, Germany

² Robert Koch-Institut, Wernigerode, Germany

³ Abt. Mikrobiologie and CellNanOs, Universität Osnabrück, Osnabrück, Germany

Structural and functional characterization of SiiA, an auxiliary protein from the SPI4-encoded type 1 secretion system from *Salmonella enterica*

Peter Kirchweger,¹ Sigrid Weiler,¹ Claudia Egerer-Sieber,¹ Anna-Theresa Blasl,¹ Stefanie Hoffmann,² Christiane Schmidt,² Nathalie Sander,³ Dorothee Merker,³ Roman G. Gerlach,² Michael Hensel³ and Yves A. Muller^{1*}

¹Division of Biotechnology, Department of Biology, Friedrich-Alexander-University Erlangen-Nürnberg, Henkestr. 91, D-91052, Erlangen, Germany.

²Robert Koch-Institut, Wernigerode, Germany.

³Abt. Mikrobiologie and CellNanOs, Universität Osnabrück, Osnabrück, Germany.

Summary

Salmonella invasion is mediated by a concerted action of the *Salmonella* pathogenicity island 4 (SPI4)-encoded type one secretion system (T1SS) and the SPI1-encoded type three secretion system (T3SS-1). The SPI4-encoded T1SS consists of five proteins (SiiABCDF) and secretes the giant adhesin SiiE. Here, we investigated structure–function relationships in SiiA, a non-canonical T1SS subunit. We show that SiiA consists of a membrane domain, an intrinsically disordered periplasmic linker region and a folded globular periplasmic domain (SiiA-PD). The crystal structure of SiiA-PD displays homology to that of MotB and other peptidoglycan (PG)-binding domains. SiiA-PD binds PG *in vitro*, albeit at an acidic pH, only. Mutation of Arg162 impedes PG binding of SiiA and reduces *Salmonella* invasion efficacy. SiiA forms a complex with SiiB at the inner membrane (IM), and the observed SiiA-MotB homology is paralleled by a predicted SiiB-MotA homology. We show that, similar to MotAB, SiiAB translocates protons across the IM. Mutating Asp13 in SiiA impairs proton translocation. Overall, SiiA shares numerous properties with MotB. However, MotAB uses the proton motive force (PMF)

to energize the bacterial flagellum, it remains to be shown how usage of the PMF by SiiAB assists T1SS function and *Salmonella* invasion.

Abbreviations: Aa, amino acid; CD, circular dichroism; IM, inner membrane; LR, linker region; MD, membrane domain; OM, outer membrane; PEM, periplasmic region essential for mobility; PG, peptidoglycan; PD, periplasmic domain; PMF, proton motive force; ppr, periplasmic region; rmsd, root mean square deviation; RT, room temperature; SPI, *Salmonella* pathogenicity island; T1SS, type one secretion system; T3SS-1, type three secretion system encoded by SPI1; T_M , melting temperatures; WT, wild-type.

Introduction

Salmonella enterica are facultative anaerobe, Gram-negative, pathogenic bacteria that infect a wide range of hosts (Barlag and Hensel, 2015). Infections of humans by typhoidal and nontyphoidal *S. enterica* serovars are responsible for a pleiotropy of medical conditions including intestinal inflammation and typhoid fever (Crump *et al.*, 2015; Arya *et al.*, 2017). For successful infection of polarized epithelial cells, a concerted action between the *Salmonella* pathogenicity island 4 (SPI4)-encoded type one secretion system (T1SS) and the SPI1-encoded type three secretion system (T3SS-1) is required (Gerlach *et al.*, 2008; Barlag and Hensel, 2015). While the SPI4-T1SS establishes adhesion to the apical side of polarized epithelial cells by action of SiiE (Barlag and Hensel, 2015), the T3SS-1 mediates invasion by translocating various effector molecules (reviewed in LaRock *et al.*, 2015). Lack of SPI4-T1SS mediated adhesion also dramatically attenuates invasion of polarized epithelial cells by *S. enterica* serovar Typhimurium (*S. Typhimurium*) (Gerlach *et al.*, 2008).

We have shown that SPI4 of *S. Typhimurium* harbours the *sii* operon encoding six proteins, namely SiiA to SiiF (SiiABCDEF) (Gerlach *et al.*, 2007). The three proteins SiiCDF form a canonical T1SS, i.e. SiiC corresponds to the outer membrane (OM) pore protein, SiiD to the periplasmic adapter protein and SiiF to the inner membrane

*For correspondence. E-mail yves.muller@fau.de; Tel. +49-9131-8523082; Fax +49-9131-8523080.

(IM) ATP-binding cassette (ABC) protein. T1SSs often secrete only a single protein, and the substrate of the SPI4-encoded T1SS corresponds to the largest protein present in the *Salmonella* proteome, namely the 595 kDa adhesin SiiE (Gerlach *et al.*, 2007; Morgan *et al.*, 2007; Griessl *et al.*, 2013; Peters *et al.*, 2017). In contrast to all previous proteins, the function of the two remaining proteins SiiA and SiiB is currently only poorly understood.

It has been shown that SiiA and SiiB are integral membrane proteins that form a complex within the IM (Wille *et al.*, 2014). Detailed experimental data highlighted that the transmembrane regions of the SiiAB complex share similarities in sequence and in the topological arrangement of the membrane-spanning segments with a number of heteromeric ion-conducting channels, such as the MotAB, PomAB, ExbBD and TolQR complexes (Wille *et al.*, 2014). A critical aspartate residue (Asp13) in SiiA has been proposed to be located at a position homologous to Asp33 in MotB (from *S. enterica*), Asp24 in PomB (from *Vibrio alginolyticus*), Asp25 in ExbD and Asp23 in TolR (both from *Escherichia coli*) (Braun *et al.*, 1996; Zhou *et al.*, 1998; Cascales *et al.*, 2001; Zhu *et al.*, 2014; Wille *et al.*, 2014). ExbBD together with TonB transduce energy from the proton motive force (PMF) of the IM to high-affinity OM ion transporters (Ollis *et al.*, 2009). MotAB, PomAB and TolQR are involved in coupling the PMF to specific protein actions at the IM. Thus, MotA and MotB (or likewise PomA and PomB) form a heteromeric complex with a 4 to 2 stoichiometry at the IM and participate in the torque generation of the flagellum of Gram-negative bacteria (Zhu *et al.*, 2014; Minamino and Imada, 2015). Once activated by interaction with the C-ring of the flagellum, the complex fixes the flagellum in the membrane through the interaction of the MotB or PomB peptidoglycan (PG)-binding domain with the PG layer (Minamino and Imada, 2015). Torque is generated by translocating either H⁺ or Na⁺ across the IM, and the above-mentioned aspartate residues are predicted to be directly implicated in the translocation mechanism (Zhou *et al.*, 1998; Wille *et al.*, 2014). The exact function of TolR is currently less well understood; overall, the Tol-Pal system plays a role in assuring the integrity of the OM (Wojdyla *et al.*, 2015).

The SiiA structure possibly matches the protein architecture of MotB, PomB and TolR. In the 309 residue-long MotB from *S. Typhimurium* this architecture consists of a transmembrane helix (aa 29-50), a plug helix (aa 53-66), and a C-terminal segment named 'periplasmic region essential for mobility' (PEM, aa 111-270) that also contains an OmpA-like PG-binding domain (aa 149-269) (De Mot and Vanderleyden, 1994; Hosking *et al.*, 2006; Kojima *et al.*, 2009; Minamino *et al.*, 2018). The PG-binding domain enables interaction with the PG layer in Gram-negative bacteria. This layer consists of a mesh-like structure made up of

glycan strands interconnected by short peptides. The glycan strands are built from multiple molecules of N-acetylglucosamine and N-acetylmuramic acid carbohydrate molecules linked by β -1,4 glycosidic bonds. The peptide stem is a pentapeptide made up of L-Ala-D-*iso*-Glu-*meso*-A₂pm-D-Ala-D-Ala, with *iso*-Glu being the γ -bonded Glu and *meso*-A₂pm is the *meso*-2,6-diaminopimelic acid (Vollmer, 2015).

OmpA-like PG-binding domains occur in many proteins. They harbour a PG-binding sequence motif, i.e. TD-X₁₀-LS-X₂-RA-X₂-V-X₃-L, that is highly conserved in proteins from Gram-negative bacteria involved in PG binding, such as OmpA, MotB, PomB and PALs (PG-associated lipoproteins) (De Mot and Vanderleyden, 1994). Atomic insight into the structures of the OmpA-like PG-binding domain is available from many proteins; insight into the details of the interaction between PG-binding domains and PG fragments is however scarce. Positive exceptions are the crystal structure of the PG-binding domain of OmpA from *Acinetobacter baumannii* in complex with *meso*-A₂pm-containing PG-derived pentapeptide as well as the NMR structure of the PG-binding domain of Pal from *Haemophilus influenza* in complex with a PG precursor (Parsons *et al.*, 2006; Park *et al.*, 2012). Although the individual functions of proteins containing PG-binding domains are as diverse as forming OM pores, involved in antibiotic and small molecules export (OmpA), or generating torque for propelling the flagellum (MotB and PomB), they all share a common domain core fold with a β 1/ α 1/ β 2/ α 2/ β 3/ β 4 secondary structure topology (Roujeinikova, 2008; Kojima *et al.*, 2009).

Here, we analysed the structure and function of SiiA from *S. Typhimurium*. The recombinantly produced periplasmic region of SiiA (ppr-SiiA, aa 40-210) was studied using structure predictions, limited proteolysis, mass spectrometry and circular dichroism (CD). The crystal structure revealed that SiiA shares structural homology with other OmpA-like PG-binding domains, among them MotB. With the help of *in vivo* and *in vitro* PG-binding studies, we observed a pH-dependent binding of SiiA to PG and unravelled a link between PG binding and *Salmonella* invasion efficacy. We also showed that the IM-located SiiAB complex pumps indeed protons across the membrane similar to what has been observed for MotAB and other members of the family of heteromeric ion-conducting channels, which use the PMF to generate work.

Results

Domain architecture of SiiA

Weak sequence homologies were detected between the transmembrane regions of the SiiAB proteins and MotAB, ExbBD and TolQR, and additional experimental

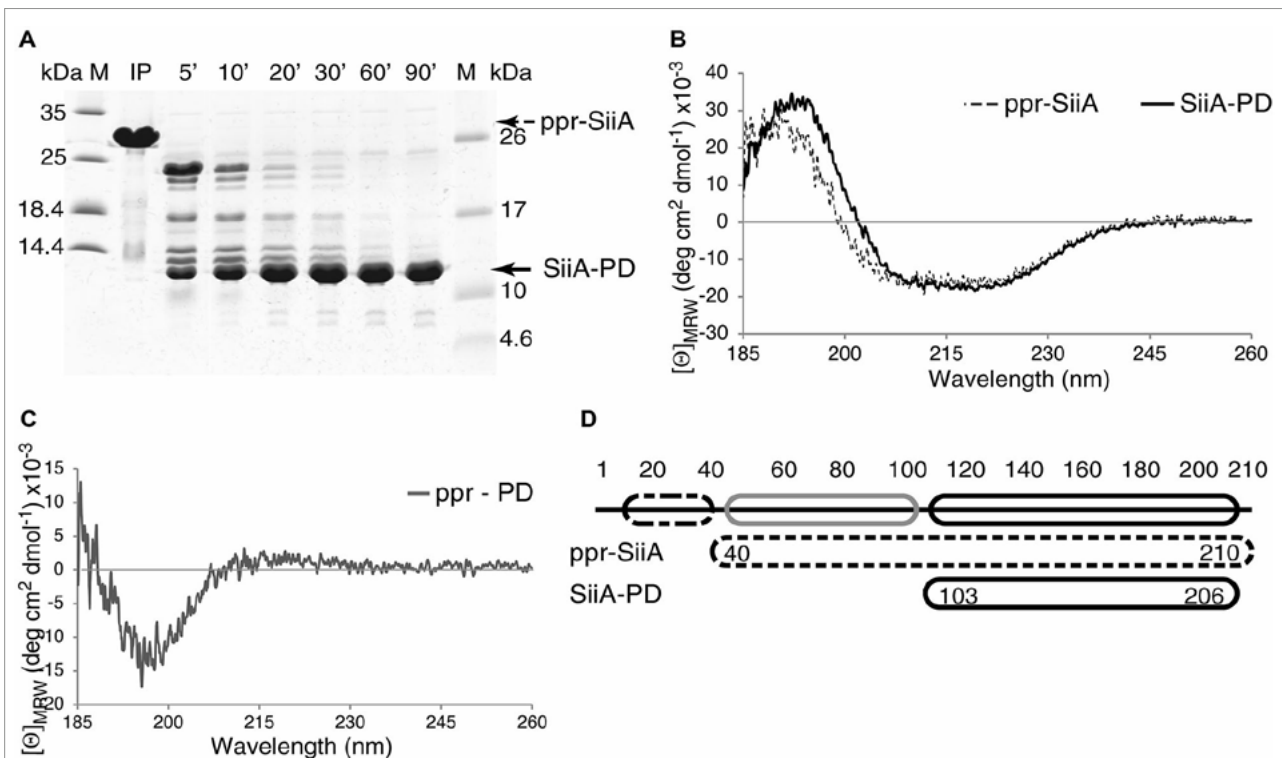


Fig. 1. Domain structure of SiiA.

A. Limited proteolysis of ppr-SiiA (about 26 kDa) with the unspecific protease thermolysin monitored by SDS-PAGE. Limited proteolysis yields SiiA-PD (about 12 kDa), the folded C-terminal domain of SiiA.

B. CD spectrum of ppr-SiiA (after removal of the HisTag with thrombin) and of SiiA-PD recorded at pH 7.4.

C. CD difference spectrum calculated by subtracting the spectrum of SiiA-PD from the spectrum of ppr-SiiA.

D. Schematic representation of the domain structure of SiiA, consisting of a predicted transmembrane region, an intrinsically unstructured region and a folded periplasmic domain (SiiA-PD). The existence of the latter two has been corroborated by the experimental data presented here. In (A), (B) and (D) ppr-SiiA data are displayed/marked with dashed lines and SiiA-PD with black continuous lines; in (D) the intrinsically disordered region is indicated with a grey box.

data confirmed that SiiAB are integral membrane proteins (Wille *et al.*, 2014). However, no sequence homologies were initially observed for the remaining regions of SiiA and SiiB. Therefore, the sequence of SiiA was analysed with the program XtalPred in order to gain more detailed insight into the entire domain organization of 210 residue-long SiiA, (Slabinski *et al.*, 2007). This bioinformatics analysis underlines that SiiA consists of a transmembrane (TM) helix (residues 14-38) and suggests the additional presence of a disordered and unfolded linker (aa 51-92) and a C-terminal globular domain that extends from residues 93 to 210.

Ppr-SiiA was purified from *E. coli* in order to experimentally validate the predicted domain architecture. When subjecting purified ppr-SiiA to a limited proteolysis experiment with the unspecific protease thermolysin then a single stable fragment of about 12 kDa is readily formed (Fig. 1A). Such a behaviour is commonly observed for proteins that consist of a folded globular domain from which disordered segments extend. Access of these segments by

proteases is facilitated; hence, these segments are especially prone to proteolytic degradation (see for example (Heilingloh *et al.*, 2017)). We named the protease-resistant 12 kDa fragment: SiiA periplasmic domain (SiiA-PD). Its composition was analysed by mass spectrometry, and analysis of peptides obtained through tryptic digestion reveals multiple sequence coverage for SiiA residues 104 to 206 (Fig. S1A). Please note that this analysis does not allow for the unambiguous determination of the exact starting and ending residue of the protease-generated SiiA-PD fragment.

CD spectroscopy measurements were performed, and the secondary structure composition of ppr-SiiA and of SiiA-PD compared. The CD spectra recorded at pH 7.4 show that both protein variants display spectra corresponding to folded proteins with mixed secondary structure elements (Fig. 1B). Differences in the secondary structure composition become apparent when calculating a difference CD spectrum in which the CD signal of SiiA-PD is subtracted from ppr-SiiA (Fig. 1C). The

difference spectrum corresponds to the CD spectrum of an unfolded protein devoid of any secondary structure elements. These measurements indicate that any segments that are not part of SiiA-PD, but present in addition in ppr-SiiA, are likely disordered in solution. In order to investigate the possibility that these segments become ordered at slightly acidic and basic pHs, the measurements were repeated at pH 5.8 and 8.0 (Fig. S1). When considering the secondary structure detection limits of these CD measurements, then these experiments strongly suggest that segments present in addition in pprSiiA remain disordered within the pH 5.8 to 8.0 range. This is in line with the observation that both protein variants display nearly identical melting temperatures (T_M) (Fig. S1, Table S1). While SiiA-PD unfolds at 79°C at pH 7.4, the entire periplasmic region of SiiA unfolds at 77°C showing that segments that are present in addition in ppr-SiiA do not provide any further stabilizing interactions in SiiA.

SiiA-PD and ppr-SiiA elute both as dimers in an analytical size exclusion chromatography run (Fig. S1B, Table S2). Hence, the supplemental protein segments present in ppr-SiiA do not alter the oligomerization state of ppr-SiiA. The experiments from above show that, following the membrane domain (SiiA-MD, aa 1-39), SiiA consists of an unstructured periplasmic linker region (SiiA-LR) and a dimeric periplasmic domain (SiiA-PD) (Fig. 1D).

Crystal structure of SiiA-PD

We determined the crystal structure of SiiA-PD at 1.9 Å with the MAD method using SeMet-labelled protein (Table 1). Six molecules are present in the asymmetric unit and form three identical dimers. The terminal residues 103 and 203 are visible in all six monomers, and up to three additional C-terminal residues visible in some of the molecules. Absence of electron density for residues in the loop segment that interconnects the secondary structure elements $\beta 2$ and $\alpha 2$ (aas 153 to 156) leads to a chain break in three monomers. When calculating an anomalous difference density map with phases derived from the refined structure then electron density is observed for all methionines present in the asymmetric unit (Table S3) thereby corroborating model building and structure refinement.

When the six monomers of the asymmetric unit are compared to each other then two groups of molecules can be identified (group 1: chains A, C and E; group 2: chains B, D and F). Molecules within each group can be pairwise superimposed with low rmsd values ranging from 0.2 to 0.3, whereas rmsd values around 1.0 Å are obtained when comparing molecules between groups (calculated with $C\alpha$ -atoms, only) (Table S4). The main divergences between the two groups occur in loop regions, namely in the loop connecting $\beta 1$ to $\alpha 1$ and in the $\beta 2$ to $\alpha 2$ loop.

Table 1. Crystallographic data collection, phasing and refinement statistics.

PDB deposition code	6QVP		
<i>Data collection</i>			
Space group	P1		
Cell dimensions ^a			
<i>a</i> , <i>b</i> , <i>c</i> (Å)	58.33, 58.36, 65.83		
α , β , γ (°)	93.9, 94.0, 119.00		
	Peak	Inflection	Remote ^b
Wavelength (Å)	0.9797	0.9799	0.9184
Resolution (Å)	42.0–1.9	42.5–1.94	42.5–1.9
	(2.01–1.9) ^c	(2.05–1.94)	(2.01–1.90)
R_{meas} (%)	12.0 (62.6)	9.2 (58.9)	11.4 (54.4) ^d
I/σ (I)	7.1 (2.0)	8.6 (1.9)	7.5 (2.3)
CC _{1/2} (%)	99.1 (67.1)	99.5 (75.1)	99.1 (72.6) ^d
Resolution limit anomalous signal (Å) ^e	2.4	3.9	4.7
Completeness (%)	95.9 (93.7)	95.5 (93.6)	95.9 (93.8)
Redundancy	1.7	1.7	1.7
<i>Refinement</i>			
Resolution range (Å)	19.9 – 1.9		
No. of unique reflections	57795		
R_{work}/R_{free}	18.6/24.6		
Ramachandran (%)			
Favored/outlier	97.6/0.0		
Total no. of atoms	5533		
No. of protein atoms	4899		
No. of water atoms	619		
No. of ligand atoms	15		
<i>B</i> -factors (Å) ²			
Protein	35.3		
Water	33.9		
Ligands	42.0		
R.m.s deviations			
Bond lengths (Å)	0.013		
Bond angles (°)	1.182		

^aA single crystal was used for phasing and refinement.

^bThe remote dataset was used for the refinement of the model.

^cValues in parentheses refer to the highest resolution shell.

^dValues calculated with the Friedel's law equal false setting. Prior to refinement, however, the Friedel pairs were merged.

^eDefined as the resolution value where the correlation between anomalous differences drops below 30% and as calculated with program SHELXC (Sheldrick, 2010).

Each dimer is formed by one molecule from group 1 and one molecule from group 2. Low rmsd values of around 0.2 Å are obtained when comparing the dimers in such a way that monomers belonging to the same group are superimposed. In contrast, when monomers are superimposed crosswise then values of around 2.6 Å are obtained. These results show that the SiiA-PD dimers are slightly asymmetric. At the same time, this asymmetry is highly conserved among all three dimers present in the asymmetric unit (Table S5).

The SiiA-PD monomer structure displays a central β -sheet, consisting of five β -strands with mixed parallel and antiparallel strand pairing and with a $\beta 0$, $\beta 1$, $\beta 4$, $\beta 2$ and $\beta 3$ strand order (Fig. 2A). On one side, the β -sheet is flanked by two α -helices ($\alpha 1$ and $\alpha 2$). These interconnect

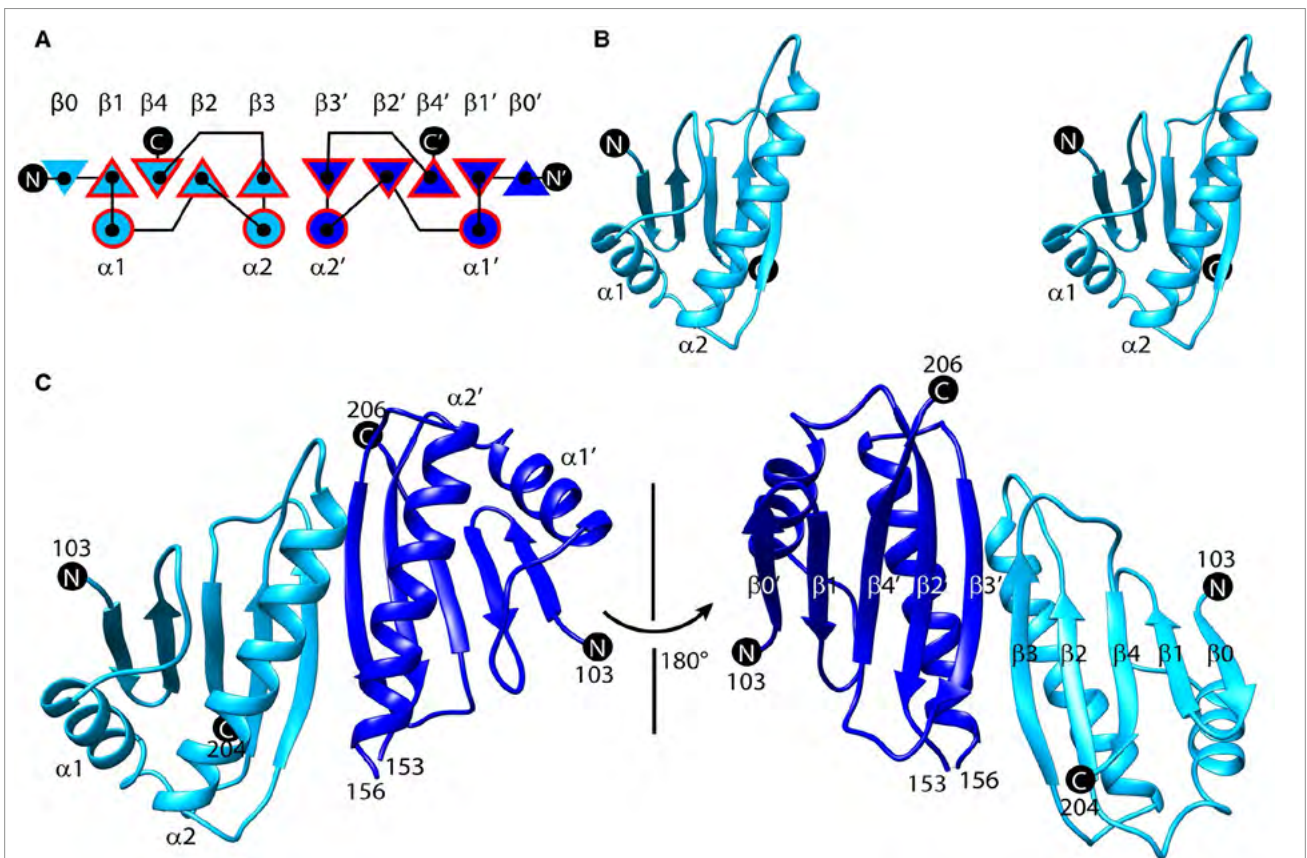


Fig. 2. Crystal structure of SiiA-PD.

A. Topology plot of the SiiA-PD monomer (light blue) and dimer (light and dark blue). The red frame highlights the core domain fold observed in OmpA-like domains consisting of $\beta 1/\alpha 1/\beta 2/\alpha 2/\beta 3/\beta 4$ (see also Fig. 3).
 B. Stereo image of a SiiA-PD monomer.
 C. Ribbon representation of the SiiA-PD dimer. The two chains are coloured in light and dark blue. The N- and C-termini in (B) and (C) are marked with black circles. [Colour figure can be viewed at wileyonlinelibrary.com]

strands $\beta 1$ and $\beta 2$ (helix $\alpha 1$) and strands $\beta 2$ and $\beta 3$ ($\alpha 2$) (Fig. 2B). Homodimer formation is accomplished through an antiparallel edge to edge pairing of $\beta 3$ from two adjacent SiiA molecules and results in the formation of a contiguous 10-stranded β -sheet (Fig. 2C). Overall, the SiiA-PD dimer displays nearly C_2 point group symmetry with the twofold symmetry axis oriented perpendicular to the plane of the contiguous β -sheet. Next to $\beta 3$, helix $\alpha 2$ also participates in the dimer interface and makes ample contacts with the homologous helix $\alpha 2$ from the second protomer. As shown in Fig. 2C, dimerization leads to the formation of a molecular surface that displays four α -helices and a surface which is composed of β -strands, only. Each monomer buries 780 \AA^2 of its surface in the dimer interface, and this amounts to about 12% of the total monomer surface. Eleven hydrogen bonds and two salt bridges are formed between the two monomers in the dimer interface. The presence of a high number of additional hydrophobic interactions suggests that the

SiiA-PD dimer constitutes a permanent dimer (Jones and Thornton, 1996). These results confirm earlier data where stable homodimer formation of full length SiiA was demonstrated using bacterial two hybrid assays (Wille *et al.*, 2014). Hence, it appears highly unlikely that transient self-association and re-dissociation events contribute to the cellular function of SiiA in *Salmonella*.

SiiA-PD shares structural homology to numerous PG-binding proteins

The monomer structure of SiiA-PD was used as a search template to identify homologous structures with the DALI server (Holm and Laakso, 2016). This search revealed that SiiA shares structural homology with numerous OmpA-like PG-binding proteins (Table 2). Several of the identified proteins were superimposed onto SiiA using the MatchMaker program in Chimera (Fig. 3, Fig. S2) (Pettersen *et al.*, 2004; Meng *et al.*,

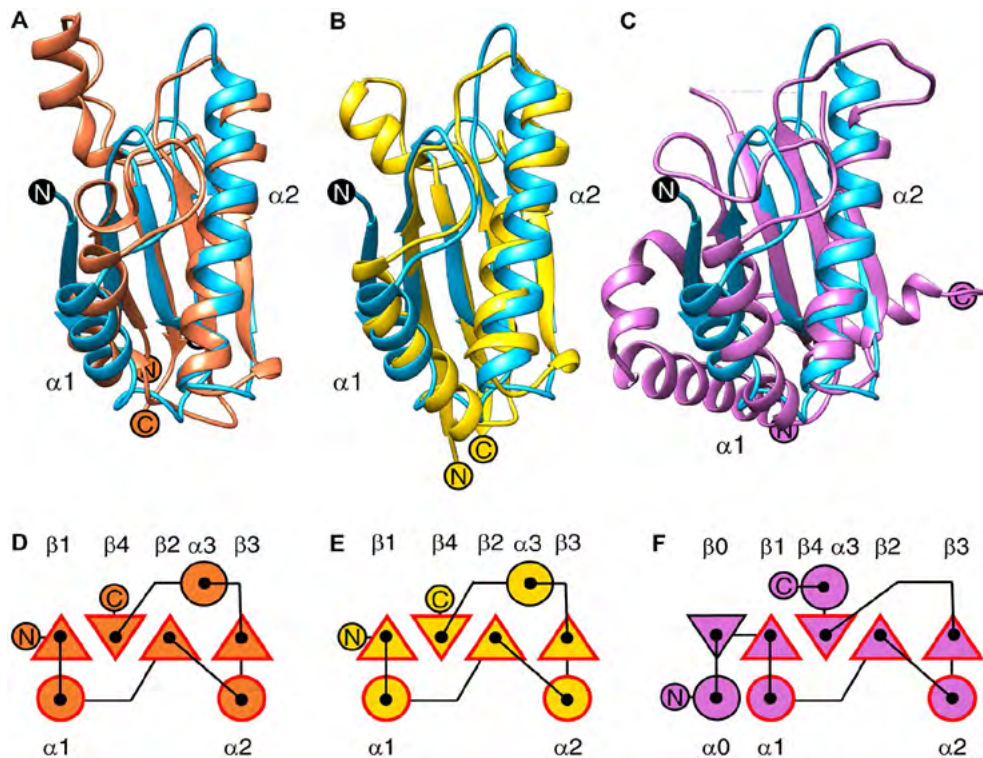


Fig. 3. SiiA shares structural homology to OmpA-like PG-binding domains. SiiA-PD (in light blue) is structurally homologous to the PG-binding domain of A. OmpA from *S. Typhimurium* (PDB-ID: 5VES, orange), B. OmpA from *A. baumannii* (PDB-ID: 3TD5, yellow), and C. MotB from *S. Typhimurium* (PDB-ID: 2ZOV, orchid), among others (Table 2, Fig. S3). N- and C-termini are marked with black circles in SiiA-PD and with coloured circles in case of the compared proteins. Helices $\alpha 1$ and $\alpha 2$ of SiiA-PD are annotated. Panels (D), (E) and (F) depict the secondary structure topology of the SiiA homologous proteins shown in panels (A), (B) and (C) respectively. All these proteins share an OmpA-like fold, consisting of a common core of $\beta 1/\alpha 1/\beta 2/\alpha 2/\beta 3/\beta 4$ secondary structure elements (framed in red). [Colour figure can be viewed at wileyonlinelibrary.com]

2006). All of these OmpA-like domains share a common core of secondary structure elements with a $\beta 1/\alpha 1/\beta 2/\alpha 2/\beta 3/\beta 4$ topology. Depending on the protein, additional secondary structure elements also occur. Thus, SiiA-PD harbours an additional strand $\beta 0$ at the N-terminus (Fig. 2A). OmpA from *S. Typhimurium* (PDB-ID: 5VES, (Rose *et al.*, 2015)) and *A. baumannii* (PDB-ID: 3TD5) display an additional $\alpha 3$ helix present between β -strands $\beta 3$ and $\beta 4$ (Fig. 3). MotB from *S. Typhimurium* (PDB-ID: 2ZOV) harbors additional $\alpha 0$ and $\beta 0$ secondary elements at the N-terminus as well as an additional $\alpha 3$ helix at the C-terminus (Fig. 3).

When comparing the dimerization modes of OmpA-like protein domains that are homologous to SiiA-PD then it becomes apparent that the dimerization modes of the periplasmic domain of MotB (MotB-PD, e.g. PDB-IDs: 2ZVY, 3S02), PomB (PDB-ID: 3WPW) and OmpA from *Klebsiella pneumoniae* (PDB-ID: 5NHX) are identical to that of SiiA-PD. In these proteins, dimerization is achieved by a juxtaposition of the $\alpha 2$ and $\beta 3$ secondary structure elements from the two protomers (see above). In contrast, only monomers are observed in the crystal structures

of the structurally homologous PAL protein (e.g. PDB-IDs: 5JIR, 5LKW and 5N2C). Interestingly, a different dimerization mode is observed in two crystal structures of OmpA from *A. baumannii* (e.g. PDB-IDs: 4G88 and, 3TD5). Here, dimer formation occurs *via* a juxtaposition of strand $\beta 1$. However, in PDB-entry 3TD5, a second OmpA dimerization mode can be observed, too, which is similar to that of SiiA-PD. It is also notable that, among all proteins compared here, SiiA-PD shares the highest sequence identity with OmpA (13%, Table 2). Overall, it appears that, of the different OmpA-like domain-containing proteins, all proteins proposed to be involved in ion translocation, e.g. MotB, PomB and SiiA, share an identical dimerization mode.

De Mot and Vanderleyden (De Mot and Vanderleyden, 1994) analysed the sequence of various OmpA-like domains and identified a so-called PG-binding motif with the sequence TD-X₁₀-LS-X₂-RA-X₂-V-X₃-L. Whereas almost all of the proteins identified by the DALI server share most of the amino acids present in this motif, SiiA harbours only a very reduced PG-binding motif restricted to the sequence L-X₃-R (Fig. 4A and B). The general motif spans from the

Table 2. SiiA homologous structures.

Protein	PDB-ID	Z-score	C α -rmsd (Å) ^a	Seq. -ID (%)	Organism	Reference
YfiB	4zhw	9.9 ^b	2.3 (91/168)	8	<i>P. aeruginosa</i>	(Li <i>et al.</i> , 2015)
OmpA	5nhx	9.7	2.4 (93/344)	8	<i>K. pneumoniae</i>	(Rose <i>et al.</i> , 2015)
MotB	2zov	9.4	2.8 (95/309)	6	<i>S. Typhimurium</i>	(Kojima <i>et al.</i> , 2009)
PAL	5jir	9.3	2.7 (97/476)	12	<i>T. pallidum</i>	(Parker <i>et al.</i> , 2016)
TagL	5m38	9.3	2.9 (93/576)	5	<i>E. coli</i>	(Rose <i>et al.</i> , 2015)
PAL	5lkw	9.3	2.5 (94/170)	11	<i>B. cenocepacia</i>	(Dennehy <i>et al.</i> , 2017)
PomB	3wpw	9.1	2.9 (96/315)	7	<i>V. alginolyticus</i>	(Zhu <i>et al.</i> , 2014)
PAL	5n2c	9.1	2.4 (90/170)	11	<i>B. cenocepacia</i>	(Capelli <i>et al.</i> , 2017)
OmpA	4g88	9.1	2.4 (94/356)	13	<i>A. baumannii</i>	(Rose <i>et al.</i> , 2015)
OmpA	3td5	9.1	2.3 (93/356)	13	<i>A. baumannii</i>	(Park <i>et al.</i> , 2012)
MotB	3s02	9.1	2.7 (95/171)	8	<i>H. pylori</i>	(O'Neill <i>et al.</i> , 2011)
OmpA	5ves	8.9	2.5 (92/350)	9	<i>S. Typhimurium</i>	(Rose <i>et al.</i> , 2015)

^aNumbers in parentheses indicate the number of aligned/overall residues.

^bThe proteins are ranked according to their Z-scores.

end of strand β 2 to the middle of α 2 in the canonical OmpA-like domain fold (Fig. 4C). The two residues Leu163 and Arg167 from the reduced L-X₃-R motif are displayed from the first half of helix α 2 in SiiA (Fig. 4C). It is notable that, even though only a very low sequence homology exists between SiiA and OmpA-like domains from other proteins, i.e. ranging from 6 to 13%, the overall structures of these proteins remain very similar (Fig. 4D, Table 2).

SiiA-PD binds to peptidoglycan in vitro

SiiA-PD shares a high structural similarity with OmpA-like PG-binding domains, but, at the same time, displays a poorly conserved PG-binding motif. We used a PG pulldown assay in order to assess whether SiiA-PD actually binds to PG isolates from *S. Typhimurium*. For comparison and as a control, we also monitored binding of MotB-PD from *S. Typhimurium* to PG (residues 99 to 276 of MotB, fragment identical to that in PDB-ID: 2ZVY (Kojima *et al.*, 2009)). The binding behaviour of the latter has been extensively studied before (for a recent review see (Minamino *et al.*, 2018)).

We observe that SiiA-PD is able to bind PG, albeit in a highly pH-dependent manner. SiiA binds to PG in a potassium phosphate-based buffer at a weak acidic pH, i.e. 5.8, whereas no binding is observed at a weak basic pH, i.e. 8.0. (Fig. 5, Fig. S3). This contrasts with the behaviour of MotB-PD, which binds to PG at pH 5.8 and 8.0 (Fig. 5). Upon a further division of the pH 5.8 to 8.0 interval into smaller pH steps, it becomes apparent that SiiA-PD binds to PG at pH 5.8 and 6.2 but not at pH 6.7, 7.2, 7.6 and 8.0 (Fig. 5D, Fig. S3). Binding of SiiA-PD to PG is fully reversible; when transferring the PG-bound SiiA-PD sample from pH 5.8 to 8.0 then a rapid release of PG-bound SiiA-PD into the supernatant can be observed (Fig. 5E).

In order to rule out that co-sedimentation of PG and SiiA-PD is caused by a pH-induced denaturation and

precipitation of SiiA-PD, we investigated the stability and solubility of SiiA-PD (and MotB-PD) at pH 5.8 and 8.0 using CD spectroscopy. At both pH values, the two proteins show well-defined CD spectra (Fig. S4). In addition, the T_M values of both proteins remain unaltered at pH 5.8 and 8.0. These were measured in a CD-monitored thermal unfolding experiment and correspond to 77°C and 74°C (SiiA-PD), and 63°C and 63°C (MotB-PD) at pH 5.8 and 8.0 respectively (Fig. S4, Table S1). These values also compare well to the T_M value of SiiA-PD determined at pH 7.4 (79° C, see above).

These results show that the observed structural similarities between SiiA-PD and MotB-PD are paralleled by a shared function, namely the ability to bind to PG. However, the two proteins display considerably different pH-dependent affinity profiles.

Arg162 and Arg167 participate in PG binding

An arginine residue, structurally homologous to Arg167 from the reduced PG-binding motif of SiiA, has been observed to directly participate in PG binding, before. Thus, in the crystal structure of the complex formed between the PG-binding domain of OmpA from *A. baumannii* and a PG-derived pentapeptide, the guanidinium group of Arg286 of OmpA directly interacts with the carboxylate group of the *meso*-A₂pm moiety of the bound PG-derived pentapeptide fragment (PDB-entry 3TD5, (Park *et al.*, 2012)). A highly similar interaction also occurs in the complex formed between the PG-binding domain of Pal and a PG precursor (Parsons *et al.*, 2006).

We produced two different mutants, namely SiiA-R167L and SiiA-S197E, in order to probe any participation of Arg167 in PG binding in SiiA. The scope of the R167L substitution was to ablate the guanidinium head group of the amino acid and, at the same time, retain the hydrophobic interactions observed between the aliphatic part of

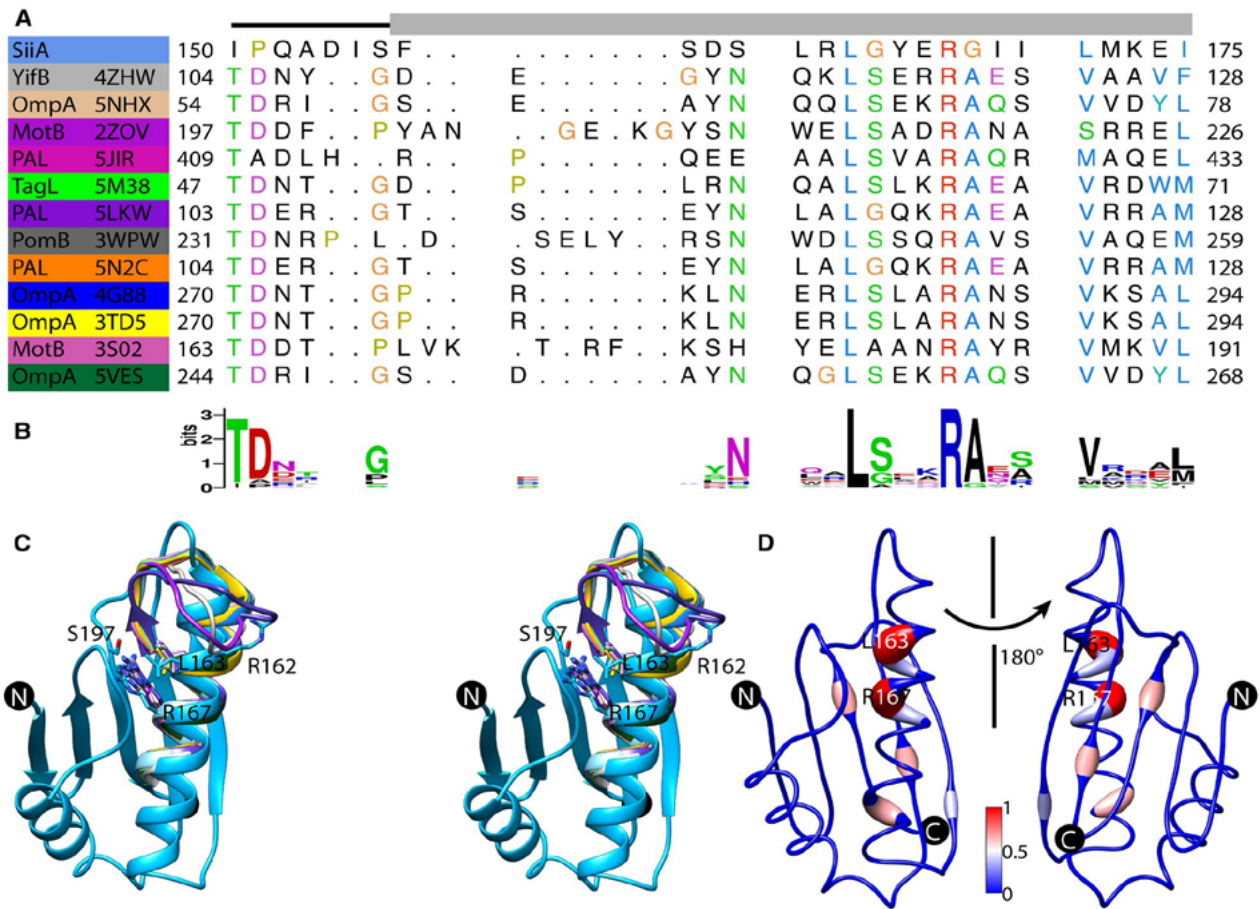


Fig. 4. PG-binding motif of SiiA in comparison to other OmpA-like PG-binding proteins.

A. Structure-based sequence alignment of the PG-binding motif of SiiA-PD and other OmpA-like proteins. A black line (loop $\beta 2$ to $\alpha 2$) and a grey box (helix $\alpha 2$) indicate the secondary structure of the aligned segment in SiiA-PD. On the left side of the alignment are reported the names and PDB-IDs of the aligned proteins (see also Table 2).

B. The PG-binding motif TDX10LSX2RAX2VX3L displayed as a sequence logo (Crooks *et al.*, 2004).

C. Stereo image depicting the PG-binding motifs of various OmpA-like structures superimposed onto SiiA. Colour coding of the proteins as in (a). Two important residues of SiiA-PD (R162 and S197) and two selected conserved residues from the PG-binding motif (L163 and R167) are shown in a stick representation.

D. Mapping of the sequence conservation of OmpA-like PG-binding proteins onto the structure of SiiA-PD. Sequence conservation (by clustal histogram), ranging from low and high, is color-coded by a blue to red gradient and emphasized by an enlarged cartoon tube radius. The structure-based sequence alignment and the sequence conservation mapping was calculated with the full-length proteins listed in Table 2. [Colour figure can be viewed at wileyonlinelibrary.com]

Arg167 and the SiiA protein core. The goal of the S197E substitution was to shield off the guanidinium group of Arg167 without perturbing the numerous intra-protein interactions that Arg167 is involved in. The mutant proteins display CD spectra that are indistinguishable from WT SiiA. In comparison to the latter, they show either an increased (R167L) or comparable (S197E) melting temperature. This suggests that the two point mutations do not negatively affect the structural integrity of SiiA-PD (Fig. S4C and D, Table S1). In the PG-binding assay, the two mutants share a very similar PG-binding profile. As previously observed for WT SiiA, the variants do not bind to PG at pH of 8.0. At the same time, they display

a reduced PG-binding ability at pH 5.8 in comparison to WT SiiA (Fig. 5, Fig. S3). These observations strongly hint that, similar to OmpA and Pal, Arg167 represents a PG-binding determinant in SiiA.

We also tested the contribution of Arg162 to PG binding and produced the mutant variant SiiA-R162A. Arg162 is a non-conserved residue that is contained within the segment that covers the extended PG-binding motif (De Mot and Vanderleyden, 1994). Arg162 and Arg167 are both part of helix $\alpha 2$ with the former residue being located closer to the dimerization interface (Figs 2C and 4C). Interestingly, an alanine substitution of Arg162 completely abolishes PG binding at pH 5.8 and, as for the

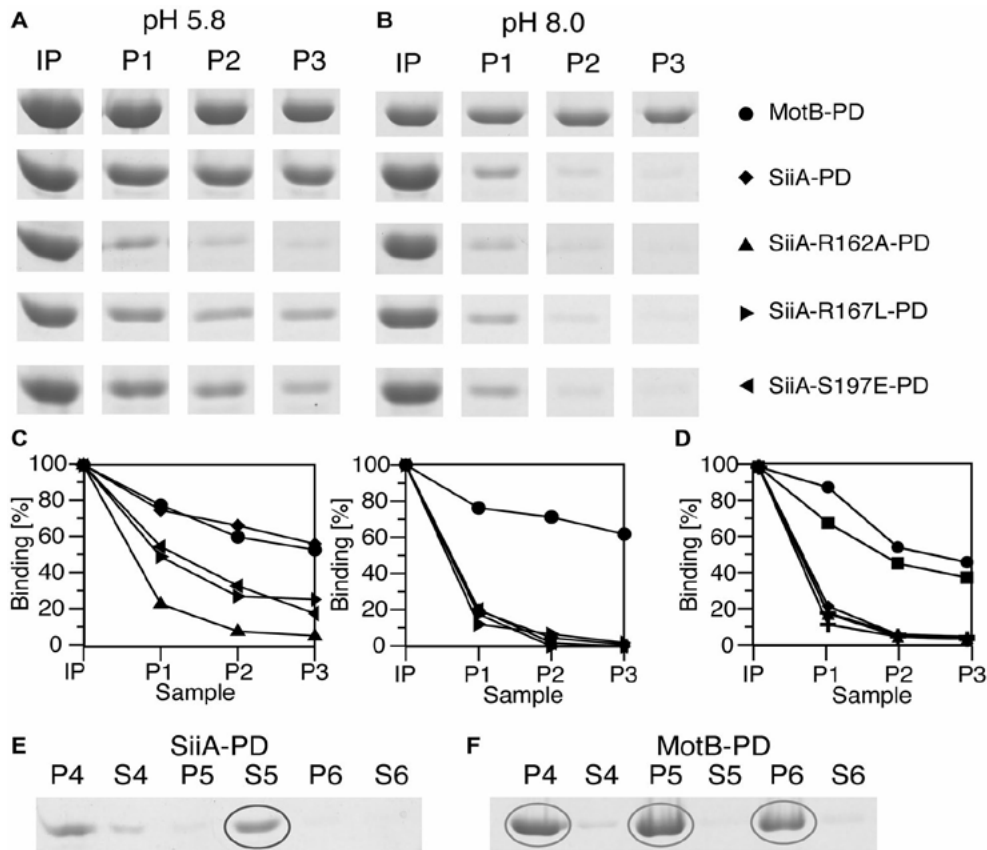


Fig. 5. SiiA binds to PG in a pH-dependent manner.

A. and B. PG pull-down assays of MotB-PD (dot symbol), SiiA-PD (diamond), SiiA-R162A-PD (triangle pointing upwards), SiiA-R167L-PD (triangle pointing right) and SiiA-S197E-PD (triangle pointing left) performed at pH 5.8 (A) and pH 8.0 (B). Input (IP) and pellet (P1-3) bands of the SDS-PAGE analysis of the pull-down fractions are shown. The complete SDS-PAGE gels of these assays are depicted in Fig. S3.

C. Band intensity analyses of the pull-down experiments at pH 5.8 (left panel) and pH 8.0 (right panel). The integrated intensities of the input bands were set to 100%. The symbols used for the different proteins are as in (A).

D. PG binding of SiiA-PD at different pH values. Band intensity analyses of PG-pulldowns at pH 5.8 (dot symbol), pH 6.25 (square), pH 6.74 (hyphen), pH 7.23 (cross), pH 7.65 (triangle) and pH 8.0 (diamond). The associated SDS-PAGE gels are depicted in Fig. S3.

E. pH-dependent dissociation of SiiA-PD from PG.

F. No pH-dependent dissociation is observed for MotB-PD. In panels (E) and (F) the P3 samples of SiiA-PD and MotB-PD from panel (A) were washed three times with a pH 8.0 buffer. P4-6 and S4-6 indicate pellet and supernatant fractions respectively. Whereas SiiA-PD dissociates from the PG upon washing with pH 8.0 (band S5, encircled), MotB-PD remains attached to PG after all washing steps (bands P4, P5, P6, encircled).

wild-type protein, displays no binding at pH 8.0 (Fig. 5, Fig. S3). Thus, it appears that the substitution of Arg162 impairs PG binding more drastically than the substitution or shielding of Arg167. To confirm that mutation of Arg162 did not impair the structural integrity of SiiA, we investigated the mutant protein with analytical SEC and CD spectroscopy. These experiments show that dimerization of SiiA is retained in SiiA-R162A (Fig. S1) and that SiiA-R162A displays a CD spectrum and melting temperature that is similar to the WT protein (Fig. S4B, Table S1).

It is possible that Arg162 contributes indirectly to PG binding, namely through long-range electrostatic interactions. Indeed, when viewing SiiA from the side from which Arg162 is displayed then a surface patch with a

striking positive electrostatic potential becomes apparent. In contrast to this, the opposite side displays an extended patch of negative electrostatic potential (Fig. 6A). If the two Arg162 residues present in the dimer are mutated *in silico* to alanine then this positive patch displays a neutral to negative potential in support of the possibility that Arg162 contributes to PG binding through electrostatic effects (Fig. 6B).

A co-isolation of either WT SiiA or mutant variant SiiA-R162A in complex with PG directly from *S. Typhimurium* further corroborates the involvement of Arg162 in PG binding. The co-isolation experiment shows that the amount of co-isolated SiiA-R162A is reduced by a factor of two in comparison to WT SiiA when analysed with

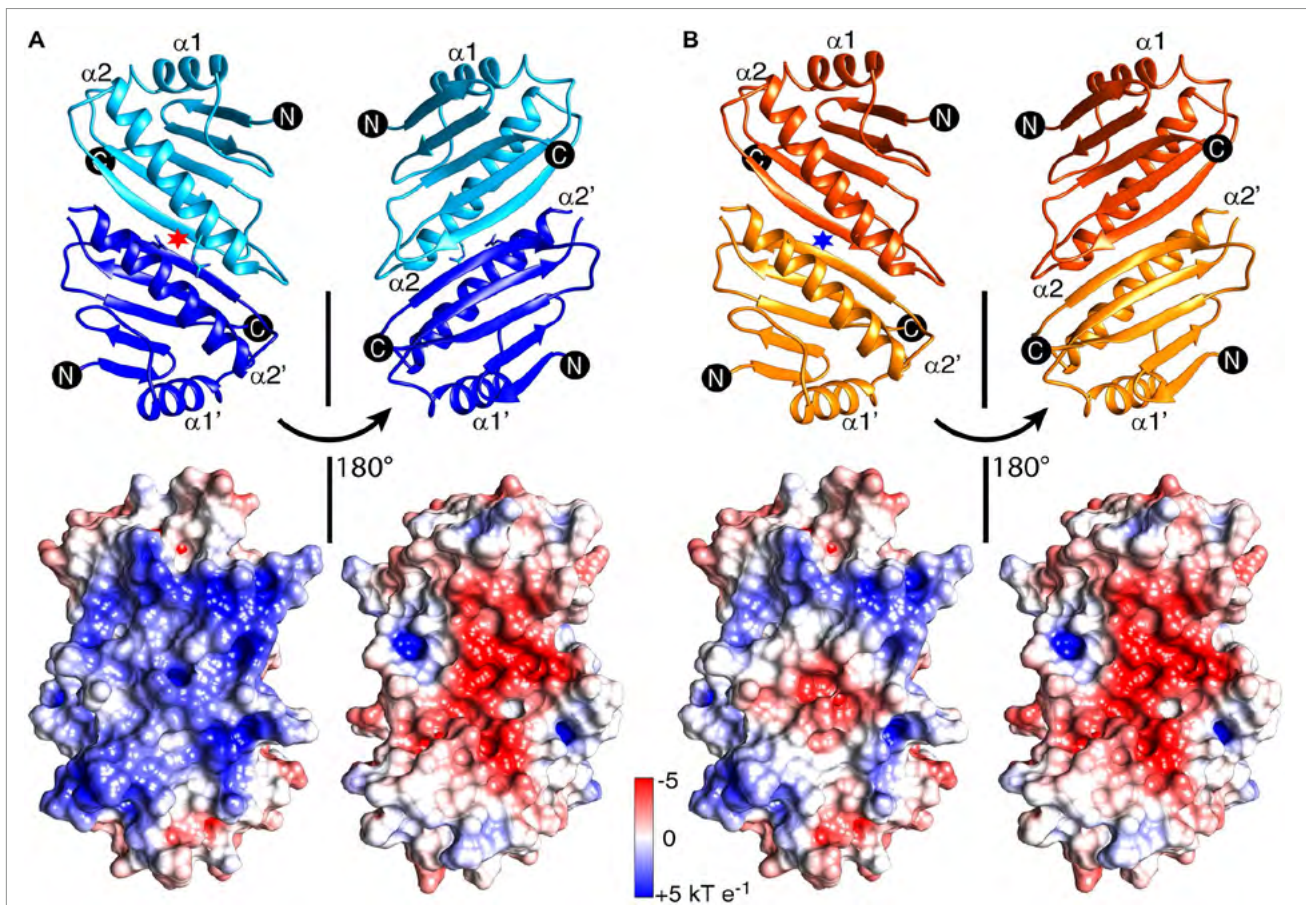


Fig. 6. Changes in the electrostatic surface potential of SiiA-PD upon introduction of the R162A substitution.

A. The SiiA-PD dimer is displayed in light and dark blue.

B. In silico analysis of the R162A mutant mapped onto the SiiA-PD dimer structure shown in orange and dark yellow. In the bottom half the electrostatic surface potential is displayed from -5 to neutral to $+5 \text{ kT e}^{-1}$ with a red-white-blue color gradient. Residue R162 in panel A and in silico mutated residue A162 in B are shown as sticks and further highlighted by a red and blue stars respectively. [Colour figure can be viewed at wileyonlinelibrary.com]

an antibody directed against the HA-Tag contained in either WT SiiA or the mutant variant (Fig. 7, Table S6). At the same time, antibody staining against OmpA indicates that in both co-isolated samples similar amounts of PG material are present (Table S6). Taken together, these results show that SiiA binds to PG with the help of two arginine residues. Of the two arginines, Arg 162 and Arg167, Arg162 contributes more significantly to PG binding.

A substitution of Arg162 reduces the Salmonella invasion of polarized epithelial cells

Previous studies demonstrated that the concerted actions of SiiE, the cognate T1SS and SiiAB are required to mediate adhesion to, and invasion of polarized epithelial cells (Gerlach *et al.*, 2007; Gerlach *et al.*, 2008). Mutant strains deficient in *siiA* are highly attenuated in invasion of polarized epithelial cells (Wille *et al.*, 2014). We therefore set

out to investigate if the PG-binding domain of SiiA is also important for the overall function of the SPI4-encoded T1SS. First, a mutational analysis was performed by C-terminal truncations or internal deletions to various extents of the PG-binding domain. We observed that the cellular amounts of the resulting mutant forms of SiiA were highly reduced, thus impeding further functional analyses (data not shown).

We investigated next whether a substitution of individual amino acids affects invasion of polarized epithelial cells. In order to identify candidate residues, in addition to R162A, R167L and S197E, we superimposed the structure of SiiA onto the structure of OmpA in complex with a PG fragment (PDB-entry 3TD5, (Park *et al.*, 2012)) and considered all SiiA residues that were located within 5 \AA of the OmpA-bound ligand as potential substitution candidates.

We performed site-directed mutagenesis of *siiA* and generated R120A, D159A, R162A, L163A, R167L and

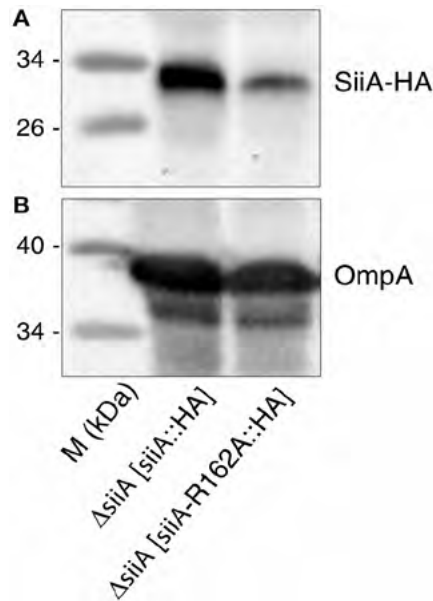


Fig. 7. Arg162 is critical for PG binding of SiiA. *S. Typhimurium* *siiA* deletion strains harbouring plasmids for expression of WT *siiA*::HA or *siiA*-R162A::HA were subcultured to induce expression of genes of the SPI4-T1SS. Cells were harvested, lysed by sonication and cell wall material was isolated. PG-binding proteins were extracted by incubation with buffer containing 2% of SDS and TCA precipitated. Pellets of equal amounts of bacteria were separated by SDS-PAGE and transferred onto nitrocellulose membranes. A. SiiA was detected by anti-HA antibody. B. The blot was stripped and reprobred for detection of OmpA by polyclonal antiserum.

S197E variant alleles. The synthesis of WT and mutant forms of SiiA was analysed in total cell lysates of *S. Typhimurium* strains. We observed that, while the cellular amounts of SiiA mutants D159A, L163A and R167L were highly reduced, the amounts of SiiA variants R120A, R162A and S197E were comparable to the levels of WT SiiA (Fig. 8A).

We compared phenotypes of a *siiA* deletion strains harbouring plasmids for the production of WT SiiA and SiiA mutants and studied the effect of aa exchanges in SiiA on invasion of polarized cells in an assay conducted at neutral pH (Fig. 8B). SiiA-R120A and SiiA-S197E restored invasion similar to WT SiiA. SiiA-D159A, SiiA-R162A, SiiA-L163A and SiiA-R167L did not restore invasion and entry levels were comparable to a strain harbouring the empty vector. However, since the cellular amounts of SiiA-D159A, SiiA-L163A and SiiA-R167L were highly reduced, it is not possible to estimate the contribution of the mutated residues to SiiA function.

In contrast, SiiA-R120A, SiiA-R162A and SiiA-S197E levels were not decreased compared to WT SiiA. Of these three mutants, only the mutant R162A showed reduced invasion. Thus, we conclude that residue Arg162 is

critical for the function of SiiA, while amino acid exchanges R120A and S197E are compatible with SiiA function. It is interesting to note that the substitution of Arg162 leads to both an abolishment of PG binding and a reduction of the invasion efficacy, whereas substitution of S197E causes only a reduction of the PG-binding affinity.

Transmembrane substitutions alter the proton-conducting activity of SiiAB

Encouraged by the anticipated structural similarities between SiiAB and MotAB and ExbBD, we previously suggested that SiiAB resembles a proton-conducting channel in the IM (Wille *et al.*, 2014). In order to test this proposed function of SiiAB, we established an assay that allows assessing the impact of SiiAB onto the intracellular pH of living bacteria, as previously demonstrated for MotAB (Nakamura *et al.*, 2009). For that, a pH-sensing GFP variant, namely R-pHluorin-M153R, was co-produced with either SiiAB or MotAB (Morimoto *et al.*, 2011). Co-production of either complexes led to a significantly more acidic cytosolic pH, which argues for the occurrence of a functional proton influx through both proton channels (Fig. 8C).

Consistent with the proposed crucial role of a transmembrane aspartate in proton conductance (Zhou *et al.*, 1998; Wille *et al.*, 2014), the acidification of the cytoplasm was strongly impeded when either the mutant complexes MotA-MotB-D33N or SiiA-D13N-SiiB were expressed (Fig. 8C). At the same time, WT and mutant SiiA proteins showed equal expression levels as detected by Western blot (Fig. S5).

In a similar set of experiments, we measured the intracellular pH of *Salmonella* expressing SiiAB-complexes containing the R162A substitution in the PG-binding domain of SiiA. Expression of SiiA-R162A-SiiB was controlled again *via* Western blot (Fig. S5). Expression of the mutant induced a cytosolic acidification comparable to that observed for WT SiiAB (Fig. 8D). Thus, no distinction can be made between the behaviour of WT SiiA and SiiA-R162A with regard to cytosolic acidification.

Discussion

In the present study, we investigated the atomic structure and function of SiiA, a protein that forms a complex with SiiB in the IM (Wille *et al.*, 2014). The SiiAB complex shares a number of properties with MotAB as well as with other members of the family of heteromeric ion-conducting channels, such as PomAB, ExbBD and TolQR. These latter complexes, by means of ion translocation across the IM, generate mechanical work that translates into the rotation of the flagellum or the uptake of nutrients at the

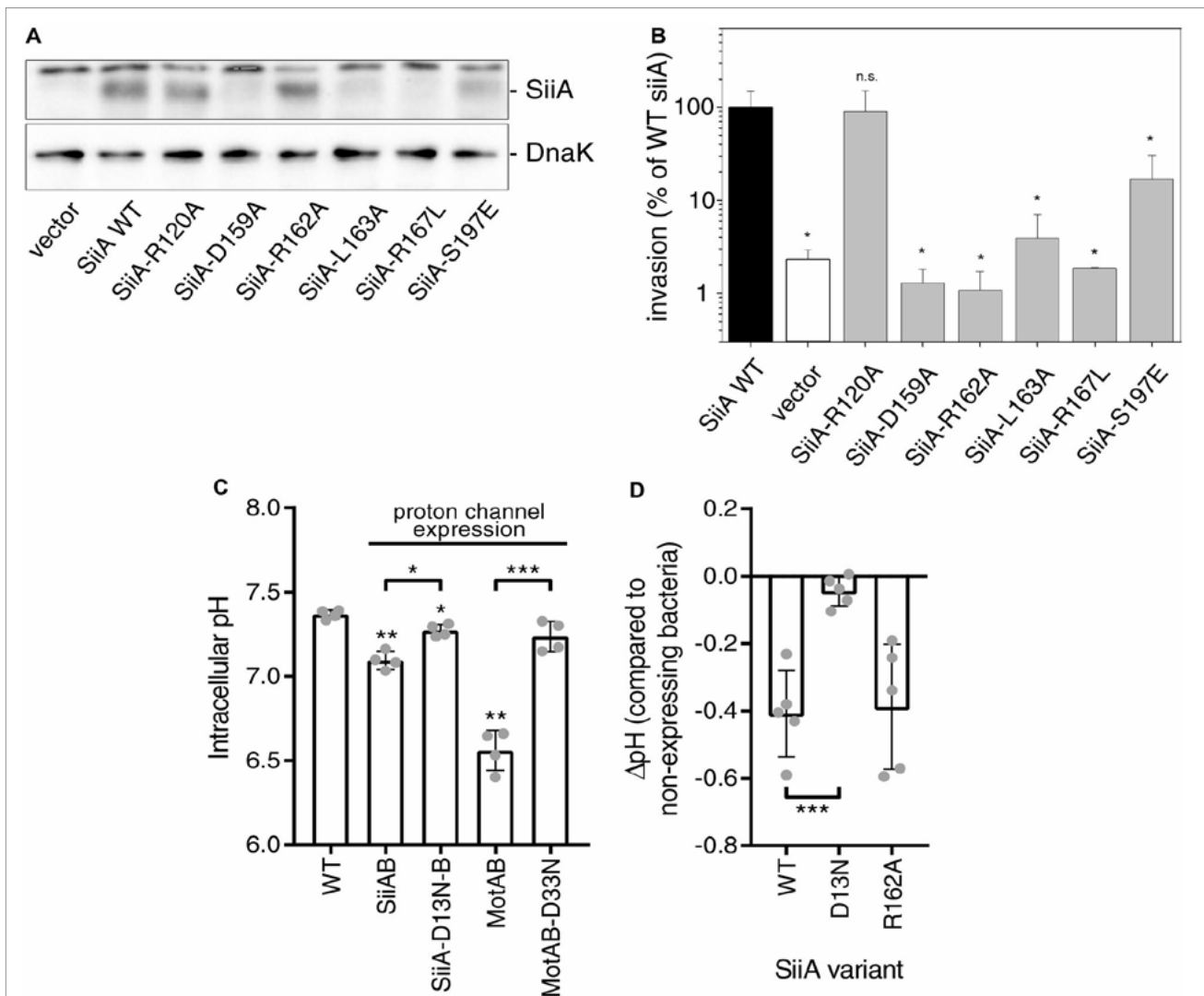


Fig. 8. Mutational analysis of SiiA *in vivo*.

A. Effect of *siiA* site-directed mutagenesis (SDM) on cellular amounts of SiiA. *S. Typhimurium* MvP771 harbouring the empty vector or various plasmids for the expression of *siiA* WT or various mutant alleles were subcultured in LB broth for 3.5 h. Equal amounts of bacterial cells as adjusted by OD600 were harvested and protein denatured by SDS-PAGE sample buffer. Protein was separated by SDS-PAGE on 12% gels and transferred onto nitrocellulose membranes. SiiA was detected using antibody against the HA tag. As loading control, blots were stripped and developed using an antibody against DnaK.

B. Effect of SDM of *siiA* on SPI4-dependent invasion of polarized epithelial cells. The Δ *siiA* strain MvP771 harbouring plasmids for the expression of WT *siiA*, various mutant alleles, or the empty vector were subcultured for 3.5 h to induce expression of genes for adhesion to, and invasion of polarized epithelial cells. The canine kidney epithelial cell line MDCK was grown as polarized monolayer and infected with *Salmonella* at a multiplicity of infection (MOI) of 5. After incubation for 25 min, non-internalized *Salmonella* were removed by washing and remaining extracellular bacteria were killed by incubation in medium containing 100 μ g ml⁻¹ Gentamicin for 1 h. Cells were washed again and lysed by addition of PBS containing 0.5% of desoxycholate. Serial dilutions of lysates were plated onto Mueller-Hinton agar to determine the number of colony forming units. Invasion is expressed as percentage of internalized inoculum. Means and standard deviations of triplicate samples are shown and the data are representative for three independent experiments.

C. Intracellular pH was detected using ratiometric fluorescence measurement of R-pHluorin-M153R in *S. Typhimurium* NCTC 12023 without (WT) or with co-expression of SiiAB, SiiA-D13N-SiiB, MotAB or MotA-MotB-D33N as indicated. Data of four independent experiments are shown and statistical significance was calculated against WT or between indicated data sets using paired, two-tailed Student's *t*-test and was defined as * for $P < 0.05$, ** for $P < 0.01$ or *** for $P < 0.001$.

D. Change in intracellular pH after expression of SiiAB complexes with WT SiiA, SiiA-D13N or SiiA-R162A compared to bacteria without induction of expression. Data of five independent experiments are shown and statistical significance was calculated using unpaired, two-tailed Student's *t*-test defined as *** for $P < 0.001$.

OM (Kojima *et al.*, 2009; Zhu *et al.*, 2014; Wojdyla *et al.*, 2015; Celia *et al.*, 2016). The question arises whether any structural similarities between SiiAB, and for example, MotAB are paralleled by similarities in the regulatory mechanisms that these proteins contribute to. If so, then available knowledge on MotAB could help to better understand how SiiAB contributes to SPI4-mediated adhesion of *Salmonella* (Wille *et al.*, 2014).

Here, we experimentally showed that indeed the architecture of SiiA closely resembles that of MotB. SiiA consists of a single transmembrane domain followed by an intrinsically disordered region and a stably folded domain referred to as SiiA-PD. Prior work demonstrated that residue Asp13 in the transmembrane region of SiiA is essential for SiiA function. Exchange of Asp13 in SiiA resulted in a highly attenuated invasion of polarized epithelial cells. Here, we now showed that the complex SiiAB is indeed involved in proton translocation across the IM. However, at the external pH value tested, i.e. pH 6.0, SiiAB was not able to reduce the cytosolic pH to the same extent as MotAB (Fig. 8C) (Nakamura *et al.*, 2009). This notwithstanding, our experiments show that mutation of Asp13 in SiiA as well as Asp33 in MotB directly impeded proton influx. Therefore, mutation of Asp13 in SiiA affects both proton translocation and, as previously shown, invasion of polarized epithelial cells (Wille *et al.*, 2014). These results strongly hint that proton translocation through SiiAB and hence energy derived from the PMF directly contribute to SPI4-mediated adhesion of *Salmonella*.

We solved the crystal structure of the stably folded periplasmic domain of SiiA, i.e. SiiA-PD. The structure of SiiA-PD resembles the structures of PG-binding domains from proteins present in either the IM or OM of Gram-negative bacteria. SiiA-PD forms a homodimer, and an identical dimerization mode is observed in MotB and PomB. In contrast, the dimerization mode of the PG-binding domain of OmpA, a protein located in the OM, is remarkably different. The OmpA-like domain of PAL, however, is monomeric in solution and in the crystal structure (Dennehy *et al.*, 2017). Thus, it appears that PG-binding domains of proteins involved in ion translocation across the IM, i.e. MotB, PomB and SiiA, share the same dimerization mode, whereas this is not the case for proteins with other functions.

SiiA harbours a reduced PG-binding motif. Only two residues, namely Leu163 and Arg167, are strictly conserved between the motif in SiiA-PD and the motif in other OmpA-like PG-binding domains (Fig. 4A). Here, we now showed for the first time that SiiA binds indeed to PG *in vitro* in a pH-dependent manner and that mutation or the shielding-off of Arg167 leads to a reduction of its PG-binding affinity. Moreover, mutation of additional residue Arg162, located in close proximity to Arg167, abolished PG binding *in vitro*. SiiA binds to PG with high affinity only at pH

values lower than 6.5, whereas MotB that we used as a control protein bound PG at low and high pH (pH 5.8 and 8.0). We also observed that increasing the salt concentration in the SiiA buffer negatively affected PG binding of SiiA (data not shown). It is difficult to anticipate how the *in vitro* observed binding behaviour translates into the number of PG-bound *versus* unbound SiiA molecules *in vivo*. Free diffusion of SiiA is restricted *in vivo* by both the attachment of SiiA to the membrane and its confinement to the periplasmic space. As a result, high local apparent concentrations prevail. Hence, the fraction of PG-bound SiiA molecules could be high despite SiiA displaying only a moderate PG-binding affinity under physiological conditions (Kuriyan and Eisenberg, 2007).

Our experiments suggest that the segment that links the transmembrane region of SiiA to the stably folded SiiA-PD is intrinsically disordered. Bioinformatics analyses, limited proteolysis experiments and difference CD spectra fail to reveal the presence of any secondary structure elements in this segment. This appears to be different for other members of this family. In MotB, PomB and TolR, this segment is proposed to play an important role in regulating both the anchoring of the PD domain to the PG layer and in controlling the translocation of ions across the translocation pore (Kojima *et al.*, 2009; Zhu *et al.*, 2014; Wojdyla *et al.*, 2015). In the inactive form of MotB, a so-called plug helix, contained in the segment that interlinks the transmembrane region of MotB to MotB-PD, is proposed to obstruct the proton-pore and inhibit proton translocation. Once the MotB-binding partner MotA interacts with the flagellum protein FliG, a structural rearrangement occurs that opens both the channel and induces a conformational change in the linker segment allowing for the attachment of MotB-PD to the PG layer. Overall, highly similar mechanisms have been proposed for how the linker segment controls the PG layer attachment in MotB, PomB and TolR (Kojima *et al.*, 2009; Zhu *et al.*, 2014; Wojdyla *et al.*, 2015; Kojima *et al.*, 2018). In these proteins, the function of the linker segment resembles that of a train pantograph. The latter either sits flat on the train roof (PG-domain remaining attached to the IM) or extends and connects the train to the overhead electric line (PG-domain attached to the PG layer).

Our present experiments fail to reveal that the segment that interconnects the transmembrane region of SiiA to the SiiA-PD is able to adopt different conformations. Moreover, MotB-SiiA chimeric proteins, in which the MotB PEM has been substituted against corresponding segments from SiiA, are not able to rescue flagellum function in the $\Delta motAB$ mutant (data not shown). Nevertheless, the structural similarities between SiiA and MotB strongly suggest that attachment of SiiA-PD to the PG is interlinked with the conductivity of the pore. If this is true, then the 60 residue-long disordered linker segment in SiiA

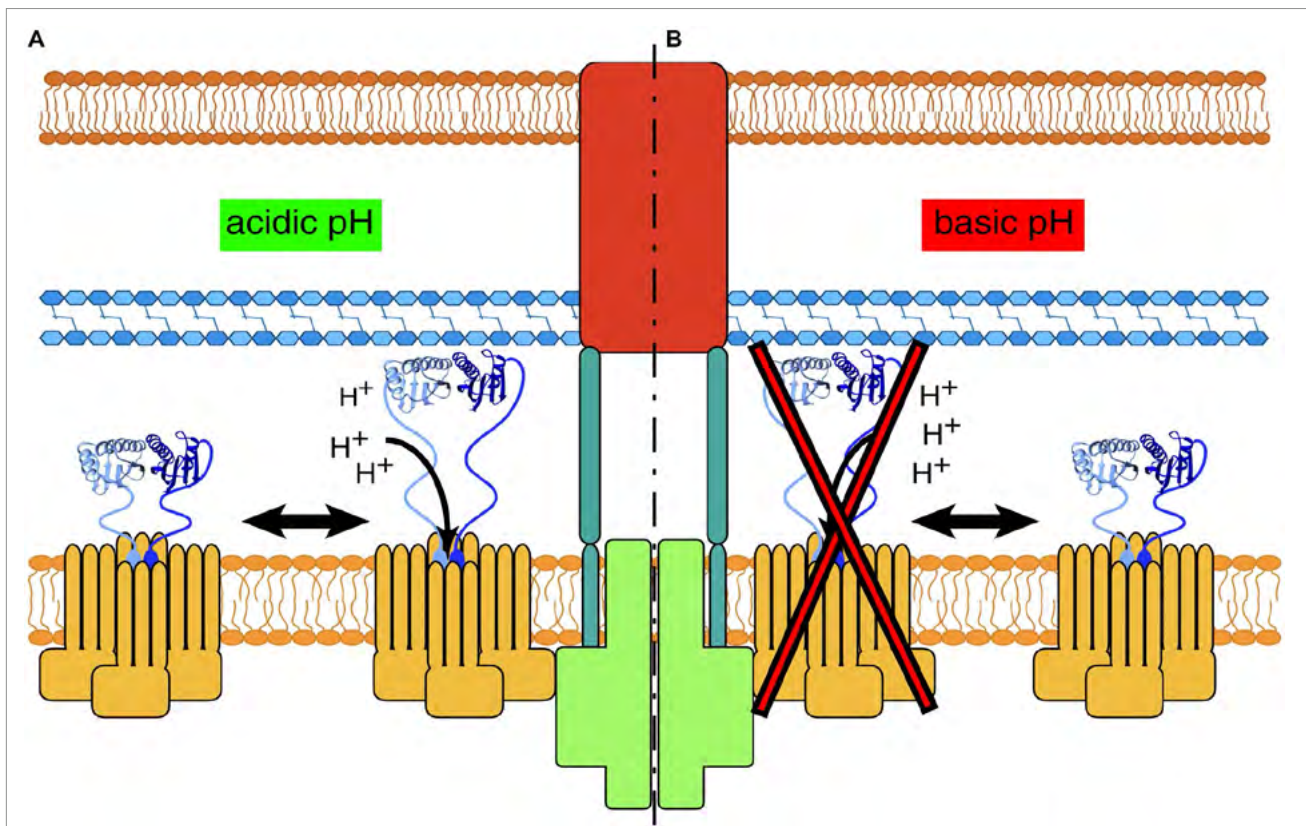


Fig. 9. Model of the SiiAB-complex and its integration into the SPI4-T1SS.

A. Upon acidification of the periplasmic space SiiA-PD attaches to the PG-layer and to SiiF and the proton influx is enabled.

B. At a basic pH, SiiA-PD is not able to bind to PG and the proton influx is reduced. At present it is still not known how proton influx or possibly any work that is generated by the influx of protons contribute to the function of the T1SS. SiiA and SiiB are shown in blue and yellow respectively. The canonical components of the SPI4-encoded T1SS are shown in red (SiiC), light green (SiiF) and cyan (SiiD). [Colour figure can be viewed at wileyonlinelibrary.com]

would be the prime candidate for linking these functional sites. Moreover, the pH-dependency of the attachment of SiiA-PD to the PG could be a contributor to the regulation of the conductivity of the pore, a mechanism so far not observed in MotB, PomB and TolR (Fig. 9).

It is tempting to speculate that a pH change might provide for a general trigger signal that modulates T1SS function, and that SiiA-PD plays an important role as a pH sensor. Taking the oral infection route, *Salmonella* survive the highly acidic pH in the stomach (pH 0 to 3) and are exposed to a rising pH gradient within the gut lumen reaching neutral levels in the ileum (pH 6 to 8) and decreasing again to mildly acidic levels in the colon (pH 5.5 to 7) (Evans *et al.*, 1988). So *Salmonella* are exposed to a low pH environment *in vivo* before it gets neutralized by bicarbonate-containing mucus overlaying the enterocytes (Atuma *et al.*, 2001).

Nevertheless, it remains to be determined how exactly the observed *in vitro* pH dependency of SiiA binding to PG influences the mechanism of the infection process *in vivo* since our current link between the *in vitro* and *in*

in vivo data doesn't appear to be fully conclusive. Thus, for example, mutation of Arg162 in SiiA abolishes PG binding and reduces *Salmonella* infectivity. However, mutation of Arg162 alters PG binding of SiiA-PD *in vitro*, only at slightly acidic pH values and not at neutral pH values where *in vivo* infection experiments on polarized MDCK cells were performed. At neutral pH values, no PG binding is observed for both wild-type SiiA and SiiA-R162A in our *in vitro* experiments. Similarly, the *in vivo* proton conductance assays were performed at an external pH of 6.0, and no differences in proton conductance were observed between wild-type SiiA and SiiA-R162A. At the same time, we observe clear differences in the PG-binding behaviour of these two variants at pH 6.0 *in vitro*. Clearly, additional experiments are needed to better reconcile these *in vivo* and *in vitro* observations. Thus, it is quite possible that the PG-binding pH window is altered in the context of the periplasmic space and in membrane-anchored full-length SiiA in comparison to SiiA-PD used in the *in vitro* experiments. A strong hint that these findings can be reconciled is provided by the results from the co-isolation experiment of

SiiA and mutant SiiA-R162A from *S. Typhimurium*. These results show that *in vivo* full-length wild-type SiiA and mutant SiiA-R162A still bind to PG at pH 7.0 but that the binding affinity of SiiA-R162A is reduced. Concomitantly, invasion efficiency of variant SiiA-R162A is also reduced in invasion assays conducted at the same pH.

Presently, it still remains unclear how SiiAB contributes in detail to the function of the SPI4-encoded T1SS and ultimately invasion of epithelial cells by *Salmonella*. Here and in past experiments, it is shown that SiiA mediates proton translocation at the inner membrane and PG attachment in the periplasmic space. Furthermore it is shown that residues in SiiA involved in either proton translocation or PG attachment contribute to proper T1SS function. Moreover, the structural and functional similarities observed between SiiAB and MotAB strongly suggest that SiiAB is able to 'tap' into the PMF. Clearly, it remains to be shown how exactly this 'tapping' contributes to *Salmonella* infectivity.

Experimental procedures

Protein production

For the production of ppr-SiiA, the *siiA* gene was cloned into a pET15b vector (Novagen, Darmstadt, Germany). The translated gene product consists of an N-terminal hexa-histidine tag (MGSSHHHHHH) followed by a thrombin cleavage site (SSGLVPRGSHM) and residues 40 to 210 of SiiA from *S. Typhimurium* (Uniprot entry H9L4G5, (The UniProt, 2017)). The SiiA-R162A mutant was generated using a two-stage mutagenesis protocol (Wang and Malcolm, 1999). Two separate 50 μ l PCR mixtures, containing either the forward or the reverse PCR primer listed, were prepared and seven PCR cycles performed (Table S7). Subsequently, 25 μ l of each mixture were combined, additional Q5 polymerase (NEB, Frankfurt, Germany) added and 17 additional PCR cycles performed. DpnI (NEB) was added, and the mixture incubated at 37°C for 1 h prior to the transformation into XL10Gold cells (NEB) (Table S8). The correctness of all plasmid constructs generated in this study was confirmed by DNA sequencing.

Additional mutant variants were generated with the oligonucleotides listed in Table S7 and using a protocol that adhered to the manufacturer's instructions of the Q5 SDM kit (NEB). The protocol contained several modifications: the kinase-ligase-DpnI reaction was performed by mixing 10, 400 and 20 units of T4-polynucleotide kinase, T4-ligase and DpnI (all NEB) respectively. The reaction was incubated for 2 h at room temperature (RT). Five microlitre of this reaction mixture was transformed into XL10Gold cells (NEB).

WT ppr-SiiA protein and mutant variants were produced using freshly transformed BL21(DE3) (Novagen) cells. The transformed cells were incubated in LB medium (Carl Roth, Karlsruhe, Germany) supplemented with 100 μ g ml⁻¹ ampicillin. The cells were harvested by centrifugation, resuspended in a sodium phosphate/imidazole buffer (20 mM sodium phosphate pH 7.5, 30 mM imidazole, 500 mM NaCl, EDTA-free protease inhibitor cocktail (Roche, Mannheim, Germany))

and lysed by sonication. Cell debris was removed by centrifugation at 95,000 \times *g* and 4°C for 1 h. The proteins were purified by affinity chromatography *via* the hexa-histidine tag (elution buffer: 20 mM sodium phosphate pH 7.5, 500 mM imidazole, 500 mM NaCl) and dialysed into a 20 mM Tris-HCl pH 7.5 buffer. The hexa-histidine tag was removed overnight with thrombin (5 U thrombin (Sigma-Aldrich, Darmstadt, Germany) per mg SiiA protein) resulting in a fragment covering the periplasmic part of SiiA. The cleavage reaction was stopped by adding 5 mM AEBSF, and the protein was further purified by size exclusion chromatography using a Superdex 75 16 600 column (GE Healthcare, Freiburg, Germany) and a 20 mM Tris-HCl pH 7.5 buffer.

The production of seleno-methionine (SeMet)-labelled ppr-SiiA was accomplished using the protocol of Studier *et al.* (Studier, 2005). The transformed BL21(DE3) cells were grown overnight in PAG media supplemented with 100 μ g ml⁻¹ ampicillin (Studier, 2005). This preculture was then diluted into the auto-inducing PSAM 5052 medium and supplemented with 100 μ g ml⁻¹ carbenicillin (Studier, 2005). The cells were grown for 3.5 days at 20°C before harvesting by centrifugation. SeMet-labelled SiiA protein isolation and purification was carried out as described above, except that the buffer used for size exclusion chromatography consisted of 20 mM of Tris-HCl pH 7.5, 10 mM of EDTA and 150 mM of NaCl. The protein was stored at a concentration of 1.0 mg ml⁻¹ at -80°C for later usage.

In order to have a positive control protein sample in the PG-binding assay (see below), the PG-binding domain of *Salmonella* MotB (aa 99-276, Uniprot entry P55892, (The UniProt, 2017)) was produced using a similar gene construct as for SiiA. MotB was cloned into a pET15b vector (Novagen) resulting in a construct that contains an N-terminal His-tag and a thrombin cleavage site. BL21(DE3) cells were transformed with the plasmids, and the transformed cells incubated in TB medium (Carl Roth) supplemented with 100 μ g ml⁻¹ ampicillin. The cells were harvested by centrifugation, resuspended in a Tris/imidazole buffer (20 mM Tris-HCl, 20 mM imidazole, pH 7.4, 500 mM NaCl, EDTA-free protease inhibitor cocktail) and lysed by sonication. Cell debris was removed by centrifugation at 108,000 \times *g* and 4°C for 1 h. MotB was purified by affinity chromatography *via* the hexa-histidine tag (elution buffer: 20 mM Tris-HCl, 500 mM Imidazole pH 7.4 and 500 mM NaCl) and subsequently dialysed against 20 mM Tris-HCl pH 8.0, 100 mM NaCl buffer. MotB was further purified by size exclusion chromatography (Superdex 75 16 600 column) using a 20 mM of Tris-HCl pH 8.0, 100 mM of NaCl buffer.

Proteolysis with thermolysin

In order to investigate the domain structure of ppr-SiiA and to identify alternative SiiA fragments for crystallization trials, we incubated a purified ppr-SiiA sample over a period of 2 days at 20°C with limited amounts of thermolysin (Hampton Research, Aliso Viejo, USA; 1 μ g thermolysin per mg SiiA). The formation of proteolytic degradation products was monitored by retrieving aliquots at fixed time intervals and analysing the aliquots with SDS-PAGE.

For preparative production of WT and mutant SiiA-PD (either SeMet-labelled or not), thermolysin was added to

ppr-SiiA (1 μg thermolysin per mg SiiA) after the initial His-tag affinity chromatography step in a 20 mM of Tris-HCl pH 7.5 buffer. The thermolysin-SiiA mixture was incubated for 1.5 h on ice. Proteolysis was stopped by adding 10 mM of EDTA. The resulting protein fragment was purified using a DEAE-sepharose column (GE Healthcare). Elution from the column was accomplished with a linear gradient ranging from 0 to 500 mM NaCl in a buffer containing 20 mM of Tris-HCl pH 7.4 and 10 mM of EDTA. The final purification step consisted of a size exclusion chromatography (Superdex 75 16 600 column, GE Healthcare) and using the same buffer as above but without NaCl. SiiA-PD was then concentrated to 20 mg ml^{-1} and stored at -80°C for later usage.

CD measurements

The secondary structure composition of the different protein variants was analysed *via* CD spectroscopy, using a Jasco J-815 CD spectropolarimeter (Jasco, Gross-Umstadt, Germany). Prior to the recording of the CD signal, the protein variants were dialyzed against buffers consisting of 10 mM of potassium phosphate with different pH values, namely pH 5.8, 7.4 and 8.0. All spectra were recorded in a 0.1 cm cuvette with protein concentrations of 5 μM protein. The absorption range was scanned from 185 to 260 nm using a step size of 0.1 nm, a data integration time of 1 s, a bandwidth of 1 nm and a scanning speed of 20 nm min^{-1} . For further analysis of the CD signal, the mean residue ellipticity was calculated (Kelly *et al.*, 2005). Thermal denaturation analysis was performed in a 1 cm cuvette with a protein concentration of 0.7 μM . The CD signal was recorded at a single wavelength, namely at 222 nm, and the temperature increased from 20 to 100°C at a rate of 1°C per min .

Protein crystallization and crystal structure determination

SeMet-labelled SiiA-PD was crystallized using the hanging drop method (Rupp, 2009). The reservoir solution consisted of 200 mM of sodium phosphate dibasic pH 8.8 ± 0.1 and 20% of PEG 3350. The protein droplet was formed by mixing 2 μl of protein solution (17 mg ml^{-1} SeMet-labelled SiiA-PD in 20 mM Tris-HCl pH 7.5, 1 mM EDTA and 15 mM NaCl) with 1 μl reservoir solution and 2 μl of perfluoropolyether cryo-oil (Hampton research). The crystals were harvested, cryo-protected with additional perfluoropolyether cryo-oil and flash frozen in liquid nitrogen prior to any diffraction data collection.

Diffraction data were collected on beamline BL14.1 operated by the Helmholtz-Zentrum Berlin (HZB) and BL14.2 operated by the Joint Berlin MX-Laboratory at the BESSY II electron storage ring (Berlin-Adlershof, Germany) (Mueller *et al.*, 2015). The structure of SiiA-PD was solved using the multi-wavelength anomalous dispersion (MAD) method (Rupp, 2009). A complete MAD dataset was collected from a single triclinic SeMet-labelled SiiA-PD crystal at beamline BL14.2, and the data processed with XDS and XDSAPP (Kabsch, 2010; Sparta *et al.*, 2016). The values of the triclinic unit cell dimensions (a , b , c and α , β , γ equal to 58.3, 58.4, 65.8 (\AA) and 93.9, 94.0, 119.0°) respectively are very close to values that would allow for an alternative crystal lattice assignment, namely a monoclinic C-centred

Bravais lattice with dimensions 59.2, 100.6, 65.8 (\AA) and 90.0, 97.8, 90.0°). However, an analysis of the structure factor amplitudes of the remote dataset (used for the final model refinement) with programs XDS and POINTLESS revealed unambiguously the absence of a twofold rotational symmetry ($R_{\text{meas}} \sim 11\%$ in Laue group -1 versus $R_{\text{meas}} \sim 37\%$ in group $2/m$) and confirmed the triclinic space group (Table 1) (Evans, 2006; Kabsch, 2010). Data were scaled with program XSCALE, and the localization of the selenium sites and partial model building accomplished with program AUTOSOL of the PHENIX software suite (Terwilliger *et al.*, 2009; Adams *et al.*, 2010). Model building was completed, and the structure refined to convergence in an iterative process, consisting of steps of manual inspection with program COOT, automated model rebuilding and refinement, using program AUTOBUILD and single model refinement steps with program PHENIX.REFINE (Terwilliger *et al.*, 2008; Emsley *et al.*, 2010; Afonine *et al.*, 2012). The triclinic crystals contain six protein molecules grouped into three dimers in the asymmetric unit. Data collection and refinement statistics are summarized in Table 1.

Bioinformatics analyses

A monomeric chain of SiiA was used with the DALI server to identify protein structures that are homologous to SiiA (Holm and Laakso, 2016). The identified structures were ranked based on Z-scores. Crystal structures with a Z-score > 8.9 were chosen for a structure-based sequence alignment. The structures were aligned with the MATCHMAKER program in CHIMERA (Pettersen *et al.*, 2004; Meng *et al.*, 2006). The sequence conservation mapping was performed with the full-length proteins and the MULTIALIGN VIEWER in CHIMERA (Pettersen *et al.*, 2004; Meng *et al.*, 2006).

The electrostatic surface representation was generated *via* the APBS-PDB2PQR-server version 2.1.1 with default settings (http://nbc-222.ucsd.edu/pdb2pqr_2.1.1/) (Jurrus *et al.*, 2018). The PDB2PQR settings included the use of the PARSE-force field (Sitkoff *et al.*, 1994), the treatment of the N- and C-terminus as neutral and a pH of 7.0.

Rmsd values between monomers and dimers were calculated with LSQKAB (Kabsch, 1976). Changes in solvent accessible surface areas were calculated with the PISA-server (Krissinel and Henrick, 2007). All structure illustrations were drawn with program chimera (Pettersen *et al.*, 2004).

Peptidoglycan (PG) isolation

The isolation of PG from *S. Typhimurium* was performed according to a protocol adapted from Glauner (1988). In short, bacteria were grown in LB medium (Carl Roth) to mid-exponential log phase (OD_{600} of 0.6–0.8). The cells were chilled rapidly in an ice bath and harvested via centrifugation. The cell pellet was resuspended in MQ-water and added dropwise to a boiling SDS-solution (8%). The volume was adjusted with MQ to 4% SDS and further boiled for 30 min. From now on, the solution was kept at RT. The next day, the solution was centrifuged at $108,000\times g$ at

RT for 45 min. The pellet was washed with MQ-water five times in order to remove any residual SDS. The PG pellet was suspended in 50 mM Tris-HCl pH 7.0 and subsequently treated with 100 $\mu\text{g ml}^{-1}$ α -amylase (Sigma-Aldrich) for 2 h at 37°C. The solution was then supplemented with 20 mM MgSO_4 and treated with 50 $\mu\text{g ml}^{-1}$ RNase A (Roche) and 10 $\mu\text{g ml}^{-1}$ DNase (Sigma-Aldrich) for additional 2 h at 37°C. Subsequently, 10 mM CaCl_2 and 100 $\mu\text{g ml}^{-1}$ trypsin (Sigma-Aldrich) were added and the mixture incubated at 37°C overnight. The next day, 10 mM EDTA pH 7.4 were added. The solution was supplemented with SDS to a final concentration of 1% (v/v) and boiled for 15 min in a bain-marie. This solution was cooled down to RT and centrifuged at 108,000 \times g at RT for 45 min. The pellet was washed five times to remove any SDS traces. The isolated PG was dried in a SpeedVac (Thermo Scientific, Osterode, Germany) and stored at -20°C until further usage.

Generation of *siiA* mutant alleles

Site-directed mutagenesis of low copy number vector p3187 harbouring *siiA*::HA under control of P_{siiA} was performed using the Q5 SDM kit according to the manufacturer instructions (NEB) (Table S9), with oligonucleotides (IDT, Munich, Germany) listed Table S7. The resulting plasmids were confirmed by DNA sequencing and introduced in *S. Typhimurium* strain MvP771 ($\Delta siiA$::FRT, Table S8).

PG-binding assays

For *in vitro* binding assays, the proteins SiiA-PD, SiiA-R162A-PD, SiiA-R167L-PD, SiiA-S197E-PD and MotB-PD were dialyzed against buffer A (10 mM potassium phosphate pH 5.8) and/or buffer B (10 mM potassium phosphate 8.0). After buffer exchange, the protein variants were centrifuged at 16,100 \times g for 15 min at 4°C in order to remove any precipitate. Isolated PG from *Salmonella* was resuspended and washed three times with buffer A or B. About 0.2 mg of PG were mixed with 0.25 mg of purified protein in a 1.5 ml reaction tube. This was the input sample (sample IP). This mixture was incubated at RT for 1 h. The PG and PG-bound protein were pelleted via centrifugation at 16,100 \times g for 10 min at 22°C and the supernatant collected in a separate tube. The pellet was re-suspended in 200 μl with the respective buffer. Unbound protein was removed from the insoluble PG by two additional centrifugation and resuspension steps, as described above. Samples for SDS-PAGE were taken from the resuspended pellet (samples P1, P2, P3...) and the supernatant (samples S1, S2, S3...) at each of the steps. The samples were analysed via SDS-PAGE and stained with Coomassie Blue. The band intensities were quantified with program ImageJ (<https://imagej.nih.gov/ij/>).

For analyses of PG binding in *S. Typhimurium* cells, assays were performed basically as described by Mizuno (1979) (Table S8). The *S. Typhimurium* *siiA* deletion strain MvP771 harbouring plasmids for expression of WT *siiA*::HA or *siiA*-R162A::HA was grown overnight in LB, diluted 1:31 on LB and subcultured for 2.5 h for induction of SPI4 genes. Bacterial cells were harvested and resuspended in PBS, pH 7.4. Cells were disrupted by sonication using a Branson sonifier. The

lysates were centrifuged for 60 min at 130,000 \times g at 4°C and pellets were washed in PBS. Pellets were incubated in 900 μl extraction buffer (100 mM Tris-HCl, pH 7.3, 100 mM CaCl_2 , 10% glycerol and 2% SDS) at 34.6°C. After centrifugation at 130,000 \times g for 1 h at 34.6°C, the supernatant was recovered and protein was precipitated by addition of TCA to a final concentration of 10%. Precipitated protein was recovered by centrifugation at 16,100 \times g for 46 min at 25°C. Pellets were washed with acetone, dried and protein was dissolved in SDS-PAGE sample buffer. If required, pH was neutralized by addition of 1 M Tris-HCl, pH 10.0 and samples were denatured by boiling of 5 min.

Infection of polarized epithelial cells

S. Typhimurium strains were grown over night in LB containing 50 $\mu\text{g ml}^{-1}$ carbenicillin with aeration by continuous rotation in a roller drum at 37°C. Cultures were diluted 1:31 in LB and grown for 3.5 h at the same conditions in order to induce expression of SPI1 and SPI4 genes. Infection of the polarized epithelial cell line MDCK was performed as described before, and the amounts of internalized *Salmonella* were determined 1 h after infection (Wille *et al.*, 2014).

Measurement of intracellular pH

Plasmids were constructed using assembly cloning of PCR products (Gibson *et al.*, 2009). All primers used for PCR are listed in Table S7. For the cloning of plasmids that allow co-expression of *siiAB*, *siiA*-D13N-B or *motAB* with pHluorin, pTAC-MAT-Tag-2 (Sigma-Aldrich) was PCR-amplified with primers pTAC-Gbs-for/rev (Table S9). As inserts, a tetracycline-inducible promoter was amplified from pWRG603 with primers TetR-Gbs-for/rev (Wille *et al.*, 2014). A codon-optimized version of R-pHluorin-M153R was synthesized (IDT) and amplified with primers R-pHluorin-tetR-Gbs-for/R-pHluorin-pTAC-Gbs-rev, and *siiAB*, *motAB* or *siiA*-D13N-B from *S. Typhimurium* genomic DNA or pWRG648 using primer pairs pTAC-SiiA-Gbs-for/SiiB462-tetR-Gbs-rev or pTAC-MotA-Gbs-for/MotB-pTAC-Gbs-rev (Morimoto *et al.*, 2011; Wille *et al.*, 2014). Plasmids containing further site-specific mutations in *siiA* (R162A) and *motB* (D33N) were generated by assembly cloning using primers listed in Table S7.

Overnight cultures of strains carrying pHluorin constructs were reinoculated at an OD_{600} of 0.15 in fresh LB broth containing 50 $\mu\text{g ml}^{-1}$ carbenicillin (Carl Roth) and grown with aeration for 3.5 h at 37°C. Expression of *siiAB* or *motAB* together with R-pHluorin-M153R was induced after 2 h with 10 mM IPTG and 50 ng ml^{-1} anhydrotetracycline hydrochloride (Sigma-Aldrich). One millilitre of the suspension was centrifuged (8,000 \times g , 5 min.), washed once with 1 ml of 100 mM phosphate buffer pH 6.0 and finally resuspended in 500 μl of the same buffer. After 10-fold dilution fluorescence was determined with excitation at 410 and 470 nm and emission at 509 nm in a black 96-well plate (Nunc Thermo Fisher, Karlsruhe, Germany) using an Infinite M1000 plate reader (Tecan, Männedorf, Switzerland). The 410/470 nm excitation ratio was used to calculate the pH based on calibration curves. Calibration curves were generated with R-pHluorin-M153R expressing bacteria which were washed and resuspended in

phosphate buffers of different pH ranging from 6.0 to 8.0. The protonophore carbonyl cyanide *m*-chlorophenyl hydrazone (CCCP, Sigma-Aldrich) was added to a final concentration of 30 μ M and samples were incubated for 30 min. at 37°C. The ratio 410/470 nm was plotted against the pH-value and the resulting curve was fitted using a fourparameter logistic function (Fig. S6).

Western blot

Bacterial cells were grown and *siiAB* expression was induced as described for intracellular pH measurements. An aliquot of the bacterial suspension was centrifuged (8,000 \times g, 5 min.) and the pellet was resuspended in sample buffer (Roti-Load 1; Carl Roth) to normalize the volume to equal OD₆₀₀. After heating (95°C, 5 min.), 10 μ l were loaded onto 10% polyacrylamide gels and separated in Tris-Tricine buffer according to manufacturer's instructions (ProSieve; Lonza, Basel, Switzerland). The gels were wet blotted (Mini Trans-Blot Cell; Bio-Rad, Munich, Germany) onto polyvinylidene fluoride membranes (Immobilon-P, 0.45 μ m; Merck-Millipore, Darmstadt, Germany). Membranes were probed using anti-HA or anti-SiiA and anti-SiiB primary antibodies (as indicated in the respective figures) (Wille *et al.*, 2014) and horseradish peroxidase-coupled anti-rabbit secondary antibodies (Jackson ImmunoResearch, Ely, UK). Signals were visualized using a Chemi-Smart 3000 chemiluminescence system (Vilber Lourmat, Eberhardzell, Germany). Blot images were processed (marker overlay, tonal range, 16- to 8-bit conversion) using Photoshop CS6 (Adobe Systems, Munich, Germany).

Acknowledgements

We would like to thank Manfred Weiss for help with data collection at beamline 14.1 at BESSY synchrotron and Max Kraner from the Biochemistry Division of the Department of Biology at Friedrich-Alexander University Erlangen-Nuremberg for mass spectrometry measurements. This work was supported by the Deutsche Forschungsgemeinschaft *via* GRK1962 (to YM), GE2533/2-2 (to RGG), HE1964/13-2 and SFB944, P4 (to MH) and *via* MU1477/9-2 (to YM).

Author contributions

PK, RGG, MH and YAM designed the research. PK, SW, CES, ATB, SH, CS, NS, DM, RGG, MH and YAM performed the experiments. PK, ATB, RGG, MH and YAM analysed the data. PK, RGG, MH and YAM wrote the paper with input from all authors.

Data availability statement

Coordinates and structure factor amplitudes have been deposited with the protein data bank with accession number: 6QVP.

References

- Adams, P.D., Afonine, P.V., Bunkoczi, G., Chen, V.B., Davis, I.W., Echols, N., *et al.* (2010) PHENIX: a comprehensive Python-based system for macromolecular structure solution. *Acta Crystallographica Section D*, **66**, 213–221.
- Afonine, P.V., Grosse-Kunstleve, R.W., Echols, N., Headd, J.J., Moriarty, N.W., Mustyakimov, M., *et al.* (2012) Towards automated crystallographic structure refinement with phenix.refine. *Acta Crystallographica Section D*, **68**, 352–367.
- Arya, G., Holtslander, R., Robertson, J., Yoshida, C., Harris, J., Parmley, J., *et al.* (2017) Epidemiology, pathogenesis, genoserotyping, antimicrobial resistance, and prevention and control of non-typhoidal *Salmonella* serovars. *Current Clinical Microbiology Reports*, **4**, 43–53.
- Atuma, C., Strugala, V., Allen, A. and Holm, L. (2001) The adherent gastrointestinal mucus gel layer: thickness and physical state in vivo. *American Journal of Physiology-Gastrointestinal and Liver Physiology*, **280**, G922–G929.
- Barlag, B. and Hensel, M. (2015) The Giant Adhesin SiiE of *Salmonella enterica*. *Molecules*, **20**, 1134–1150.
- Braun, V., Gaisser, S., Herrmann, C., Kampfenkel, K., Killmann, H. and Traub, I. (1996) Energy-coupled transport across the outer membrane of *Escherichia coli*: ExbB binds ExbD and TonB in vitro, and leucine 132 in the periplasmic region and aspartate 25 in the transmembrane region are important for ExbD activity. *Journal of Bacteriology*, **178**, 2836–2845.
- Capelli, R., Matterazzo, E., Amabili, M., Peri, C., Gori, A., Gagni, P., *et al.* (2017) Designing probes for immunodiagnosis: structural insights into an epitope targeting *Burkholderia* infections. *ACS Infectious Diseases*, **3**, 736–743.
- Cascales, E., Lloubes, R. and Sturgis, J.N. (2001) The TolQ-TolR proteins energize TolA and share homologies with the flagellar motor proteins MotA-MotB. *Molecular Microbiology*, **42**, 795–807.
- Celia, H., Noinaj, N., Zakharov, S.D., Bordignon, E., Botos, I., Santamaria, M., *et al.* (2016) Structural insight into the role of the Ton complex in energy transduction. *Nature*, **538**, 60–65.
- Crooks, G.E., Hon, G., Chandonia, J.M. and Brenner, S.E. (2004) WebLogo: a sequence logo generator. *Genome Research*, **14**, 1188–1190.
- Crump, J.A., Sjolund-Karlsson, M., Gordon, M.A. and Parry, C.M. (2015) Epidemiology, clinical presentation, laboratory diagnosis, antimicrobial resistance, and antimicrobial management of invasive *Salmonella* infections. *Clinical Microbiology Reviews*, **28**, 901–937.
- De Mot, R. and Vanderleyden, J. (1994) The C-terminal sequence conservation between OmpA-related outer membrane proteins and MotB suggests a common function in both Gram-positive and Gram-negative bacteria, possibly in the interaction of these domains with peptidoglycan. *Molecular Microbiology*, **12**, 333–334.
- Dennehy, R., Romano, M., Ruggiero, A., Mohamed, Y.F., Dignam, S.L., Troncoso, C.M., *et al.* (2017) The *Burkholderia cenocepacia* peptidoglycan-associated lipoprotein is involved in epithelial cell attachment and elicitation of inflammation. *Cellular Microbiology*, **19**, e12691.
- Emsley, P., Lohkamp, B., Scott, W.G. and Cowtan, K. (2010) Features and development of Coot. *Acta Crystallographica Section D*, **66**, 486–501.

- Evans, P. (2006) Scaling and assessment of data quality. *Acta Crystallographica Section D*, **62**, 72–82.
- Evans, D.F., Pye, G., Bramley, R., Clark, A.G., Dyson, T.J. and Hardcastle, J.D. (1988) Measurement of gastrointestinal pH profiles in normal ambulant human subjects. *Gut*, **29**, 1035–1041.
- Gerlach, R.G., Cláudio, N., Rohde, M., Jäckel, D., Wagner, C. and Hensel, M. (2008) Cooperation of *Salmonella* pathogenicity islands 1 and 4 is required to breach epithelial barriers. *Cellular Microbiology*, **10**, 2364–2376.
- Gerlach, R.G., Jäckel, D., Stecher, B., Wagner, C., Lupas, A., Hardt, W.-D., *et al.* (2007) *Salmonella* Pathogenicity Island 4 encodes a giant non-fimbrial adhesin and the cognate type 1 secretion system. *Cellular Microbiology*, **9**, 1834–1850.
- Gibson, D.G., Young, L., Chuang, R.-Y., Venter, J.C., Hutchison Iii, C.A. and Smith, H.O. (2009) Enzymatic assembly of DNA molecules up to several hundred kilobases. *Nature Methods*, **6**, 343–345.
- Glauner, B. (1988) Separation and quantification of muropeptides with high-performance liquid chromatography. *Analytical Biochemistry*, **172**, 451–464.
- Grieschl, M.H., Schmid, B., Kassler, K., Braunsmann, C., Ritter, R., Barlag, B., *et al.* (2013) Structural insight into the giant Ca²⁺-binding adhesin SiiE: implications for the adhesion of *Salmonella enterica* to polarized epithelial cells. *Structure*, **21**, 741–752.
- Heilingloh, C.S., Klingl, S., Egerer-Sieber, C., Schmid, B., Weiler, S., Muhl-Zurbes, P., *et al.* (2017) Crystal structure of the extracellular domain of the human dendritic cell surface marker CD83. *Journal of Molecular Biology*, **429**, 1227–1243.
- Holm, L. and Laakso, L.M. (2016) Dali server update. *Nucleic Acids Research*, **44**, W351–W355.
- Hosking, E.R., Vogt, C., Bakker, E.P. and Manson, M.D. (2006) The *Escherichia coli* MotAB proton channel unplugged. *Journal of Molecular Biology*, **364**, 921–937.
- Jones, S. and Thornton, J.M. (1996) Principles of protein-protein interactions. *Proceedings of the National Academy of Sciences of the United States of America*, **93**, 13–20.
- Jurus, E., Engel, D., Star, K., Monson, K., Brandi, J., Felberg, L.E., *et al.* (2018) Improvements to the APBS biomolecular solvation software suite. *Protein Science*, **27**, 112–128.
- Kabsch, W. (1976) A solution for the best rotation to relate two sets of vectors. *Acta Crystallographica Section A*, **32**, 922–923.
- Kabsch, W. (2010) XDS. *Acta Crystallographica Section D*, **66**, 125–132.
- Kelly, S.M., Jess, T.J. and Price, N.C. (2005) How to study proteins by circular dichroism. *Biochimica et Biophysica Acta (BBA) – Proteins and Proteomics*, **1751**, 119–139.
- Kojima, S., Imada, K., Sakuma, M., Sudo, Y., Kojima, C., Minamino, T., *et al.* (2009) Stator assembly and activation mechanism of the flagellar motor by the periplasmic region of MotB. *Molecular Microbiology*, **73**, 710–718.
- Kojima, S., Takao, M., Almira, G., Kawahara, I., Sakuma, M., Homma, M., *et al.* (2018) The helix rearrangement in the periplasmic domain of the flagellar stator b subunit activates peptidoglycan binding and ion influx. *Structure*, **26**, 590–598.e595.
- Krissinel, E. and Henrick, K. (2007) Inference of macromolecular assemblies from crystalline state. *Journal of Molecular Biology*, **372**, 774–797.
- Kuriyan, J. and Eisenberg, D. (2007) The origin of protein interactions and allostery in colocalization. *Nature*, **450**, 983–990.
- LaRock, D.L., Chaudhary, A. and Miller, S.I. (2015) *Salmonellae* interactions with host processes. *Nature Reviews Microbiology*, **13**, 191–205.
- Li, S., Li, T., Xu, Y., Zhang, Q., Zhang, W., Che, S., *et al.* (2015) Structural insights into YfiR sequestering by YfiB in *Pseudomonas aeruginosa* PAO1. *Scientific Reports*, **5**, 16915.
- Meng, E.C., Pettersen, E.F., Couch, G.S., Huang, C.C. and Ferrin, T.E. (2006) Tools for integrated sequence-structure analysis with UCSF Chimera. *BMC Bioinformatics*, **7**, 339.
- Minamino, T. and Imada, K. (2015) The bacterial flagellar motor and its structural diversity. *Trends in Microbiology*, **23**, 267–274.
- Minamino, T., Terahara, N., Kojima, S. and Namba, K. (2018) Autonomous control mechanism of stator assembly in the bacterial flagellar motor in response to changes in the environment. *Molecular Microbiology*, **109**, 723–734.
- Mizuno, T. (1979) A novel peptidoglycan-associated lipoprotein found in the cell envelope of *Pseudomonas aeruginosa* and *Escherichia coli*. *The Journal of Biochemistry*, **86**, 991–1000.
- Morgan, E., Bowen, A.J., Carnell, S.C., Wallis, T.S. and Stevens, M.P. (2007) SiiE is secreted by the *Salmonella enterica* serovar Typhimurium pathogenicity island 4-encoded secretion system and contributes to intestinal colonization in cattle. *Infection and Immunity*, **75**, 1524–1533.
- Morimoto, Y.V., Kojima, S., Namba, K. and Minamino, T. (2011) M153R mutation in a pH-sensitive green fluorescent protein stabilizes its fusion proteins. *PLoS ONE*, **6**, e19598.
- Mueller, U., Förster, R., Hellmig, M., Huschmann, F.U., Kastner, A., Malecki, P., *et al.* (2015) The macromolecular crystallography beamlines at BESSY II of the Helmholtz-Zentrum Berlin: current status and perspectives. *The European Physical Journal Plus*, **130**, 141.
- Nakamura, S., Kami-ike, N., Yokota, J.P., Kudo, Seishi, Minamino, T. and Namba, K. (2009) Effect of intracellular pH on the torque-speed relationship of bacterial proton-driven flagellar motor. *Journal of Molecular Biology*, **386**, 332–338.
- Ollis, A.A., Manning, M., Held, K.G. and Postle, K. (2009) Cytoplasmic membrane protonmotive force energizes periplasmic interactions between ExbD and TonB. *Molecular Microbiology*, **73**, 466–481.
- O'Neill, J., Xie, M., Hijnen, M. and Roujeinikova, A. (2011) Role of the MotB linker in the assembly and activation of the bacterial flagellar motor. *Acta Crystallographica Section D*, **67**, 1009–1016.
- Park, J.S., Lee, W.C., Yeo, K.J., Ryu, K.-S., Kumarasiri, M., Heseck, D., *et al.* (2012) Mechanism of anchoring of OmpA protein to the cell wall peptidoglycan of the gram-negative bacterial outer membrane. *The FASEB Journal*, **26**, 219–228.
- Parker, M.L., Houston, S., Wetherell, C., Cameron, C.E. and Boulanger, M.J. (2016) The structure of *Treponema pallidum* Tp0624 reveals a modular assembly of divergently functionalized and previously uncharacterized domains. *PLoS ONE*, **11**, e0166274.

- Parsons, L.M., Lin, F. and Orban, J. (2006) Peptidoglycan recognition by Pal, an outer membrane lipoprotein. *Biochemistry*, **45**, 2122–2128.
- Peters, B., Stein, J., Klingl, S., Sander, N., Sandmann, A., Taccardi, N., *et al.* (2017) Structural and functional dissection reveals distinct roles of Ca²⁺-binding sites in the giant adhesin SiiE of *Salmonella enterica*. *PLoS Path*, **13**, e1006418.
- Pettersen, E.F., Goddard, T.D., Huang, C.C., Couch, G.S., Greenblatt, D.M., Meng, E.C., *et al.* (2004) UCSF Chimera – a visualization system for exploratory research and analysis. *Journal of computational chemistry*, **25**, 1605–1612.
- Rose, P.W., Prlic, A., Bi, C., Bluhm, W.F., Christie, C.H., Dutta, S., *et al.* (2015) The RCSB protein data bank: views of structural biology for basic and applied research and education. *Nucleic Acids Research*, **43**, D345–D356.
- Roujeinikova, A. (2008) Crystal structure of the cell wall anchor domain of MotB, a stator component of the bacterial flagellar motor: implications for peptidoglycan recognition. *Proceedings of the National Academy of Sciences of the United States of America*, **105**, 10348–10353.
- Rupp, B. (2009) *Biomolecular Crystallography: Principles, Practice, and Application to Structural Biology*. New York: Garland Science, p. 850.
- Sheldrick, G. (2010) Experimental phasing with SHELXC/D/E: combining chain tracing with density modification. *Acta Crystallographica Section D*, **66**, 479–485.
- Sitkoff, D., Sharp, K.A. and Honig, B. (1994) Accurate calculation of hydration free energies using macroscopic solvent models. *The Journal of Physical Chemistry*, **98**, 1978–1988.
- Slabinski, L., Jaroszewski, L., Rychlewski, L., Wilson, I.A., Lesley, S.A. and Godzik, A. (2007) XtalPred: a web server for prediction of protein crystallizability. *Bioinformatics*, **23**, 3403–3405.
- Sparta, K.M., Krug, M., Heinemann, U., Mueller, U. and Weiss, M.S. (2016) XDSAPP2.0. *Journal of Applied Crystallography*, **49**, 1085–1092.
- Studier, F.W. (2005) Protein production by auto-induction in high-density shaking cultures. *Protein Expression and Purification*, **41**, 207–234.
- Terwilliger, T.C., Adams, P.D., Read, R.J., McCoy, A.J., Moriarty, N.W., Grosse-Kunstleve, R.W., *et al.* (2009) Decision-making in structure solution using Bayesian estimates of map quality: the PHENIX AutoSol wizard. *Acta Crystallographica Section D*, **65**, 582–601.
- Terwilliger, T.C., Grosse-Kunstleve, R.W., Afonine, P.V., Moriarty, N.W., Zwart, P.H., Hung, L.-W., *et al.* (2008) Iterative model building, structure refinement and density modification with the PHENIX AutoBuild wizard. *Acta Crystallographica Section D*, **64**, 61–69.
- The UniProt, C. (2017) UniProt: the universal protein knowledgebase. *Nucleic Acids Research*, **45**, D158–D169.
- Vollmer, W. (2015) Chapter 6 – Peptidoglycan. In: Tang, Y.-W., Sussman, M., Liu, D., Poxton, I. and Schwartzman, J. (Eds.) *Molecular Medical Microbiology (Second Edition)*. Boston: Academic Press, pp. 105–124.
- Wang, W. and Malcolm, B.A. (1999) Two-stage PCR protocol allowing introduction of multiple mutations, deletions and insertions using QuikChange Site-Directed Mutagenesis. *BioTechniques*, **26**, 680–682.
- Wille, T., Wagner, C., Mittelstadt, W., Blank, K., Sommer, E., Malengo, G., *et al.* (2014) SiiA and SiiB are novel type I secretion system subunits controlling SPI4-mediated adhesion of *Salmonella enterica*. *Cellular Microbiology*, **16**, 161–178.
- Wojdyla, J.A., Cutts, E., Kaminska, R., Papadakos, G., Hopper, J.T.S., Stansfeld, P.J., *et al.* (2015) Structure and function of the *Escherichia coli* Tol-Pal stator protein TolR. *Journal of Biological Chemistry*, **290**, 26675–26687.
- Zhou, J., Sharp, L.L., Tang, H.L., Lloyd, S.A., Billings, S., Braun, T.F. and Blair, D.F. (1998) Function of protonatable residues in the flagellar motor of *Escherichia coli*: a critical role for Asp 32 of MotB. *Journal of Bacteriology*, **180**, 2729–2735.
- Zhu, S., Takao, M., Li, N., Sakuma, M., Nishino, Y., Homma, M., *et al.* (2014) Conformational change in the periplasmic region of the flagellar stator coupled with the assembly around the rotor. *Proceedings of the National Academy of Sciences of the United States of America*, **111**, 13523–13528.

Supporting Information

Additional supporting information may be found online in the Supporting Information section at the end of the article.

SUPPLEMENTARY INFORMATION

Structural and functional characterisation of SiiA, an auxiliary protein from the SPI-4-encoded type I secretion system from *Salmonella enterica*

Peter Kirchweber¹, Sigrid Weiler¹, Claudia Egerer-Sieber¹, Anna-Theresa Blasl¹, Stefanie Hoffmann², Christiane Schmidt², Nathalie Sander³, Dorothee Merker³, Roman G. Gerlach², Michael Hensel³ and Yves A. Muller¹

¹ Division of Biotechnology, Department of Biology, Friedrich-Alexander-University Erlangen- Nürnberg, D-91052 Erlangen, Germany

² Robert Koch-Institut, Wernigerode, Germany

³ Abt. Mikrobiologie and CellNanos, Universität Osnabrück, Osnabrück, Germany

Table S1. Melting temperatures analysed by CD-monitored thermal unfolding

Table S2. Analytical size exclusion chromatography results

Table S3. Peak assignment in the anomalous difference density map

Table S4. Ca-rmsd values between SiiA-PD monomers

Table S5. Ca-rmsd values obtained upon comparing SiiA-PD dimers

Table S6. Peptidoglycan co-isolation quantification

Table S7. Primers used for generation of expression constructs, site-directed mutagenesis, and pH sensors

Table S8. Bacterial strains used in this study

Table S9. Plasmids strains used in this study

Fig. S1. Characterisation of SiiA-PD and ppr-SiiA

Fig. S2. Structure comparison of SiiA-PD with various OmpA-like PG-binding domains

Fig. S3. PG binding of MotB-PD, SiiA-PD, SiiA-R162A-PD, SiiA-R167L-PD and SiiA-S197E-PD

Fig. S4. Structural integrity of SiiA variants and of MotB-PD probed by CD spectroscopy at various pH values

Fig. S5. Inducible expression of *siiAB*

Fig. S6. Calibration curve of R-pHluorin-M153R Additional references

Table S1. Melting temperatures analysed by CD-monitored thermal unfolding

Protein	T_m [°C]	pH	Figure
ppr-SiiA	76.8 ± 0.4	7.4	S1D
SiiA-PD	76.9 ± 0.3	5.8	S4A
SiiA-PD	79.1 ± 1.5	7.4	S1D
SiiA-PD	74.0 ± 0.3	8.0	S4A
ppr-SiiA-R162A	86.1 ± 0.8	7.4	S4G
SiiA-R162A-PD	76.2 ± 0.7	5.8	S4B
SiiA-R162A-PD	75.2 ± 0.3	8.0	S4B
SiiA-R167L-PD	92.7 ± 2.8	5.8	S4C
SiiA-R167L-PD	90.4 ± 1.8	8.0	S4C
SiiA-S197E-PD	81.6 ± 0.6	5.8	S4D
SiiA-S197E-PD	75.9 ± 0.4	8.0	S4D
MotB-PD	63.2 ± 0.1	5.8	S4E
MotB-PD	63.2 ± 0.2	8.0	S4E

Table S2. Analytical size exclusion chromatography results

Protein	MW [kDa]	V_e [mL]	
Dextranblue		7.856 (= V_0)	a ^a
Coalbumin	75	9.2	b ^a
Carboanhydrase	29	11.4	c ^a
RNase A	13.7	12.9	d ^a
Aproteine	6.5	14.9	e ^a
ppr-SiiA	44.84 ^b	10.34	
SiiA-PD	17.31 ^b	12.52	
ppr-SiiA-R162A	44.34 ^b	10.37	
SiiA-R162-PD	17.07 ^b	12.56	

^a The elution volumes of the protein standards are marked with the letters a, b, c, d and e in Fig. S1b, c).

^b Apparent molecular weights (MW) calculated via a least squared fit of a trendline based upon the elution volume (V_e). Formular: $y = -0.189 * x + 3.609$ ($R^2 = 0.999$).

Table S3. Peak assignment in the anomalous difference density map

Number	Peak height (peak intensity/standard deviation)	Corresponding aa ^a
1	18.7	MSE, E.172
2	18.1	MSE, F.186
3	17.9	MSE, D.186
4	17.0	MSE, E.186
5	17.0	MSE, E.172
6	16.5	MSE, F.172
7	16.0	MSE, C.148/A
8	15.5	MSE, B.148/A
9	15.4	MSE, D.148/A
10	15.0	MSE, A.148
11	13.8	MSE, F.148
12	13.6	MSE, E.148
13	13.3	MSE, B.186
14	13.0	MSE, C.186
15	12.8	MSE, A.186
16	11.3	MSE, A.172
17	11.2	MSE, C.172
18	9.5	MSE, B.172
19	6.5	MSE, B.148/B
20	5.8	MSE, C.148/B
21	5.4	MSE, D.148/B

^a Residues are numbered as follows: residue, chain.residue number/alternative conformation. MSE = Seleno-methionine residue.

Table S4. C_α-rmsd values between SiiA-PD monomers

	SiiA_A ^a	SiiA_B	SiiA_C	SiiA_D	SiiA_E	SiiA_F
SiiA_A	-	1.0 ^b	0.1	1.0	0.2	0.9
SiiA_B		-	1.0	0.2	1.0	0.2
SiiA_C			-	1.0	0.1	0.9
SiiA_D				-	1.0	0.3
SiiA_E					-	0.9
SiiA_F						-

^a White- and grey-shaded protein chain entries belong to group 1 and 2, respectively.

^b Values calculated with program LSQKAB (Kabsch, 1976).

Table S5. C_α-rmsd values obtained upon comparing SiiA-PD dimers

	SiiA_AB	SiiA_BA	SiiA_CD	SiiA_DC	SiiA_EF	SiiA_FE
SiiA_AB	-	2.6 ^{a,b}	0.2	2.6	0.2	2.6
SiiA_BA		-	2.6	0.2	2.6	0.2
SiiA_CD			-	2.6	0.3	2.6
SiiA_DC				-	2.6	0.3
SiiA_EF					-	2.7
SiiA_FE						-

^a Values calculated with program LSQKAB (Kabsch, 1976).

^b The SiiA-AB dimer is compared to the SiiA-BA dimer such that chain A is superimposed onto chain B and at the same time chain B onto chain A. This applies accordingly to all dimer comparisons.

Table S6. Peptidoglycan co-isolation quantification

	Signal intensity anti HA	Signal intensity anti OmpA ^a	Ratio SiiA/OmpA
WT SiiA	30,774	14,594	2.11
SiiA-R162A	13,459	14,203	0.95
Ratio WT /mut	2.29	1.02	

^a Antibody staining against WT OmpA was used as a control to normalize the precipitated PG amount.

Table S7. Primers used for generation of expression constructs, site-directed mutagenesis, and pH sensors

Primer	Sequence (5' -> 3')	Usage
R162A-fwd	GACATCTCTTCTCTGACTCTCTAGCACTGGGATATGAAG	Recombinant protein expression
R162A-rev	GTTCCATATCCAGTGCTAGAGAGTCAGAGAAAGAGATGTC	Recombinant protein expression
R167L-fwd	GGGATATGAACTGGGAATTATTTTG	Recombinant protein expression
R167L-rev	AGTCGTAGAGAGTCAGAG	Recombinant protein expression
S197E-fwd	AAGTACAACGGAAAAAGCTATTATCACGAC	Recombinant protein expression
S197E-rev	GATGCTGCGGAGTTAACAC	Recombinant protein expression
R120A-For	GTATCATGGCGCTGAGAAGCTTTTC	SDM ^a
R120A-Rev	GTAATAACAAGCTCATTTTTGTAG	SDM
D159A-For	CTCTTCTCTGCCTCTACGAC	SDM
D159A-Rev	ATGTCTGCCTGAGGAATAAC	SDM
R162A-For	TGACTCTAGCACTGGGATATGAACG	SDM
R162A-Rev	GAGAAAGAGATGCTGCC	SDM
L163A-For	CTCTCTACGAGCGGATATGAACGG	SDM
L163A-Rev	TCAGAGAAAGAGATGCTG	SDM
R167L-For	GGGATATGAACTGGGAATTATTTTG	SDM
R167L-Rev	AGTCGTAGAGAGTCAGAG	SDM
S197E-For	AAGTACAACGGAAAAAGCTATTATCACGAC	SDM
S197E-Rev	GATGCTGCGGAGTTAACAC	SDM
MotB-D32N-Gbs-for	GGAAAATTGCCTACGCCAATTTTATGACGGCGATGATGCC	Intracellular pH measurements
MotB-D32N-Gbs-rev	GCCATCATCGCGCTATAAAATGGCGTAGCAATTTTCC	Intracellular pH measurements
MotB-pTAC-Gbs-rev	AACCAAGATGTCGAGTTAACCCATCATGACCTCGTTCCGCTTTTG	Intracellular pH measurements
pTAC-Gbs-for	CGATCTCGACGAGTGAGAGAAG	Intracellular pH measurements
pTAC-Gbs-rev	CATATTATCTCTGTGTGAAATTGTTATCC	Intracellular pH measurements
pTAC-MotA-Gbs-for	GATAACAATTTACACAGGAGATATAATATGCTTATCTTATTAGGTTACCTG	Intracellular pH measurements
pTAC-SiiA-Gbs-for	GATAACAATTTACACAGGAGATATAATATGGAAGACGAAAGTAATCCG	Intracellular pH measurements
pWRG692-Gbs-for	CCATGGATCGATAGCTGGTC	Intracellular pH measurements
R-pHluorin-pTAC-Gbs-rev	TGAAAATCTTCTCACTCGTCGAGATCGTTATTATTATACAGTTCATC	Intracellular pH measurements
R-pHluorin-pTAC-Gbs-rev	TGAAAATCTTCTCACTCGTCGAGATCGTTATTATTATACAGTTCATC	Intracellular pH measurements
R-pHluorin-tetR-Gbs-for	ATAGAGAAAGATGGCAAGAGGAGATATCATGTCTAAAGGCGAAGAAGCTG	Intracellular pH measurements
R-pHluorin-tetR-Gbs-for	ATAGAGAAAGATGGCAAGAGGAGATATCATGTCTAAAGGCGAAGAAGCTG	Intracellular pH measurements
SiiA-R162A-pTAC-Gbs-for	ATCTCTTCTCTGACTCTCTAGCGCTGGGATATGAACGGGAATTATTTGATGAAAGAG	Intracellular pH measurements
SiiA-R162A-pTAC-Gbs-rev	CTCTTTCATCAAATAATCCCCGTTATATCCAGCGCTAGAGAGTCAGAGAAAGAGAT	Intracellular pH measurements
SiiB462-tetR-Gbs-rev	GTAACCAAGATGTCGAGTTAACCCATCGATTAATCTTCATTTTTTCTCCTTG	Intracellular pH measurements
TetR-Gbs-for	TCGATGGGTGGTTAACTCGAC	Intracellular pH measurements
TetR-Gbs-rev	GATATCCTCCTCTTGCCATC	Intracellular pH measurements

^a SDM, site-directed mutagenesis.

Table S8. Bacterial strains used in this study

Designation	relevant genotype	Source/reference
<i>Salmonella enterica</i> serovar Typhimurium		
NCTC 12023	WT	NCTC Colindale, lab collection
MvP771	Δ <i>siIA</i> ::FRT	(Wille <i>et al.</i> , 2014)
MvP103	Δ <i>sseC</i> :: <i>aphT</i> , Kan ^R	(Medina <i>et al.</i> , 1999)
<i>Escherichia coli</i>		
OneShot Mach1-T1 ^R	F- ϕ 80(<i>lacZ</i>) Δ M15 Δ <i>lacX74</i> <i>hsdR</i> (rK-mK+) Δ <i>recA1398</i> <i>endA1</i> <i>tonA</i> <i>hsdR</i> (rK-mK+) Δ <i>recA1398</i> <i>endA1</i> <i>tonA</i>	Sigma-Aldrich
XL10Gold	F' <i>proA</i> ⁺ <i>B</i> ⁻ <i>lacI</i> ⁻ Δ (<i>lacZ</i>)M15 <i>zzf</i> ::Tn10 (Tet ^R)/ <i>thiA</i> Δ (<i>argF-lacZ</i>)U169 <i>phoA</i> <i>glnV44</i> Φ 80 Δ (<i>lacZ</i>)M15 <i>gyrA96</i> <i>recA1relA1</i> <i>endA1</i> <i>thi-1</i> <i>hsdR17</i>	NEB
BL21(DE3)	F ⁻ <i>ompT</i> <i>hsdS</i> ₈ (<i>r</i> _S m ₈) <i>gal</i> <i>dcm</i> (DE3)	Novagen

Table S9. Plasmids strains used in this study

Designation	relevant genotype	Source/reference
pWSK29	low copy number vector, Amp ^R	(Rong Fu & Kushner, 1991)
p3187	P _{<i>siIA</i>} <i>siIA</i> ::HA in pWSK29	(Gerlach <i>et al.</i> , 2007)
p4478	P _{<i>siIA</i>} <i>siIA</i> ::HA R120A	This study
p4479	P _{<i>siIA</i>} <i>siIA</i> ::HA D159A	This study
p4480	P _{<i>siIA</i>} <i>siIA</i> ::HA R162A	This study
p4481	P _{<i>siIA</i>} <i>siIA</i> ::HA L163A	This study
p4482	P _{<i>siIA</i>} <i>siIA</i> ::HA R167A	This study
p4483	P _{<i>siIA</i>} <i>siIA</i> ::HA S197E	This study
pTAC-MAT-Tag-2	<i>tac</i> promoter, Amp ^R	Sigma-Aldrich
pWRG603	P _{<i>tsdA</i>} :: <i>siIF</i> G500E:: <i>scfp3a</i> P _{<i>tsdA</i>} :: <i>siIB</i> :: <i>syfp2</i> , Amp ^R	(Wille <i>et al.</i> , 2014)
pWRG850	P _{<i>tsdA</i>} :: <i>siAB</i> - <i>tetR</i> P _{<i>tsdA</i>} :: <i>pHluorin</i> -M153R, Amp ^R	This study
pWRG851	P _{<i>tsdA</i>} :: <i>siA</i> D13N- <i>B</i> - <i>tetR</i> P _{<i>tsdA</i>} :: <i>pHluorin</i> -M153R, Amp ^R	This study
pWRG855	P _{<i>tsdA</i>} :: <i>motAB</i> - <i>tetR</i> P _{<i>tsdA</i>} :: <i>pHluorin</i> -M153R, Amp ^R	This study
pWRG862	P _{<i>tsdA</i>} :: <i>motAB</i> D32N- <i>tetR</i> P _{<i>tsdA</i>} :: <i>pHluorin</i> -M153R, Amp ^R	This study
pWRG898	P _{<i>tsdA</i>} :: <i>siA</i> R162A- <i>B</i> - <i>tetR</i> P _{<i>tsdA</i>} :: <i>pHluorin</i> -M153R, Amp ^R	This study
pET-15B	Expression vector, Amp ^R	Novagen
pBT127	pET-15B, <i>ppr-siIA</i>	This study
pBT380	pET-15B, <i>ppr-siIA</i> R162A	This study
pBT427	pET-15B, <i>motB</i> -PD	This study
pBT444	pET-15B, <i>ppr-siIA</i> R167L	This study
pBT445	pET-15B, <i>ppr-siIA</i> S197E	This study

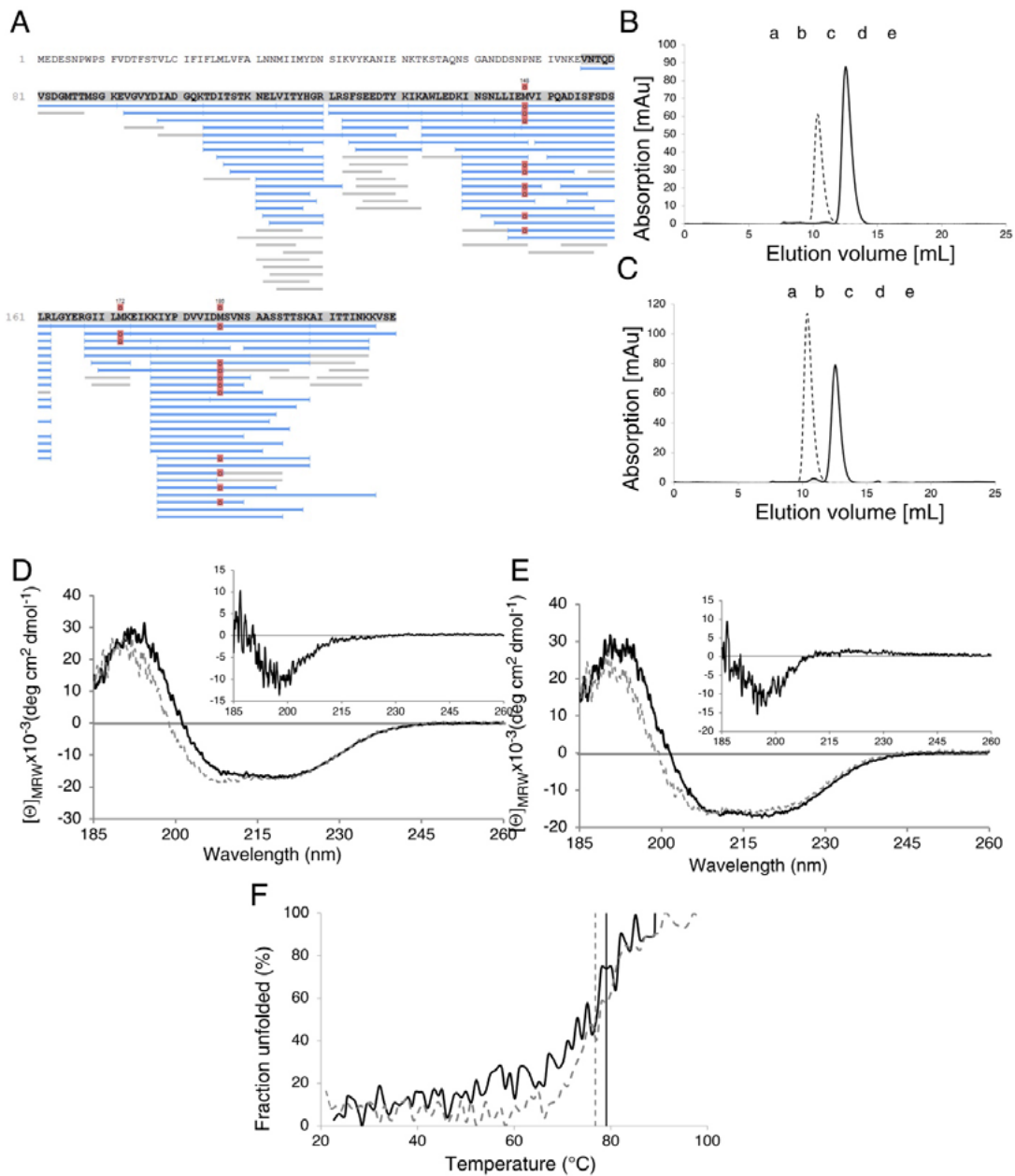


Fig. S1. Characterisation of SiiA-PD and ppr-SiiA. **A.** ESI mass spectrometry analysis of tryptic fragments of SiiA-PD (blue lines). Grey lines indicate observed fragments below the quality score (false discovery rate < 20%). Red dots mark oxidized methionines. Good sequence coverage is observed from residue Thr104 to Lys206. However, additional fragments are observed beyond this range. The analysis does not allow for the unambiguous determination of the exact starting and ending residue of the protease-generated SiiA-PD fragment. **B.** Analytical size exclusion chromatography analysis of ppr-SiiA (broken line) and SiiA-PD (black line). **C.** Analytical size exclusion chromatography analysis of ppr-SiiA-R162A (broken line) and SiiA-R162A-PD (black line). In panels B and C, the labels a, b, c, d and e indicate the elution volumes of the protein standards listed in Table S2. **D** and **E** display the CD spectra of SiiA-PD (black solid line) and ppr-SiiA (grey dashed line) recorded at pH 5.8 (panel D) and pH 8.0 (panel E). The insets in D and E show the difference spectrum calculated by subtracting the CD-signal of SiiA-PD from ppr-SiiA. **F** shows the thermal denaturation analysis of SiiA-PD (black solid line) and ppr-SiiA (grey dashed line) recorded at pH 7.4. The T_M -values are marked with vertical lines in the respective shading. The results are summarized in Table S1.

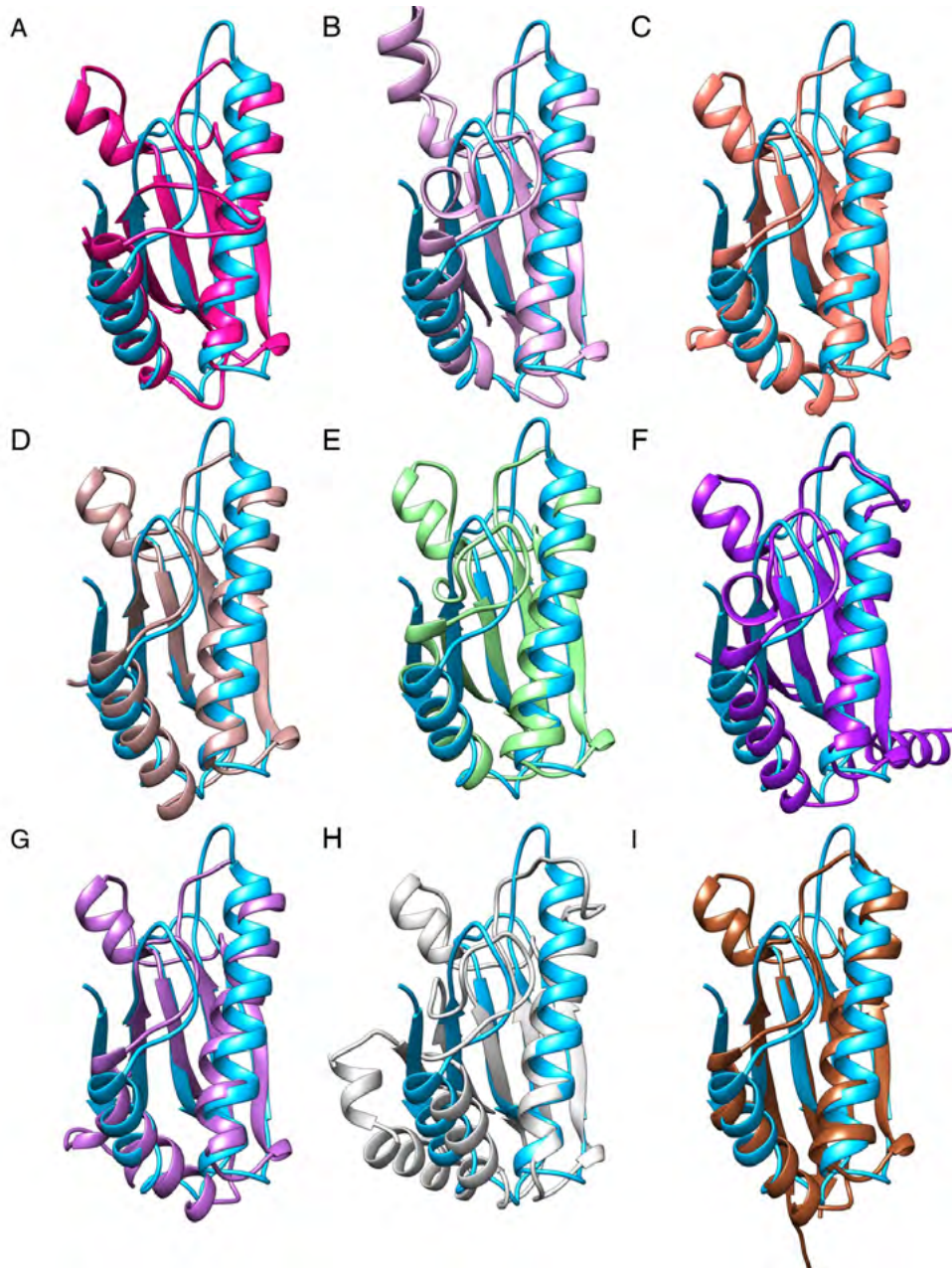


Fig. S2. Structure comparison of SiiA-PD with various OmpA-like PG-binding domains. Structural homologues of SiiA-PD identified with the DALI server (Holm & Laakso, 2016) (see also Table 2 in main text): SiiA-PD (light blue) in comparison to A. PAL from *T. pallidum* (PDB-ID: 5IJR, (Rose *et al.*, 2015)), B. OmpA from *K. pneumoniae* (PDB-ID: 5NHX), C. PAL from *B. cenocepacia* (PDB-ID: 5N2C), D. YifB from *P. aeruginosa* (PDB-ID: 4ZHW), E. TagL from *E. coli* (PDB-ID: 5M38), F. MotB from *H. pylori* (PDB-ID: 3S02), G. PAL from *B. cenocepacia* (PDB-ID: 5LKW), H. PomB from *V. alginolyticus* (PDB-ID: 3WPW) and I. OmpA from *A. baumannii* (PDB-ID: 4G88).

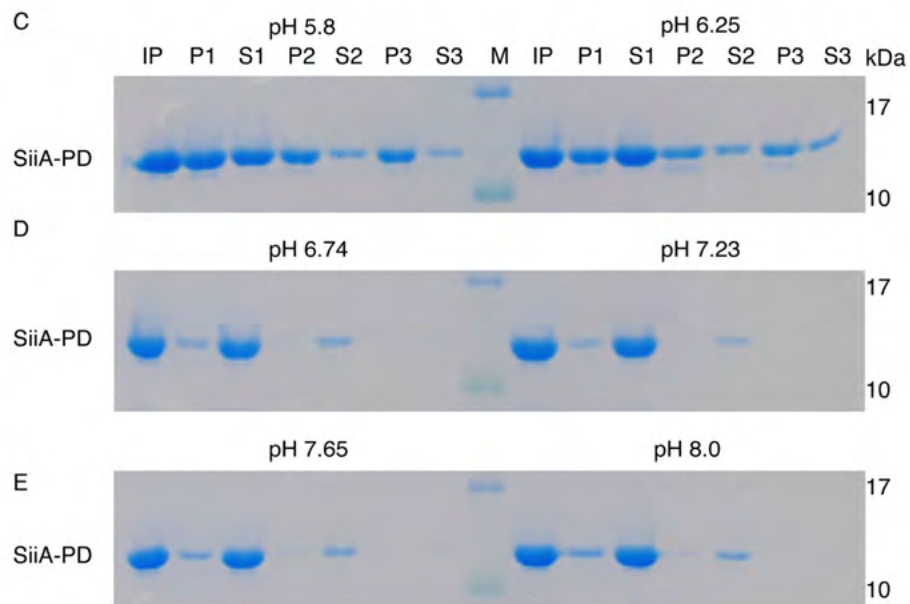


Fig. S3. PG binding of MotB-PD, SiiA-PD, SiiA-R162A-PD, SiiA-R167L-PD and SiiA-S197E-PD. A. PG pulldown assays performed at pH 5.8 (left side) and pH 8.0 (right side) with the different protein variants and analysed by SDS-PAGE. Input (IP), pellet (P1-3) and supernatant (S1-3) fractions, as well as the relevant marker bands are indicated. Shown are the original electrophoretic gels from which the bands that are displayed individually in Fig. 5 of the main text have been extracted. B. SDS-PAGE analysis of the input samples of the protein variants used in A. The molecular weights of selected marker bands are reported on the left side of the gel. C, D and E. Binding of SiiA-PD to PG at different pH values investigated with PG pulldown assays. The lanes are labelled as in panel A.

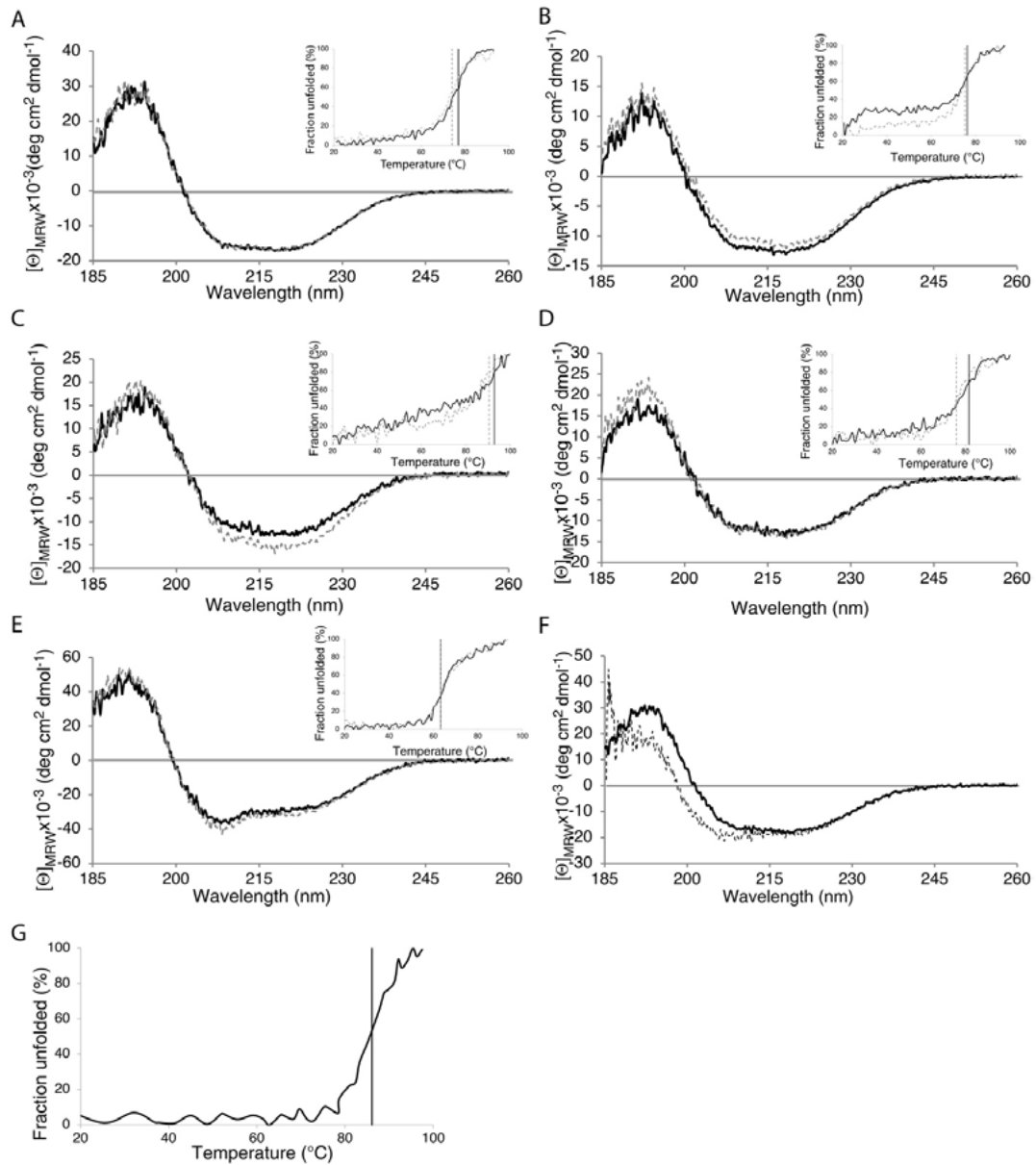


Fig. S4. Structural integrity of SiiA variants and of MotB-PD probed by CD spectroscopy at various pH values. CD spectra of A. SiiA-PD, B. SiiA-R162A-PD, C. SiiA-R167L-PD, D. SiiA-S197E-PD and E. MotB-PD fragments. Insets display the CD-monitored thermal denaturation of the respective proteins. In panels A to E contiguous black lines and dashed grey lines show the proteins in 10 mM potassium phosphate-based buffers at pH 5.8 and 8.0, respectively. F. CD spectra of SiiA-R162A-PD (black line) and ppr-SiiA-R162A (grey dashed line) recorded in 10 mM potassium phosphate-based buffers at pH 7.4. G. shows the thermal denaturation of ppr-SiiA-R162A at pH 7.4. The observed melting temperatures are summarized in Table S1 and indicated by vertical lines in all panels/insets.

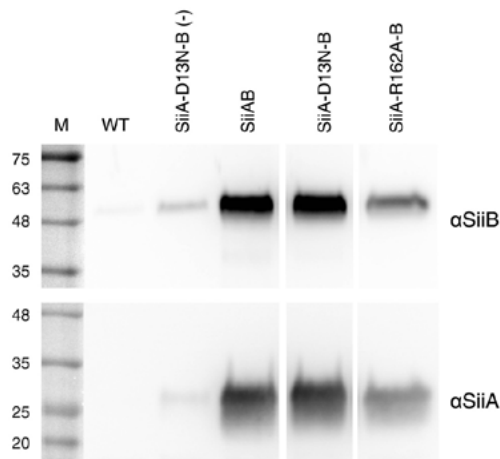


Fig. S5. Inducible expression of *siiAB*. *S. Typhimurium* NCTC 12023 WT bacteria were transformed with plasmids allowing for co-production of SiiAB with R-pHluorin-M153R. Bacteria were subcultured with or without (-) the addition of 10 mM IPTG to induce expression of the indicated SiiAB complexes as described for intracellular pH measurements. The samples were separated in a 10% SDS polyacrylamide gel and blotted. The proteins were detected by specific antibodies against SiiA and SiiB. WT bacteria without plasmid served as control. One Western blot from three independent experiments with similar results is shown. M = protein marker with molecular sizes in kDa as indicated.

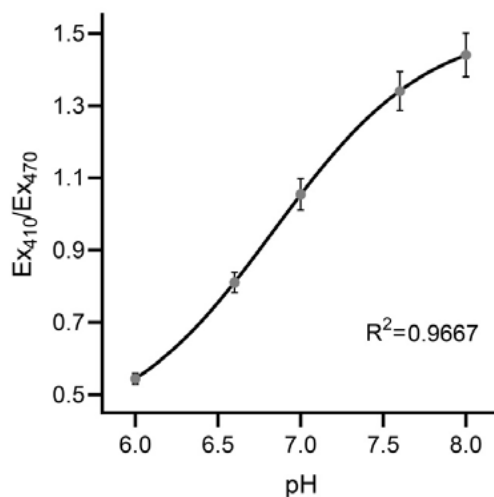


Fig. S6. Calibration curve of R-pHluorin-M153R. Defined external pH values were correlated to the ratio of pHluorin fluorescence in the presence of 30 μ M CCCP with excitation 410 nm, emission 509 nm / excitation 470 nm, emission 509 nm (Ex410/Ex470). The coefficient of determination (R^2) is supplied for the 4-parameter logistic function used to fit the data. Data shown are mean and SEM of three independent experiments.

Additional references

Gerlach, R.G., Jäckel, D., Stecher, B., Wagner, C., Lupas, A., Hardt, W.-D., and Hensel, M. (2007) Salmonella Pathogenicity Island 4 encodes a giant non-fimbrial adhesin and the cognate type I secretion system. *Cellular Microbiology* **9**: 1834-1850.

Holm, L., and Laakso, L.M. (2016) Dali server update. *Nucleic Acids Research* **44**: W351-W355. Kabsch, W. (1976) A solution for the best rotation to relate two sets of vectors. *Acta Crystallographica Section A* **32**: 922-923.

Medina, E., Paglia, P., Nikolaus, T., Müller, A., Hensel, M., and Guzmán, C.A. (1999) Pathogenicity Island 2 Mutants of *Salmonella typhimurium* Are Efficient Carriers for Heterologous Antigens and Enable Modulation of Immune Responses. *Infection and Immunity* **67**: 1093-1099.

Rong Fu, W., and Kushner, S.R. (1991) Construction of versatile low-copy-number vectors for cloning, sequencing and gene expression in *Escherichia coli*. *Gene* **100**: 195-199.

Rose, P.W., Prlic, A., Bi, C., Bluhm, W.F., Christie, C.H., Dutta, S., Green, R.K., Goodsell, D.S., Westbrook, J.D., Woo, J., Young, J., Zardecki, C., Berman, H.M., Bourne, P.E., and Burley, S.K. (2015) The RCSB Protein Data Bank: views of structural biology for basic and applied research and education. *Nucleic Acids Res* **43**: D345-356.

Wille, T., Wagner, C., Mittelstadt, W., Blank, K., Sommer, E., Malengo, G., Dohler, D., Lange, A., Sourjik, V., Hensel, M., and Gerlach, R.G. (2014) SiiA and SiiB are novel type I secretion system subunits controlling SPI-4-mediated adhesion of *Salmonella enterica*. *Cell Microbiol* **16**: 161-178.

III.3. Scarless deletion of up to seven methyl-accepting chemotaxis genes with an optimized method highlights key function of CheM in *Salmonella Typhimurium*

Stefanie Hoffmann¹, Christiane Schmidt¹, Steffi Walter¹, Jennifer K. Bender² and Roman G. Gerlach¹

¹ Project Group 5, Robert Koch Institute, Wernigerode, Germany

² Division of Nosocomial Pathogens and Antibiotic Resistances, Department of Infectious Diseases, Robert Koch Institute, Wernigerode, Germany

RESEARCH ARTICLE

Scarless deletion of up to seven methyl-accepting chemotaxis genes with an optimized method highlights key function of CheM in *Salmonella* Typhimurium

Stefanie Hoffmann¹, Christiane Schmidt¹, Steffi Walter¹, Jennifer K. Bender², Roman G. Gerlach^{1*}

1 Project Group 5, Robert Koch Institute, Wernigerode, Germany, **2** Division of Nosocomial Pathogens and Antibiotic Resistances, Department of Infectious Diseases, Robert Koch Institute, Wernigerode, Germany

* GerlachR@rki.de

Abstract

Site-directed scarless mutagenesis is an essential tool of modern pathogenesis research. We describe an optimized two-step protocol for genome editing in *Salmonella enterica* serovar Typhimurium to enable multiple sequential mutagenesis steps in a single strain. The system is based on the λ Red recombinase-catalyzed integration of a selectable antibiotic resistance marker followed by replacement of this cassette. Markerless mutants are selected by expressing the meganuclease I-SceI which induces double-strand breaks in bacteria still harboring the resistance locus. Our new dual-functional plasmid pWRG730 allows for heat-inducible expression of the λ Red recombinase and tet-inducible production of I-SceI. Methyl-accepting chemotaxis proteins (MCP) are transmembrane chemoreceptors for a vast set of environmental signals including amino acids, sugars, ions and oxygen. Based on the sensory input of MCPs, chemotaxis is a key component for *Salmonella* virulence. To determine the contribution of individual MCPs we sequentially deleted seven MCP genes. The individual mutations were validated by PCR and genetic integrity of the final seven MCP mutant WRG279 was confirmed by whole genome sequencing. The successive MCP mutants were functionally tested in a HeLa cell infection model which revealed increased invasion rates for non-chemotactic mutants and strains lacking the MCP CheM (Tar). The phenotype of WRG279 was reversed with plasmid-based expression of CheM. The complemented WRG279 mutant showed also partially restored chemotaxis in swarming assays on semi-solid agar. Our optimized scarless deletion protocol enables efficient and precise manipulation of the *Salmonella* genome. As demonstrated with whole genome sequencing, multiple subsequent mutagenesis steps can be realized without the introduction of unwanted mutations. The sequential deletion of seven MCP genes revealed a significant role of CheM for the interaction of *S. Typhimurium* with host cells which might give new insights into mechanisms of *Salmonella* host cell sensing.

OPEN ACCESS

Citation: Hoffmann S, Schmidt C, Walter S, Bender JK, Gerlach RG (2017) Scarless deletion of up to seven methyl-accepting chemotaxis genes with an optimized method highlights key function of CheM in *Salmonella* Typhimurium. PLoS ONE 12(2): e0172630. doi:10.1371/journal.pone.0172630

Editor: Nicholas J. Mantis, New York State Department of Health, UNITED STATES

Received: December 19, 2016

Accepted: February 7, 2017

Published: February 17, 2017

Copyright: © 2017 Hoffmann et al. This is an open access article distributed under the terms of the [Creative Commons Attribution License](https://creativecommons.org/licenses/by/4.0/), which permits unrestricted use, distribution, and reproduction in any medium, provided the original author and source are credited.

Data Availability Statement: All sequencing data files are available through BioProject (<http://www.ncbi.nlm.nih.gov/bioproject/>) PRJNA355390 and SRA (<http://www.ncbi.nlm.nih.gov/sra/>), e.g. NGS sequencing reads can be accessed through SRR5062192 and SRR5062193.

Funding: This project was funded in part by the 'Deutsche Forschungsgemeinschaft' (www.dfg.de) grant GE 2533/2-2 and an intramural research grant of the Robert Koch Institute (www.rki.de) to RGG.

Competing interests: The authors have declared that no competing interests exist.

Introduction

The ability for precise manipulation of bacterial genomes is of utmost importance in modern microbiological research. Although there is a long history of manipulating bacterial genomes, the application of phage-derived recombinases constitute a breakthrough in bacterial genetics [1, 2]. These “recombineering” strategies jointly exploit the ability of phage λ Red RecE/T or of phage λ Red recombinases to use DNA fragments of less than 40 bp as substrates for homologous recombination [3]. Direct integration of these homologous sequences within short oligonucleotides is a great advantage which makes cloning of helper plasmids obsolete.

Over the years a vast number of different strategies and ever more refined protocols have been developed with a clear trend towards “scarless” genome manipulations [4–9]. These techniques are usually based on two steps starting with the integration of a selectable marker (e.g. an antibiotic resistance gene) followed by seamless replacement of that particular marker. For the second step efficient methods to select for loss of the marker are required. Here, accumulation of toxic metabolites based on *tetAR* [6, 10], sucrose sensitivity utilizing the *sacB* gene [7, 9], *rpsL*-mediated streptomycin sensitivity in resistant hosts [11, 12], the CcdA/CcdB toxin-antitoxin system [13] or I-SceI induced double-strand breaks (DSB) [4, 5, 14–17] were successfully used. The meganuclease I-SceI of *S. cerevisiae* has an unusually long recognition site of 18 bp which is statistically not present in bacterial genomes [18]. Mechanistically, the I-SceI site is co-integrated into the genome with the antibiotic resistance cassette during the first recombination step. Expression of the I-SceI enzyme after the second step selects for successful recombinants. Thus the precise and independent regulated expression of λ Red recombinase and I-SceI is a prerequisite for maximum efficiency and reliability of this method. Whereas the above mentioned methods rely on double-stranded DNA (dsDNA) as substrate for recombination, the chromosomal integration of short single-stranded DNA (ssDNA) oligonucleotides has also been demonstrated [3]. Recombineering of ssDNA requires only the function of λ Beta/RecT ssDNA binding proteins and functions without selectable or counter-selectable markers [19, 20]. However, methyl-directed mismatch repair reduces efficiency of the method and thereby increasing the effort of screening for correct clones [21].

Recombineering techniques are not only limited by the efficiency of the applied systems but also in general by the amenability of microorganisms to the Red/Rec recombinases. Alternative approaches are explored not only to avoid this limitation but to make genome editing even more efficient. The CRISPR/Cas9 (clustered regularly interspaced short palindromic repeats and its associated protein, Cas9) system promises many advantages and is tremendously successful for editing eukaryotic genomes. Unfortunately, its application in bacteria is still limited. Amongst other reasons this is mainly due to the lack of a non-homologous end joining mechanism for DNA repair in most bacteria (reviewed in [22]). Nevertheless, successful CRISPR/Cas9-mediated genome editing including the introduction of deletions, insertions, and point mutations, was demonstrated when combined with λ Red recombinase functions [23]. The system was especially promoted for introducing multiple genome modifications since it does not rely on the cyclic integration and excision of a selectable marker [24]. However, the method requires careful design of the specific sequences for the gene-targeting protospacer adjacent motif (PAM) in order to prevent potential off-target activity. In addition, the PAM sequence together with the single guide RNA has to be supplied on a plasmid which needs to be cloned and, ideally, sequence-verified for each target gene to achieve high efficiency in bacteria [8, 23, 24]. Until further optimization of CRISPR/Cas9 system for bacteria, refined scarless recombineering protocols are an efficient and cost-effective tool for genome editing. Based on our previously developed method [4] we optimized the system to enhance efficiency and enable fast and reliable sequential modifications of the *Salmonella Typhimurium* (STM) genome.

We wanted to demonstrate the functionality of the optimized protocol in STM deleting seven genes encoding for methyl-accepting chemotaxis proteins (MCPs). MCPs are sensor molecules which respond to a variety of environmental cues including amino acids, sugars, ions and oxygen. Receptor signaling is initiated by reversible ligand binding at the periplasmic domains of dimeric MCPs [25]. Upon activation the receptor-bound kinase CheA phosphorylates the response regulator CheY. Through binding to the flagellar motor complex CheY influences the direction of flagellar rotation. As a result environmental signals perceived by MCPs control chemotactic swimming (reviewed in [26]). *Salmonella* expresses homologs to the *E. coli* MCPs Tsr, Tar, Trg and Aer. Tsr and Tar detect the amino acids serine and aspartate, respectively [27, 28]. Although the *Salmonella* Tar homolog CheM shows only 79% sequence identity with Tar of *E. coli* it was also demonstrated to bind and respond to aspartate [29, 30]. Trg is responsible for the sensing of the sugars glucose, galactose and ribose [31]. Alterations of the redox potential can be detected by Aer [32]. In contrast to the above mentioned MCPs the chemotaxis sensors Tap, Tip, McpA, McpB and McpC are only found in *Salmonella*. Tap was shown to sense citrate and phenol [33] whereas McpB/C mediate a repellent response towards L-cystine [34]. Currently no function for McpA [35], lacking a transmembrane domain, and Tip which is devoid of the periplasmic sensor domain is known.

We used a thoroughly defined set of MCP mutants to investigate the impact of individual MCPs on the ability of *Salmonella* to invade HeLa cells. Our infection experiments revealed an increased invasion rate for mutants lacking CheM indicating a detrimental effect of CheM-mediated chemotaxis in this infection model.

Results and discussion

Design and construction of system components

In our previously published system [4] the arabinose-inducible expression of the λ Red recombinase was combined with the meganuclease I-SceI under control of the *tetA* promoter in plasmid pWRG99 [36]. Although the system allowed for efficient generation of scarless deletions or single nucleotide exchanges, it required curing and re-transformation of pWRG99 between each recombination step [4]. We speculated that leaky expression of the λ Red proteins from the P_{BAD} promoter in the absence of glucose [37] could have selected for inactive recombinases. Therefore we reasoned that a differently regulated λ Red expression plasmid might circumvent this problem. The pSC101-based pSIM5 harbors the phage λ p_L operon comprising the genes *exo*, *bet* and *gam* under the control of the temperature-sensitive repressor CI857 that enables heat-inducible expression of λ Red recombinase functions [38]. Moreover, the pSIM5 plasmid allows for simple curing by its temperature-sensitive *repA_{ts}* origin of replication. From the functional perspective pSIM5 exhibited 10- to 60-fold higher recombination efficiency compared to the arabinose-inducible λ Red expression plasmid pKD119, which is similar to pKD46 except for the tetracycline resistance gene [38]. The combined λ Red/I-SceI expression plasmid pWRG730 was constructed by integrating the tetracycline-inducible I-SceI expression cassette of pWRG99 into the highly efficient pSIM5 vector (Fig 1A).

Together with pWRG730 new FRT-free template plasmids were constructed based on pBluescript II SK+. Flp recombinase target (FRT) sites as present on the old template plasmid pWRG100 negatively interfered with DSB-based counterselection [4]. To circumvent this problem, the kanamycin resistance cassette of pKD4 [36] was integrated in two orientations relative to the I-SceI cleavage site thereby producing pWRG717 (Fig 1B) and pWRG832 (not shown). To provide an alternative selection marker, a spectinomycin resistance cassette originating from pDL1098 [39] was cloned in both orientations which resulted in pWRG829 and

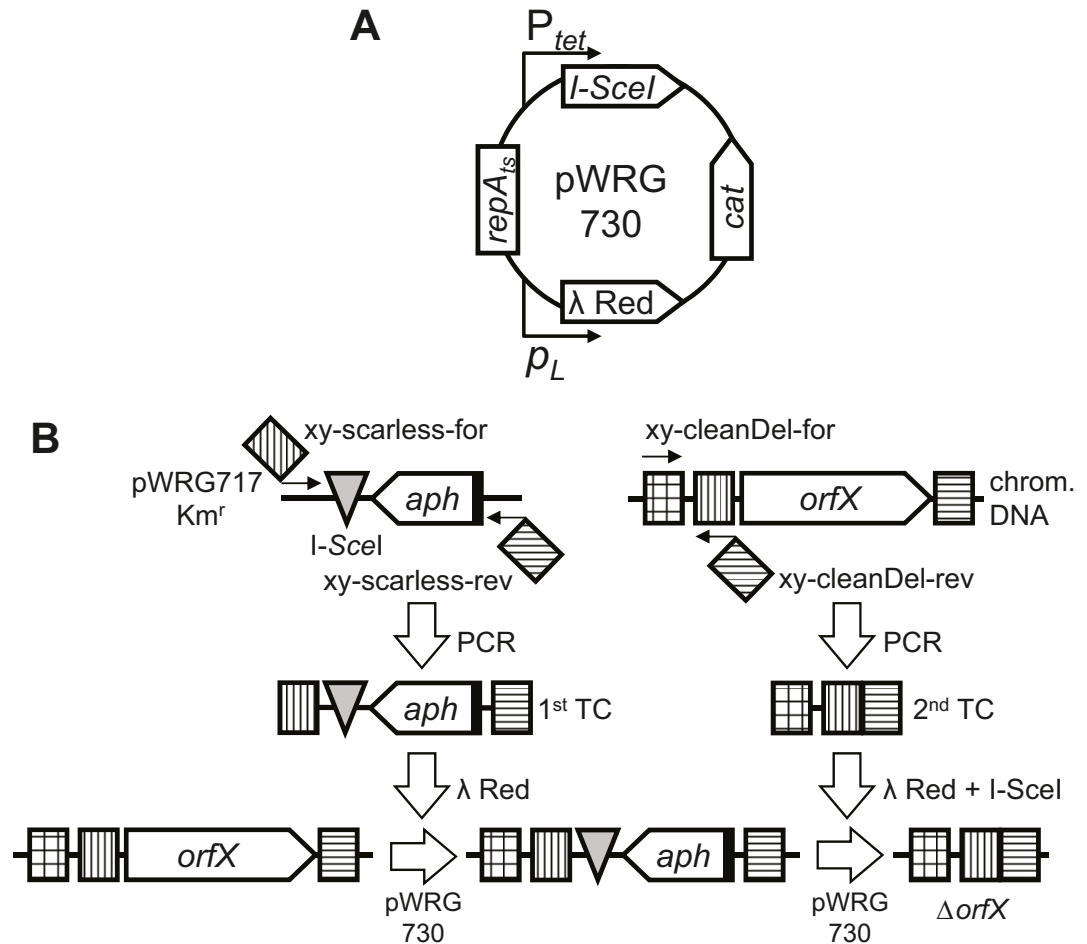


Fig 1. Overview of the method. (A) Schematic representation of the functional units of plasmid pWRG730. The operon containing λ Red recombinase functions is under control of the heat-inducible phage-derived promoter p_L . Expression of the I-SceI meganuclease is controlled by a tetracycline-inducible promoter (P_{tet}). A chloramphenicol resistance cassette (*cat*) is used for selection purposes. Due to its temperature-sensitive origin of replication (*repA_{ts}*) the plasmid can be easily cured at elevated growth temperatures. (B) Representation of the two-step scarless deletion methodology. A kanamycin resistance cassette (*aph*) is amplified together with an I-SceI cleavage site (grey triangle) from pWRG717 with two 60-mer primers each containing site-specific homology extensions at their 5'-ends (striped squares). Chromosomal integration of this first targeting construct (TC) is achieved by λ Red recombinase expression from pWRG730. The 2nd TC is also generated by PCR using chromosomal DNA as template and contains a direct fusion of up- and downstream homology regions. After genomic integration of the 2nd TC using λ Red recombinase, successful recombinants are selected by I-SceI expression from pWRG730. A detailed description of the method can be found in the main text.

doi:10.1371/journal.pone.0172630.g001

pWRG865 (data not shown). Although all four template vectors are suitable for the introduction of deletions, heterologous DNA or nucleotide exchanges, we routinely used the template vectors with the resistance gene in reversed orientation compared to the I-SceI cleavage site (pWRG717, pWRG829) (Fig 1B and not shown) to minimize polar effects in the first recombination step. The vectors with the resistance cassette in same orientation to the I-SceI cleavage site enable the simple integration of the antibiotic resistance gene in an artificial operon structure to serve as a reporter gene as described for *Vibrio cholerae* [39].

Sequential deletion of MCP genes

To evaluate the functionality of the system we decided to sequentially delete all genes encoding for known MCPs in *S. Typhimurium* strain NCTC 12023. The MCP genes were deleted in the following order: *aer*, *tcp*, *tsr*, *trg*, *cheM* (*tar*), *mcpC* (STM14_3893) and *mcpB* (STM14_3817) [35]. Each scarless deletion involved two successive recombination steps: (i) integration of a kanamycin resistance cassette amplified from pWRG717 and (ii) replacement of that resistance cassette by a PCR fragment containing the fused flanking regions of the gene to be deleted (Fig 1B) [4]. Similar strategies have been described before but with Red recombinase and I-SceI functionality provided on different plasmids [5] or requiring multiple rounds of culturing in selective medium for maximum efficiency [17]. In contrast to our first approach [4] the new plasmid pWRG730 encoding the recombinase and I-SceI meganuclease could be maintained within the bacteria during the whole sequential gene deletion process through selection with chloramphenicol (Cm) and keeping the cells at 30 °C.

Primers 'xy-scarless-for' and 'xy-scarless-rev' were used for amplification of an I-SceI cleavage site together with a kanamycin resistance cassette from template vector pWRG717 to produce the 1st targeting construct (TC) for recombination. Whereas the 20 bases at the 3' ends of the primers were designed to bind to the template vectors, the 40 bases at each 5' end are homologous to regions up- and downstream of '*orfX*' and thus determine the genome integration site (Fig 1B). Electrocompetent *Salmonella* with heat-induced λ Red recombinase were transformed with the 1st TC and transformants were selected on kanamycin (Km) and Cm-containing LB agar plates. Proper integration of the I-SceI/kanamycin cassette and replacement of each MCP gene was verified in both directions by PCR. The TC for the second recombination step was also generated by PCR. The construct represents a fusion of upstream and downstream homologous regions of the target deletion site. The homologous upstream sequence was amplified from wild-type (WT) chromosomal DNA as template using a short upstream-binding 'xy-cleanDel-for' primer and a 60-mer 'xy-cleanDel-rev' primer. The downstream homology region comprises the 40 bases of the 5' end of 'xy-cleanDel-rev' (Fig 1B). This PCR-based approach to obtain a 2nd TC is much more flexible and cost-effective for introducing deletions or for site-directed mutagenesis compared to phosphorylated oligonucleotides [4]. PCR using 60-mer primers with 40 bases homology extensions would be also the means of choice for insertion of heterologous DNA sequences. Alternatively, synthetic DNA with compatible terminal homology regions can be used in the 2nd recombination step hence providing maximal flexibility. This step was selected on anhydrotetracycline (AHT) containing LB agar plates which induced I-SceI expression from pWRG730 allowing only the growth of successful recombinants devoid of the I-SceI site (Fig 1B).

Verification of mutants

Successful scarless deletion of each MCP gene was verified after the 2nd recombination step by PCR using primers which bind up- and downstream of the site of deletion, respectively. Using these primer combinations, mutant alleles should result in shorter fragments compared to the WT situation. The theoretical fragment lengths for mutant and WT of each MCP gene are listed in Table 1. Starting from the single deletion strain WRG246 Δ *aer* all scarless mutants were checked whether their MCP alleles corresponded to the expected genotype. Agarose gels that summarize the individual allele types for each of the MCP genes of the seven sequential deletion strains are depicted in S1 Fig. No PCR fragments were observed for the '*aer*' locus in the Δ 6 (WRG277) and Δ 7 (WRG279) strains. Since the *mcpC* gene is located adjacent to *aer*, deletion of *mcpC* removed the reverse primer binding site in these mutants. All other observed fragments were of the expected size as listed in Table 1. Fig 2A shows a direct comparison of

Table 1. Expected fragment sizes of verification PCRs.

Locus	Forward primer	Reverse primer	Fragment WT [bp]	Fragment after deletion [bp]
<i>aer</i>	Aer-Delcheck-for2	McpC-Delcheck-rev	2605	1370
<i>tcp</i>	Tcp-Delcheck-for	Tcp-Delcheck-rev	2150	509
<i>tsr</i>	Tsr-Delcheck-for	Tsr-Delcheck-rev	2203	544
<i>trg</i>	Trg-Delcheck-for	Trg-Delcheck-rev	2153	530
<i>cheM (tar)</i>	CheM-Delcheck-for	CheM-Delcheck-rev	2555	896
<i>mcpC</i>	McpC-Delcheck-for	McpC-Delcheck-rev	2330	768
<i>mcpB</i>	McpB-Delcheck-for2	McpB-Delcheck-rev	2414	813

doi:10.1371/journal.pone.0172630.t001

the PCR products originating from WT genomic DNA or from WRG279 lacking all seven MCP genes ($\Delta 7$) which confirmed the absence of the MCP genes in the $\Delta 7$ strain. Finally, Sanger sequencing of the PCR fragments verified the expected nucleotide sequence of all MCP deletion sites (data not shown).

Expression of highly efficient phage recombinases such as λ Red can cause unwanted recombination events within the chromosome [40]. This is especially evident if “scars” e.g. from recombinases such as Flp or Cre accumulate in the genome during multi-step mutagenesis protocols. It has been shown that a set of mutated recombination sites provides one possible but laborious solution to circumvent this problem [41]. There is no need for such amendments using a scarless protocol as presented in this study. Given the mutagenic activity of extended high-level expression of λ Red recombinase [40], it is very important to strictly limit λ Red expression when multiple successive mutation steps are carried out in the same bacterial background. With the pSIM5-based Red expression plasmid pWRG730 10–15 minutes of heat induction is sufficient for efficient recombination [42].

Despite all these precautions we could not completely exclude accumulation of mutations in the strain WRG279. To address this, Illumina-based whole genome sequencing of our NCTC 12023 WT laboratory strain and of the $\Delta 7$ MCP mutant WRG279 was carried out. The obtained sequencing reads were mapped to the published genome sequence of STM ATCC 14028S which is isogenic with strain NCTC 12023. In contrast to NCTC 12023 WT, no sequencing reads of WRG279 were mapped to the deleted MCP genes (Fig 2B). Furthermore, the coverage data of WRG279 confirmed the precise deletion sites as determined by the homology regions of the 2nd TC (not shown). The ATCC 14028S genome data was also used as a reference to identify single nucleotide polymorphisms (SNPs). From the total 23 SNPs identified comparing ATCC 14028S with NCTC 12023 and WRG279 (data not shown) only two were unique for WRG279 (Table 2). One SNP resulted in a silent substitution within STM14_2710 and was detectable in all MCP mutants (Table 2). The other SNP was located within the putative ribosome binding site (RBS) of the *yceB* gene (STM14_1333) and appeared only in the last three mutants generated (Table 2). YceB is a predicted outer membrane lipoprotein and found to be downregulated in a resistant *Salmonella* strain isolated after a single challenge with nalidixic acid. Thus, this isolate exhibited additional resistance to tetracycline and chloramphenicol [43]. In contrast the WRG279 mutant showed minimal inhibitory concentrations (MICs) for both antibiotics similar to the parental NCTC 12023 WT strain in broth dilution assays (S2 Fig). However, modulation of YceB activity beyond antibiotic resistance due to altered protein levels cannot be excluded. These results argue against the *yceB* RBS mutation as an adaptation to the prolonged exposure to chloramphenicol, AHT, or both. Furthermore, both identified mutations are at chromosomal loci distantly located from the sites of recombination which makes their emergence unlikely to be directly linked to the recombination procedures applied. These low impact mutations might rather reflect natural

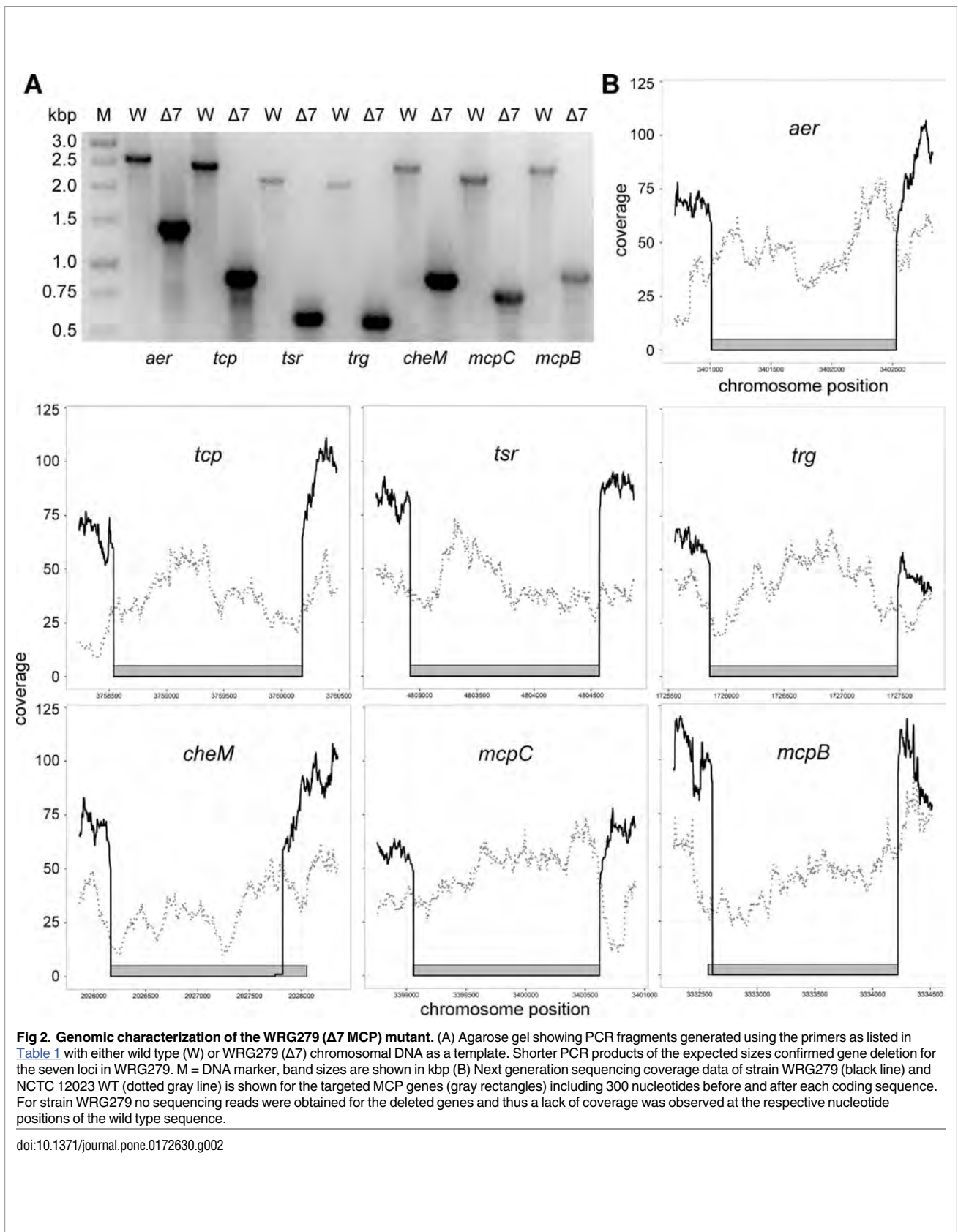


Table 2. Distribution of single nucleotide polymorphisms unique for WRG279.

Strain	Position* 1,208,402 RBS of <i>yceB</i> (STM14_1333)	Position* 2,345,688 synonymous mutation within STM14_2710
NCTC 12023 WT	A	G
WRG246	A	A
WRG255	A	A
WRG260	A	A
WRG264	A	A
WRG269	G	A
WRG277	G	A
WRG279	G	A

* reference: ATCC 14028S genome.

doi:10.1371/journal.pone.0172630.t002

genomic plasticity from prolonged laboratory handling as shown recently for chronic *Salmonella* infections [44, 45].

In summary our data highlight that the optimized system based on the dual-functional pWRG730 in combination with the pWRG717-derived kanamycin resistance cassette allows for fast and reliable manipulation of the *Salmonella* genome. This highly efficient tool is likely applicable in other bacteria amenable for the Red recombinase system, for example *E. coli* [36], *Shigella* spp. [46], *Yersinia enterocolitica* [47], *Y. pestis* [9], *Pseudomonas aeruginosa* [7] or *Pantoea ananatis* [48].

Functional characterization of the MCP deletion strains

Having confirmed the genetic integrity of the mutants we went on to functionally characterize the strains. It has been demonstrated previously that bacterial motility is an important factor for efficient invasion of host cells [49, 50]. Actively swimming bacteria encounter shear forces which bring them within close proximity of the host cell surface. This “near surface swimming” promotes *Salmonella*-cell interactions and cooperative invasion of membrane ruffles [51]. By utilizing a *cheY* mutant which uncouples motility from chemotaxis [26] it was demonstrated that directed swimming is not required for near surface swimming [51]. However, *in vivo* results using streptomycin-pretreated mice underlined the importance of chemotaxis as a major virulence function besides motility [52]. We set out to test whether the lack of multiple MCPs influences *Salmonella* invasion in a HeLa-based infection model. Quantification of intracellular bacteria was done after one hour and was normalized to STM WT (set to 1). Very low amounts of intracellular bacteria were detected for an *invC* deletion mutant harboring a non-functional SPI-1 encoded type three secretion system (T3SS-1) (Fig 3A, left panel). Our data revealed an approximately 2-fold increased invasion rate for the *cheY* mutant suggesting an inhibitory effect of chemotaxis on HeLa invasion (Fig 3A, left panel). This result is in line with previous observations where “smooth” swimming mutants such as *cheY* or *cheA* exhibited increased invasion capabilities in HEp-2 cells [49]. In contrast a “tumbling only” *cheB* mutant was shown to have lower tissue culture invasion rates [49] presumably due to decreased near surface swimming. Next we used the set of successive MCP deletion mutants to elucidate the impact of specific chemotactic signaling on HeLa cell invasion. Surprisingly, we found a clear phenotypical separation of two groups of mutants. The first group comprising mutants $\Delta 1$ (WRG246 Δaer) to $\Delta 4$ (WRG264 Δaer , Δtcp , Δtsr , Δtrg) exhibited invasion rates very similar to WT whereas the remaining mutants, which lack five to seven MCP genes, showed an elevated invasion comparable to a *cheY* mutant (Fig 3A, left panel).

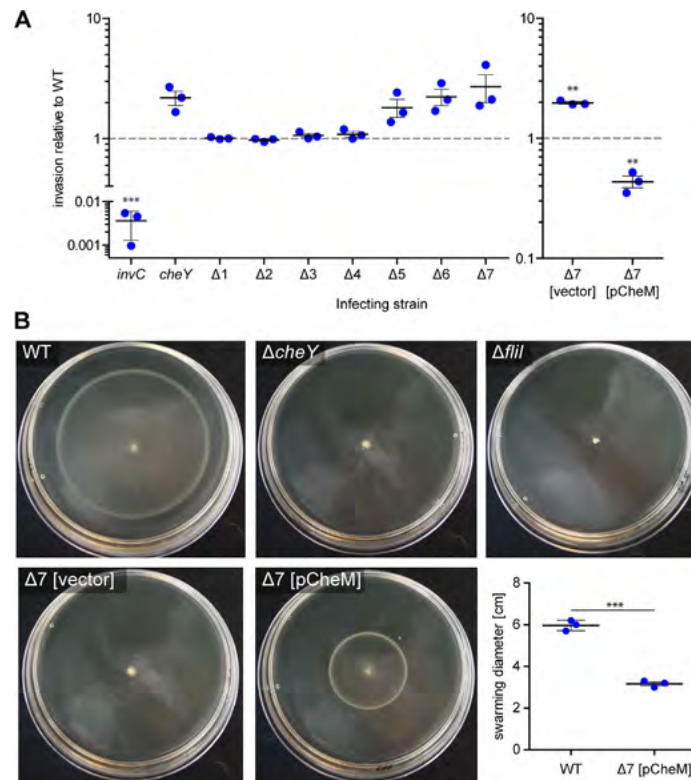


Fig 3. Functional characterization of the WRG279 mutant. (A) HeLa cells were infected with different STM strains and relative invasion rates compared to STM WT were calculated after one hour of infection. An *invC* mutant lacking a functional T3SS-1 was used as a negative control for invasion and a motile but non-chemotactic *cheY* mutant was included to evaluate the impact of directed motility. The $\Delta 1$ to $\Delta 7$ strains represent sequential MCP deletions as follows: $\Delta 1$ = WRG246 Δaer ; $\Delta 2$ = WRG255 Δaer , Δtcp ; $\Delta 3$ = WRG260 Δaer , Δtcp , Δtsr ; $\Delta 4$ = WRG264 Δaer , Δtcp , Δtsr , Δtrg ; $\Delta 5$ = WRG269 Δaer , Δtcp , Δtsr , Δtrg , $\Delta cheM$; $\Delta 6$ = WRG277 Δaer , Δtcp , Δtsr , Δtrg , $\Delta cheM$, $\Delta mcpC$; $\Delta 7$ = WRG279 Δaer , Δtcp , Δtsr , Δtrg , $\Delta cheM$, $\Delta mcpC$, $\Delta mcpB$. The right panel shows the invasion rates of the $\Delta 7$ strain complemented with pCheM (pWRG847) or transformed with the empty vector pWSK29 (vector). Statistical significance was calculated using a one sample *t* test against the hypothetical value 1.0 and was defined as ** for $p < 0.01$ and *** for $p < 0.001$. (B) Swarming phenotypes of different *Salmonella* strains as indicated on LB soft agar plates. Depicted is one representative out of three similar experiments. The diagram in the lower right panel shows the diameter of the swarming rings of *S. Typhimurium* WT and the $\Delta 7$ MCP mutant complemented with a CheM expression plasmid or a vector control as described in (B). Data of three independent biological replicates including means and standard deviations are shown. Statistical significance was calculated using a two-tailed paired Student's *t* test and was defined as *** for $p < 0.001$.

doi:10.1371/journal.pone.0172630.g003

Deletion of the *cheM* gene is the common feature of mutants $\Delta 5$ (WRG269) to $\Delta 7$ (WRG279). The observed phenotypes suggested that only CheM (Tar) is responsible for chemotactic signaling in the HeLa infection model supported by previous results obtained with HEp-2 cells [49]. To investigate this effect in more detail we complemented the $\Delta 7$ MCP strain WRG279 with the low-copy number plasmid pCheM (pWRG847) harboring the *cheM* gene under control of its natural promoter. While WRG279 transformed with the empty vector pWSK29 exhibited an elevated invasion similar to the *cheY* mutant, invasion of WRG279 [pCheM] was significantly decreased compared to WT (Fig 3A, right panel). We thus hypothesize that the six to eight plasmid copies per cell [53] led to an increased expression level of *cheM* which in turn fostered

CheM-dependent chemotactic signaling with higher tumbling rates. CheM can directly sense aspartate [29]. Aspartate is not a component of the DMEM medium but small amounts of different amino acids are present in the FCS used during infection. The cell- and receptor density-dependent signaling preference of Tar-Tsr receptor complexes for either aspartate or serine could explain the apparent lack of chemotactic response from Tsr in our assays [54]. In the HeLa infection model aspartate or other so far uncharacterized CheM ligands might be liberated from the host cells thereby triggering a chemotactic response of *Salmonella*.

In a further set of experiments we wanted to characterize the MCP mutant strains in swarming assays on soft agar plates. As expected we observed a decrease in swarming diameter with more MCP genes deleted which reflects their increasing incapacity to perceive chemotactic signals (S3 Fig). Interestingly, the mutant WRG269 expressing only the MCPs McpB and McpC did show residual chemotactic movement whereas the successive WRG277, with *mcpC* deleted, was incapable of directed motility (S3 Fig). Like for WRG277, no chemotactic swarming could be observed for mutants lacking *cheY* or for the non-motile *fliI* mutant (Fig 3B). The $\Delta 7$ mutant WRG279 harboring the empty vector pWSK29 was phenotypically indistinguishable from the *cheY* mutant. Because both mutants are still motile they exhibited a slightly “blurred” inoculation site, which is most likely the result of “tumbly” swimming (Fig 3B). Introduction of the CheM complementation plasmid pCheM in WRG279 partially restored its chemotactic capacity (Fig 3B, lower right panel). Intriguingly, a single swarming ring could be detected for the CheM-complemented $\Delta 7$ MCP mutant which diameter roughly corresponded to the inner (CheM/Tar) ring observed for STM WT (Fig 3B). For STM WT two concentric rings were observed in some experiments which expanded over time to the agar plate periphery (Fig 3B). It has been demonstrated for *E. coli* that the outer ring corresponds to cells sensing serine through Tsr and the inner ring is composed of bacteria which sense aspartate by Tar [27, 28].

Our results and those of others [49] suggest that functional chemotaxis alone is disadvantageous for *Salmonella* invasion of HeLa and HEp-2 cells *in vitro*. However, the *in vivo* environment might be far more complex with chemotaxis being an important virulence factor [52, 55]. The optimized mutagenesis protocol described in the present study enabled us to efficiently generate a set of mutants lacking up to seven MCP genes. Further functional characterization of this set of MCP mutants *in vitro* identified CheM/Tar as the only MCP responding to chemotactic signals in a HeLa-based infection model. Future *in vivo* testing of these and other mutants, successfully generated by the developed procedure, might help to decipher the environmental signals *Salmonella* responds to during natural infection.

Materials and methods

Bacterial strains and plasmids

All strains used are listed in Table 3. Bacteria were routinely grown in LB media supplemented with 50 $\mu\text{g}/\text{mL}$ carbenicillin (Cb) (Carl Roth, Mannheim, Germany), 25 $\mu\text{g}/\text{mL}$ kanamycin (Km) (Carl Roth), 10 $\mu\text{g}/\text{mL}$ chloramphenicol (Cm) (Carl Roth), 50 $\mu\text{g}/\text{mL}$ spectinomycin (Sp) (Carl Roth) or 100 ng/mL anhydrotetracycline (AHT) (# 37919 Sigma-Aldrich, Schnelldorf, Germany) if required. Table 4 gives an overview of all the plasmids used in this study.

PCR and cloning

All primers used for cloning are listed in S1 Table. For construction of the I-SceI *aph* template plasmid pWRG717, an I-SceI cleavage site was fused to the kanamycin resistance cassette of pKD4 by PCR using primers XhoI-*aph*-for2 and Aph-I-SceI-KnpI-rev2. The PCR fragment was cloned via XhoI/KpnI in pBluescript II SK+ (Agilent Technologies, Waldbronn, Germany). For

Table 3. Strains used in this study.

Strain	Relevant characteristic(s)	Source or Reference
MvP818	NCTC 12023 $\Delta invC$ FRT	[56]
MvP1212	NCTC 12023 $\Delta cheY$ FRT	[57]
MvP1213	NCTC 12023 $\Delta flil$ FRT	[58]
NCTC 12023	Wild type, Nal^s , isogenic to ATCC 14028	NCTC, Colindale, UK
WRG244	NCTC 12023 $\Delta aer::I$ -SceI <i>aph</i> , Km^r	This study
WRG246	NCTC 12023 Δaer	This study
WRG247	NCTC 12023 $\Delta aer \Delta tcp::I$ -SceI <i>aph</i> , Km^r	This study
WRG255	NCTC 12023 $\Delta aer \Delta tcp$	This study
WRG259	NCTC 12023 $\Delta aer \Delta tcp \Delta tsr::I$ -SceI <i>aph</i> , Km^r	This study
WRG260	NCTC 12023 $\Delta aer \Delta tcp \Delta tsr$	This study
WRG263	NCTC 12023 $\Delta aer \Delta tcp \Delta tsr \Delta trg::I$ -SceI <i>aph</i> , Km^r	This study
WRG264	NCTC 12023 $\Delta aer \Delta tcp \Delta tsr \Delta trg$	This study
WRG266	NCTC 12023 $\Delta aer \Delta tcp \Delta tsr \Delta trg \Delta cheM::I$ -SceI <i>aph</i> , Km^r	This study
WRG269	NCTC 12023 $\Delta aer \Delta tcp \Delta tsr \Delta trg \Delta cheM$	This study
WRG276	NCTC 12023 $\Delta aer \Delta tcp \Delta tsr \Delta trg \Delta cheM \Delta mcpC::I$ -SceI <i>aph</i> , Km^r	This study
WRG277	NCTC 12023 $\Delta aer \Delta tcp \Delta tsr \Delta trg \Delta cheM \Delta mcpC$	This study
WRG278	NCTC 12023 $\Delta aer \Delta tcp \Delta tsr \Delta trg \Delta cheM \Delta mcpC \Delta mcpB::I$ -SceI <i>aph</i> , Km^r	This study
WRG279	NCTC 12023 $\Delta aer \Delta tcp \Delta tsr \Delta trg \Delta cheM \Delta mcpC \Delta mcpB$	This study

doi:10.1371/journal.pone.0172630.t003

construction of all other plasmids including the spectinomycin template plasmid pWRG829, assembly cloning of PCR fragments was used [59]. Primers pWSK29-Gbs-for and pKD4-Gbs-rev were used with pWRG717 as template to obtain a PCR fragment containing the vector and the I-SceI cleavage site. A spectinomycin resistance cassette was amplified with primers pSK-aad9-Gbs-for and pKD-aad9-Gbs-rev from plasmid pDL1098 [39] and subsequently

Table 4. Plasmids used in this study.

Plasmid	Relevant characteristic(s)	Source or Reference
pDL1098	Temperature-sensitive <i>mTn10</i> delivery vector, Cm^r , Sp^r	[39]
pKD4	<i>aph</i> resistance cassette flanked by FRT sites, λ Pir dependent replication, Km^r , Ap^r	[36]
pSIM5	temperature-sensitive replication (30°C) and Red recombinase expression (42°C), Cm^r	[38]
pWRG99	pKD46 [36] derivative, temperature-sensitive replication (30°C), arabinose-inducible expression of Red recombinase, Tet-inducible expression of I-SceI, Ap^r	[4]
pWRG717	pBluescript II SK+ derivative, <i>aph</i> resistance cassette and I-SceI cleavage site, Km^r , Ap^r	This study
pWRG730	pSIM5 [38] derivative, temperature-sensitive replication (30°C) and Red recombinase expression (42°C), Tet-inducible expression of I-SceI, Cm^r	This study
pWRG829	pBluescript II SK+ derivative, <i>aad9</i> resistance cassette and I-SceI cleavage site, Sp^r , Ap^r	This study
pWRG832	pWRG717 derivative, <i>aph</i> resistance cassette reversed, Km^r , Ap^r	This study
pWRG841	$P_{cheM}::cheM$ in pCRII-TOPO, Km^r , Ap^r	This study
pWRG847	pCheM; $P_{cheM}::cheM$ in pWSK29, Ap^r	This study
pWRG865	pWRG829 derivative, <i>aad9</i> resistance cassette reversed, Sp^r , Ap^r	This study
pWSK29	Low-copy-number vector, Ap^r	[53]

doi:10.1371/journal.pone.0172630.t004

combined with the first PCR product to obtain pWRG829. In template plasmids pWRG832 and pWRG865 the antibiotic resistance cassettes are in reversed orientation compared to pWRG717 and pWRG829, respectively. Here, pBluescript II SK+ was amplified with primers pWSK29-Gbs-for and -rev. The resistance cassettes were amplified from pWRG717 and pWRG829 with primer pairs Aph-I-SceI-pSK-Gbs-for/Aph-pSK-Gbs-rev2 and Aad9-I-SceI-pSK-Gbs-for/Aad9-pSK-Gbs-rev, respectively. A two-fragment assembly of each of the resistance cassettes with the vector PCR fragment led to the final plasmids. The heat-inducible Red recombinase expression plasmid pSIM5 [38] was linearized by PCR using primers pSIM-Gbs-for and pSIM-Gbs-rev. The tetracycline-inducible I-SceI expression cassette was amplified with primers pSIM-TetR-Gbs-for2 and pSIM-I-SceI-Gbs-rev using pWRG99 [4] as template. The two PCR fragments were combined by assembly cloning resulting in plasmid pWRG730. The region containing the *cheM* promoter and coding sequence was amplified from chromosomal DNA using primers CheM-Delcheck-for and CheM-pWSK-Gbs-rev. The PCR fragment was blunt-cloned in pCR II-TOPO (Thermo Fisher Scientific, Karlsruhe, Germany) resulting in plasmid pWRG841 which was subsequently digested with KpnI and XbaI. The *cheM*-containing fragment was gel-purified and cloned in the similarly-digested pWSK29 to obtain pWRG847 (pCheM).

Generation of mutants

All primers used to amplify the kanamycin resistance cassette from pWRG717 and to obtain a TC from *Salmonella* genomic DNA are listed in [S1 Table](#). The desalted primers were purchased from Integrated DNA Technologies (Munich, Germany). For amplification of the first targeting construct forward primers consisting of the 3' sequence 5' -AGGGTTTCCCAGTCACGAC-3', which binds to all pBluescript II SK+ -based template vectors, and a 5' 40 bases sequence homologous to the genomic target site were used. The 60-mer reverse primers were similarly designed with the following 3'-located sequence binding to the template vectors: 5' -TGCTTCCGGCTCGTATGTTG-3'. Overnight (O/N) cultures of *Salmonella* harboring pWRG730 were grown at 30°C in LB supplemented with 10 µg/mL chloramphenicol. O/N cultures were re-inoculated 1:100 in fresh medium and grown aerated to an OD₆₀₀ of 0.3 to 0.5. Red recombinase expression was induced for 12.5 minutes in a shaking water bath at 42°C [42]. After that bacteria were immediately put on ice and electro-competent cells were prepared essentially as described before [4]. Cells were transformed with 100–500 ng purified 1st TC using a Micropulser device (Bio-Rad, Munich, Germany) at 'EC2' setting. Successful recombinants were selected on LB plates containing chloramphenicol (plasmid pWRG730) and kanamycin (*aph* cassette from pWRG717 template) and kept at 30°C to preserve pWRG730. Colony-PCRs with suitable primers were routinely used to check for correct insertion of the resistance cassette within the genome in both directions. For subsequent removal of the resistance cassette competent cells were prepared from confirmed mutants still harbouring pWRG730 as described above. After transformation a 10-fold dilution series of the cells up to 10⁻⁴ was prepared in LB and plated on LB agar containing chloramphenicol and AHT. Plates were kept O/N at 30°C and large colonies were picked and purified again on LB agar plates containing chloramphenicol and AHT. Successful deletion of a MCP gene was confirmed with PCR using primers binding to the flanking regions of the gene (see [Table 1](#)) and subsequent Sanger sequencing of the PCR products (data not shown). After going through the desired number of deletion cycles, plasmid pWRG730 was cured from the bacteria by O/N incubation at 42°C.

Whole genome sequencing and mapping

Genomic DNA of strain NCTC 12023 wild type (WT) and the isogenic 7x MCP mutant WRG279 was prepared from O/N cultures in LB medium using a GenElute Bacterial Genomic

DNA kit (Sigma-Aldrich, Schnellendorf, Germany) according to manufacturer's instructions. One ng of genomic DNA of each strain was fragmented using the Nextera sample preparation kit (Illumina, San Diego, CA, USA) and sequenced on a MiSeq (Illumina) machine running in paired end mode with 300 bp read length. All raw sequence reads of BioProject PRJNA355390 (<http://www.ncbi.nlm.nih.gov/bioproject/>) are available through SRA (<http://www.ncbi.nlm.nih.gov/sra>) accessions SRR5062192 (WT) and SRR5062193 (WRG279).

Consensus sequences for the two genomes were determined utilizing a custom in-house analysis pipeline as described earlier [60]. Briefly, MiSeq reads were mapped to the published genome sequence of *S. Typhimurium* strain ATCC 14028S (accession: CP001363) by a combination of BWA-SW version 0.7.13-r1126 [61] and SAMtools 0.1.19 [62]. VarScan 2.3 [63] was utilized for consensus calling. After mapping sequencing coverage was extracted using SAMtools 1.3.1 and visualized with 'ggplot2' [64] from 'R' 3.3.0 [65]. SNPs were extracted from the NCTC 12023 WT and WRG279 genomes obtained by reference-based mapping using a custom in-house Python script. Regions containing SNPs unique for WRG279 or sites of MCP deletion were PCR-amplified and subjected to Sanger sequencing (GATC Biotech, Cologne, Germany) using suitable primers listed in S1 Table. Sequence data is available through BioProject PRJNA355390.

Minimal inhibitory concentration assay

O/N cultures of test strains were diluted 1:100 in fresh LB and grown at 37°C to an OD₆₀₀ between 0.5 and 0.7. After adjusting the cultures to an OD₆₀₀ of 0.0002 (approximately 2×10^5 bacteria/mL) in fresh 2-fold concentrated LB, 100 µl were added to each well of a 96-well plate containing 100 µl of increasing concentrations of chloramphenicol or tetracycline in distilled water. The plates were incubated at 37°C in a humid chamber for 16 h and absorbance was measured at 600 nm (Tecan Infinite M1000). The MICs were calculated using 'R' as described before [66].

Cell culture and infection

HeLa cells (LGC Standards, Wesel, Germany) were grown in DMEM (Biowest, Germany) supplemented with 10% FCS, sodium pyruvate and 2 mM GlutaMax (Thermo Fisher Scientific, Karlsruhe, Germany) under humidified atmosphere with 5% CO₂. Gentamicin protection assays were essentially carried out as described previously [67]. Briefly, 5×10^4 HeLa per well were seeded in 24-well plates (Cell-star, Greiner bio-one, Frickenhausen, Germany) 24 h prior infection. Bacterial O/N cultures grown in LB supplemented with appropriate antibiotics were reinoculated 1:31 in fresh medium and grown aerobically for another 3.5 h. An inoculum corresponding to a multiplicity of infection (MOI) of 10 was prepared in DMEM and used to infect the HeLa cells for 25 min. After the cells were washed thrice with PBS, 500 µl of DMEM containing 100 µg/mL gentamicin was applied to each well to kill remaining extracellular bacteria. After one hour of incubation the cell layers were washed again with PBS and then lysed for 10 min with PBS containing 1% Elugent (Merck Millipore, Darmstadt, Germany) and 0,0625% Antifoam B (Sigma-Aldrich, Schnellendorf, Germany) to liberate the intracellular bacteria. Serial dilutions of the inoculum and the lysates were plated on Mueller Hinton (MH) plates to determine the colony-forming units. Based on the inoculum the percentage of invasive bacteria was calculated and subsequently normalized to WT.

Swarming assay

Swarming of different *Salmonella* strains was assessed on LB semi-solid agar plates (LB with 5 g/L NaCl, 0.5% agar). A small amount (0.2 µl) of bacterial O/N cultures was applied onto the

center of LB soft agar plate and incubated for six hours at 37°C. The diameters of the swarm colonies were measured and the plates were photographed.

Supporting information

S1 Fig. PCR fragments after colony PCR of sequential MCP deletion strains. Primer combinations as listed in Table 1 were used. One exception was the 'aer' locus where primer 'Aer-Delcheck-rev2' instead of 'McpC-Delcheck-rev' was used producing a 1087 bp fragment. Due to deletion of the reverse primer binding site during replacement of *mcpC* and *mcpB*, no product was observed (*) for WRG277 (6) and WRG279 (7). 1 = WRG246 Δ aer; 2 = WRG255 Δ aer, Δ tcp; 3 = WRG260 Δ aer, Δ tcp, Δ tsr; 4 = WRG264 Δ aer, Δ tcp, Δ tsr, Δ trg; 5 = WRG269 Δ aer, Δ tcp, Δ tsr, Δ trg, Δ cheM; 6 = WRG277 Δ aer, Δ tcp, Δ tsr, Δ trg, Δ cheM, Δ mcpC; 7 = WRG279 Δ aer, Δ tcp, Δ tsr, Δ trg, Δ cheM, Δ mcpC, Δ mcpB, M = DNA marker, band sizes indicated in kbp. (TIF)

S2 Fig. Determination of the minimal inhibitory concentration (MIC). MICs for chloramphenicol (left) and tetracycline (right) were determined for either *S. Typhimurium* NCTC 12023 wild type (WT) or the isogenic mutant WRG279 lacking seven MCP genes in broth dilution assays. Data of three independent biological replicates done in duplicates with means and standard deviations are shown. n.s. = not significant as calculated using a two-tailed unpaired Student's *t* test. (EPS)

S3 Fig. Swarming phenotypes of different MCP mutants. (A) Swarming phenotypes on LB soft agar plates of different *Salmonella* MCP mutants as indicated. Depicted is one representative out of three similar experiments. (B) Diameters of the swarming rings with means and standard deviations of the different *Salmonella* strains from (A) for three independent biological replicates are shown. Statistical significance compared to WT was calculated using a two-tailed paired Student's *t* test and was defined as * for $p < 0.05$ and *** for $p < 0.001$. (TIF)

S1 Table. Oligonucleotides used in this study. (XLSX)

Acknowledgments

We thank Monique Duwe for technical support during genome sequencing of strain WRG279.

Author Contributions

Conceptualization: RGG.

Data curation: RGG.

Formal analysis: SH RGG.

Funding acquisition: RGG.

Investigation: SH CS SW.

Methodology: RGG SH.

Project administration: RGG.

Resources: JKB.

Supervision: RGG.

Validation: SH SW CS.

Visualization: SH RGG.

Writing – original draft: RGG.

Writing – review & editing: JKB RGG SH SW.

References

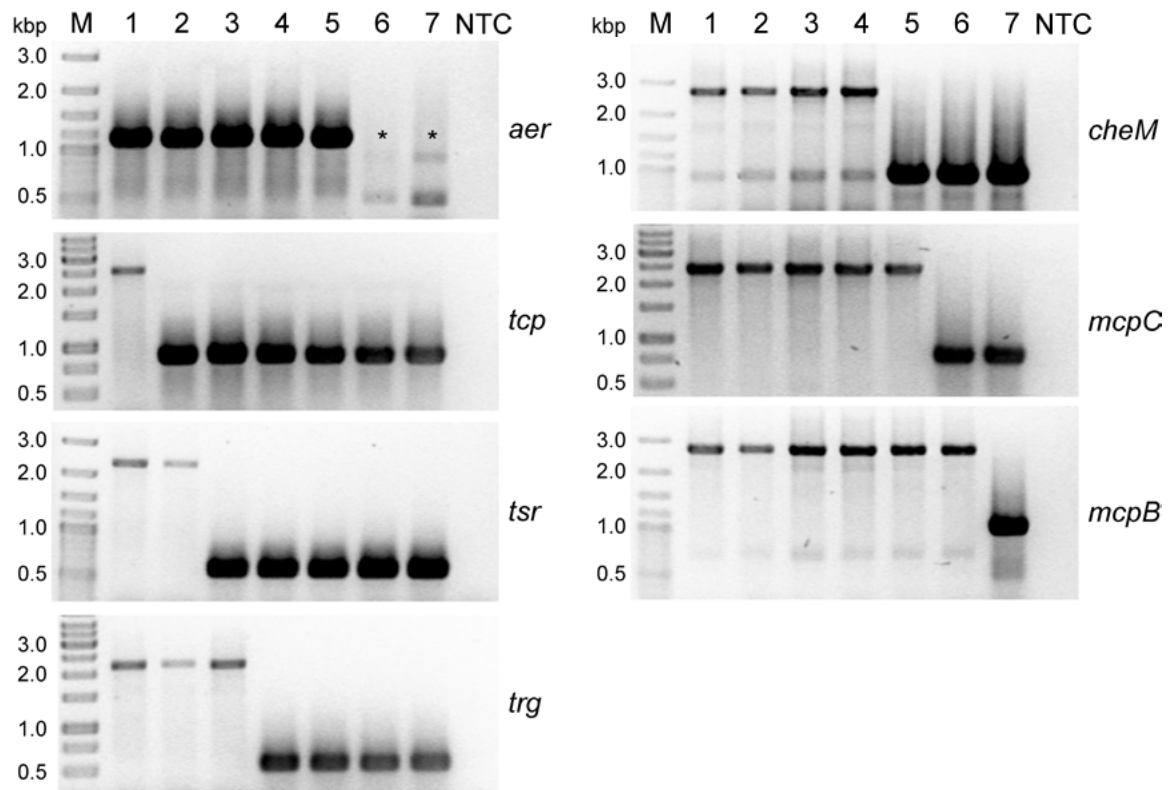
1. Thomason LC, Sawitzke JA, Li X, Costantino N, Court DL. Recombineering: genetic engineering in bacteria using homologous recombination. *Curr Protoc Mol Biol.* 2014; 106:1 16 1–39.
2. Pines G, Freed EF, Winkler JD, Gill RT. Bacterial Recombineering: Genome Engineering via Phage-Based Homologous Recombination. *ACS Synth Biol.* 2015; 4(11):1176–85. doi: [10.1021/acssynbio.5b00009](https://doi.org/10.1021/acssynbio.5b00009) PMID: [25856528](https://pubmed.ncbi.nlm.nih.gov/25856528/)
3. Sawitzke JA, Thomason LC, Costantino N, Bubunenko M, Datta S, Court DL. Recombineering: *in vivo* genetic engineering in *E. coli*, *S. enterica*, and beyond. *Methods Enzymol.* 2007; 421:171–99. doi: [10.1016/S0076-6879\(06\)21015-2](https://doi.org/10.1016/S0076-6879(06)21015-2) PMID: [17352923](https://pubmed.ncbi.nlm.nih.gov/17352923/)
4. Blank K, Hensel M, Gerlach RG. Rapid and highly efficient method for scarless mutagenesis within the *Salmonella enterica* chromosome. *PLoS One.* 2011; 6(1):e15763. Epub 2011/01/26. PubMed Central PMCID: PMC3021506. doi: [10.1371/journal.pone.0015763](https://doi.org/10.1371/journal.pone.0015763) PMID: [21264289](https://pubmed.ncbi.nlm.nih.gov/21264289/)
5. Cox MM, Layton SL, Jiang T, Cole K, Hargis BM, Berghman LR, et al. Scarless and site-directed mutagenesis in *Salmonella enteritidis* chromosome. *BMC Biotechnol.* 2007; 7:59. Epub 2007/09/19. PubMed Central PMCID: PMC2096622. doi: [10.1186/1472-6750-7-59](https://doi.org/10.1186/1472-6750-7-59) PMID: [17875218](https://pubmed.ncbi.nlm.nih.gov/17875218/)
6. Gerlach RG, Jäckel D, Hölzer SU, Hensel M. Rapid oligonucleotide-based recombineering of the chromosome of *Salmonella enterica*. *Appl Environ Microbiol.* 2009; 75(6):1575–80. Epub 2009/01/20. PubMed Central PMCID: PMC2655478. doi: [10.1128/AEM.02509-08](https://doi.org/10.1128/AEM.02509-08) PMID: [19151186](https://pubmed.ncbi.nlm.nih.gov/19151186/)
7. Liang R, Liu J. Scarless and sequential gene modification in *Pseudomonas* using PCR product flanked by short homology regions. *BMC Microbiol.* 2010; 10(1):209. Epub 2010/08/05. PubMed Central PMCID: PMC2924854.
8. Reisch CR, Prather KL. The no-SCAR (Scarless Cas9 Assisted Recombineering) system for genome editing in *Escherichia coli*. *Sci Rep.* 2015; 5:15096. PubMed Central PMCID: PMC4604488. doi: [10.1038/srep15096](https://doi.org/10.1038/srep15096) PMID: [26463009](https://pubmed.ncbi.nlm.nih.gov/26463009/)
9. Sun W, Wang S, Curtiss R, 3rd. Highly efficient method for introducing successive multiple scarless gene deletions and markerless gene insertions into the *Yersinia pestis* chromosome. *Appl Environ Microbiol.* 2008; 74(13):4241–5. Epub 2008/05/20. PubMed Central PMCID: PMC2446500. doi: [10.1128/AEM.00940-08](https://doi.org/10.1128/AEM.00940-08) PMID: [18487404](https://pubmed.ncbi.nlm.nih.gov/18487404/)
10. Karlinsky JE. λ -Red genetic engineering in *Salmonella enterica* serovar Typhimurium. In: Hughes KT, Maloy SR, editors. *Advanced Bacterial Genetics: Use of Transposons and Phage for Genomic Engineering.* *Methods Enzymol.* 421. 2007/03/14 ed. New York: Academic Press; 2007. p. 199–209.
11. Rivero-Müller A, Lajić S, Huhtaniemi I. Assisted large fragment insertion by Red/ET-recombination (ALFIRE)—an alternative and enhanced method for large fragment recombineering. *Nucleic Acids Res.* 2007; 35(10):e78. Epub 2007/05/23. PubMed Central PMCID: PMC1904275. doi: [10.1093/nar/gkm250](https://doi.org/10.1093/nar/gkm250) PMID: [17517785](https://pubmed.ncbi.nlm.nih.gov/17517785/)
12. Zhang Y, Muylers JP, Rientjes J, Stewart AF. Phage annealing proteins promote oligonucleotide-directed mutagenesis in *Escherichia coli* and mouse ES cells. *BMC Mol Biol.* 2003; 4(1):1. Epub 2003/01/18. PubMed Central PMCID: PMC149363. doi: [10.1186/1471-2199-4-1](https://doi.org/10.1186/1471-2199-4-1) PMID: [12530927](https://pubmed.ncbi.nlm.nih.gov/12530927/)
13. Wang H, Bian X, Xia L, Ding X, Müller R, Zhang Y, et al. Improved seamless mutagenesis by recombineering using *ccdB* for counterselection. *Nucleic Acids Res.* 2014; 42(5):e37. PubMed Central PMCID: PMC3950717. doi: [10.1093/nar/gkt1339](https://doi.org/10.1093/nar/gkt1339) PMID: [24369425](https://pubmed.ncbi.nlm.nih.gov/24369425/)
14. Lee DJ, Bingle LE, Heurlier K, Pallen MJ, Penn CW, Busby SJ, et al. Gene doctoring: a method for recombineering in laboratory and pathogenic *Escherichia coli* strains. *BMC Microbiol.* 2009; 9:252. Epub 2009/12/17. PubMed Central PMCID: PMC2796669. doi: [10.1186/1471-2180-9-252](https://doi.org/10.1186/1471-2180-9-252) PMID: [20003185](https://pubmed.ncbi.nlm.nih.gov/20003185/)

15. Pósfai G, Kolisnychenko V, Bereczki Z, Blattner FR. Markerless gene replacement in *Escherichia coli* stimulated by a double-strand break in the chromosome. *Nucleic Acids Res.* 1999; 27(22):4409–15. PubMed Central PMCID: PMC148724. PMID: [10536150](#)
16. Tischer BK, von Einem J, Kaufer B, Osterrieder N. Two-step red-mediated recombination for versatile high-efficiency markerless DNA manipulation in *Escherichia coli*. *Biotechniques.* 2006; 40(2):191–7. Epub 2006/03/11. PMID: [16526409](#)
17. Yu BJ, Kang KH, Lee JH, Sung BH, Kim MS, Kim SC. Rapid and efficient construction of markerless deletions in the *Escherichia coli* genome. *Nucleic Acids Res.* 2008; 36(14):e84. Epub 2008/06/24. PubMed Central PMCID: PMC2504295. doi: [10.1093/nar/gkn359](#) PMID: [18567910](#)
18. Monteilhet C, Perrin A, Thierry A, Colleaux L, Dujon B. Purification and characterization of the *in vitro* activity of I-Sce I, a novel and highly specific endonuclease encoded by a group I intron. *Nucleic Acids Res.* 1990; 18(6):1407–13. Epub 1990/03/25. PubMed Central PMCID: PMC330504. PMID: [2183191](#)
19. Ellis HM, Yu D, DiTizio T, Court DL. High efficiency mutagenesis, repair, and engineering of chromosomal DNA using single-stranded oligonucleotides. *Proc Natl Acad Sci U S A.* 2001; 98(12):6742–6. Epub 2001/06/07. PubMed Central PMCID: PMC34423. doi: [10.1073/pnas.121164898](#) PMID: [11381128](#)
20. Wang HH, Isaacs FJ, Carr PA, Sun ZZ, Xu G, Forest CR, et al. Programming cells by multiplex genome engineering and accelerated evolution. *Nature.* 2009; 460(7257):894–8. PubMed Central PMCID: PMC4590770. doi: [10.1038/nature08187](#) PMID: [19633652](#)
21. Costantino N, Court DL. Enhanced levels of λ Red-mediated recombinants in mismatch repair mutants. *Proc Natl Acad Sci U S A.* 2003; 100(26):15748–53. PubMed Central PMCID: PMC307639. doi: [10.1073/pnas.2434959100](#) PMID: [14673109](#)
22. Luo ML, Leenay RT, Beisel CL. Current and future prospects for CRISPR-based tools in bacteria. *Bio-technol Bioeng.* 2016; 113(5):930–43. PubMed Central PMCID: PMC4816669. doi: [10.1002/bit.25851](#) PMID: [26460902](#)
23. Pyne ME, Moo-Young M, Chung DA, Chou CP. Coupling the CRISPR/Cas9 System with Lambda Red Recombineering Enables Simplified Chromosomal Gene Replacement in *Escherichia coli*. *Appl Environ Microbiol.* 2015; 81(15):5103–14. PubMed Central PMCID: PMC4495200. doi: [10.1128/AEM.01248-15](#) PMID: [26002895](#)
24. Ronda C, Pedersen LE, Sommer MO, Nielsen AT. CRMAGE: CRISPR Optimized MAGE Recombineering. *Sci Rep.* 2016; 6:19452. PubMed Central PMCID: PMC4726160. doi: [10.1038/srep19452](#) PMID: [26797514](#)
25. Hazelbauer GL, Falke JJ, Parkinson JS. Bacterial chemoreceptors: high-performance signaling in networked arrays. *Trends Biochem Sci.* 2008; 33(1):9–19. PubMed Central PMCID: PMC2890293. doi: [10.1016/j.tibs.2007.09.014](#) PMID: [18165013](#)
26. Wadhams GH, Armitage JP. Making sense of it all: bacterial chemotaxis. *Nat Rev Mol Cell Biol.* 2004; 5(12):1024–37. doi: [10.1038/nrm1524](#) PMID: [15573139](#)
27. Adler J. Chemotaxis in bacteria. *Science.* 1966; 153(3737):708–16. PMID: [4957395](#)
28. Edwards JC, Johnson MS, Taylor BL. Differentiation between electron transport sensing and proton motive force sensing by the Aer and Tsr receptors for aerotaxis. *Mol Microbiol.* 2006; 62(3):823–37. PubMed Central PMCID: PMC1858650. doi: [10.1111/j.1365-2958.2006.05411.x](#) PMID: [16995896](#)
29. Blat Y, Eisenbach M. Tar-dependent and -independent pattern formation by *Salmonella typhimurium*. *J Bacteriol.* 1995; 177(7):1683–91. PubMed Central PMCID: PMC176793. PMID: [7896688](#)
30. Kolodziej AF, Tan T, Koshland DE Jr. Producing positive, negative, and no cooperativity by mutations at a single residue located at the subunit interface in the aspartate receptor of *Salmonella typhimurium*. *Biochemistry.* 1996; 35(47):14782–92. doi: [10.1021/bi961481v](#) PMID: [8942640](#)
31. Kondoh H, Ball CB, Adler J. Identification of a methyl-accepting chemotaxis protein for the ribose and galactose chemoreceptors of *Escherichia coli*. *Proc Natl Acad Sci U S A.* 1979; 76(1):260–4. PubMed Central PMCID: PMC382918. PMID: [370826](#)
32. Bibikov SI, Miller AC, Gosink KK, Parkinson JS. Methylation-independent aerotaxis mediated by the *Escherichia coli* Aer protein. *J Bacteriol.* 2004; 186(12):3730–7. PubMed Central PMCID: PMC419962. doi: [10.1128/JB.186.12.3730-3737.2004](#) PMID: [15175286](#)
33. Yamamoto K, Imae Y. Cloning and characterization of the *Salmonella typhimurium*-specific chemoreceptor Tcp for taxis to citrate and from phenol. *Proc Natl Acad Sci U S A.* 1993; 90(1):217–21. PubMed Central PMCID: PMC45631. PMID: [8419927](#)
34. Lazova MD, Butler MT, Shimizu TS, Harshey RM. *Salmonella* chemoreceptors McpB and McpC mediate a repellent response to L-cystine: a potential mechanism to avoid oxidative conditions. *Mol Microbiol.* 2012; 84(4):697–711. PubMed Central PMCID: PMC4285363. doi: [10.1111/j.1365-2958.2012.08051.x](#) PMID: [22486902](#)

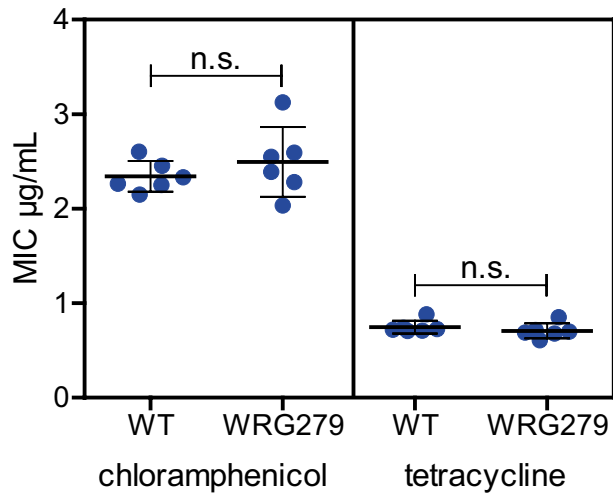
35. Frye J, Karlinsky JE, Felise HR, Marzolf B, Dowidar N, McClelland M, et al. Identification of new flagellar genes of *Salmonella enterica* serovar Typhimurium. *J Bacteriol.* 2006; 188(6):2233–43. PubMed Central PMCID: PMC1428135. doi: [10.1128/JB.188.6.2233-2243.2006](https://doi.org/10.1128/JB.188.6.2233-2243.2006) PMID: [16513753](https://pubmed.ncbi.nlm.nih.gov/16513753/)
36. Datsenko KA, Wanner BL. One-step inactivation of chromosomal genes in *Escherichia coli* K-12 using PCR products. *Proc Natl Acad Sci U S A.* 2000; 97(12):6640–5. PubMed Central PMCID: PMC18686. doi: [10.1073/pnas.120163297](https://doi.org/10.1073/pnas.120163297) PMID: [10829079](https://pubmed.ncbi.nlm.nih.gov/10829079/)
37. Guzman LM, Belin D, Carson MJ, Beckwith J. Tight regulation, modulation, and high-level expression by vectors containing the arabinose P_{BAD} promoter. *J Bacteriol.* 1995; 177(14):4121–30. PubMed Central PMCID: PMC177145. PMID: [7608087](https://pubmed.ncbi.nlm.nih.gov/7608087/)
38. Datta S, Costantino N, Court DL. A set of recombinering plasmids for gram-negative bacteria. *Gene.* 2006; 379:109–15. doi: [10.1016/j.gene.2006.04.018](https://doi.org/10.1016/j.gene.2006.04.018) PMID: [16750601](https://pubmed.ncbi.nlm.nih.gov/16750601/)
39. McDonough E, Lazinski DW, Camilli A. Identification of *in vivo* regulators of the *Vibrio cholerae xds* gene using a high-throughput genetic selection. *Mol Microbiol.* 2014; 92(2):302–15. PubMed Central PMCID: PMC4005888. doi: [10.1111/mmi.12557](https://doi.org/10.1111/mmi.12557) PMID: [24673931](https://pubmed.ncbi.nlm.nih.gov/24673931/)
40. Murphy KC, Campellone KG. Lambda Red-mediated recombinogenic engineering of enterohemorrhagic and enteropathogenic *E. coli*. *BMC Mol Biol.* 2003; 4:11. PubMed Central PMCID: PMC317293. doi: [10.1186/1471-2199-4-11](https://doi.org/10.1186/1471-2199-4-11) PMID: [14672541](https://pubmed.ncbi.nlm.nih.gov/14672541/)
41. Carter Z, Delneri D. New generation of *loxP*-mutated deletion cassettes for the genetic manipulation of yeast natural isolates. *Yeast.* 2010; 27(9):765–75. doi: [10.1002/yea.1774](https://doi.org/10.1002/yea.1774) PMID: [20641014](https://pubmed.ncbi.nlm.nih.gov/20641014/)
42. Lee SC, Wang W, Liu P. Construction of gene-targeting vectors by recombinering. *Methods Mol Biol.* 2009; 530:15–27. PubMed Central PMCID: PMC3706932. doi: [10.1007/978-1-59745-471-1_2](https://doi.org/10.1007/978-1-59745-471-1_2) PMID: [19266337](https://pubmed.ncbi.nlm.nih.gov/19266337/)
43. Dowd SE, Killinger-Mann K, Brashears M, Fralick J. Evaluation of gene expression in a single antibiotic exposure-derived isolate of *Salmonella enterica* Typhimurium 14028 possessing resistance to multiple antibiotics. *Foodborne Pathog Dis.* 2008; 5(2):205–21. doi: [10.1089/fpd.2007.0062](https://doi.org/10.1089/fpd.2007.0062) PMID: [18407759](https://pubmed.ncbi.nlm.nih.gov/18407759/)
44. Octavia S, Wang Q, Tanaka MM, Sintchenko V, Lan R. Genomic Variability of Serial Human Isolates of *Salmonella enterica* Serovar Typhimurium Associated with Prolonged Carriage. *J Clin Microbiol.* 2015; 53(11):3507–14. PubMed Central PMCID: PMC4609693. doi: [10.1128/JCM.01733-15](https://doi.org/10.1128/JCM.01733-15) PMID: [26311853](https://pubmed.ncbi.nlm.nih.gov/26311853/)
45. Marzel A, Desai PT, Goren A, Schorr YI, Nissan I, Porwollik S, et al. Persistent Infections by Nontyphoidal *Salmonella* in Humans: Epidemiology and Genetics. *Clin Infect Dis.* 2016; 62(7):879–86. PubMed Central PMCID: PMC4787607. doi: [10.1093/cid/civ1221](https://doi.org/10.1093/cid/civ1221) PMID: [26740515](https://pubmed.ncbi.nlm.nih.gov/26740515/)
46. Ranallo RT, Barnoy S, Thakkar S, Urlick T, Venkatesan MM. Developing live *Shigella* vaccines using λ Red recombinering. *FEMS Immunol Med Microbiol.* 2006; 47(3):462–9. doi: [10.1111/j.1574-695X.2006.00118.x](https://doi.org/10.1111/j.1574-695X.2006.00118.x) PMID: [16872384](https://pubmed.ncbi.nlm.nih.gov/16872384/)
47. Trülsch K, Sporleder T, Igwe EI, Rüssmann H, Heesemann J. Contribution of the major secreted Yops of *Yersinia enterocolitica* O:8 to pathogenicity in the mouse infection model. *Infect Immun.* 2004; 72(9):5227–34. Epub 2004/08/24. PubMed Central PMCID: PMC517446. doi: [10.1128/IAI.72.9.5227-5234.2004](https://doi.org/10.1128/IAI.72.9.5227-5234.2004) PMID: [15322017](https://pubmed.ncbi.nlm.nih.gov/15322017/)
48. Katashkina JI, Hara Y, Golubeva LI, Andreeva IG, Kuvaveva TM, Mashko SV. Use of the λ Red-recombinering method for genetic engineering of *Pantoea ananatis*. *BMC Mol Biol.* 2009; 10:34. PubMed Central PMCID: PMC2682490. doi: [10.1186/1471-2199-10-34](https://doi.org/10.1186/1471-2199-10-34) PMID: [19389224](https://pubmed.ncbi.nlm.nih.gov/19389224/)
49. Jones BD, Lee CA, Falkow S. Invasion by *Salmonella typhimurium* is affected by the direction of flagellar rotation. *Infect Immun.* 1992; 60(6):2475–80. PubMed Central PMCID: PMC257184. PMID: [1587617](https://pubmed.ncbi.nlm.nih.gov/1587617/)
50. Khoramian-Falsafi T, Harayama S, Kutsukake K, Pechere JC. Effect of motility and chemotaxis on the invasion of *Salmonella typhimurium* into HeLa cells. *Microb Pathog.* 1990; 9(1):47–53. PMID: [2077343](https://pubmed.ncbi.nlm.nih.gov/2077343/)
51. Misselwitz B, Barrett N, Kreibich S, Vonaesch P, Andritschke D, Rout S, et al. Near surface swimming of *Salmonella* Typhimurium explains target-site selection and cooperative invasion. *PLoS Pathog.* 2012; 8(7):e1002810. PubMed Central PMCID: PMC3406100. doi: [10.1371/journal.ppat.1002810](https://doi.org/10.1371/journal.ppat.1002810) PMID: [22911370](https://pubmed.ncbi.nlm.nih.gov/22911370/)
52. Stecher B, Hapfelmeier S, Müller C, Kremer M, Stallmach T, Hardt WD. Flagella and chemotaxis are required for efficient induction of *Salmonella enterica* serovar Typhimurium colitis in streptomycin-pre-treated mice. *Infect Immun.* 2004; 72(7):4138–50. PubMed Central PMCID: PMC427403. doi: [10.1128/IAI.72.7.4138-4150.2004](https://doi.org/10.1128/IAI.72.7.4138-4150.2004) PMID: [15213159](https://pubmed.ncbi.nlm.nih.gov/15213159/)
53. Wang RF, Kushner SR. Construction of versatile low-copy-number vectors for cloning, sequencing and gene expression in *Escherichia coli*. *Gene.* 1991; 100:195–9. PMID: [2055470](https://pubmed.ncbi.nlm.nih.gov/2055470/)

54. Kalinin Y, Neumann S, Sourjik V, Wu M. Responses of *Escherichia coli* bacteria to two opposing chemoattractant gradients depend on the chemoreceptor ratio. *J Bacteriol.* 2010; 192(7):1796–800. PubMed Central PMCID: PMC2838042. doi: [10.1128/JB.01507-09](https://doi.org/10.1128/JB.01507-09) PMID: [20118262](https://pubmed.ncbi.nlm.nih.gov/20118262/)
55. Rivera-Chávez F, Winter SE, Lopez CA, Xavier MN, Winter MG, Nuccio SP, et al. *Salmonella* uses energy taxis to benefit from intestinal inflammation. *PLoS Pathog.* 2013; 9(4):e1003267. PubMed Central PMCID: PMC3630101. doi: [10.1371/journal.ppat.1003267](https://doi.org/10.1371/journal.ppat.1003267) PMID: [23637594](https://pubmed.ncbi.nlm.nih.gov/23637594/)
56. Gerlach RG, Cláudio N, Rohde M, Jäckel D, Wagner C, Hensel M. Cooperation of *Salmonella* pathogenicity islands 1 and 4 is required to breach epithelial barriers. *Cell Microbiol.* 2008; 10(11):2364–76. doi: [10.1111/j.1462-5822.2008.01218.x](https://doi.org/10.1111/j.1462-5822.2008.01218.x) PMID: [18671822](https://pubmed.ncbi.nlm.nih.gov/18671822/)
57. Wille T, Barlag B, Jakovljevic V, Hensel M, Sourjik V, Gerlach RG. A gateway-based system for fast evaluation of protein-protein interactions in bacteria. *PLoS One.* 2015; 10(4):e0123646. PubMed Central PMCID: PMC4391838. doi: [10.1371/journal.pone.0123646](https://doi.org/10.1371/journal.pone.0123646) PMID: [25856398](https://pubmed.ncbi.nlm.nih.gov/25856398/)
58. Bender JK, Wille T, Blank K, Lange A, Gerlach RG. LPS structure and PhoQ activity are important for *Salmonella* Typhimurium virulence in the *Galleria mellonella* infection model. *PLoS One.* 2013; 8(8):e73287. PubMed Central PMCID: PMC3738532. doi: [10.1371/journal.pone.0073287](https://doi.org/10.1371/journal.pone.0073287) PMID: [23951347](https://pubmed.ncbi.nlm.nih.gov/23951347/)
59. Gibson DG, Young L, Chuang RY, Venter JC, Hutchison CA 3rd, Smith HO. Enzymatic assembly of DNA molecules up to several hundred kilobases. *Nat Methods.* 2009; 6(5):343–5. doi: [10.1038/nmeth.1318](https://doi.org/10.1038/nmeth.1318) PMID: [19363495](https://pubmed.ncbi.nlm.nih.gov/19363495/)
60. Steglich M, Nitsche A, von Müller L, Herrmann M, Kohl TA, Niemann S, et al. Tracing the Spread of *Clostridium difficile* Ribotype 027 in Germany Based on Bacterial Genome Sequences. *PLoS One.* 2015; 10(10):e0139811. PubMed Central PMCID: PMC4596877. doi: [10.1371/journal.pone.0139811](https://doi.org/10.1371/journal.pone.0139811) PMID: [26444881](https://pubmed.ncbi.nlm.nih.gov/26444881/)
61. Li H, Durbin R. Fast and accurate long-read alignment with Burrows-Wheeler transform. *Bioinformatics.* 2010; 26(5):589–95. PubMed Central PMCID: PMC2828108. doi: [10.1093/bioinformatics/btp698](https://doi.org/10.1093/bioinformatics/btp698) PMID: [20080505](https://pubmed.ncbi.nlm.nih.gov/20080505/)
62. Li H, Handsaker B, Wysoker A, Fennell T, Ruan J, Homer N, et al. The Sequence Alignment/Map format and SAMtools. *Bioinformatics.* 2009; 25(16):2078–9. PubMed Central PMCID: PMC2723002. doi: [10.1093/bioinformatics/btp352](https://doi.org/10.1093/bioinformatics/btp352) PMID: [19505943](https://pubmed.ncbi.nlm.nih.gov/19505943/)
63. Koboldt DC, Zhang Q, Larson DE, Shen D, McLellan MD, Lin L, et al. VarScan 2: somatic mutation and copy number alteration discovery in cancer by exome sequencing. *Genome research.* 2012; 22(3):568–76. PubMed Central PMCID: PMC3290792. doi: [10.1101/gr.129684.111](https://doi.org/10.1101/gr.129684.111) PMID: [22300766](https://pubmed.ncbi.nlm.nih.gov/22300766/)
64. Wickham H. *ggplot2: Elegant Graphics for Data Analysis.* New York: Springer; 2016.
65. R Core Team. *R: A language and environment for statistical computing.* Vienna, Austria: R Foundation for Statistical Computing; 2016.
66. Erhardt M, Mertens ME, Fabiani FD, Hughes KT. ATPase-independent type-III protein secretion in *Salmonella enterica*. *PLoS Genet.* 2014; 10(11):e1004800. PubMed Central PMCID: PMC4230889. doi: [10.1371/journal.pgen.1004800](https://doi.org/10.1371/journal.pgen.1004800) PMID: [25393010](https://pubmed.ncbi.nlm.nih.gov/25393010/)
67. Gerlach RG, Jäckel D, Stecher B, Wagner C, Lupas A, Hardt WD, et al. *Salmonella* Pathogenicity Island 4 encodes a giant non-fimbrial adhesin and the cognate type 1 secretion system. *Cell Microbiol.* 2007; 9(7):1834–50. doi: [10.1111/j.1462-5822.2007.00919.x](https://doi.org/10.1111/j.1462-5822.2007.00919.x) PMID: [17388786](https://pubmed.ncbi.nlm.nih.gov/17388786/)

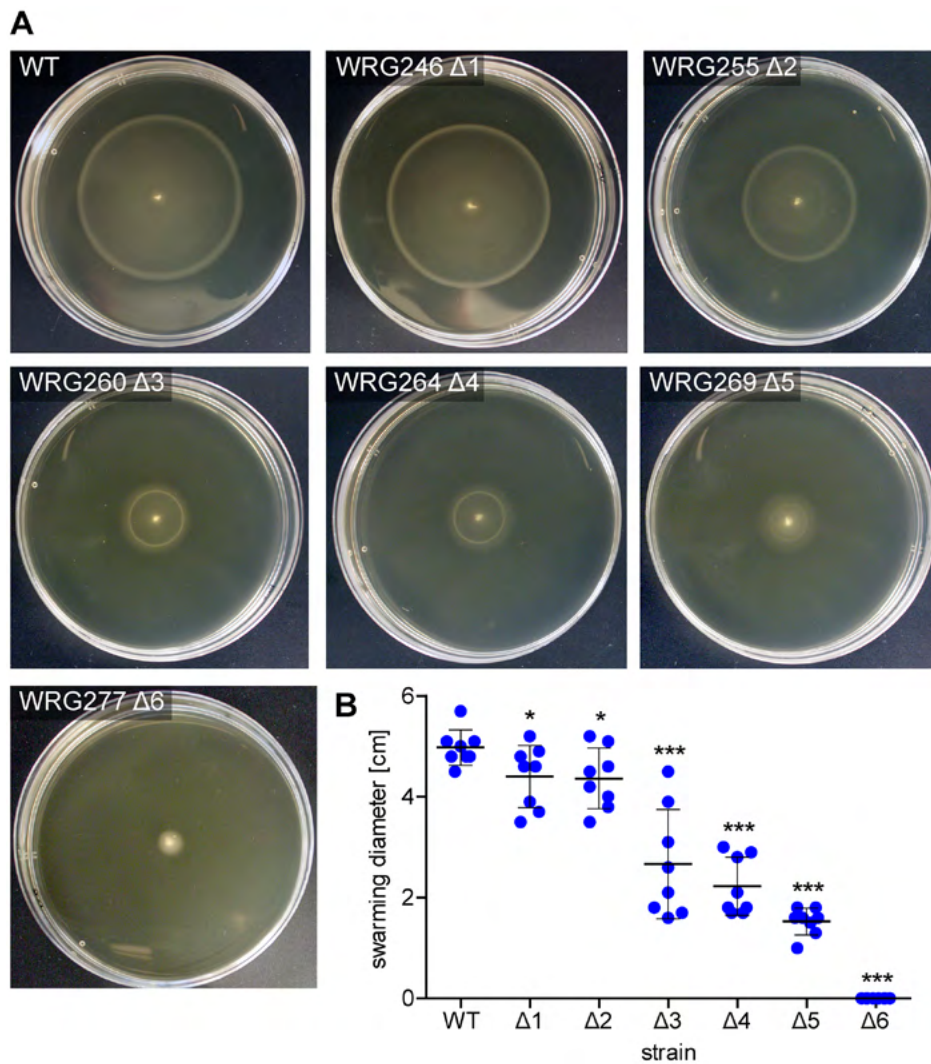
Supplementary Material

Scarless deletion of up to seven methyl- accepting chemotaxis genes with an optimized method highlights key function of CheM in *Salmonella* TyphimuriumStefanie Hoffmann¹, Christiane Schmidt¹, Steffi Walter¹, Jennifer K. Bender² and Roman G. Gerlach¹¹ Project Group 5, Robert Koch Institute, Wernigerode, Germany² Division of Nosocomial Pathogens and Antibiotic Resistances, Department of Infectious Diseases, Robert Koch Institute, Wernigerode, Germany

S1 Fig: PCR fragments after colony PCR of sequential MCP deletion strains. Primer combinations as listed in Table 1 were used. One exception was the '*aer*' locus where primer 'Aer-Delcheck-rev2' instead of 'McpC-Delcheck-rev' was used producing a 1087 bp fragment. Due to deletion of the reverse primer binding site during replacement of *mcpC* and *mcpB*, no product was observed (*) for WRG277 (6) and WRG279 (7). 1 = WRG246 Δaer ; 2 = WRG255 $\Delta aer, \Delta tcp$; 3 = WRG260 $\Delta aer, \Delta tcp, \Delta tsr$; 4 = WRG264 $\Delta aer, \Delta tcp, \Delta tsr, \Delta trg$; 5 = WRG269 $\Delta aer, \Delta tcp, \Delta tsr, \Delta trg, \Delta cheM$; 6 = WRG277 $\Delta aer, \Delta tcp, \Delta tsr, \Delta trg, \Delta cheM, \Delta mcpC$; 7 = WRG279 $\Delta aer, \Delta tcp, \Delta tsr, \Delta trg, \Delta cheM, \Delta mcpC, \Delta mcpB$, M = DNA marker, band sizes indicated in kbp.



S2 Fig: Determination of the minimal inhibitory concentration (MIC). MICs for chloramphenicol (left) and tetracycline (right) were determined for either *S. Typhimurium* NCTC 12023 wild type (WT) or the isogenic mutant WRG279 lacking seven MCP genes in broth dilution assays. Data of three independent biological replicates done in duplicates with means and standard deviations are shown. n.s. = not significant as calculated using a two-tailed unpaired Student's *t* test.



S3 Fig: Swarming phenotypes of different MCP mutants. (A) Swarming phenotypes on LB soft agar plates of different *Salmonella* MCP mutants as indicated. Depicted is one representative out of three similar experiments. (B) Diameters of the swarming rings with means and standard deviations of the different *Salmonella* strains from (A) for three independent biological replicates are shown. Statistical significance compared to WT was calculated using a two-tailed paired Student's *t* test and was defined as * for $p < 0.05$ and *** for $p < 0.001$.

S1 Table: Oligonucleotides used in this study.

Designation	Sequence 5' -> 3'
Aad9-I-SceI-pSK-Gbs-for	TAATACGACTCACTATAGGCGGAATTGGGTACCAAGTTACGCTAGGGATAACAGGGTAATATAGGCGCAACGCAATTAATGTAAG
Aad9-pSK-Gbs-rev	ATGACCATGATTACGCCAAGCGCGCAATTACCTATATCGCCGACATCACC
Aer-cleanDel-for	GCAAATTGCGATCCAGAG
Aer-cleanDel-rev	GGGCGGATGTCATTACCATTGCTACTACAATAAACTAGATAGCGTCTGTGCAGG
Aer-Delcheck-for2	CCTCTCGGTTTAGTGCTTTC
Aer-Delcheck-rev2	CGTGGTGGGATAATCATTGG
Aer-Scarless-for	CGAAAAATTAACATCCAGATAACCTGCACAGGACGCTATCAGGGTTTTCCAGTCACGAC
Aer-Scarless-rev	GGGCGGATGTCATTACCATTGCTACTACAATAAACTTAGTCTCCGGCTCGTATGTTG
Aph-I-SceI-KpnI-rev2	GCCGGTACCAGTACGCTAGGGATAACAGGGTAATATAGAGAGCGCTTTTGAAGCTGGG
Aph-I-SceI-pSK-Gbs-for	TAATACGACTCACTATAGGCGGAATTGGGTACCAAGTTACGCTAGGGATAACAGGGTAATATAGTGGGCTATCGGACAAGGG
Aph-pSK-Gbs-rev2	ATGACCATGATTACGCCAAGCGCGCAATTACGAAGCCCAACCTTTCATAG
CheM-cleanDel-for	CCGCTGCGACACTGTCATTG
CheM-cleanDel-rev	GTTCCGCAAATTAATCGATAACCGACAGCGCACGTCGATCAAAGGCACCTTCTGATAACG
CheM-Delcheck-for	CGTCGTCGGGATAGTGGTAG
CheM-Delcheck-rev	AAAGCGGTCAGGTTGGTAG
CheM-pWSK-Gbs-rev	ATGACCATGATTACGCCAAGCGCGCAATTATATGCGAACAGACGAAAGG
CheM-Scarless-for	TGCCGATAACGTTGATAACTGTTATCAGGAAGGTGCCTTAGGGTTTTCCAGTCACGAC
CheM-Scarless-rev	GTTCCGCAAATTAATCGATAACCGACAGCGCACGTCGATCATGCTCCGGCTCGTATGTTG
McpB-cleanDel-for	TAACGGTGGATAACCGTCTC
McpB-cleanDel-rev	GAAGGAAACCCATTATCAGTAGACTGTGCGGGAGCCGACATGAATTTCTTGCTGAATA
McpB-Delcheck-for2	TGGGCTATCTGGACAGATTG
McpB-Delcheck-rev	GAAGGAAAGAGGCGATAGTG
McpB-Scarless-for	GTCTGATGACTAATCTTATATTAGCAAGGAAATTCATAGGGTTTTCCAGTCACGAC
McpB-Scarless-rev	GAAGGAAACCCATTATCAGTAGACTGTGCGGGAGCCGACTGCTCCGGCTCGTATGTTG
McpC-cleanDel-for	TCCTTCTCCCTTGTCTAC
McpC-cleanDel-rev	GATTGATCGCGCGGCTGGAATCGCCGAACCTGGATTAATTTCTCCCTGGGATTGC
McpC-Delcheck-for	CGGATCGGCTCTGATAGAAG
McpC-Delcheck-rev	ACTTCGGCTGGTCATTCTTG
McpC-Scarless-for	AATCTTCTGTATGAGGATATGCAATCCAGGGAGAAAAATAGGGTTTTCCAGTCACGAC

Designation	Sequence 5'→3'
McpC-Scarless-rev	GATTGATCGCGCGCGCTGGAAATCGCCGAACTGGATTAATGCTTCCGGCTCGTATGTTG
pKD4-Gbs-rev	CAACCTGCCATCACGAGATTTC
pSIM-Gbs-for	CCGCTGTGCTTTCAGTGGATTTCCG
pSIM-Gbs-rev	GACAGTAAGACGGGTAAGCCTG
pSIM+SceI-Gbs-rev	GGCCTTTCTGTTATCCGAAATCCACTGAAAGCACAGCGGGTCTCCCTATAGTGAGTCG
pSIM-TetR-Gbs-for2	CGGTATCATCAACAGGCTTACCCGTCTACTGTCAAAGTGCCACCTGCATCG
pWSK29-Gbs-for	TAATTGCGCGCTTGGCGTAATC
pWSK29-Gbs-rev	ACCCAATTCGCCCTATAGTG
STM14_2710-seq-for	CGGTAACGTCTCTTGTCTC
STM14_2710-seq-rev	ATTCAGGCGTCAGACATTCC
Tcp-cleanDel-for	TCCCGGATATTCCTTC
Tcp-cleanDel-rev	GTAAGCGCATTAACTGCACGGCAGATACTATTCTGATTAAGTGCCAACTTCCTTATT
Tcp-Delcheck-for	TTTACCGGGCTATGGCTGGC
Tcp-Delcheck-rev	GTTGCCCTGAACCGGTAATG
Tcp-Scarless-for	ATTGATCATAACCGTCTACAAAAAAGGAATGTTAGGCACTAGGGTTTTCCAGTCACGAC
Tcp-Scarless-rev	GTAAGCGCATTAACTGCACGGCAGATACTATTCTGATTATGCTTCCGGCTCGTATGTTG
Trg-cleanDel-rev	CGCCCGGGCTAAAATAGCCCGTGGCGGACGCTTACTAGACCGTGACTCTCTGTAG
Trg-Delcheck-for	GGCGATAACTGATTCATCCG
Trg-Delcheck-rev	AGAATGCGGAAGCCCTGTTG
Trg-Scarless-for	GCGTGTTTTACGCATAAAACCTACAAGAGAGTCGACGGTCAGGGTTTTCCAGTCACGAC
Trg-Scarless-rev	CGCCCGGGCTAAAATAGCCCGTGGCGGACGCTTACTATGCTTCCGGCTCGTATGTTG
Tsr-cleanDel-rev	ACGGTCGTCTGTAGGCCGACTGTTCACTACTACGCCCTTAGTTTTCTCTTCCGCTAGAC
Tsr-Delcheck-for	GTTGTTGTTGAGGAGGTAG
Tsr-Delcheck-rev	ACCGCACACCTTCACTCAAC
Tsr-Scarless-for	AGGCCGAAAATCTGTATCTGTAGCGGAAAGAGAAAACAGGGTTTTCCAGTCACGAC
Tsr-Scarless-rev	ACGGTCGTCTGTAGGCCGACTGTTCACTACTACGCCCTTAGTTTTCTCTTCCGCTAGAC
XhoI-aphI-for2	GAACTCGAGACTGGGTATCTGGACAAGG
YceB-seq-for	CCAATCTGGCTGACAAGGTTAG
YceB-seq-rev	CGGCGAATTATCGGAAGATG

III.4. A chemotactic sensor controls *Salmonella*-host cell interaction

Stefanie Hoffmann¹, Kathrin Gendera¹, Christiane Schmidt¹, Peter Kirchweger², Axel Imhof³,
Christian Bogdan⁴, Yves Muller², Michael Hensel⁵ and Roman G. Gerlach^{1,4}

¹ Project Group 5, Robert Koch Institute, Wernigerode, Germany

² Division of Biotechnology, Department of Biology, Friedrich-Alexander-University (FAU) Erlangen-Nuremberg, Erlangen, Germany

³ BioMedical Center and Center for Integrated Protein Sciences Munich, Ludwig-Maximilians-Universität München, München, Germany

⁴ Mikrobiologisches Institut – Klinische Mikrobiologie, Immunologie und Hygiene, Universitätsklinikum Erlangen and Friedrich-Alexander-Universität Erlangen-Nürnberg, Erlangen, Germany

⁵ Abteilung Mikrobiologie, Universität Osnabrück, Osnabrück, Germany and CellNanOs – Center for Cellular Nanoanalytics Osnabrück, Universität Osnabrück, Osnabrück, Germany

A chemotactic sensor controls *Salmonella*-host cell interaction

Stefanie Hoffmann¹, Kathrin Gendera¹, Christiane Schmidt¹, Peter Kirchweger^{2*}, Axel Imhof³, Christian Bogdan⁴, Yves A. Muller², Michael Hensel⁵, Roman G. Gerlach^{1,4*}

Keywords: *Salmonella*, chemotaxis, adhesion, aspartate

Abstract

Intimate cell contact and subsequent type three secretion system-dependent cell invasion are key steps in host colonization of *Salmonella*. Adhesion to complex glycostructures at the apical membrane of polarized cells is mediated by the giant adhesin SiiE. This protein is secreted by a type 1 secretion system (T1SS) and needs to be retained at the bacterial surface to exert its adhesive function. Here, we show that SiiE surface expression was linked to the presence of L-aspartate sensed by the *Salmonella*-specific methyl-accepting chemotaxis protein CheM. Bacteria lacking CheM were attenuated for invasion of polarized cells, whereas increased invasion was seen with *Salmonella* exposed to the nonmetabolizable aspartate analog α -methyl-D, L-aspartate (MeAsp). While components of the chemotaxis phosphorelay or functional flagella were dispensable for the increased invasion, CheM directly interacted with proteins associated with the SiiE T1SS arguing for a novel non-canonical signaling mechanism. As a result, CheM attractant signaling caused a shift from secreted to surface-retained and adhesion-competent SiiE. Thus, CheM controls the virulence function of SiiE in a precise spatio-temporal fashion depending on the host micro-milieu.

Introduction

Many pathogenic bacteria strongly rely on their ability to get into close contact to eukaryotic host cell surfaces. By means of different adhesins, they are able to colonize mucosal surfaces or invade cells and establish their niches in host organisms. *Salmonella enterica* subsp. *enterica* serovar Typhimurium (STM) is a pathogen that is capable to infect diverse hosts and usually causes a self-limiting gastrointestinal infection. STM can invade non-phagocytic cells by deploying a type III secretion system (T3SS) that is encoded by the *Salmonella* pathogenicity island 1 (SPI-1) (1). An intimate contact between the pathogen and the host cell is essential for the subsequent translocation of effector molecules by the SPI-1-dependent

¹ Project Group 5, Robert Koch Institute, Wernigerode, Germany

² Division of Biotechnology, Department of Biology, Friedrich-Alexander-Universität Erlangen-Nürnberg (FAU), Erlangen, Germany

³ BioMedical Center and Center for Integrated Protein Sciences Munich, Ludwig-Maximilians-Universität München, München, Germany

⁴ Mikrobiologisches Institut – Klinische Mikrobiologie, Immunologie und Hygiene, Universitätsklinikum Erlangen and Friedrich-Alexander-Universität Erlangen-Nürnberg, Erlangen, Germany

⁵ Abteilung Mikrobiologie, Universität Osnabrück, Osnabrück, Germany and CellNanOs – Center for Cellular Nanoanalytics Osnabrück, Universität Osnabrück, Osnabrück, Germany

* present address: Department of Chemical and Structural Biology, Faculty of Chemistry, Weizmann Institute of Science, Rehovot, Israel

* **Corresponding author:** Roman G. Gerlach

Email: roman.gerlach@uk-erlangen.de

Author Contributions: R.G.G., S.H., M.H. and Y.A.M. designed research; S.H., K.G., C.S. and P.K. performed research; R.G.G., S.H. and A.I. analyzed the data; and R.G.G., C.B., M.H. and Y.A.M. wrote the paper.

T3SS (T3SS-1). This triggers an inflammatory host immune response, which does not only weaken the enterocyte barrier function, but also helps STM to compete with the intestinal microbiota (2). While the T3SS-1 itself can already mediate adhesion (3), additional adhesive structures such as Fim fimbriae (4) or the giant non-fimbrial adhesin SiiE (5) are also critical for bacterial attachment, depending on the type of host cell. Transcriptional co-regulation of SPI-1 with the SiiE-encoding *Salmonella* pathogenicity island 4 (SPI-4) is the basis of this functional cooperation (5, 6).

In line with previous findings on other polarized cells (7), it was recently shown that apical invasion of intestinal epithelial cells requires SiiE (8). SiiE likely functions as a lectin recognizing glycostructures with terminal *N*-acetylglucosamine (GlcNAc) and/or α 2,3-linked sialic acid residues (9). The unique structural features of the ~175 nm long 600 kDa adhesin SiiE allow *Salmonella* to overcome the antiadhesive barrier function of the transmembrane, epithelial mucin MUC1, the extracellular domain of which is heavily decorated with O-linked glycans terminating in negatively charged sialic acids (8). SiiE comprises 53 bacterial immunoglobulin-like (BIg) domains that show distinct Ca^{2+} binding motifs crucial for its rigid tertiary structure (10, 11). SiiE is the only known substrate of the SPI-4-encoded T1SS and contains a complex C-terminal secretion signal (7). Based on similarity to other T1SS, e.g., the *E. coli* hemolysin system (12), secretion is likely achieved in a single step without a periplasmic intermediate. Considering these structural features, SiiE is thought to be permanently secreted into the extracellular space. A recent study showed that secreted SiiE suppressed the humoral immune response against *Salmonella* by reducing the number of IgG-secreting plasma cells in the bone marrow. Mechanistically, an N-terminal region of SiiE with high similarity to laminin β 1 bound to β 1 integrin (CD29) on IgG⁺ plasma cells, thereby preventing their interaction with laminin β 1⁺CXCL12⁺ stromal cells which otherwise form a survival niche for plasma cells in the bone marrow (13). However, in line with its function as an adhesin, the protein was also found temporally retained on the surface of *Salmonella* (7, 8, 14). Nonetheless, it is still unclear how the surface expression of SiiE and hence the switch between its function as adhesin vs. immunosuppressant is regulated.

Here, we show that the presence of aspartate (Asp) promotes the surface expression of SiiE and the adhesion of *Salmonella*, which turned out to be dependent on the *Salmonella*-specific methyl-accepting chemotaxis protein (MCP) CheM, an ortholog of *E. coli* Tar/MCP-II. Using mass spectrometry, CheM and other MCPs were identified as interaction partners of the SPI-4 encoded SiiA and SiiB. SiiAB are associated with the T1SS and form an inner membrane proton (H⁺) channel with similarities to the ExbB/TolQ and MotAB family (15, 16). Using a set of consecutive MCP deletion mutants, we found that invasion of polarized cells by STM was attenuated upon deletion of *cheM*. Binding of Asp to CheM usually triggers bacterial chemotaxis towards the attractant gradient (17). We discovered that the addition of a non-metabolizable aspartate analog, α -methyl-D,L-aspartate (MeAsp), elevated host cell invasion by STM. Using mutants lacking downstream components of the chemotaxis phosphorelay or functional flagella, we observed that neither classical chemotaxis signaling nor bacterial motility contributed to the increased invasion. Instead, attractant-stimulation of CheM caused a shift from secreted to surface-retained and adhesion-competent SiiE. We therefore suggest that aspartate acts as microenvironmental cue that elicits the SPI-4-dependent adhesion to and invasion of polarized epithelial cells by *Salmonella* through a novel, non-canonical signaling pathway of the MCP CheM via SiiAB to the SPI-4 T1SS and SiiE.

Results

SiiAB interact with CheM

Our previous results suggested that SiiE-mediated adhesion depends on the function of the SPI-4 T1SS-associated SiiAB proton channel (15). We set out to identify protein interaction partners as potential regulators of SiiA and/or SiiB. Epitope-tagged SiiA or SiiB was expressed from low copy-number plasmids and used as bait proteins to purify complexes after cross-linking. Composition of complexes was determined by liquid chromatography coupled to mass spectrometry (LC-MS/MS). As expected, both bait proteins were under the top five identified proteins (Fig 1A). Moreover, our data confirmed the previously found (15) interaction between SiiA and SiiB, since both proteins were identified as prey while using the other as bait. Interestingly, a set of MCPs (Aer, Trg, McpB, McpC and CheM) was enriched in the SiiA complex while in the SiiB complex the MCP CheM was identified. MCPs act as sensors controlling flagellar movement towards attractants and away from repellants (18). In the following, we focused on CheM because the protein was previously implicated to have a role in *Salmonella* invasion of HeLa cells (19, 20) and appears to interact with both SiiA and SiiB. CheM is a *Salmonella*-specific MCP and an ortholog of *E. coli* Tar, but shares only 79% of sequence identity. Like known for Tar, the amino acid L-aspartate functions as an attractant stimulus for CheM while Co^{2+} and Ni^{2+} ions act as repellants (17, 21). However, in contrast to Tar, CheM does not respond to maltose (22).

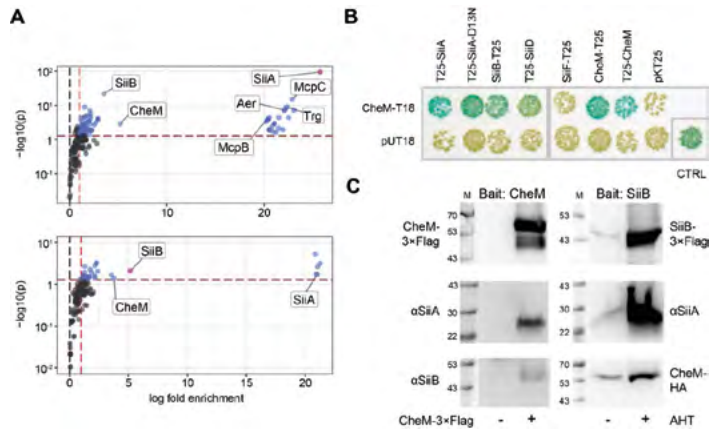


Figure 1. SPI-4 components interact with CheM. (A) Analysis of affinity purification mass spectrometry data using SiiA-3×Flag (upper panel) or SiiB-3×Flag (lower panel) as bait proteins (magenta dots). Red dashed lines show limits of significant enrichment (>2-fold, $p < 0.05$). Interacting proteins within these limits are depicted in blue with SPI-4 components and MCPs labeled. Summarized data of three independent experiments are shown. (B) Bacterial two hybrid assays evaluating the interaction between the T18 fragment of CyaA alone (pUT18, negative control) or fused to the Cterminus of CheM (CheM-T18) with the CyaA T25 fragment alone (pKT25, negative control) or T25 fused to the indicated SPI-4 proteins or CheM. Functional reconstitution of CyaA activity through protein-protein interactions resulted in blue color of the *E. coli* BTH101 reporter strain colonies. A positive control (CTRL) was included based on the interaction of GCN4 leucine zippers. (C) Co-immunoprecipitation using CheM-3×Flag (left panels) or SiiB-3×Flag (right panels) as bait proteins. A plasmid-encoded copy of *cheM* was expressed from its natural promoter either without (left lane) or with (right lane) 3×Flag epitope tag. SiiA and SiiB were detected using polyclonal antibodies. Expression of SiiAB-3×Flag from plasmid pWRG905 was induced with addition of 50 ng/mL anhydrotetracycline (AHT) or left uninduced (left lane). While SiiA was detected with a specific antiserum, a plasmid encoding for CheM-HA was cotransformed allowing CheM detection via HA tag. M = molecular weight marker with protein sizes in kDa.

To confirm the interactions between SiiAB and CheM identified by MS, we performed a bacterial twohybrid (B2H) assay which is based on the functional complementation of *Bordetella pertussis* adenylate cyclase (CyaA) from T25 and T18 fragments (23). The T25 fragment was fused to SiiA, SiiB, SiiD, SiiF or to a non-functional SiiA^{D13N} mutant (15), while the T18 fragment was fused to CheM. Blue colonies of the *cyaA*-deficient *E. coli* reporter strain BTH101 (24) indicated functional CyaA protein complementation and thus protein-protein interaction. We observed a strong interaction (dark blue colonies) between CheM-T18 and T25 fusions of SiiA and SiiA-D13N (Fig 1B). Moreover, high reporter activity was also observed when testing for the known dimerization of Tar/CheM (18) with co-expression of CheM-T18 and T25-CheM or CheM-T25 (Fig 1B). Lighter blue colonies were observed for the coexpression of CheM-T18 and SiiB-T25 or T25-SiiD showing β -galactosidase activity comparable to that of the positive control (Fig 1B). Furthermore, we performed co-immunoprecipitation (co-IP) using epitope tagged proteins. When CheM-3 \times Flag was used as bait, both SiiA and SiiB were identified as prey proteins. Vice versa, using SiiB-3 \times Flag as bait, SiiA and epitope-tagged CheM-HA were detected as interaction partners (Fig 1C). Thus, using three independent approaches, we established that CheM interacts with both SiiA and SiiB while confirming the known SiiAB complex (15) and CheM dimerization (18).

Role of MCPs for invasion of polarized MDCK

Bacterial motility is required for efficient invasion of *Salmonella* into HeLa (25) and polarized Caco-2 cells (26). In a previously published study, we further assessed the impact of chemotaxis on invasion efficiency of non-polarized HeLa cells using sequential deletion of up to seven MCP genes (19). We found that loss of CheY or CheM led to an increase of *Salmonella* invasion (19) as observed earlier for smooth swimming mutants (20, 27). Because SPI-4 function was shown to play a role for adhesion to polarized cells only (5, 7, 8), we aimed to investigate the role of individual MCPs on *Salmonella* invasion of polarized Madin-Carby Canine Kidney (MDCK) cells. Host cells were infected with STM wild-type (WT), a smooth swimming *cheY* mutant, Δ *siiF* (non-functional SPI-4 T1SS) and MCP mutant strains as described (19), followed by quantification of intracellular bacteria and subsequent normalization to STM WT. Interestingly, all MCP mutants missing the *cheM* gene exhibited reduced invasion in polarized MDCK cells. In contrast, elevated invasion rates were observed for the same *cheM*-lacking mutants when using non-polarized HeLa cells as described before (19) (Fig 2). While a smooth swimming Δ *cheY* strain showed a 2-fold increased invasion rate in HeLa, the mutant was significantly attenuated in MDCK arguing for a role of chemotaxis for efficient invasion of polarized cells. In line with the known importance of SPI-4 for the adhesion to and invasion of MDCK cells (7), very few intracellular bacteria harboring an E627Q mutation within the Walker B motif of the SiiF ABC protein were detected (Fig 2). Thus, the type of infection model (non-polarized vs. polarized cells) determine the impact of CheM function on STM invasion which mirrors the differences seen for SPI-4 function (7).

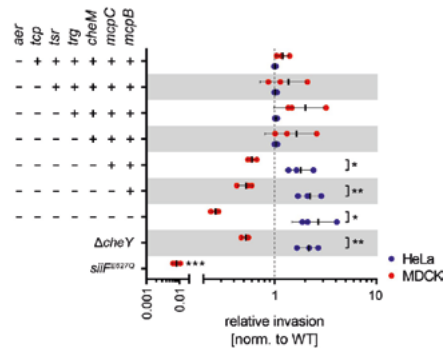


Fig 2. Role of MCPs for bacterial invasion. Relative invasion rates as normalized to *S. Typhimurium* (STM) wild-type (WT, dotted line) after one hour of infection of indicated sequential MCP deletion strains into HeLa (blue) and MDCK (red) cells are shown. The non-chemotactic $\Delta cheY$ strain and a *sifE627Q* mutant with a non-functional SPI-4 were included as controls. Data of three independent experiments done in triplicates are depicted. Statistical significance was calculated using unpaired, two-tailed *t* test between groups or a one sample *t* test against the hypothetical value 1 (*sifE627Q*) and were defined as * for $p < 0.05$ and ** for $p < 0.01$ and *** for $p < 0.001$.

CheM attractant binding fosters *Salmonella* invasion of polarized cells

To characterize a possible functional link of CheM to the SPI-4-encoded T1SS, we constructed two lowcopy-number plasmids that encode *Salmonella cheM* or, as a control, *E. coli tar*, each modified with a C-terminal 3×Flag-tag under control of the STM *cheM* promoter (P_{cheM}). After introducing the plasmids in a mutant lacking all seven MCP genes ($\Delta 7$ MCP) (19), Western blot demonstrated similar expression of both proteins with the cytosolic protein DnaK as loading control (Fig 3A). Next, $\Delta 7$ MCP was transformed with the empty vector control (pWSK29) and plasmids encoding for CheM (pCheM) or Tar (pTar) without epitope tag and these strains were further functionally characterized in swarming assays using soft agar plates. While the strain harboring pWSK29 did not swarm, pCheM and pTar conferred swarming ability to the mutant. However, compared to STM WT (> 5 cm, not shown), both plasmidcomplemented $\Delta 7$ MCP showed a reduced swarming distance with ~4 cm (pCheM) and ~1 cm (pTar), respectively (Fig 3B). To test more specifically the ability to respond to CheM attractants, we performed a capillary assay as described by Adler (28) using MeAsp (29) (Fig 3C, left panel). Quantifying the bacteria within the fixed-volume capillary revealed significantly more cells in case of the pCheMcomplemented strain, compared not only to the vector control, but also compared to WT (Fig 3C, right panel).

We hypothesized that not the CheM protein itself, but rather CheM signaling elicited by the binding of CheM ligands (i.e. attractants) may have an impact on SPI-4 function and subsequently on invasion of polarized epithelial cells. Usually, attractant binding inactivates autokinase activity of MCP-coupled CheA, thus reducing phosphoryl transfer to the response regulators CheY and CheB. While low CheY~P results in counter-clockwise (CCW) flagellar rotation and straight swimming, receptor methylation is high due to low CheB~P methyltransferase activity (18). Therefore, STM WT and the $\Delta 7$ MCP mutant containing either the vector control, pCheM or pTar were tested for invasion of MDCK without attractant, in the presence of 10 mM MeAsp or, as a control, 10 mM of the non-metabolizable Tsr attractant α -aminoisobutyrate (AiBu) (30, 31). While AiBu had no or, in case of STM WT, even a

detrimental effect on invasion, addition of MeAsp elevated invasion capability of WT and pCheM-complemented $\Delta 7$ MCP (Fig 3D). The pCheM vector partially complemented the invasion defect of the $\Delta 7$ MCP mutant in the absence of attractant or with addition of AiBu, while the strains carrying pTar or the vector control were attenuated for invasion regardless of attractant supplementation (Fig 3D).

To verify our findings obtained with MDCK cells, we employed HT29-MTX cells (8, 32) as an alternative infection model. In contrast to non-polarized 1-day cultures (Fig S1A, upper panel), polarized monolayers with significant amounts of mucus were formed after 21 days of culture (Fig S1A, lower panel). Similar to HeLa cells (7), *Salmonella* invasion of non-polarized HT29-MTX cells required T3SS-1 but was independent of SPI-4 (Fig S1B). Invasion of polarized HT29-MTX cells, however, was strongly dependent on an intact SPI-4 locus (Fig 3E) as observed before (8). In close accordance with the MDCK data, elevated invasion of HT29-MTX cells was observed for WT and $\Delta 7$ MCP [pCheM] in the presence of MeAsp (Fig 3E). However, pCheM was able to complement the $\Delta 7$ MCP mutant to the level of WT STM without attractant or with 10 mM AiBu. In contrast, low invasion rates were observed for cells without CheM (Fig 3E).

Taken together, using two infection models based on polarized cells, we observed a stimulating effect of the CheM ligand MeAsp on *Salmonella* invasion. The phenotype was specifically dependent on the presence of CheM. No increase in invasion was seen in strains only expressing *E. coli* Tar or with addition of the Tsr ligand AiBu.

Augmented invasion after CheM stimulation is independent of motility and chemotaxis

Bacterial motility and chemotaxis towards energy sources was shown to be required for *Salmonella* virulence *in vivo* (33-35). Because our data also suggest a promoting effect of chemotaxis for invasion of polarized cells, we set out to characterize the role of motility and the chemotaxis phosphorelay pathway for the observed phenotype in more detail. We generated a non-motile mutant lacking the flagella-specific ATPase *fliI* and employed, besides the *cheY*-deficient strain, a mutant lacking the histidine autokinase CheA. Together with MCPs and the coupling protein CheW, CheA dimers form a ternary complex that is the minimum requirement for chemosensing (18, 36). The *cheA* and *cheY* mutations were further combined with the $\Delta 7$ MCP mutant. These mutant strains were all attenuated for invasion of MDCK. Interestingly, the non-motile $\Delta fliI$ and the two 8-fold mutants ($\Delta 7$ MCP plus $\Delta cheA$ and $\Delta 7$ MCP plus $\Delta cheY$) exhibited an even stronger phenotype with almost no invasion detectable (Fig 4A). While significantly more intracellular WT STM bacteria were found when grown in the presence of MeAsp, the mutants responded neither to this attractant nor to AiBu (Fig 4A).

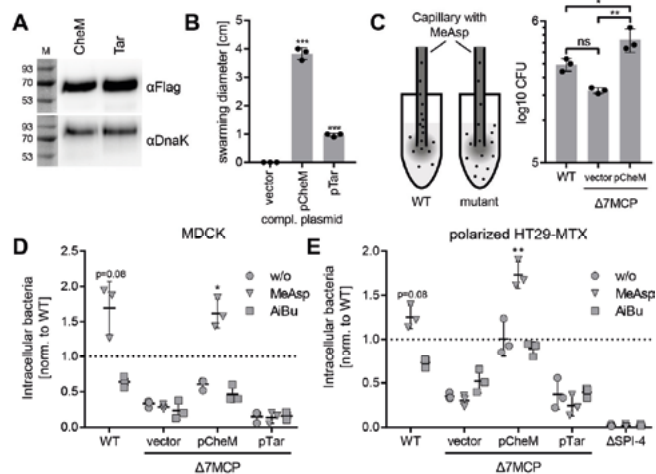


Fig 3. CheM complementation and impact of CheM signaling on invasion of polarized cells. (A) Expression of either CheM-3×Flag or Tar-3×Flag from the CheM promoter in a *S. Typhimurium* (STM) strain lacking all 7 MCP genes ($\Delta 7$ MCP) was detected with a Flag-specific monoclonal antibody. Equal sample loading was demonstrated by DnaK. M = molecular weight marker with protein sizes in kDa. (B) The $\Delta 7$ MCP strain transformed with the empty vector pWSK29 (vector) or vectors encoding for CheM (pCheM) or Tar (pTar) were subjected to swarming assays on soft agar plates. Mean swarming diameters \pm SD after 8.5 h of growth are depicted for three independent experiments. Statistical significance was calculated using a one sample *t* test against the hypothetical value 0 (vector control) and were defined as *** for $p < 0.001$. (C) Principle of capillary assay. Wild-type (WT) bacteria with functional CheM-dependent chemotaxis swim towards a gradient of α -methyl-D, L-aspartate (MeAsp) generated by an attractant-filled capillary. No enrichment within the capillary is observed for mutants with defects in CheM-signaling (left panel). Mean amount \pm SD of STM WT or the $\Delta 7$ MCP with empty vector (vector) or pCheM within the capillary after 1 h. of chemotactic movement from three independent experiments are shown (right panel). One way ANOVA with Tukey's multiple comparison test was calculated and was defined as * for adj. $p < 0.05$ and ** for adj. $p < 0.01$. (D and E) Relative invasion rates as normalized to STM WT (black dotted line) after one hour of infection of the indicated strains into polarized MDCK (D) or HT29-MTX (E) cells are shown. The strains were either grown without (w/o) attractant or with addition of 10 mM MeAsp or 10 mM AiBu. A SPI-4 deficient strain (Δ SPI-4) was included as control for HT29-MTX. Mean \pm SD from three independent experiments are depicted. Statistical significance of strains with increased invasiveness was calculated using a one sample *t* test against the hypothetical value 1 and were defined as * for $p < 0.05$ and ** for $p < 0.01$.

Motile bacteria exhibit an invasion advantage due to near surface swimming and thus higher probability to encounter a host cell (25). To compensate for the lack of motility, we used centrifugation to bring bacteria into close proximity to the host cells, which allows investigating bacterial invasion following adhesion despite the absence of bacterial motility. Under these conditions, the Δ *fliI* mutant behaved like WT with significantly increased invasion in the presence of MeAsp (Fig 4B). The invasion capability of the $\Delta 7$ MCP mutant was not altered by centrifugation. While Δ *cheA* and Δ *cheY* mutants behaved similar to WT bacteria without attractant or with AiBu, they showed vastly increased invasion rates when MeAsp was added (Fig 4B). In contrast, *Salmonella* with a *cheA* or *cheY* mutation and simultaneous deletion of all MCPs (Δ *cheA* $\Delta 7$ MCP or Δ *cheY* $\Delta 7$ MCP) lost the responsiveness to MeAsp and the ability to invade host cells. Thus, MeAsp fosters *Salmonella* invasion in a CheM-dependent manner, but this process is independent of bacterial motility and the chemotaxis phosphorelay pathway.

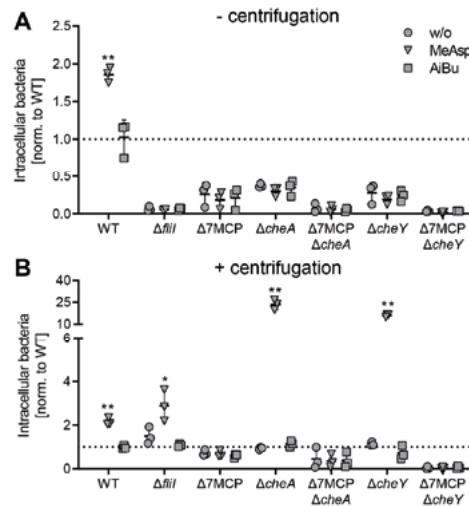


Fig 4. Impact of motility and chemotaxis components on *Salmonella* invasion of polarized MDCK. *S. Typhimurium* (STM) wild-type (WT), the non-motile $\Delta filI$ mutant, the $\Delta 7$ MCP deletion strain, the chemotaxis mutants $\Delta cheA$ and $\Delta cheY$ or strains lacking besides *cheA* or *cheY* additionally all 7 MCPs were grown without attractant (w/o), in the presence of 10 mM MeAsp or 10 mM AiBu. Inoculi were added to the MDCK cells (A) or bacteria were brought in close host cell contact through centrifugation to compensate for lack of chemotaxis or motility (B). Intracellular bacteria were quantified after one hour of infection and relative invasion rates were calculated based on STM WT without attractant. Data of three independent experiments done in triplicates are depicted. Statistical significance of strains with increased invasiveness was calculated using a one sample *t* test against the hypothetical value 1.0 and was defined as * for $p < 0.05$ and ** for $p < 0.01$.

CheM signaling shifts SiiE from release to retention

The experiments described above excluded a motility-related effect to be responsible for elevated *Salmonella* invasion after MeAsp stimulation. Instead, the pronounced phenotype in conjunction with polarized cells and the identification of CheM as a SiiAB interaction partner argues for CheM as a regulator of SPI-4 dependent adhesion. Previous studies suggested that SPI-4 adhesion capability is determined by the amount and/or binding strength of surface-localized SiiE (7, 14). Therefore, mechanisms regulating SiiE surface expression might account for SPI-4 dependent adhesion.

To test whether attractant binding to CheM affects localization of SiiE, we quantified the amounts of surface-retained and secreted SiiE adhesin after 3.5 h of growth (late logarithmic phase) with or without addition of MeAsp. Bacteria-associated SiiE was quantified in a dot blot assay using a SiiE-specific antibody and normalization to the LPS signal. Upon addition of MeAsp, elevated amounts of retained SiiE were detected for WT STM and the $\Delta 7$ MCP mutant carrying pCheM (Fig 5A). In contrast, no upregulation of surface-localized SiiE in response to MeAsp was observed for the $\Delta 7$ MCP mutant harboring the empty vector or for the $\Delta siiE$ mutant which served as negative control (Fig 5A). Quantification of secreted SiiE using a specific ELISA (6) revealed an inhibitory effect of CheM attractant binding reciprocal to SiiE surface localization. MeAsp inhibited SiiE secretion of WT and $\Delta 7$ MCP [pCheM] to the level of the $\Delta siiE$ control. Interestingly, compared to WT STM, almost 2-fold more SiiE was secreted from the $\Delta 7$ MCP strain harboring the empty vector control (Fig 5B).

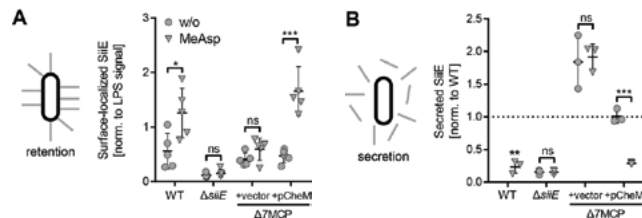


Fig 5. CheM-specific attractant binding promotes SiiE surface localization. (A) Dot-blots were used to quantify surface-localized SiiE and LPS (used for normalization) of *S. Typhimurium* (STM) wild-type (WT), a Δ *siiE* mutant or the Δ 7MCP deletion strain, transformed with the empty vector (vector) or pCheM. Bacteria were either grown without (w/o) or in the presence of 10 mM MeAsp. Mean data \pm SD of five independent experiments are shown. (B) Secreted SiiE was quantified using an ELISA after 3.5 h of growth of the strains and under the conditions as described in (A). Mean data \pm SD of three independent experiments done in triplicates are shown. Statistical significance was calculated using unpaired, two-tailed *t* test between groups or a one sample *t* test against the hypothetical value 1.0 (WT in (B)) and was defined as ns = not significant, * for $p < 0.05$, ** for $p < 0.01$ and *** for $p < 0.001$.

Our findings support a model where the interplay of CheM with the SPI-4 components SiiAB regulates SiiE localization. Attractant binding by CheM resulted in more surface-localized SiiE. To test whether indeed surface-retained SiiE can function as an adhesin, we combined competitive index experiments with a screen for ligand expression using immunomagnetic particles (SIMPLE) (37) (Fig 6A). The test and reference strains harboring different antibiotic resistance cassettes were mixed equally and an aliquot was plated on appropriate selective media to verify the proportion of the two strains. Subsequently, α -SiiE antibodies and magnetic protein A beads were added to the mixture. SiiE-positive bacteria were enriched through magnetic separation of beads coated with antibodies that have bound their antigen. Finally, the proportion of test and reference strain was determined through parallel plating (Fig 6A). Using STM WT as test strain and Δ *siiE* as reference, we achieved \sim 8-fold enrichment using this assay. As expected, there was no effect of MeAsp on enrichment of STM WT over Δ *siiE* (Fig 6B).

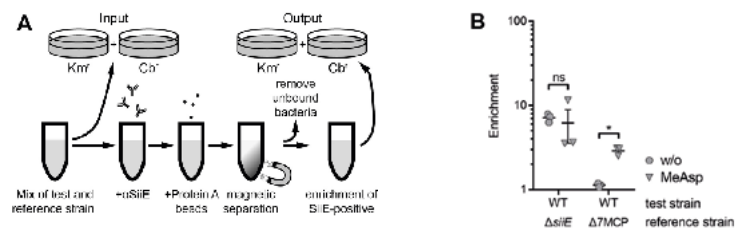


Fig 6. Increase of adhesion-competent SiiE in the presence of MeAsp. (A) Principle of a modified screening with immunomagnetic particles for ligand expression (SIMPLE) assay. (B) Enrichment of the test strains compared to the reference strains as indicated without (w/o) or in the presence of 10 mM MeAsp was determined using the SIMPLE assay as shown in (A). Data of three independent experiments done in triplicates are shown. Statistical significance was calculated using unpaired, two-tailed *t* test between groups as indicated and was defined as ns = not significant and * for $p < 0.05$.

When the $\Delta 7$ MCP strain was used as reference, WT STM was ~ 3 -fold enriched in the presence of MeAsp, while no enrichment was seen without attractant (Fig 6B). These results demonstrate that addition of MeAsp enhanced the localization of SiiE on the surface of *Salmonella* in a MCP-dependent manner.

Discussion

In the present study, we identified the MCP CheM as a novel SiiAB interaction partner and the binding of attractants to CheM as a positive regulator of SPI-4 dependent adhesion. We found that straight swimming *cheA* or *cheY* mutants, which resemble an attractant-bound “always off” state of the MCPs and are incapable of phosphoryl transfer, were attenuated for invasion in polarized cells. In contrast, straight swimming *Salmonella* showed a higher probability to invade other cell types (19, 25). Recently, the *Salmonella* MCP McpC was shown to promote a straight swimming phenotype that was dependent on the SPI-1 transcription factor HilD (38). When we bypassed the impact of motility and chemotaxis on bacteria-host cell interaction by centrifugation, addition of the CheM attractant MeAsp was still able to enhance invasion of polarized cells. This was particularly remarkable for the non-motile $\Delta fliI$ strain, which by itself rules out any involvement of the “classical” chemotaxis-motility pathway. In the absence of MeAsp, centrifugation of $\Delta cheA$ and $\Delta cheY$ mutants led to invasion rates comparable to WT. Strikingly, in the presence of the CheM attractant, these strains were hyperinvasive (~ 20 - 25 -fold of WT). In contrast, invasion capability was completely abolished with additional deletion of all 7 MCP genes. These observations cannot be explained with the chemotaxis phosphorelay signaling (18). Therefore, we propose a novel, non-canonical signal transduction from the MCP to SPI-4 encoded proteins resulting in increased adhesion and subsequent bacterial invasion. Links between chemotaxis and bacterial virulence functions are not unprecedented. In *Pseudomonas aeruginosa*, the putative MCP encoded by PA2573 regulates genes involved in virulence and antibiotic resistance and the soluble chemoreceptor McpB was shown to be important for virulence in several infection models (39, 40). In *Cronobacter sakazakii*, a plasmid-encoded MCP was reported to have an impact on adhesion, invasion, motility and biofilm formation (41). The MCPs TcpI and AcfB of *Vibrio cholerae* were shown to be important for infant mouse colonization (42). For plant pathogenic bacteria such as *Agrobacterium tumefaciens* or *Xanthomonas oryzae* pv. *oryzae*, many chemoattractants can also act as virulence inducers (43, 44). However, in all these examples chemotaxis signaling is mechanistically linked to virulence through transfer of phosphoryl groups to alternative response regulators resulting in a virulence-specific transcriptional response (36).

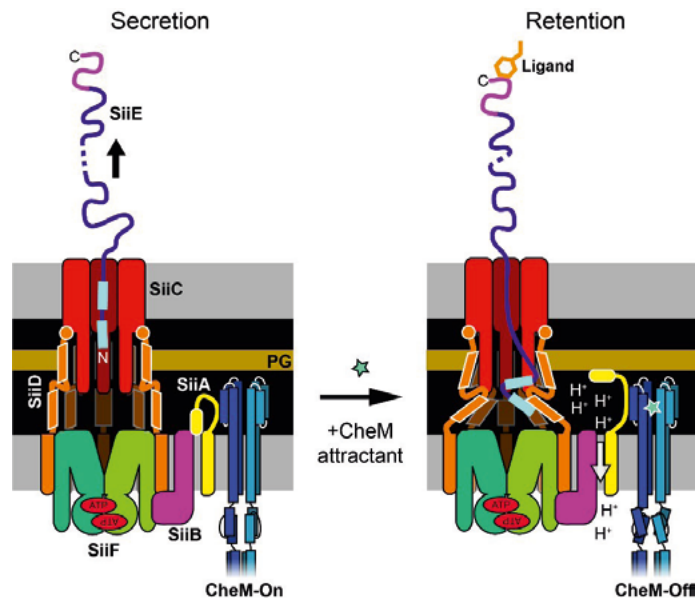


Figure 7. Proposed model how CheM could control SiiE-mediated adhesion. In the absence of attractant, CheM is in the kinase "on" state and the SiiAB proton channel is inactive, presumably due to the periplasmic peptidoglycan (PG) binding domain of SiiA functioning as a plug (left panel). Upon addition of CheM attractant, structural changes in the ligand binding domain of CheM induce displacement of the periplasmic SiiA portion and subsequent association with PG. Proton flux through SiiAB could energize structural changes in the T1SS thus retaining the N-terminal domain of SiiE within the channel (right panel).

The transduction of the CheM attractant signal is presumably based on the identified interaction of the MCP with the SPI-4 T1SS-associated SiiAB proton channel. It is tempting to postulate a regulation of SiiAB proton flux through direct interaction with attractant-bound CheM (Fig 7). The peptidoglycan (PG) binding domain of MotB was shown to function as a plug sealing the proton channel. Upon association with the flagellar motor complex, the MotB domain is shifted through PG binding and thereby enables proton flux and energy conversion of the system (45). Similarly, the SiiA PG binding domain (16) could be displaced from the SiiAB proton channel through interaction with attractant-bound CheM. In orthologous *E. coli* Tar dimers, Asp binding induces a piston-like movement of one alpha helix within the sensory domain. This movement is amplified in the cytosolic HAMP domains and finally transmitted to the hairpin tip bundle controlling CheA autokinase activity (18). In our model, the structural changes within the CheM ligand binding domain, and perhaps other portions of the molecule, would change the molecular interface between CheM and the SiiAB channel, thus enabling PG binding of SiiA and proton flux. The energy harvested from the transmembrane H^+ gradient would then be transferred to the SPI-4 encoded T1SS by means of an energy-rich conformation resulting in retention of the SiiE molecule (Fig 7). Such energy transfer has been described for the SiiAB homologs ExbBD and TolQR inducing conformational changes in TonB and TolA, respectively (46, 47). Interestingly, *in vitro* studies with the isolated periplasmic domain of SiiA showed a pH-dependency of PG binding activity. SiiA PG-binding was observed at pH 5.8-6.2, but not

between pH 6.7 and pH 8.0 (16). Here, slightly acidic pH as found in some parts of the gut could serve as another environmental signal to regulate the adhesion capacity of SPI-4. Alternatively, the observed pH-dependent PG binding could function as a proxy to ensure sufficient energization by detecting periplasmic protons contributing to the proton motive force (PMF). According to our model (Fig 7), *Salmonella* utilizes Asp as an environmental cue to control SiiE surface expression. Aspartate and other free amino acids are generated from oligopeptides originating from food through the activity of peptidases at the apical side of polarized enterocytes (48). The bulk of this amino acid liberation, and subsequent absorption, takes place in the proximal jejunum and is usually complete at the terminal ileum (48, 49). Although there is extensive catabolism of enteral Asp by enterocytes (50) and gut bacteria (51), the microbiota also releases free Asp through peptide degradation (52). Recently, Asp was found to contribute to initial murine gut colonization of STM by enabling hydrogen/fumarate-dependent anaerobic respiration. Aspartate is taken up in exchange of succinate by the high-affinity antiporter DcuABC and converted to the alternative electron acceptor fumarate (53). Therefore, the availability of Asp within the small intestine not only enables bacterial expansion in competition to the intestinal microbiota, but also contributes, amongst other environmental stimuli, to precise spatiotemporal control of bacterial adhesion to polarized epithelial cells.

In summary, we found that the MCP CheM interacted with the SPI-4 encoded SiiAB proton channel.

Asp was identified as an attractant of CheM that elicited a change in the localization of the giant SPI-4-encoded adhesin SiiE of *Salmonella*: in the absence of Asp, SiiE was primarily secreted, whereas in the presence of Asp, SiiE was retained on the bacterial surface. Surface-bound, but not secreted SiiE functions as an adhesin. Thus, the CheM attractant L-aspartate acts as positive regulator of SPI-4-dependent adhesion to polarized cells. Although CheM directly interacts with the SPI-4 encoded SiiAB proton channel, the exact molecular mechanisms of signal transductions and adhesin retention remain to be characterized.

Materials and methods

Bacterial strains and plasmids

All strains used are listed in Table S1. Bacteria were routinely grown in LB media supplemented with 50 µg/mL carbenicillin (Cb) (Carl Roth, Mannheim, Germany), 25 µg/mL kanamycin (Km) (Carl Roth), 10 µg/mL chloramphenicol (Cm) (Carl Roth), 50 ng/mL anhydrotetracycline (AHT) (# 37919 SigmaAldrich, Schnelldorf, Germany), 10 mM α-aminoisobutyrate (AiBu) (#850993 Sigma-Aldrich) or 10 mM α-methyl-D, L-aspartate (MeAsp) (#M6001 Sigma-Aldrich), if required. For details on the construction of mutant strains and plasmids, the reader is referred to the supplementary information. Tables S2 and S3 give an overview of all the plasmids and primers used in this study, respectively.

Protein-protein interaction assays

Bacterial two hybrid (B2H) assays were essentially carried out as described before (15). Briefly, *E. coli* reporter strain BTH101 was co-transformed with plasmids encoding for protein fusions with the T18 and T25 fragments of *Bordetella pertussis* CyaA. Transformants were spread on LB plates containing 25 µg/mL kanamycin,

100 µg/mL carbenicillin, 100 µM IPTG (Thermo Scientific, St. Leon-Rot, Germany) and 40 µg/mL X-Gal (5-bromo-4-chloro-3-indolyl-β-D-galactopyranoside; Thermo Scientific). Plates were incubated at room temperature for 48-72 h, and blue colonies indicated protein interaction resulting in functional CyaA-complementation.

For co-immunoprecipitation (co-IP), STM were either transformed with pWRG868 (CheM-3×Flag) or cotransformed with pWRG903 (CheM-HA) and pWRG905 (P_{tet}::*siiAB*-3×Flag). O/N cultures were reinoculated 1:31 into 500 mL fresh medium and grown with aeration for 3.5 h. The expression of SiiAB3×Flag was induced for 2 h with AHT. Cells were pelleted (8,000 × g, 10 min, room temperature (RT)), re-suspended in 250 mL of pre-warmed MEM medium (Capricorn Scientific, Ebsdorfergrund, Germany) and allowed to grow for additional 30 min. Proteins were crosslinked with addition of 0.5 % (w/v) paraformaldehyde (#43368 Alfa Aesar, Heysham, UK). After 15 min, the reaction was quenched with 0.125 M glycine. Cells were washed thrice with ice-cold MEM medium and then stored at -20 °C. Pellets were re-suspended in 10 mL PBS supplemented with 1 % *n*-dodecyl β-D-maltoside (# A0819, AppliChem, Darmstadt, Germany), 1× EDTA-free halt protease inhibitor cocktail (#87785, Thermo Fisher Scientific, Karlsruhe, Germany), 0.5 mM MgSO₄ and 5 µL TURBO DNase (Ambion).

Subsequently, cells were lysed through a French pressure cell (EmulsiFlex-C3, Avestin, Mannheim, Germany) and debris was removed by low speed centrifugation (11,000 × g, 20 min, 4°C). The protein extract, containing either SiiB-3×Flag or CheM-3×Flag, was further cleared by additional centrifugation (20,000 × g, 15 min, 4°C). The protein concentration was measured by BCA assay (#23225, Thermo Fisher) and similar protein amounts were used for co-IP of all samples. Immunoprecipitation of 3×Flagtagged proteins was performed using α-FLAG M2 affinity gel (Sigma-Aldrich) following the manufacturer's recommendations. Therefore, 100 µL of the gel suspension (50 µL of packed gel volume) were washed 3× with 1 mL of PBS and subsequently added to each sample. Protein binding was allowed over night at 4°C. After three further washing steps, bound proteins were eluted from the beads with addition of 50 µL reducing sample buffer (Carl Roth) and heating for 15 min to 98°C.

Western blot

Aliquots of protein samples were mixed with reducing sample buffer (Carl Roth) to a final concentration of 1×. After heating to 98°C for 15 min, 10 µL of each sample was analyzed by SDS-PAGE electrophoresis (ProSieve, Lonza, Cologne, Germany) and subsequent Western blot (Bio-Rad, Munich, Germany) on a polyvinylidene difluoride membrane (Thermo Fisher). Membranes were probed with antibodies against DnaK (clone 8E2/2, Enzo Life Science, Lörrach, Germany), SiiA, SiiB (15), HA (clone 3F10, Roche, Mannheim, Germany) or Flag (M2, Sigma-Aldrich) and appropriate horseradish-coupled secondary antibodies (Dianova, Hamburg, Germany).

Mass spectrometry

STM was co-transformed with pWRG416 (P_{tet}::*hila*, resulting in mild SPI-1/4 over-expression) plus pWRG461 (*siiA*-3×Flag) or with pWRG416 plus pWRG462 (*siiAB*-3×Flag). Protein complexes were purified with α-FLAG M2 affinity gel (Sigma-Aldrich) as described for co-IP. After washing, bead-bound proteins were eluted twice with 450 µL of 0.1 M glycine pH3.5 and 180 µL of 0.5 M Tris-HCl pH7.4, 1.5 M NaCl was added for neutralization.

To precipitate the proteins, trichloroacetic acid was added to a final concentration of 10% and the samples were incubated O/N at 4°C. After centrifugation (20,000 × g, 45 min, 4°C), the pellets were washed twice with ice-cold acetone. The air-dried pellet was finally suspended in 100 µL fresh 50 mM NH₄HCO₃, pH 7.8. The samples were subjected to tryptic digestion and the resulting peptide mixtures were analyzed by nano-ESI-LC-MS/MS (Thermo Scientific LTQ Orbitrap). Proteins were identified using Mascot (Matrix Science, London, UK) based on a custom proteome file of *S. Typhimurium* strain ATCC 14028s. Spectral counts were extracted using Scaffold Viewer (Proteome Software, Portland, OR, USA) and compared to controls (similar treated *S. Typhimurium* WT without 3×Flag tagged proteins) with the 'R' (54) package 'apmsWAPP' (55) applying upper quartile normalization and interquartile range filtering. Data is summarized in Table S4.

Cell culture and infection

HT29-MTX human colonic epithelial cells (kind gift of G. Grassl, Hannover, Germany) were cultured in DMEM medium (high glucose, stable glutamine, sodium pyruvate) (Biowest, Nuaille, France) supplemented with 10% FCS and non-essential amino acids (Biowest). HeLa cells (ATCC CCL-2, LGC Standards, Wesel, Germany) were grown in DMEM (Biowest) supplemented with 10% FCS, sodium pyruvate and 2 mM GlutaMax (Thermo Fisher) and MDCK cells (subclone Pf, Department of Nephrology, FAU Erlangen-Nürnberg) were kept in MEM medium (Biowest) supplemented with 10% FCS, 2 mM Glutamax (Thermo Fisher) and non-essential amino acids (Biowest). To each medium 100 U/mL penicillin and 100 µg/mL streptomycin (Biowest) were added. Cultures were incubated at 37°C in a humidified 5% (v/v) CO₂ atmosphere. For invasion assays, HT29-MTX cells were seeded in 24-well culture plates (#662160, Cellstar, Greiner Bio-One, Frickenhausen, Germany) at a density of 4×10⁴ cells per well 21 days prior infection. MDCK and HeLa cells were seeded in 96-well plates (#655180, Greiner Bio-One) at a density of 8×10⁴ or 6×10³ per well, respectively. MDCK cells were allowed to polarize for 10–11 days. The culture medium was changed every other day and medium without antibiotics was used for the last medium change.

Gentamicin protection assays were essentially carried out as described previously [7]. Briefly, bacterial overnight (O/N) cultures grown in LB supplemented with appropriate antibiotics were re-inoculated 1:31 in fresh medium and grown aerobically for another 3.5 h. An inoculum corresponding to a multiplicity of infection (MOI) of 10 (HeLa) or 25 (MDCK, HT29-MTX) was prepared in MEM/DMEM and used to infect the cells for 25 min. After the cells had been washed thrice with PBS, MEM/DMEM containing 100 µg/mL gentamicin was applied to each well to kill remaining extracellular bacteria. After 1 h of incubation, the cell layers were washed again with PBS and then lysed for 10 min with PBS containing 1% Elugent (Merck Millipore, Darmstadt, Germany) and 0.0625% Antifoam B (Sigma-Aldrich, Schnelldorf, Germany) to liberate the intracellular bacteria. Serial dilutions of the inoculum and the lysates were plated on Mueller Hinton (MH) plates to determine the colony-forming units. Based on the inoculum the percentage of invasive bacteria was calculated and subsequently normalized to WT.

Swarming assay

Swarming of different *Salmonella* strains was assessed on semi-solid agar LB plates (LB with 5 g/L NaCl, 0.5% agar) as described before (19). Briefly, a small amount (0.2 µL) of bacterial O/N cultures was applied onto the center of LB soft agar plate and incubated for six hours at 37°C. The diameters of the swarm colonies were measured and the plates were photographed.

Capillary assay

Capillary assays were essentially performed as described before (28) with the following modifications: An U-shaped dam created from a piece of modelling clay and parafilm was mounted onto a microscopy slide. The chamber thus created was sealed with a cover slip and filled with 500 μ L of a 3.5 h bacterial sub-culture. A 1 μ L capillary (BLAUBRAND intraEND, Brand, Wertheim, Germany) was heat-sealed at one end and then filled with a 100 mM MeAsp solution. The capillary prepared in this way was immersed in the chamber for 1 h at 37°C. The capillary was then rinsed, the sealed end broken off and the capillary contents was emptied using a pipetting aid (Brand). Serial dilutions were plated and CFUs determined. **ELISA** Antisera were raised in rabbits against the recombinant C-terminal moiety of SiiE (7). For detection of SiiE, culture supernatants were filter-sterilized (0.45 μ m syringe filters, Corning Life Sciences, Amsterdam, Netherlands), and aliquots of 50 μ L were directly applied to 96-well Nunc MultiSorp microtiter plates (#467340 Thermo Fisher) overnight at 4°C in a humid chamber. The plates were washed three times with 200 μ L/well of PBS supplemented with 0.05 % Tween20 (PBS-Tween), and the rabbit anti-glutathione S-transferase(GST)-SiiE-C detection antibody diluted 1:1,000 in PBS plus 10 % inactivated FCS (PBS-FCS) was applied for 2 h at RT. After five washes with PBS-Tween, 100 μ L of the anti-rabbit horseradish peroxidase-coupled secondary antibody diluted 1:2,500 in PBS-FCS was added to each well for 30 min at RT. The wells were washed again seven times with PBS-Tween, and 50 μ L of enzyme-linked immunosorbent assay (ELISA) horseradish peroxidase substrate (#555214, Becton Dickinson, Heidelberg, Germany) was added. After incubation in the dark at RT for 8 to 15 min, the reaction was stopped by the addition of 25 μ L/well 0.5 M H₂SO₄ and A₄₅₀ was measured using a M1000 plate reader (Tecan, Männedorf, Switzerland).

Dot Blot

Bacterial strains were diluted 1:31 in LB from O/N cultures and grown at 37°C for 3.5 h. Aliquots of 1 mL of bacterial culture were collected, cells pelleted and re-suspended in 1 mL of sterile LB. After an additional washing step with sterile LB, bacterial suspensions were adjusted to OD₆₀₀=1 in 500 μ L of 3 % PFA in PBS. After fixation of bacterial cells for 15 min at RT, cells were pelleted (10,000 \times g, 5 min., RT) and re-suspended in 500 μ L PBS. Five microliters of bacterial suspensions were spotted on nitrocellulose membrane pieces, set in a black 24-well plate, which have been pre-wetted with PBS and dried again before adding bacteria. After drying of the spots, membranes were blocked with 5 % dry milk powder and 3 % BSA in PBS/T (PBS + 0.1 % Tween20) for at least 30 min. For detection of SiiE on the bacterial surface, antiserum against the C-terminal moiety of SiiE was diluted 1:5,000 in blocking solution and applied to the membrane. LPS was detected using antiserum against Salmonella O-antigen (Becton Dickinson) at the same dilution. After incubation O/N at 4°C, membranes were washed thrice with PBS/T and HRP-linked secondary antibody was added in a 1:50,000 dilution in PBS/T. After three additional washing steps with PBS/T, membranes were rinsed in PBS, substrate for HRP was applied and signals were quantified using a Tecan M1000 plate reader in luminescence mode.

SIMPLE Assay

A screen for ligand expression using immunomagnetic particles (SIMPLE) assay was carried out as described by Nuccio *et al.* (37) with the following modifications. *Salmonella* strains were sub-cultured 1:31 from O/N for 3.5 h at 37°C and adjusted to OD₆₀₀=2 in fresh PB buffer (=TN buffer (0.1 M Tris-HCl pH 7.5, 0.15 M NaCl) plus 1 % casein). Strains carried either plasmid pWSK29 or derivatives to exhibit carbenicillin resistance or plasmid pWSK129 for a kanamycin resistance. The strains were mixed at a ratio of 1:1 and bacteria were then pre-incubated with α-SiiE antibody or pre-immune serum in 650 μL PB-buffer for 1 h at RT with head-over-head rotation. Then, 100 μL of washed magnetic beads (BioMag Protein A, Qiagen, Hilden, Germany) resuspended in 100 μL TN-buffer were added to each sample (total volume of 750 μL) and incubated for two additional hours. After three washing steps with 750 μL TN buffer, beads were suspended in 1 mL PBS. Serial dilutions of all probes were plated in parallel on MH plates containing carbenicillin or kanamycin, CFU were determined and enrichment based on the competitive index and normalization to pre-immune serum controls was calculated.

Acknowledgements

We thank Guntram Grassl (Hannover, Germany) for providing cell line HT29-MTX. This work was funded by grants of the German research foundation (www.DFG.de) to Y.A.M. (MU 1477 9/2), M.H. (HE 1964 13/2) and R.G.G. (GE 2533 2/2).

References

1. I. Behlau, S. I. Miller, A PhoP-repressed gene promotes *Salmonella typhimurium* invasion of epithelial cells. *J Bacteriol* **175**, 4475-4484 (1993).
2. B. Stecher *et al.*, *Salmonella enterica* serovar Typhimurium exploits inflammation to compete with the intestinal microbiota. *PLoS Biol* **5**, 2177-2189 (2007).
3. M. Lara-Tejero, J. E. Galán, *Salmonella enterica* serovar typhimurium pathogenicity island 1 encoded type III secretion system translocases mediate intimate attachment to nonphagocytic cells. *Infect Immun* **77**, 2635-2642 (2009).
4. B. Misselwitz *et al.*, *Salmonella enterica* serovar Typhimurium binds to HeLa cells via Fimmediated reversible adhesion and irreversible type three secretion system 1-mediated docking. *Infect Immun* **79**, 330-341 (2011).
5. R. G. Gerlach *et al.*, Cooperation of *Salmonella* pathogenicity islands 1 and 4 is required to breach epithelial barriers. *Cell Microbiol* **10**, 2364-2376 (2008).
6. R. G. Gerlach, D. Jäckel, N. Geymeier, M. Hensel, *Salmonella* pathogenicity island 4-mediated adhesion is coregulated with invasion genes in *Salmonella enterica*. *Infect Immun* **75**, 46974709 (2007).
7. R. G. Gerlach *et al.*, *Salmonella* Pathogenicity Island 4 encodes a giant non-fimbrial adhesin and the cognate type 1 secretion system. *Cell Microbiol* **9**, 1834-1850 (2007).
8. X. Li *et al.*, MUC1 is a receptor for the *Salmonella* SiiE adhesin that enables apical invasion into enterocytes. *PLoS Pathog* **15**, e1007566 (2019).
9. C. Wagner, B. Barlag, R. G. Gerlach, J. Deiwick, M. Hensel, The *Salmonella enterica* giant adhesin SiiE binds to polarized epithelial cells in a lectin-like manner. *Cell Microbiol* **16**, 962975 (2014).
10. M. H. Grieschl *et al.*, Structural insight into the giant Ca²⁺-binding adhesin SiiE: implications for the adhesion of *Salmonella enterica* to polarized epithelial cells. *Structure* **21**, 741-752 (2013).
11. B. Peters *et al.*, Structural and functional dissection reveals distinct roles of Ca²⁺-binding sites in the giant adhesin SiiE of *Salmonella enterica*. *PLoS Pathog* **13**, e1006418 (2017).
12. S. Thomas, I. B. Holland, L. Schmitt, The Type 1 secretion pathway – The hemolysin system and beyond. *Biochimica et biophysica acta* **10.1016/j.bbamcr.2013.09.017** (2013).
13. C. Männe *et al.*, *Salmonella* SiiE prevents an efficient humoral immune memory by interfering with IgG⁺ plasma cell persistence in the bone marrow. *Proc Natl Acad Sci U S A* **116**, 74257430 (2019).
14. C. Wagner *et al.*, Functional dissection of SiiE, a giant non-fimbrial adhesin of *Salmonella enterica*. *Cell Microbiol* **13**, 1286-1301 (2011).
15. T. Wille *et al.*, SiiA and SiiB are novel type I secretion system subunits controlling SPI4-mediated adhesion of *Salmonella enterica*. *Cell Microbiol* **16**, 161-178 (2014).
16. P. Kirchweber *et al.*, Structural and functional characterization of SiiA, an auxiliary protein from the SPI4-encoded type 1 secretion system from *Salmonella enterica*. *Mol Microbiol* **112**, 14031422 (2019).
17. Y. Blat, M. Eisenbach, Tar-dependent and -independent pattern formation by *Salmonella typhimurium*. *J Bacteriol* **177**, 1683-1691 (1995).
18. J. S. Parkinson, G. L. Hazelbauer, J. J. Falke, Signaling and sensory adaptation in *Escherichia coli* chemoreceptors: 2015 update. *Trends Microbiol* **23**, 257-266 (2015).
19. S. Hoffmann, C. Schmidt, S. Walter, J. K. Bender, R. G. Gerlach, Scarless deletion of up to seven methyl-accepting chemotaxis genes with an optimized method highlights key function of CheM in *Salmonella* Typhimurium. *PLoS One* **12**, e0172630 (2017).
20. B. D. Jones, C. A. Lee, S. Falkow, Invasion by *Salmonella typhimurium* is affected by the direction of flagellar rotation. *Infect Immun* **60**, 2475-2480 (1992).

21. A. F. Kolodziej, T. Tan, D. E. Koshland, Jr., Producing positive, negative, and no cooperativity by mutations at a single residue located at the subunit interface in the aspartate receptor of *Salmonella typhimurium*. *Biochemistry* **35**, 14782-14792 (1996).
22. T. Mizuno, N. Mutoh, S. M. Panasenko, Y. Imae, Acquisition of maltose chemotaxis in *Salmonella typhimurium* by the introduction of the *Escherichia coli* chemosensory transducer gene. *J Bacteriol* **165**, 890-895 (1986).
23. G. Karimova, J. Pidoux, A. Ullmann, D. Ladant, A bacterial two-hybrid system based on a reconstituted signal transduction pathway. *Proc Natl Acad Sci U S A* **95**, 5752-5756 (1998).
24. G. Karimova, A. Ullmann, D. Ladant, A bacterial two-hybrid system that exploits a cAMP signaling cascade in *Escherichia coli*. *Methods Enzymol* **328**, 59-73 (2000).
25. B. Misselwitz *et al.*, Near surface swimming of *Salmonella Typhimurium* explains target-site selection and cooperative invasion. *PLoS Pathog* **8**, e1002810 (2012).
26. F. J. Van Asten, H. G. Hendriks, J. F. Koninkx, B. A. Van der Zeijst, W. Gaastra, Inactivation of the flagellin gene of *Salmonella enterica* serotype Enteritidis strongly reduces invasion into differentiated Caco-2 cells. *FEMS microbiology letters* **185**, 175-179 (2000).
27. T. Khoramian-Falsafi, S. Harayama, K. Kutsukake, J. C. Pechere, Effect of motility and chemotaxis on the invasion of *Salmonella typhimurium* into HeLa cells. *Microb Pathog* **9**, 47-53 (1990).
28. J. Adler, A method for measuring chemotaxis and use of the method to determine optimum conditions for chemotaxis by *Escherichia coli*. *J Gen Microbiol* **74**, 77-91 (1973).
29. R. Mesibov, J. Adler, Chemotaxis toward amino acids in *Escherichia coli*. *J Bacteriol* **112**, 315326 (1972).
30. S. Neumann, C. H. Hansen, N. S. Wingreen, V. Sourjik, Differences in signalling by directly and indirectly binding ligands in bacterial chemotaxis. *EMBO J* **29**, 3484-3495 (2010).
31. M. L. Hedblom, J. Adler, Genetic and biochemical properties of *Escherichia coli* mutants with defects in serine chemotaxis. *J Bacteriol* **144**, 1048-1060 (1980).
32. T. Lesuffleur, A. Barbat, E. Dussaulx, A. Zweibaum, Growth adaptation to methotrexate of HT29 human colon carcinoma cells is associated with their ability to differentiate into columnar absorptive and mucus-secreting cells. *Cancer Res* **50**, 6334-6343 (1990).
33. F. Rivera-Chávez *et al.*, Energy Taxits toward Host-Derived Nitrate Supports a *Salmonella* Pathogenicity Island 1-Independent Mechanism of Invasion. *mBio* **7** (2016).
34. F. Rivera-Chávez *et al.*, *Salmonella* uses energy taxis to benefit from intestinal inflammation. *PLoS Pathog* **9**, e1003267 (2013).
35. B. Stecher *et al.*, Flagella and chemotaxis are required for efficient induction of *Salmonella enterica* serovar Typhimurium colitis in streptomycin-pretreated mice. *Infect Immun* **72**, 41384150 (2004).
36. M. A. Matilla, T. Krell, The effect of bacterial chemotaxis on host infection and pathogenicity. *FEMS Microbiol Rev* **42** (2018).
37. S. P. Nuccio *et al.*, SIMPLE approach for isolating mutants expressing fimbriae. *Appl Environ Microbiol* **73**, 4455-4462 (2007).
38. K. G. Cooper *et al.*, Regulatory protein Hild stimulates *Salmonella Typhimurium* invasiveness by promoting smooth swimming via the methyl-accepting chemotaxis protein McpC. *Nat Commun* **12**, 348 (2021).
39. C. García-Fontana *et al.*, The involvement of McpB chemoreceptor from *Pseudomonas aeruginosa* PAO1 in virulence. *Sci Rep* **9**, 13166 (2019).
40. H. P. McLaughlin, D. L. Caly, Y. McCarthy, R. P. Ryan, J. M. Dow, An orphan chemotaxis sensor regulates virulence and antibiotic tolerance in the human pathogen *Pseudomonas aeruginosa*. *PLoS One* **7**, e42205 (2012).
41. Y. Choi *et al.*, Plasmid-encoded MCP is involved in virulence, motility, and biofilm formation of *Cronobacter sakazakii* ATCC 29544. *Infect Immun* **83**, 197-204 (2015).
42. A. P. Chaparro, S. K. Ali, K. E. Klose, The ToxT-dependent methyl-accepting chemoreceptors AcfB and TcpI contribute to *Vibrio cholerae* intestinal colonization. *FEMS microbiology letters* **302**, 99-105 (2010).
43. M. Guo, Z. Huang, J. Yang, Is there any crosstalk between the chemotaxis and virulence induction signaling in *Agrobacterium tumefaciens*? *Biotechnol Adv* **35**, 505-511 (2017).
44. R. Kumar Verma, B. Samal, S. Chatterjee, *Xanthomonas oryzae* pv. *oryzae* chemotaxis components and chemoreceptor Mcp2 are involved in the sensing of constituents of xylem sap and contribute to the regulation of virulence-associated functions and entry into rice. *Mol Plant Pathol* **19**, 2397-2415 (2018).
45. S. Kojima *et al.*, The Helix Rearrangement in the Periplasmic Domain of the Flagellar Stator B Subunit Activates Peptidoglycan Binding and Ion Influx. *Structure* **26**, 590-598 e595 (2018).
46. K. Postle, R. A. Larsen, TonB-dependent energy transduction between outer and cytoplasmic membranes. *Biometals* **20**, 453-465 (2007).
47. P. Germon, M. C. Ray, A. Vianney, J. C. Lazzaroni, Energy-dependent conformational change in the TolA protein of *Escherichia coli* involves its N-terminal domain, TolQ, and TolR. *J Bacteriol* **183**, 4110-4114 (2001).
48. A. Jahan-Mihan, B. L. Luhovyy, D. El Khoury, G. H. Anderson, Dietary proteins as determinants of metabolic and physiologic functions of the gastrointestinal tract. *Nutrients* **3**, 574-603 (2011).
49. N. van der Wielen, P. J. Moughan, M. Mensink, Amino Acid Absorption in the Large Intestine of Humans and Porcine Models. *J Nutr* **147**, 1493-1498 (2017).
50. H. G. Windmueller, A. E. Spaeth, Respiratory fuels and nitrogen metabolism in vivo in small intestine of fed rats. Quantitative importance of glutamine, glutamate, and aspartate. *J Biol Chem* **255**, 107-112 (1980).
51. Z. L. Dai, G. Wu, W. Y. Zhu, Amino acid metabolism in intestinal bacteria: links between gut ecology and host health. *Front Biosci (Landmark Ed)* **16**, 1768-1786 (2011).
52. S. P. Claus *et al.*, Systemic multicompartmental effects of the gut microbiome on mouse metabolic phenotypes. *Mol Syst Biol* **4**, 219 (2008).
53. B. D. Nguyen *et al.*, Import of Aspartate and Malate by DcuABC Drives H₂/Fumarate Respiration to Promote Initial *Salmonella* Gut-Lumen Colonization in Mice. *Cell Host Microbe* **27**, 922-936 e926 (2020).
54. R Core Team (2021) R: A language and environment for statistical computing. (R Foundation for Statistical Computing, Vienna, Austria).
55. M. Fischer, S. Zilkenat, R. G. Gerlach, S. Wagner, B. Y. Renard, Pre- and post-processing workflow for affinity purification mass spectrometry data. *J Proteome Res* **13**, 2239-2249 (2014).

SUPPLEMENTARY INFORMATION

A chemotactic sensor controls *Salmonella*-host cell interaction

Stefanie Hoffmann¹, Kathrin Gendera¹, Christiane Schmidt¹, Peter Kirchweber², Axel Imhof³,
Christian Bogdan⁴, Yves Muller², Michael Hensel⁵ and Roman G. Gerlach^{1,4}

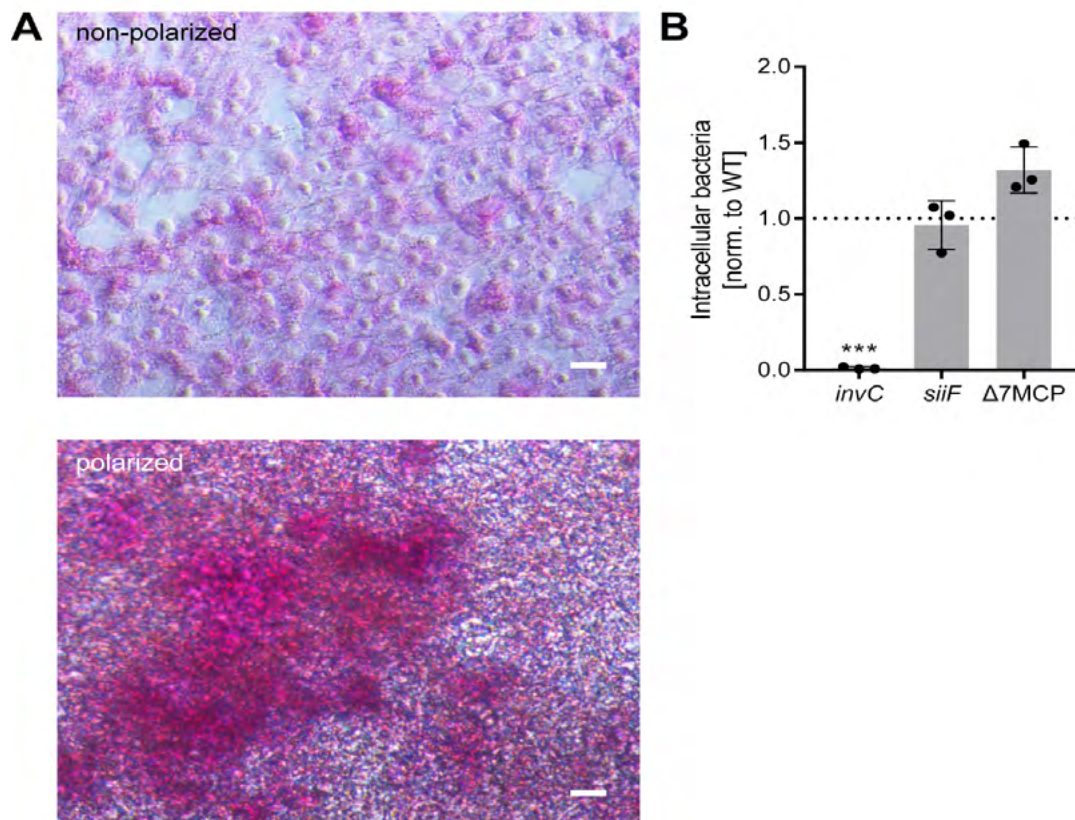
¹ Project Group 5, Robert Koch Institute, Wernigerode, Germany

² Division of Biotechnology, Department of Biology, Friedrich-Alexander-University (FAU) Erlangen-Nuremberg, Erlangen, Germany

³ BioMedical Center and Center for Integrated Protein Sciences Munich, Ludwig-Maximilians-Universität München, München, Germany

⁴ Mikrobiologisches Institut – Klinische Mikrobiologie, Immunologie und Hygiene, Universitätsklinikum Erlangen and Friedrich-Alexander-Universität Erlangen-Nürnberg, Erlangen, Germany

⁵ Abteilung Mikrobiologie, Universität Osnabrück, Osnabrück, Germany and CellNanOs – Center for Cellular Nanoanalytics Osnabrück, Universität Osnabrück, Osnabrück, Germany



S1 Fig. Phenotype of HT29-MTX cells. (A) Periodic acid-Schiff (PAS) staining of mucins (purple) produced by HT29-MTX after one day (non-polarized, upper panel) and after 21 days (polarized, lower panel) of differentiation. Scale bar = 20 μ m. (B) Relative invasion rates in non-polarized HT29-MTX cells as normalized to *S. Typhimurium* WT (black dotted line) after one hour of infection with strains *invC* (non-functional T3SS-1), *siiF* (non-functional SPI-4) and $\Delta 7$ MCP are depicted. Statistical significance was calculated using a one sample *t* test against the hypothetical value 1 and were defined as *** for $p < 0.001$.

Table S1. Strains used in this study.

Strain	Relevant characteristic(s)	Source or Reference
<i>E. coli</i> strains		
BTH101	F, <i>cya-99</i> , <i>araD139</i> , <i>galE15</i> , <i>galK16</i> , <i>rpsL1</i> (Str ^r), <i>hsdR2</i> , <i>mcrA1</i> , <i>mcrB1</i>	[24]
<i>Salmonella</i> strains		
MvP818	NCTC 12023 $\Delta invC$ FRT	[6]
MvP1212	NCTC 12023 $\Delta cheY$ FRT	[61]
MvP1213	NCTC 12023 $\Delta flhJ$ FRT	[62]
NCTC 12023	Wild type, Nal ^r , isogenic to ATCC 14028	NCTC, Colindale, UK
WRG246	NCTC 12023 Δaer	[18]
WRG255	NCTC 12023 $\Delta aer \Delta tcp$	[18]
WRG260	NCTC 12023 $\Delta aer \Delta tcp \Delta tsr$	[18]
WRG264	NCTC 12023 $\Delta aer \Delta tcp \Delta tsr \Delta trg$	[18]
WRG269	NCTC 12023 $\Delta aer \Delta tcp \Delta tsr \Delta trg \Delta cheM$	[18]
WRG277	NCTC 12023 $\Delta aer \Delta tcp \Delta tsr \Delta trg \Delta cheM \Delta mcpC$	[18]
WRG279	NCTC 12023 $\Delta aer \Delta tcp \Delta tsr \Delta trg \Delta cheM \Delta mcpC \Delta mcpB$	[18]
WRG469	NCTC 12023 $\Delta cheA$	This study
WRG521	NCTC 12023 $\Delta aer \Delta tcp \Delta tsr \Delta trg \Delta cheM \Delta mcpC \Delta mcpB \Delta cheY$	This study
WRG522	NCTC 12023 $\Delta aer \Delta tcp \Delta tsr \Delta trg \Delta cheM \Delta mcpC \Delta mcpB \Delta cheA$	This study
WRG238	NCTC 12023 <i>siiF</i> ^{Δ270} , Walker B motif disruption	
WRG384	$\Delta hilE$	This study

Table 2. Plasmids used in this study.

Plasmid	Relevant characteristic(s)	Source or Reference
p25-N	encodes the T25 fragment (aa 1–224) of CyaA for C-terminal fusions; Km ^r	
pKD4	<i>aph</i> resistance cassette flanked by FRT sites, λ Pir dependent replication, Km ^r , Ap ^r	[63]
pKNT25-ZIP	pKT25 derivative; leucine zipper of GCN4 fused in frame to T25 fragment; Km ^r	[23]
pKT25	encodes the T25 fragment (aa 1–224) of CyaA; for N-terminal fusions; Km ^r	[23]
pUT18	T18 fragment (aa 225–399) of CyaA; for C-terminal fusions, Ap ^r	[23]
pUT18C-ZIP	pUT18C derivative; leucine zipper of GCN4 fused in frame T18 fragment, Ap ^r	[23]
pWRG717	pBluescript II SK+ derivative, <i>aph</i> resistance cassette and I-SceI cleavage site, Km ^r , Ap ^r	[18]
pWRG730	pSIM5 [64] derivative, temperature-sensitive replication (30°C) and Red recombinase expression (42°C), Tet-inducible expression of I-SceI, Cm ^r	[18]
pWRG406	P _{src} :: <i>HilA</i> in pBAD24, Ap ^r	
pWRG847	pCheM; P _{cheM} :: <i>cheM</i> in pWSK29, Ap ^r	[18]
pWRG868	P _{cheM} :: <i>cheM</i> -3×FLAG in pWSK29, Ap ^r	This study
pWRG890	pTar; P _{cheM} :: <i>tar</i> -3×FLAG in pWSK29, Ap ^r	This study
pWRG903	P _{cheM} :: <i>cheM</i> -HA in pWSK29, Ap ^r	This study
pWRG905	P _{src} :: <i>siiAB</i> -3×FLAG in pETcoco-1, Cm ^r	This study
pWSK29	Low-copy-number vector, Ap ^r	[65]

References

- Behlau I, Miller SI. A PhoP-repressed gene promotes *Salmonella typhimurium* invasion of epithelial cells. *J Bacteriol.* 1993;175(14):4475-84. PubMed PMID: 8392513; PubMed Central PMCID: PMCPMC204888.
- Stecher B, Robbiani R, Walker AW, Westendorf AM, Barthel M, Kremer M, *et al.* *Salmonella enterica* serovar Typhimurium exploits inflammation to compete with the intestinal microbiota. *PLoS Biol.* 2007;5(10):2177-89. doi: 10.1371/journal.pbio.0050244. PubMed PMID: 17760501; PubMed Central PMCID: PMCPMC1951780.
- Agbor TA, McCormick BA. *Salmonella* effectors: important players modulating host cell function during infection. *Cell Microbiol.* 2011;13(12):1858-69. doi: 10.1111/j.1462-5822.2011.01701.x. PubMed PMID: 21902796; PubMed Central PMCID: PMCPMC3381885.
- Lara-Tejero M, Galán JE. *Salmonella enterica* serovar typhimurium pathogenicity island 1-encoded type III secretion system translocases mediate intimate attachment to nonphagocytic cells. *Infect Immun.* 2009;77(7):2635-42. doi: 10.1128/IAI.00077-09. PubMed PMID: 19364837; PubMed Central PMCID: PMCPMC2708559.
- Misselwitz B, Kreibich SK, Rout S, Stecher B, Periaswamy B, Hardt WD. *Salmonella enterica* serovar Typhimurium binds to HeLa cells via Fim-mediated reversible adhesion and irreversible type three secretion system 1-mediated docking. *Infect Immun.* 2011;79(1):330-41. doi: 10.1128/IAI.00581-10. PubMed PMID: 20974826; PubMed Central PMCID: PMCPMC3019867.
- Gerlach RG, Cláudio N, Rohde M, Jäckel D, Wagner C, Hensel M. Cooperation of *Salmonella* pathogenicity islands 1 and 4 is required to breach epithelial barriers. *Cell Microbiol.* 2008;10(11):2364-76. doi: 10.1111/j.1462-5822.2008.01218.x. PubMed PMID: 18671822.
- Gerlach RG, Jäckel D, Stecher B, Wagner C, Lupas A, Hardt WD, *et al.* *Salmonella* Pathogenicity Island 4 encodes a giant non-fimbrial adhesin and the cognate type I secretion system. *Cell Microbiol.* 2007;9(7):1834-50. doi: 10.1111/j.1462-5822.2007.00919.x. PubMed PMID: 17388786.
- Gerlach RG, Jäckel D, Geymeier N, Hensel M. *Salmonella* pathogenicity island 4-mediated adhesion is coregulated with invasion genes in *Salmonella enterica*. *Infect Immun.* 2007;75(10):4697-709. doi: 10.1128/IAI.00228-07. PubMed PMID: 17635868; PubMed Central PMCID: PMCPMC2044552.
- Wagner C, Barlag B, Gerlach RG, Deiwick J, Hensel M. The *Salmonella enterica* giant adhesin SiiE binds to polarized epithelial cells in a lectin-like manner. *Cell Microbiol.* 2013. doi: 10.1111/cmi.12253. PubMed PMID: 24345213.
- Griessl MH, Schmid B, Kassler K, Braunsmann C, Ritter R, Barlag B, *et al.* Structural insight into the giant Ca²⁺-binding adhesin SiiE: implications for the adhesion of *Salmonella enterica* to polarized epithelial cells. *Structure.* 2013;21(5):741-52. doi: 10.1016/j.str.2013.02.020. PubMed PMID: 23562396.
- Peters B, Stein J, Klingl S, Sander N, Sandmann A, Taccardi N, *et al.* Structural and functional dissection reveals distinct roles of Ca²⁺-binding sites in the giant adhesin SiiE of *Salmonella enterica*. *PLoS Pathog.* 2017;13(5):e1006418. doi: 10.1371/journal.ppat.1006418. PubMed PMID: 28558023; PubMed Central PMCID: PMCPMC5466336.
- Bumba L, Masin J, Macek P, Wald T, Motlova L, Bibova I, *et al.* Calcium-Driven Folding of RTX Domain b-Rolls Ratchets Translocation of RTX Proteins through type I Secretion Ducts. *Mol Cell.* 2016;62(1):47-62. doi: 10.1016/j.molcel.2016.03.018. PubMed PMID: 27058787.
- Thomas S, Holland IB, Schmitt L. The type I secretion pathway – The hemolysin system and beyond. *Biochimica et biophysica acta.* 2013. doi: 10.1016/j.bbamcr.2013.09.017. PubMed PMID: 24129268.
- Wagner C, Polke M, Gerlach RG, Linke D, Stierhof YD, Schwarz H, *et al.* Functional dissection of SiiE, a giant non-fimbrial adhesin of *Salmonella enterica*. *Cell Microbiol.* 2011;13(8):1286-301. Epub 2011/07/07. doi: 10.1111/j.1462-5822.2011.01621.x. PubMed PMID: 21729227.
- Wille T, Wagner C, Mittelstädt W, Blank K, Sommer E, Malengo G, *et al.* SiiA and SiiB are novel type I secretion system subunits controlling SPI-4-mediated adhesion of *Salmonella enterica*. *Cell Microbiol.* 2014;16(2):161-78. doi: 10.1111/cmi.12222. PubMed PMID: 24119191.
- Kirchweber P, Weiler S, Egerer-Sieber C, Blasl AT, Hoffmann S, Schmidt C, *et al.* Structural and functional characterization of SiiA, an auxiliary protein from the SPI-4-encoded type I secretion system from *Salmonella enterica*. *Mol Microbiol.* 2019;112(5):1403-22. Epub 2019/08/17. doi: 10.1111/mmi.14368. PubMed PMID: 31419359.
- Parkinson JS, Hazelbauer GL, Falke JJ. Signaling and sensory adaptation in *Escherichia coli* chemoreceptors: 2015 update. *Trends Microbiol.* 2015;23(5):257-66. Epub 2015/04/04. doi: 10.1016/j.tim.2015.03.003. PubMed PMID: 25834953; PubMed Central PMCID: PMCPMC4417406.
- Hoffmann S, Schmidt C, Walter S, Bender JK, Gerlach RG. Scarless deletion of up to seven methyl-accepting chemotaxis genes with an optimized method highlights key function of CheM in *Salmonella* Typhimurium. *PLoS One.* 2017;12(2):e0172630. doi: 10.1371/journal.pone.0172630. PubMed PMID: 28212413; PubMed Central PMCID: PMC5315404.
- Jones BD, Lee CA, Falkow S. Invasion by *Salmonella typhimurium* is affected by the direction of flagellar rotation. *Infect Immun.* 1992;60(6):2475-80. PubMed PMID: 1587617; PubMed Central PMCID: PMC257184.
- Blat Y, Eisenbach M. Tar-dependent and -independent pattern formation by *Salmonella typhimurium*. *J Bacteriol.* 1995;177(7):1683-91. PubMed PMID: 7896688; PubMed Central PMCID: PMC176793.
- Kolodziej AF, Tan T, Koshland DE, Jr. Producing positive, negative, and no cooperativity by mutations at a single residue located at the subunit interface in the aspartate receptor of *Salmonella typhimurium*. *Biochemistry.* 1996;35(47):14782-92. doi: 10.1021/bi961481v. PubMed PMID: 8942640.
- Mizuno T, Mutoh N, Panasenka SM, Imae Y. Acquisition of maltose chemotaxis in *Salmonella typhimurium* by the introduction of the *Escherichia coli* chemosensory transducer gene. *J Bacteriol.* 1986;165(3):890-5. Epub 1986/03/01. doi: 10.1128/jb.165.3.890-895.1986. PubMed PMID: 3512528; PubMed Central PMCID: PMCPMC214512.
- Karimova G, Pidoux J, Ullmann A, Ladant D. A bacterial two-hybrid system based on a reconstituted signal transduction pathway. *Proc Natl Acad Sci U S A.* 1998;95(10):5752-6. PubMed PMID: 9576956; PubMed Central PMCID: PMCPMC20451.

24. Karimova G, Ullmann A, Ladant D. A bacterial two-hybrid system that exploits a cAMP signaling cascade in *Escherichia coli*. *Methods Enzymol.* 2000;328:59-73. PubMed PMID: 11075338.
25. Misselwitz B, Barrett N, Kreibich S, Vonaesch P, Andrichschke D, Rout S, *et al.* Near surface swimming of *Salmonella* Typhimurium explains target-site selection and cooperative invasion. *PLoS Pathog.* 2012;8(7):e1002810. doi: 10.1371/journal.ppat.1002810. PubMed PMID: 22911370; PubMed Central PMCID: PMC3406100.
26. Van Asten FJ, Hendriks HG, Koninkx JF, Van der Zeijst BA, Gaastra W. Inactivation of the flagellin gene of *Salmonella enterica* serotype Enteritidis strongly reduces invasion into differentiated Caco-2 cells. *FEMS microbiology letters.* 2000;185(2):175-9. PubMed PMID: 10754244.
27. Khoramian-Falsafi T, Harayama S, Kutsukake K, Pechere JC. Effect of motility and chemotaxis on the invasion of *Salmonella typhimurium* into HeLa cells. *Microb Pathog.* 1990;9(1):47-53. PubMed PMID: 2077343.
28. Adler J. A method for measuring chemotaxis and use of the method to determine optimum conditions for chemotaxis by *Escherichia coli*. *Microbiology.* 1973;74(1):77-91.
29. Mesibov R, Adler J. Chemotaxis toward amino acids in *Escherichia coli*. *J Bacteriol.* 1972;112(1):315-26. Epub 1972/10/01. PubMed PMID: 4562400; PubMed Central PMCID: PMCPMC251414.
30. Neumann S, Hansen CH, Wingreen NS, Sourjik V. Differences in signalling by directly and indirectly binding ligands in bacterial chemotaxis. *EMBO J.* 2010;29(20):3484-95. Epub 2010/09/14. doi: 10.1038/emboj.2010.224. PubMed PMID: 20834231; PubMed Central PMCID: PMCPMC2964171.
31. Hedblom ML, Adler J. Genetic and biochemical properties of *Escherichia coli* mutants with defects in serine chemotaxis. *J Bacteriol.* 1980;144(3):1048-60. PubMed PMID: 6777365; PubMed Central PMCID: PMCPMC294770.
32. Lesuffleur T, Barbat A, Dussaulx E, Zweibaum A. Growth adaptation to methotrexate of HT-29 human colon carcinoma cells is associated with their ability to differentiate into columnar absorptive and mucus-secreting cells. *Cancer Res.* 1990;50(19):6334-43. Epub 1990/10/01. PubMed PMID: 2205381.
33. Rivera-Chávez F, Lopez CA, Zhang LF, García-Pastor L, Chávez-Arroyo A, Lokken KL, *et al.* Energy Taxis toward Host-Derived Nitrate Supports a *Salmonella* Pathogenicity Island 1-Independent Mechanism of Invasion. *mBio.* 2016;7(4). Epub 2016/07/21. doi: 10.1128/mBio.00960-16. PubMed PMID: 27435462; PubMed Central PMCID: PMCPMC4958259.
34. Rivera-Chávez F, Winter SE, Lopez CA, Xavier MN, Winter MG, Nuccio SP, *et al.* *Salmonella* uses energy taxis to benefit from intestinal inflammation. *PLoS Pathog.* 2013;9(4):e1003267. doi: 10.1371/journal.ppat.1003267. PubMed PMID: 23637594; PubMed Central PMCID: PMC3630101.
35. Stecher B, Hapfelmeier S, Müller C, Kremer M, Stallmach T, Hardt WD. Flagella and chemotaxis are required for efficient induction of *Salmonella enterica* serovar Typhimurium colitis in streptomycin-pretreated mice. *Infect Immun.* 2004;72(7):4138-50. doi: 10.1128/IAI.72.7.4138-4150.2004. PubMed PMID: 15213159; PubMed Central PMCID: PMC427403.
36. Matilla MA, Krell T. The effect of bacterial chemotaxis on host infection and pathogenicity. *FEMS Microbiol Rev.* 2018;42(1). Epub 2017/10/27. doi: 10.1093/femsre/fux052. PubMed PMID: 29069367.
37. Nuccio SP, Chessa D, Weening EH, Raffatellu M, Clegg S, Bäumlér AJ. SIMPLE approach for isolating mutants expressing fimbriae. *Appl Environ Microbiol.* 2007;73(14):4455-62. doi: 10.1128/AEM.00148-07. PubMed PMID: 17526787; PubMed Central PMCID: PMCPMC1932825.
38. Newell PD, Boyd CD, Sondermann H, O'Toole GA. A c-di-GMP effector system controls cell adhesion by inside-out signaling and surface protein cleavage. *PLoS Biol.* 2011;9(2):e1000587. Epub 2011/02/10. doi: 10.1371/journal.pbio.1000587. PubMed PMID: 21304920; PubMed Central PMCID: PMCPMC3032545.
39. Smith TJ, Font ME, Kelly CM, Sondermann H, O'Toole GA. An N-Terminal Retention Module Anchors the Giant Adhesin LapA of *Pseudomonas fluorescens* at the Cell Surface: a Novel Subfamily of type I Secretion Systems. *J Bacteriol.* 2018;200(8). Epub 2018/02/14. doi: 10.1128/JB.00734-17. PubMed PMID: 29437852; PubMed Central PMCID: PMCPMC5869472.
40. Guo S, Langelaan DN, Phippen SW, Smith SP, Voets IK, Davies PL. Conserved structural features anchor biofilm-associated RTX-adhesins to the outer membrane of bacteria. *FEBS J.* 2018;285(10):1812-26. Epub 2018/03/27. doi: 10.1111/febs.14441. PubMed PMID: 29575515.
41. Pérez-Mendoza D, Coulthurst SJ, Humphris S, Campbell E, Welch M, Toth IK, *et al.* A multi-repeat adhesin of the phytopathogen, *Pectobacterium atrosepticum*, is secreted by a type I pathway and is subject to complex regulation involving a non-canonical diguanylate cyclase. *Mol Microbiol.* 2011;82(3):719-33. Epub 2011/10/14. doi: 10.1111/j.1365-2958.2011.07849.x. PubMed PMID: 21992096.
42. García-Fontana C, Vilchez JI, González-Requena M, González-López J, Krell T, Matilla MA, *et al.* The involvement of McpB chemoreceptor from *Pseudomonas aeruginosa* PAO1 in virulence. *Sci Rep.* 2019;9(1):13166. Epub 2019/09/13. doi: 10.1038/s41598-019-49697-7. PubMed PMID: 31511598; PubMed Central PMCID: PMCPMC6739360.
43. McLaughlin HP, Caly DL, McCarthy Y, Ryan RP, Dow JM. An orphan chemotaxis sensor regulates virulence and antibiotic tolerance in the human pathogen *Pseudomonas aeruginosa*. *PLoS One.* 2012;7(8):e42205. Epub 2012/08/08. doi: 10.1371/journal.pone.0042205. PubMed PMID: 22870303; PubMed Central PMCID: PMCPMC3411652.
44. Choi Y, Kim S, Hwang H, Kim KP, Kang DH, Ryu S. Plasmid-encoded MCP is involved in virulence, motility, and biofilm formation of *Cronobacter sakazakii* ATCC 29544. *Infect Immun.* 2015;83(1):197-204. Epub 2014/10/22. doi: 10.1128/IAI.02633-14. PubMed PMID: 25332122; PubMed Central PMCID: PMCPMC4288869.
45. Chaparro AP, Ali SK, Klose KE. The ToxT-dependent methyl-accepting chemoreceptors AcfB and TcpI contribute to *Vibrio cholerae* intestinal colonization. *FEMS microbiology letters.* 2010;302(2):99-105. Epub 2009/11/26. doi: 10.1111/j.1574-6968.2009.01835.x. PubMed PMID: 19929967.

46. Guo M, Huang Z, Yang J. Is there any crosstalk between the chemotaxis and virulence induction signaling in *Agrobacterium tumefaciens*? *Biotechnol Adv.* 2017;35(4):505-11. Epub 2017/03/28. doi: 10.1016/j.biotechadv.2017.03.008. PubMed PMID: 28342941.
47. Kumar Verma R, Samal B, Chatterjee S. *Xanthomonas oryzae* pv. *oryzae* chemotaxis components and chemoreceptor Mcp2 are involved in the sensing of constituents of xylem sap and contribute to the regulation of virulence-associated functions and entry into rice. *Mol Plant Pathol.* 2018;19(11):2397-415. Epub 2018/07/17. doi: 10.1111/mpp.12718. PubMed PMID: 30011125; PubMed Central PMCID: PMC6638100.
48. Kojima S, Takao M, Almira G, Kawahara I, Sakuma M, Homma M, *et al.* The Helix Re-arrangement in the Periplasmic Domain of the Flagellar Stator B Subunit Activates Peptidoglycan Binding and Ion Influx. *Structure.* 2018;26(4):590-8 e5. Epub 2018/03/27. doi: 10.1016/j.str.2018.02.016. PubMed PMID: 29576320.
49. Postle K, Larsen RA. TonB-dependent energy transduction between outer and cytoplasmic membranes. *Biometals.* 2007;20(3-4):453-65. Epub 2007/01/18. doi: 10.1007/s10534-006-9071-6. PubMed PMID: 17225934.
50. Germon P, Ray MC, Vianney A, Lazzaroni JC. Energy-dependent conformational change in the TolA protein of *Escherichia coli* involves its N-terminal domain, TolQ, and TolR. *J Bacteriol.* 2001;183(14):4110-4. Epub 2001/06/22. doi: 10.1128/JB.183.14.4110-4.114.2001. PubMed PMID: 11418549; PubMed Central PMCID: PMC6638100.
51. Jahan-Mihan A, Luhovyy BL, El Khoury D, Anderson GH. Dietary proteins as determinants of metabolic and physiologic functions of the gastrointestinal tract. *Nutrients.* 2011;3(5):574-603. Epub 2012/01/19. doi: 10.3390/nu3050574. PubMed PMID: 22254112; PubMed Central PMCID: PMC3257691.
52. van der Wielen N, Moughan PJ, Mensink M. Amino Acid Absorption in the Large Intestine of Humans and Porcine Models. *J Nutr.* 2017;147(8):1493-8. Epub 2017/06/16. doi: 10.3945/jn.117.248187. PubMed PMID: 28615378.
53. Windmueller HG, Spaeth AE. Respiratory fuels and nitrogen metabolism in vivo in small intestine of fed rats. Quantitative importance of glutamine, glutamate, and aspartate. *J Biol Chem.* 1980;255(1):107-12. Epub 1980/01/10. PubMed PMID: 7350142.
54. Dai ZL, Wu G, Zhu WY. Amino acid metabolism in intestinal bacteria: links between gut ecology and host health. *Front Biosci (Landmark Ed).* 2011;16:1768-86. Epub 2011/01/05. doi: 10.2741/3820. PubMed PMID: 21196263.
55. Claus SP, Tsang TM, Wang Y, Cloarec O, Skordi E, Martin FP, *et al.* Systemic multicompartmental effects of the gut microbiome on mouse metabolic phenotypes. *Mol Syst Biol.* 2008;4:219. Epub 2008/10/16. doi: 10.1038/msb.2008.56. PubMed PMID: 18854818; PubMed Central PMCID: PMC6638100.
56. Faure M, Moennoz D, Montigon F, Mettraux C, Mercier S, Schiffrin EJ, *et al.* Mucin production and composition is altered in dextran sulfate sodium-induced colitis in rats. *Dig Dis Sci.* 2003;48(7):1366-73. Epub 2003/07/23. doi: 10.1023/a:1024175629909. PubMed PMID: 12870797.
57. Gibson DG, Young L, Chuang RY, Venter JC, Hutchison CA, 3rd, Smith HO. Enzymatic assembly of DNA molecules up to several hundred kilobases. *Nat Methods.* 2009;6(5):343-5. doi: 10.1038/nmeth.1318. PubMed PMID: 19363495.
58. Team RC. R: A language and environment for statistical computing. 3.4.1 ed. Vienna, Austria: R Foundation for Statistical Computing; 2017.
59. Fischer M, Zilkenat S, Gerlach RG, Wagner S, Renard BY. Pre- and post-processing workflow for affinity purification mass spectrometry data. *J Proteome Res.* 2014;13(5):2239-49. doi: 10.1021/pr401249b. PubMed PMID: 24641689.
60. Adler J. A method for measuring chemotaxis and use of the method to determine optimum conditions for chemotaxis by *Escherichia coli*. *J Gen Microbiol.* 1973;74(1):77-91. doi: 10.1099/00221287-74-1-77. PubMed PMID: 4632978.
61. Wille T, Barlag B, Jakovljevic V, Hensel M, Sourjik V, Gerlach RG. A gateway-based system for fast evaluation of protein-protein interactions in bacteria. *PLoS One.* 2015;10(4):e0123646. doi: 10.1371/journal.pone.0123646. PubMed PMID: 25856398; PubMed Central PMCID: PMC4391838.
62. Bender JK, Wille T, Blank K, Lange A, Gerlach RG. LPS structure and PhoQ activity are important for *Salmonella* Typhimurium virulence in the *Galleria mellonella* infection model. *PLoS One.* 2013;8(8):e73287. doi: 10.1371/journal.pone.0073287. PubMed PMID: 23951347; PubMed Central PMCID: PMC3738532.
63. Datsenko KA, Wanner BL. One-step in-activation of chromosomal genes in *Escherichia coli* K-12 using PCR products. *Proc Natl Acad Sci U S A.* 2000;97(12):6640-5. doi: 10.1073/pnas.120163297. PubMed PMID: 10829079; PubMed Central PMCID: PMC18686.
64. Datta S, Costantino N, Court DL. A set of recombinering plasmids for gram-negative bacteria. *Gene.* 2006;379:109-15. doi: 10.1016/j.gene.2006.04.018. PubMed PMID: 16750601.
65. Wang RF, Kushner SR. Construction of versatile low-copy-number vectors for cloning, sequencing and gene expression in *Escherichia coli*. *Gene.* 1991;100:195-9. PubMed PMID: 2055470.

IV. DISCUSSION

IV.1. Virtual Colony Count

The putative proton channel SiiAB was previously shown to interact with different methyl-accepting chemotaxis proteins. In the course of this work we wanted to address how the deletion of one or more MCPs affects the invasion capabilities of *S. Typhimurium* in *in vitro* cell culture-based infection assays. For this, we were strongly dependent on a reliable bacterial enumeration method.

In case of intracellular bacteria such as *Salmonella*, one must quantify the proportion of a defined inoculum that was able to gain access to intracellular compartments of the host cell. Most commonly used for this purpose is the gentamicin protection assay first described by Devenish and Schiemann in 1981. The gold standard to enumerate bacteria in this assay is still the plating of a dilution series on solid agar plates and the counting of the resulting colony forming units (CFU).

We were able to establish a method called “Virtual Colony Count” (VCC) as an alternative enumeration analysis method for the classical, time-consuming CFU assay. It was tested in cell culture-based infection models using three different cell types for invasion- and intracellular replication assays. We got robust cell counts that were in good agreement with data obtained by CFU counting (Hoffmann *et al.*, 2018).

The expected T3SS-1 phenotype could be reproduced in HeLa and MDCK cells using the VCC to enumerate the intracellular bacteria. For replication inside of host cells *Salmonella* needs a functional T3SS-2 (Hensel *et al.*, 1998; Fàbrega and Vila, 2013). In accordance, SPI-2 mutants displayed almost no net replication 24 h post infection when tested in RAW264.7 macrophagelike cells using VCC-based enumeration (Hoffmann *et al.*, 2018).

VCC is a label-free method that only depends on bacterial growth and has a very high sensitivity because of the logarithmic signal amplification. We were able to quantify bacteria over six orders of magnitude with a detection limit of 10 bacteria per well (Hoffmann *et al.*, 2018). It is not necessary to label bacteria in contrast to, for example, the method described by Grant *et al.* (2008) utilizing wild-type isogenic tagged strains (WITS) and quantification via qRT-PCR or sequencing. Here strains that shall be enumerated have to contain a barcoded sequence in their genome and an additional DNA-extraction step is required prior analysis. Several other alternative methods for the quantification of intracellular bacteria have been described. The In-cell Western assay uses immunofluorescence for the quantification (Sarshar *et al.*, 2019). This method is highly specific and efficient, allowing for accurate quantification of differences ranging over four orders of magnitude. It is also well suited for automation and high-throughput, however, the availability of a specific primary antibody is the major limitation of this assay.

In 2004, Acord *et al.* presented an assay using firefly luciferase for the quantification of adhered bacteria to eukaryotic cells. There are some problems that should be taken into account by using this method. Bacteria have to be transformed with a plasmid encoding luciferase providing an optimal expression level. The detection limit of the luciferase-based assay lies at ~100 bacteria, making it less sensitive than other approaches, e.g. VCC. Martens-Habbena and Sass (2006) used the fluorescent nucleic acid stain SYBR green I to quantify between 50,000 and 1.5×10^8 bacterial cells per ml sample. This and similar methods would not be applicable in the context of an infection model due to the excess of host cell DNA. Another approach to enumerate bacteria in infection models is the use of fluorescently labeled bacteria and the subsequent analysis via flow cytometry (Helaine *et al.*, 2014; Claudi *et al.*, 2014). This method is highly sensitive and offers a wide variety of application. Disadvantages are here the high costs for the hardware as well as the relatively time consuming sample analysis. It was also shown that the overexpression of fluorescent proteins may negatively influences the virulence of bacteria (Knodler *et al.*, 2005; Mutoji and Ennis, 2012). The use of different fluorescent markers with distinguishable spectral properties allows for simultaneous quantification of two or more strains in one sample. In the case of VCC the analysis of different strains is only possible in parallel analyses using different antibiotic resistances. For all the described methods bacteria either have to be tagged, transformed or specific antibodies are needed, which is not the case for the VCC method. The only requirement here is a separate calibration curve for different species or mutants with different growth behavior. For the actual enumeration analysis there is no manual step, like staining, needed. It can therefore be easily automated using absorbance detection equipment for measurement of optical density in a 96-well plate. Due to open source software the subsequent data analysis is simple, reproducible and without additional costs. VCC is nearly operator independent and well standardizable in different laboratories. Furthermore, hardware requirements for the absorption detection in a 96-well plate are moderate.

Limitations of the VCC method that should be considered are that mutants with different growth rates must be analyzed separately. Mutants with growth defects for example show a prolonged lag-phase (Broach *et al.*, 1976; Lifshits *et al.*, 1992) and therefore need longer times to reach the absorbance threshold compared to the respective WT strain, even when there are the exact same numbers of bacteria per well. This would falsify the cell counts when analyzed with the calibration curve recorded with the faster growing WT strain. In these cases the recording of additional calibration curves would be necessary. The method is also not suitable for dormant strains because it depends on active bacterial growth (Kell and Young, 2000), or for obligate intracellular bacteria, like *Chlamydia trachomatis* (Heinzen und Hackstadt, 1996; Ooij *et al.*, 1997). Another problem of this assay is the correlation of VCC calibration curves to actual colony counts because the quantification via CFU on agar plates as a reference inherits an inaccuracy (Naghili *et al.*, 2013).

All in all VCC is a good alternative to speed up infection assays if strains should, for example, be tested in various invasion environments that do not hamper with the sub-

sequent growth conditions. Because of its high accuracy, even slight differences in invasion rates are detectable. We used the method to investigate the SPI-4 dependent adhesion to and invasion of polarized epithelial host cells of different chemotaxis mutant strains under varying invasion conditions *in vitro*.

IV.2. SiiAB functions as a proton channel and exhibits peptidoglycan-binding

SiiAB shares some properties with the MotAB proton channel (Braun *et al.*, 2004) as well as with other members of the family of heteromeric proton-conducting channels such as ExbBD/TonB (Zhai *et al.*, 2003), PomAB (Yonekura *et al.*, 2011) or TolQR (Zhang *et al.*, 2011). These complexes generate mechanical work leading to the rotation of the flagellum or energize the uptake of nutrients via the OM (Lloubès *et al.*, 2001; Minamino *et al.*, 2008; Noinaj *et al.*, 2010). Energy is harvested from the proton motive force (PMF) through translocation of protons across the IM (Kojima *et al.*, 2009; Wojdyla *et al.*, 2015; Celia *et al.*, 2016; Zhu *et al.*, 2014). The question arises if the structural similarities between SiiAB and MotAB are an indication of similar functions of these protein complexes.

It was shown that the residue D32 of MotB, D25 of ExbD, D23 of TolR and D13 of SiiA are essential for the proper function of the respective complex (Zhou *et al.*, 1998; Cascales *et al.*, 2001; Ollis *et al.*, 2009; Wille *et al.*, 2014) and it is thought that these negatively charged amino acids get directly protonated during the process of proton conduction (Braun and Blair, 2001; Zhai *et al.*, 2003; Goemaere *et al.*, 2007).

Results obtained in a SiiA[D13N] mutant concerning the acidification of the bacterial cytosol as well as adhesion/ invasion of polarized cells (Wille *et al.*, 2014; Kirchweiger *et al.*, 2019) give strong reason to suspect that proton translocation via SiiAB and the energy derived from the PMF directly contribute to SPI-4 mediated adhesion of *Salmonella* to polarized epithelial cells.

SiiA harbors a reduced peptidoglycan-binding motif (PG) and shows the same dimerization mode as other proteins located in the IM that are involved in ion translocation like MotB or PomB (Roujeinikova, 2008; Kojima *et al.*, 2009). However, the experiments gave no hint that the linker domain which interconnects the transmembrane region of SiiA to the PG-binding domain fulfills the same function as for example in MotB. Here, this segment is proposed to play an important role in regulating the anchoring of the PG domain to the PG layer and in controlling the proton translocation across the IM (Kojima *et al.*, 2009; Zhu *et al.*, 2014; Wojdyla *et al.*, 2015). Only after the linker is removed from the channel entrance PG-binding and anchoring of the complex in the PG-layer as well as proton flux is initiated. The linker domain seals the proton channel until it is associated with the rotor complex of the flagellum. One could speculate that SiiA only anchors the SiiAB complex in the PG-layer under an acidic intracellular pH leading to the translocation of SiiE as shown in Figure IV.1. Surprisingly, the mutation of Arg162, which leads to the inability of

SiiA to bind PG as well as to reduced invasiveness of *Salmonella*, had no impact on the proton conductance (Kirchweger *et al.*, 2019). Our results also show that SiiAB's function as a proton channel is only obligate for SiiE retention not for its secretion. This might not be the whole story as all the applied assays have some limitations. PG-binding was only tested with a truncated SiiA protein in the absence of SiiB as well as maybe other, still unknown, factors. The pHLuorin assay for determination of bacterial cytosolic pH highly depends on the accuracy of the underlying standard curves which are prone to variations of external pH and temperature (Kirchweger *et al.*, 2019).

PG binding of MotAB is essential for anchoring of the flagellar complex within the bacterial envelope and to transfer the generated torque to the bacterial cell (Kojima *et al.*, 2018). Anchoring of the flagellar motor is the final step in the assembly process of this multiprotein complex. The rotor of the flagella motor is the first subcomplex to get assembled. Afterwards the actual flagellum is secreted and, finally, this complex is anchored in the PG-layer through interaction with multiple stator complexes (MotAB) (Thormann and Paulick, 2010). Depending on the external load and ion availability there are up to ten stator complexes per motor (Reid, 2006; Terahara *et al.*, 2017). A T1SS on the other hand is usually assembled after interaction of its substrate with the ABCprotein and can freely diffuse through the IM (Masi and Wandersman, 2010). In order to act as an adhesin and transmit the forces generated by the bacterium's adhesion to the host cell, anchoring of SiiE within the envelope would be a prerequisite. Given the interaction of SiiAB with T1SS-4 components (Wille *et al.*, 2014), the PG-binding of SiiA could therefore fulfill an anchoring/fixation function for the whole system.

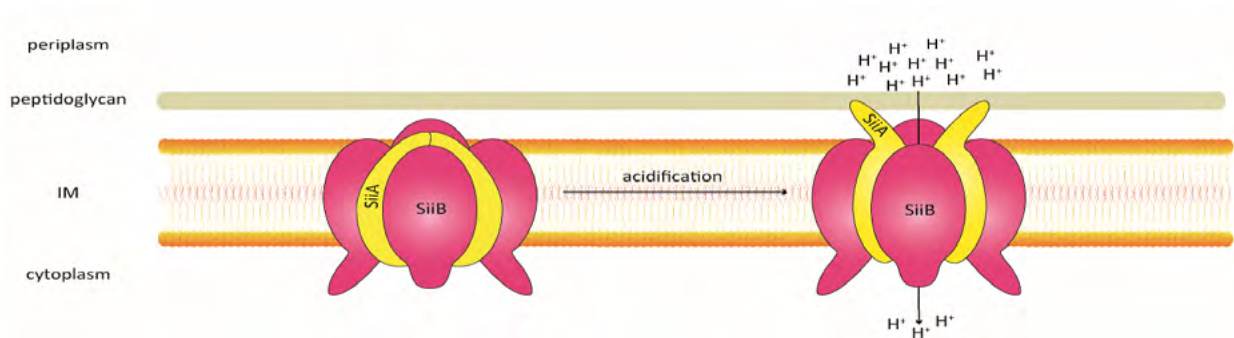


Figure IV.1 Mechanism of SiiAB. The acidification of the external pH leads to the binding of SiiA to peptidoglycan and therefore anchoring of the proton channel in the inner membrane. It also leads to the activation of proton flux along the proton motive force gradient from the periplasm in the cytoplasm.

Interestingly, our results show a pH-dependent binding of SiiA to PG (Kirchweger *et al.*, 2019). The protein has only high affinity for PG at pH values lower than 6.5. One could speculate that the acidic environment of the stomach (Ovesen *et al.*, 1986) triggers the SiiA binding to PG and assembly of the complex, so that *Salmonella* gets primed for the

imminent invasion of host cells. Proton flux through SiiAB could then be used to energize the conformational change of T1SS components finally resulting in the retention of SiiE on the bacterial surface. Maybe the transition from a lower pH environment in the lumen of the small intestine (pH 5.5) to a neutral pH (7.0) in the mucoid vicinity of enterocytes represents another signal for *Salmonella* to modulate its virulence factors. The pH is neutralized by bicarbonate-containing mucus which overlays the enterocytes (Atuma *et al.*, 2001). One could also speculate that the transition of *Salmonella* to higher pH environments would lead to detachment of SiiA from the PG-layer and therefore inactivation of proton conduction and disassembly of the proton channel from the T1SS.

Salmonella senses external pH with the two-component system PhoPQ where the binding of cationic peptides or acidic pH induces conformational changes in the PhoQ periplasmic sensor domain. This leads to the activation of autophosphorylation of PhoQ and subsequently to phosphorylation of the response regulator PhoP. As a result, stress response genes are activated (Fang *et al.*, 2016). So maybe a signal transduction from PhoPQ to SiiAB via phosphorylation or direct interaction would be conceivable. Therefore, we set out to identify possible interaction partners of SiiAB.

IV.3. Signal transduction from the chemotaxis system

Previously it had been shown that motility as well as chemotaxis are important virulence factors *in vivo* (Stecher *et al.*, 2004). We were able to identify MCPs as SiiAB interaction partners and could verify these interactions in different assays especially between CheM and SiiABD (Hoffmann *et al.*, 2021).

The deletion of CheM, the aspartate sensor, leads to decreased invasion of polarized cells (Hoffmann *et al.*, 2017) and addition of the CheM attractant aspartate had the opposite effect (Hoffmann *et al.*, 2021). In contrast to the aspartate sensor of *E. coli*, Tar, CheM does not mediate taxis towards maltose, because it is not interacting with the maltose binding protein (MBP) (Blat *et al.*, 1995; Kolodziej *et al.*, 1996). We think that the structural differences that prohibit interaction with MBP could result in additional functions of CheM instead. Biemann and Koshland (1994) showed for example that the aspartate receptor of *E. coli* only binds one Asp molecule whereas the CheM of *Salmonella* is able of binding two Asp molecules with different affinities. After binding of one molecule, there are conformational changes in the receptor altering the second binding site. This might somehow contribute to our observed phenotype. CheM shows strong protein-protein-interactions with components of the T1SS-4, mainly SiiA and SiiB, arguing for a functional link to SPI-4 (Hoffmann *et al.*, 2021). So far, some links from chemotaxis to virulence are described. These mechanisms depend on the phosphorylation of alternative response regulators, therefore altering virulence-specific transcriptional responses (Matilla *et al.*, 2018). In *Xanthomonas oryzae* pv. *oryzae*, a bacterial pathogen of rice, the chemoreceptor

mcp2 is required not only for taxis towards xylem sap but also for the entry into rice as well as for virulence (Verma *et al.*, 2018). *Pseudomonas aeruginosa* synthesizes a putative MCP, PA2573, which alters motility, virulence and antibiotic resistances when mutated (McLaughlin *et al.*, 2012). *Campylobacter jejuni* and *Helicobacter pylori* also strongly depend on chemotaxis and motility for efficient colonization and invasion of their hosts (Hendrixson and DiRita 2004; Vegge *et al.*, 2009; Chandrashekar *et al.*, 2015; Day *et al.*, 2016; de Vries *et al.*, 2017; Rolig *et al.*, 2012; Keilberg and Ottemann 2016; Huang *et al.*, 2017). So far there are no indications of such a mechanism for SPI-4.

There are some putative phosphorylation sites in SiiB. The signal transduction from the MCP to the SiiAB proton channel could therefore function via the transfer of phosphoryl groups. However, there is no intrinsic kinase activity of MCPs known and domain predictions of SiiB do not suggest such an activity for this protein (Wille *et al.*, 2014) speaking against such a mechanism. Another possibility would be the involvement of a so far unknown kinase which should get activated upon CheM signaling and would phosphorylate SiiB. This mechanism might be rather unlikely since no such protein was identified in our pulldown assays, but it cannot be completely excluded.

We tested the role of CheM for SPI-4 dependent adhesion using mutants resembling an attractant-bound, kinase “always-off”, state of the MCP ($\Delta cheA$, $\Delta cheY$) (Sukomon *et al.*, 2016). $\Delta cheA$ and *cheY* mutants are no longer able to transfer phosphoryl groups and show a straight-swimming phenotype. A non-flagellated ($\Delta flil$) mutant was included as another control. These experiments showed that the elevated invasion rates were independent of bacterial motility or chemotaxis. Bacteria had to be only in close proximity to host cells as ensured by centrifugation (Hoffmann *et al.*, 2021). Under this prerequisite, the presence of MeAsp led to higher invasion rates depending on functional CheM indicating a second role of CheM independent of the chemotaxis phosphorelay signaling (Parkinson *et al.*, 2015). Surprisingly, CheA as well as CheY mutant strains displayed about 20-fold higher invasion rates compared to bacteria grown without MeAsp (Hoffmann *et al.*, 2021). This would rule out signaling based on phosphoryl transfer, at least involving the ‘classical’ chemotaxis-associated components. The phenotype could be this extremely strong because the signal from CheM is solely transferred to the SiiAB proton channel and not “shared” with the chemotaxis cascade. The loss of CheA/Y could possibly lead to additional binding sites for SiiA and / or SiiB so that more complexes could be activated. Because of the “kinase off” state of the receptor CheB, the methyl esterase, is not phosphorylated and methyl groups added to CheM via CheR are not removed (Sourjik, 2004). This would cause the permanent displacement of the HAMP domain of the receptor and therefore also the activation of SiiAB. Another reason for the observed phenotype could be the better accessibility of CheM based on the missing of CheA which is necessary for the formation of polar clusters (Kentner *et al.*, 2006). These clusters were described by Hazelbauer *et al.* in 2008. They evaluated the distribution of MCP over the bacterial surface and proposed the arrangement of MCPs in large clusters at the cell poles. The T1SS-4 on the other hand is spread uniformly over the whole bacterial envelope (Gerlach

et al., 2008; Barlag *et al.*, 2016). Due to the missing CheA it would be conceivable that these clusters do not form properly. There are also studies showing that MCPs are not exclusively localized at the poles (Sourjik and Berg, 2000). To finally proof our observed protein-protein-interactions it would be necessary to determine the (dynamic) spatial distribution of CheM and SiiAB within the bacterial cell envelope in future experiments.

IV.4. Environmental control of SiiE retention

Our data support that upon attractant binding, CheM interacts not only with the classical chemotaxis cascade but also with SiiAB. In the presence of Asp the proportion of secreted and retained SiiE is shifted towards the retention of the adhesin. This naturally results in elevated adhesion to host cells and finally to increased invasion (Hoffmann *et al.*, 2021).

The bound adhesin has to withstand high shearing forces under hydrodynamical flow (Liu *et al.*, 2020). *Lactobacillus reuteri*, inhabiting the human gastrointestinal tract, uses a large multi-repeat cell-surface adhesin, a mucin-binding protein (MUB) for its adhesion to mucins. The binding of the full-length MUB to mucus happens via multiple interactions involving terminal sialylated mucin glycans (Gunning *et al.*, 2016). Such a mechanism would also be conceivable for *Salmonella* SiiE. The actual binding takes place via either specific (ligand-binding) or unspecific (unfolding and hydrophobic binding) forces that can be measured by atomic force microscopy (Dufrêne, 2015). During the multiple washing steps in the course of the applied SIMPLE assay, the binding of SiiE to magnetic beads has to be very strong (Hoffmann *et al.*, 2021). This indicates that the retained SiiE is functional as an adhesin and able to withstand mechanical forces that would also occur *in vivo*.

Unfortunately, the exact retention mechanism of SiiE remains elusive. Recently, multiple mechanisms have been described concerning the control of type I-secreted adhesin surface location in response to different environmental signals. For example, the type I-secreted *Pseudomonas fluorescence* protein LapA is anchored within the outer membrane in response to inorganic phosphate (Pi) (Newell *et al.*, 2011). Low Pi leads to depletion of second messenger c-di-GMP by the phosphodiesterase RapA. Hereupon LapD (c-di-GMP binding protein) releases LapG, a periplasmic protease. LapG cleaves an N-terminal retention signal off LapA, releasing the adhesin from the OMP (Newell *et al.*, 2011; Smith *et al.*, 2018). A similar 2-step mechanism is described for the multi-repeat adhesin (MRP) of *Pectobacterium atrosepticum* (Pérez-Mendoza *et al.*, 2011). For the ice-binding protein of *Marinomonas primoryensis* (MplBP) there is an intrinsically folding N-terminal domain (RIN) anchoring it within the OMP (Guo *et al.*, 2018). However, the release mechanism of this protein has to be revealed yet. A similar mechanism could be envisaged for SiiE, but we have no evidence of the involvement of c-di-GMP nor for the processing of the N-terminal domain of SiiE *in vitro* as described for LapA (M. Hensel, personal communication).

In case of SiiE a retention mechanism involving the SiiAB proton channel is very likely (Wille 2014). Due to the binding of Asp in the periplasm and the resulting piston-like motion of the TM helices and HAMP domain of CheM, the structural changes could alter the binding interface to the SiiAB channel. We speculate that a displacement of SiiA PG-binding domain could be induced. This would not only result in the activation of the channel but also in anchoring of the complex within the IM. This could converge with the dynamic association of SiiAB with the tripartite T1SS (Park *et al.*, 2011). In this case, the secretion of SiiE would be independent of the presence and function of the SiiAB complex, which was shown by Wille *et al.* (2014). Based on these data, we propose that CheM links two important virulence factors, namely chemotaxis / motility and SPI-4 dependent adhesion. The acidification of the environment on *Salmonella's* way through the body to its preferred site of invasion could hereby lead to the assembly of the proton channel and the actual T1SS via SiiA-mediated PG binding. This lead to a new working model shown in Figure IV.2.

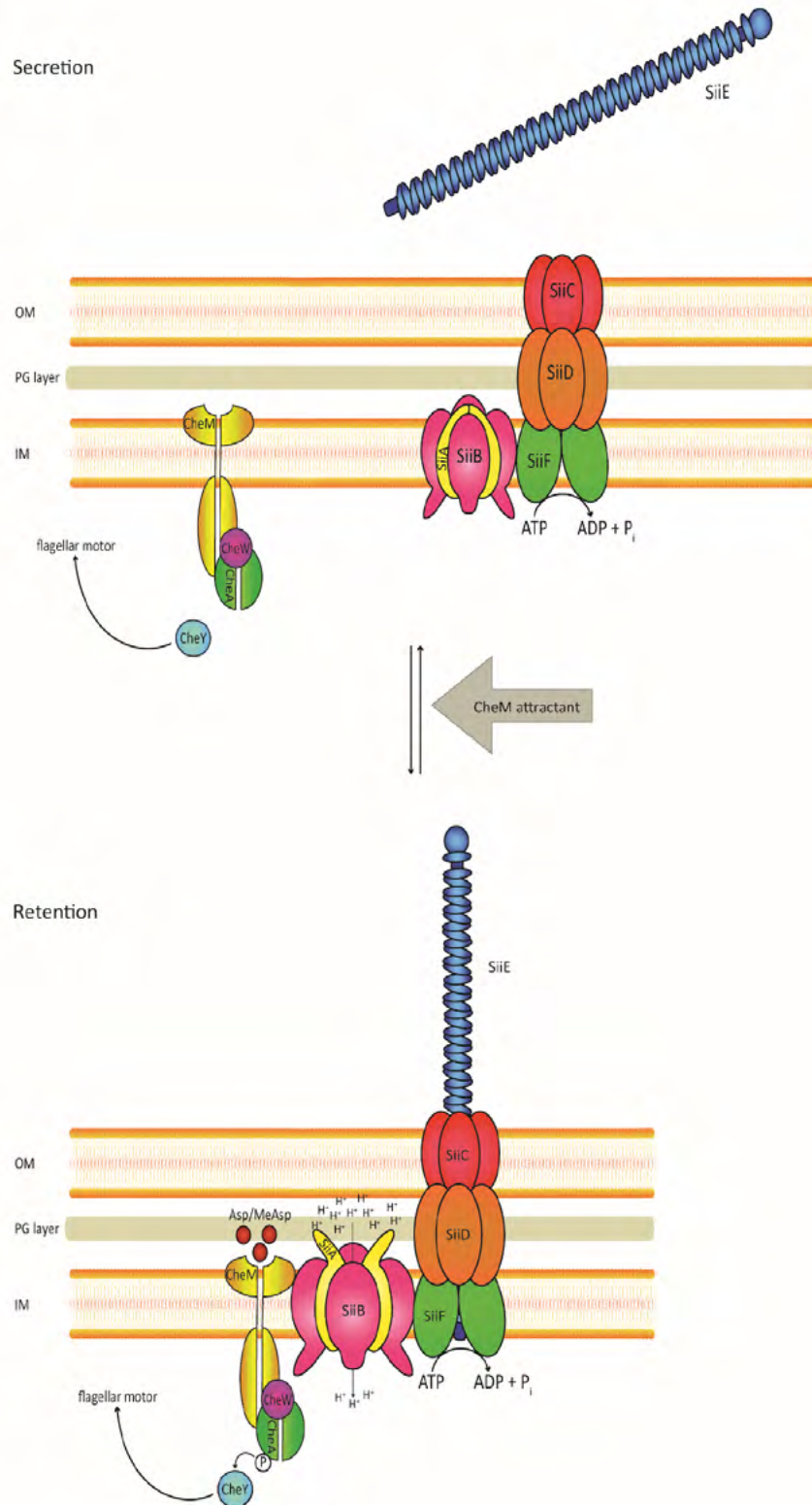


Figure IV.2 working model. CheM is sensing the presence of its attractant aspartate and interacts on the one hand with the flagellum via the chemotaxis cascade and on the other and directly with SiiAB. It functions therefore as a linker between motility and SPI-4 induced adherence.

IV.5. Mucus as a potential signal for CheM

The observed impact of CheM signaling on SPI-4 dependent adhesion was strongest in mucin-producing HT29-MTX cells (Hoffmann *et al.*, 2021). One could speculate that mucus or some of its components are important for the CheM-SPI-4 interaction. It would also be possible that components of the mucus function as attachment points for *Salmonella* facilitating adhesion.

HT29-MTX cells produce MUC1. MUC1 is a membrane-associated mucin consisting of an O-glycosylated extracellular region, a transmembrane domain and a cytoplasmic tail (Carrington *et al.*, 2009). It is ubiquitously expressed on the apical surface of epithelial cells and normally hinders adhesion because it forms a sterical barrier. It was shown that SiiE is binding MUC1 enabling *Salmonella* to breach the epithelial mucin barrier and invade into MUC1-expressing enterocytes from the apical site (Li *et al.*, 2019).

However the major intestinal mucin is the gel-forming MUC2. It is heavily O-glycosylated in the golgi. After secretion Ca^{2+} is removed from MUC2 by the increased pH allowing the mucin polymer to unfold into a flat net-like structure (Hansson *et al.*, 2019).

Next to its protective function mucus also serves as an energy source for different bacteria and is therefore permanently renewed (Dharmani *et al.*, 2009; Lievin-Le Moal *et al.*, 2006). Bacteria can for example use mucus glycans as a carbon source (Ouwkerk *et al.*, 2013). There are different bacterial species of the microbiota that use their enzymatic activities to release monosaccharides attached to the mucin glycoproteins e.g. *Akkermansia muciniphila* (Png *et al.*, 2010), *Bifidobacterium bifidum* (Png *et al.*, 2010; Garrido *et al.*, 2011) or *Ruminococcus gnavus* (Png *et al.*, 2010; Crost *et al.*, 2013). This explains why also bacteria without enzymes necessary for cleaving these sugar linkages can profit from mucus-derived nutrients (Arike and Hansson, 2016). *Salmonella* can bind to glycostructures with terminal N-acetyl-glucosamine (GlcNAc) and/or a 2,3-linked sialic acid in a lectin-like manner (Vimal *et al.*, 2000; Wagner *et al.*, 2014) and has the ability to release the carbohydrate using its sialidase (Hoyer *et al.*, 1992). Maybe some of these so produced sugars can trigger the signaling of CheM and also the resulting interaction with SiiAB. To evaluate if by-products of the residual microbiota can function as potential CheM signals *in vivo* mouse model experiments would be necessary. Here the comparison of different mutant bacteria in different backgrounds (Muc2^{-/-} mice) would be interesting. Gagnon *et al.* (2013) also saw higher adhesion of *Salmonella* to mucin producing HT29-MTX cells than to non- and low-mucus producing cells.

According to our results, *Salmonella* uses Asp as environmental signal to modulate its secretion/retention behavior of SiiE. Asp is generated at the apical side of polarized enterocytes due to the activity of peptidases. This mostly takes place in the jejunum (Jahan-Mihan *et al.*, 2011). Free Asp additionally is generated due to peptide degradation by the microbiota (Claus *et al.*, 2008). The proportion of Asp contained in mucins is higher in the jejunum than in the colon (Faure *et al.*, 2003). This coincides with *Salmonella*'s preferred locus of invasion. Recently, it was shown by Nguyen *et al.* (2020) that *Salmonella* uses Asp from the environment to synthesize fumarate. Fumarate is an electron acceptor

and promotes *Salmonella*'s anaerobic respiration in the colonized gut. This is also in favor of the hypothesis that Asp functions as signal for *Salmonella* invasion.

If the CheM signal is not derived from mucus or its components it would be possible that *Salmonella* “sees” aspartate on its way through the body to its preferred infection site so that the T1SS-4 gets primed for the retention of SiiE.

Another explanation for the observed phenotype could be the presence of alternative signals of other MCPs leading to changed SiiE surface expression. So maybe the sensing of different attractants like other amino acids, sugars or chemicals would influence the interaction between CheM and SPI-4 due to the organization of MCPs in heterologous clusters. Therefore the pronounced phenotype in HT29-MTX cells might be the product of many accumulating effects.

IV.6. Conclusion

In summary, we could show that CheM directly interacts with the SiiAB proton channel and that upon attractant-binding the adhesin SiiE is mainly localized on the bacterial surface instead of being secreted. It was shown that secreted SiiE is reducing IgG-secreting plasma cells in the bone marrow therefore hindering an efficient humoral immune response (Männe *et al.*, 2019). This shows that the secretion of SiiE is as important as its retention for the efficient invasion of *Salmonella*. Therefore the switch from secretion to retention and *vice versa* has to be perfectly timed. Here we saw that Asp is utilized as environmental cue by *Salmonella* to determine its preferred locus of invasion which also induces the switch from SiiE secretion to retention. However the exact mechanism by which the signal is conferred from CheM to the T1SS-4 has yet to be characterized.

V. REFERENCES

- » Adam, D., Doerr, H.W., Link, H. and Lode, H. (2004) *Die Infektiologie*, Springer-Verlag Berlin Heidelberg.
- » Ahmer, B.M., van Reeuwijk, J., Watson, P.R., Wallis, T.S. and Heffron, F. (1999). Salmonella SirA is a global regulator of genes mediating enteropathogenesis. *Molecular microbiology* **31**, 971-982.
- » Acord, J., Maskell, J., Sefton, A. (2005). A rapid microplate method for quantifying inhibition of bacterial adhesion to eukaryotic cells. *Journal of Microbiological Methods* **60**, 55-62.
- » Arike, L. and Hansson, G.C. (2016). The Densely O-Glycosylated MUC2 Mucin Protects the Intestine and Provides Food for the Commensal Bacteria. *Journal of Molecular Biology* **428**, 3221-3229.
- » Ashida, H., Ogawa, M., Kim, M., Mimuro, H., Sasakawa, C. (2012). Bacteria and host interactions in the gut epithelial barrier. *Nature Chemical Biology* **8**, 36-45.
- » Atuma, C., Strugala, V., Allen, A., Holm, L. (2001). The adherent gastrointestinal mucus gel layer: thickness and physical state in vivo. *American Journal of Physiology Gastrointestinal and Liver Physiology* **280**, 922-929.
- » Audia, J.P., Webb, C.C. and Foster, J.W. (2001). Breaking through the acid barrier: an orchestrated response to proton stress by enteric bacteria. *International journal of medical microbiology* **291**, 97-106.
- » Bailey, M.J., Hughes, C. and Koronakis, V. (1997). RfaH and the ops element, components of a novel system controlling bacterial transcription elongation. *Molecular microbiology* **26**, 845-851.
- » Baker, A.E. and O'Toole, G.A. (2017). Bacteria, Rev Your Engines: Stator Dynamics Regulate Flagellar Motility. *Journal of Bacteriology* **199**.
- » Barlag, B., Beutel, O., Janning, D., Czarniak, F., Richter, C.P., Kommnick, C., Göser, V., Kurre, R., Fabiani, F., Erhardt, M., Piehler, J. and Hensel, H. (2016). Single molecule super-resolution imaging of proteins in living *Salmonella enterica* using self-labelling enzymes. *Scientific Reports* **6**:31601.
- » Berg, H.C. (2003). The Rotary Motor of Bacterial Flagella. *Annual Review of Biochemistry* **72**, 19-54.
- » Bertelsen, L.S., Paesold, G., Marcus, S.L., Finlay, B.B., Eckmann, L. and Barrett, K.E. (2004). Modulation of chloride secretory responses and barrier function of intestinal epithelial cells by the Salmonella effector protein SigD. *American journal of physiology. Cell physiology* **287**, C939-948.
- » Bibikov, S.I., Miller, A.C., Gosink, K.K., Parkinson, J.S. (2004). Methylation-Independent Aerotaxis Mediated by the Escherichia coli Aer Protein. *Journal of Bacteriology* **186**, 3730-3737.
- » Blat, Y., Eisenbach, M. (1995). Tar-dependent and -independent pattern formation by Salmonella typhimurium. *J Bacteriol.* **177**, 1683-91.
- » Blat, Y., Eisenbach, M. (1995). Tar-dependent and -independent pattern formation by Salmonella typhimurium. *J Bacteriol.* **177**(7), 1683-91.
- » Boyle, E.C., Brown, N.F. and Finlay, B.B. (2006). Salmonella enterica serovar Typhimurium effectors SopB, SopE, SopE2 and SipA disrupt tight junction structure and function. *Cellular microbiology* **8**, 1946-1957.
- » Brands, D.A. and Alcamo, I.E. (2006) *Salmonella Philadelphia*, Chelsea House Publishers, pp. **102** p.
- » Braun, T.F. and Blair, D.F. (2001). Targeted Disulfide Cross-Linking of the MotB Protein of Escherichia Coli: Evidence for Two H(+) Channels in the Stator Complex. *Biochemistry* **40**(43), 13051-9.
- » Braun, T.F., Al-Mawsawi, L.Q., Kojima, S., Blair, D.F. (2004). Arrangement of Core Membrane Segments in the MotA/MotB Proton-Channel Complex of Escherichia coli. *Biochemistry* **43**, 35-45.
- » Brenner, F.W., Villar, R.G., Angulo, F.J., Tauxe, R. and Swaminathan, B. (2000). Salmonella nomenclature. *Journal of clinical microbiology* **38**, 2465-2467.
- » Brewster, J.D. (2003). A simple micro-growth assay for enumerating bacteria. *Journal of Microbiological Methods* **53**, 77 - 86.
- » Broach, J., Neumann, C., Kustu, S. (1976). Mutant Strains (nit) of Salmonella Typhimurium with a Pleiotropic Defect in Nitrogen Metabolism. *Journal of Bacteriology* **128**, 86-98.
- » Bumba, L., Masin, J., Macek, P., Wald, T., Motlova, L., Bibova, I., (2016). Calcium-Driven Folding of RTX Domain b-Rolls Ratchets Translocation of RTX Proteins through type I Secretion Ducts. *Mol Cell.* **62**, 47-62.
- » Byndloss, M.X., Olsan, E.E., Rivera-Chávez, F., Tiffany, C.R., Bäumlner, A.J. et al. (2017). Microbiota-activated PPAR-γ signaling inhibits dysbiotic Enterobacteriaceae expansion. *Science* **357**, 570-575.
- » Carrington, S., Clyne, M., Reid, C.J., FitzPatrick, E., Corfield, A.P. (2010). Microbial interaction with mucus and mucins. *Microbial Glycobiology* **33**, 655-671.
- » Cascales, E., Lloubes, R., Sturgis, J.N. (2001). The TolQ-TolR proteins energize TolA and share homologies with the flagellar motor proteins MotA-MotB. *Molecular Microbiology* **42**(3), 795-807.
- » Celia, H., Noinaj, N., Zakharov, S.D., Bordignon, E., Botos, I., Santamaria, M., Barnard, T.J., Cramer, W.A., Lloubes, R., Buchanan, S.K. (2016). Structural insight into the role of the Ton complex in energy transduction. *Nature* **538**, 60-65.
- » Chaparro, A.P., Ali, S.K., Klose, K.E. (2010). The ToxT-dependent methyl-accepting chemoreceptors AcfB and Tcpl contribute to Vibrio cholerae intestinal colonization. *FEMS microbiology letters* **302**(2), 99-105.
- » Chessa, D., Winter, M.G., Jakomin, M., Bäumlner, A.J. (2009). Salmonella enterica serotype Typhimurium Std fimbriae bind terminal alpha(1,2)fucose residues in the cecal mucosa. *Mol Microbiol* **71**(4).
- » Claudi, B., Spröte, P., Chirkova, A., Personnic, N., Zankl, J., Schürmann, N., Schmidt, A., Bumann, D. (2014). Phenotypic Variation of Salmonella in Host Tissues Delays Eradication by Antimicrobial Chemotherapy. *Cell* **158**, 722-733.
- » Claus, S.P., Tsang, T.M., Wang, Y., Cloarec, O., Skordi, E., Martin, F.-P., Rezzi, S., Ross, A., Kochhar, S., Holmes, E. and Nicholson, J.K. (2008). Systemic multicompartmental effects of the gut microbiome on mouse metabolic phenotypes. *Molecular Systems Biology* **4**, 219.
- » Cornelis, G.R. (2006). The type III secretion injectisome. *Nature reviews. Microbiology* **4**, 811-825.

- » Costa, T.R.D., Felisberto-Rodrigues, C., Meir, A., Prevost, M.S., Redzej, A., Martina Trokter, M., Waksman, G. (2015). Secretion systems in Gram-negative bacteria: structural and mechanistic insights. *Nature Reviews Microbiology* **13**, 343-359
- » Crost, E.H., Tailford, L.E., Le Gall, G., Fons, M., Henrissat, B., Juge, N. (2013). Utilisation of Mucin Glycans by the Human Gut Symbiont *Ruminococcus gnavus* Is Strain-Dependent. *PLoS One* **8**(10), e76341.
- » De Keersmaecker, S.C.J., Marchal, K., Verhoeven, T.V.A., Engelen, K., Vanderleyden, J., Detweiler, C.S. (2015). Microarray Analysis and Motif Detection Reveal New Targets of the *Salmonella enterica* Serovar Typhimurium HilA Regulatory Protein, Including HilA Itself. *Journal of Bacteriology* **187**, 4381-4391.
- » Delepelaire, P. (2004). type I secretion in Gram-negative bacteria. *Biochimica et biophysica acta* **1694**, 149-161.
- » Demerec, M. and Hartman, P.E. (1959). Complex Loci In Microorganisms. *Annu. Rev. Microbiol.* **13**, 377-406.
- » Desai, P.T., Porwollik, S., Long, F., Cheng, P., Wollam, A., Clifton, S.W., Weinstock, G.M., McClelland, M. (2013). Evolutionary Genomics of *Salmonella enterica* Subspecies. *mBio* **4**(2), e00579-12.
- » Devenish, J.A. and Schiemann, D.A. (1981). HeLa Cell Infection by *Yersinia enterocolitica*: Evidence for Lack of Intracellular Multiplication and Development of a New Procedure for Quantitative Expression of Infectivity. *INFECTION AND IMMUNITY* **32**, 48-55.
- » Dharmani, P., Srivastava, V., Kissoon-Singh, V. and Chadee, K. (2009). Role of intestinal mucins in innate host defense mechanisms against pathogens. *Journal of innate immunity* **1**, 123-135.
- » Duan, X. and He, Z.G. (2011). Characterization of the specific interaction between archaeal FHA domain-containing protein and the promoter of a flagellar-like gene-cluster and its regulation by phosphorylation. *Biochem Biophys Res Commun* **407**, 242-7.
- » Dufréne, Y.F. (2015). Sticky microbes: forces in microbial cell adhesion. *Trends in Microbiology*, 1-7
- » Durand, E., Verger, D., Rego, A. T., Chandran, V., Meng, G., Fronzes, R., Waksman, G. (2009). Structural Biology of Bacterial Secretion Systems in Gram-Negative Pathogens- Potential for New Drug Targets.: *Infectious Disorders - Drug Targets* **9**, 518-547.
- » Edwards, R.A., Olsen, G.J. and Maloy, S.R. (2002). Comparative genomics of closely related *Salmonellae*. *Trends in microbiology* **10**, 94-99.
- » Ellermeier, J.R. and Slauch, J.M. (2007). Adaptation to the host environment: regulation of the SPI-1 type III secretion system in *Salmonella enterica* serovar Typhimurium. *Current opinion in microbiology* **10**, 24-29.
- » Fàbrega, A. and Vila, J. (2013). *Salmonella enterica* Serovar Typhimurium Skills To Succeed in the Host: Virulence and Regulation. *Clinical Microbiology Reviews* **26**, 308-341.
- » Falke, J.J. and Hazelbauer, G.L. (2001). Transmembrane signaling in bacterial chemoreceptors. *Trends in Biochemical Sciences* **26**, 257-265.
- » Fang, F.C., Frawley, E.R., Tapscott, T., Vazquez-Torres, A. (2016). Bacterial Stress Responses during Host Infection. *Cell Host Microbe* **20**(2), 133-143.
- » Fattinger, S.A., Böck, D., Di Martino, M.L., Deuring, S., Samperio Ventayo, P., Ek, V., Furter, M., Kreibich, S., Bosisia, F., Müller-Hauser, A.A., Nguyen, B.D., Rohde, M., Pilhofer, M., Hardt, W.D., Sellin, M.E. (2020). *Salmonella* Typhimurium discreet-invasion of the murine gut absorptive epithelium. *PLOS Pathogens* **16**(5).
- » Finlay, B.B. and Falkow, S. (1990). *Salmonella* interactions with polarized human intestinal Caco-2 epithelial cells. *The Journal of infectious diseases* **162**, 1096-1106.
- » Finlay, B.B., Starnbach, M.N., Francis, C.L., Stacker, B.A.D., Chatfield, S., Dougan, G., Falkow, S. (1988). Identification and characterization of TnpHoA mutants of *Salmonella* that are unable to pass through a polarized MDCK epithelial cell monolayer. *Molecular Microbiology* **2**, 757-766.
- » Fookes, M., Schroeder, G.N., Langridge, G.C., Blondel, C.J., Thomson, N.R. *et al.* (2011). *Salmonella bongori* Provides Insights into the Evolution of the *Salmonellae*. *PLoS Pathogens* **7**, e1002191.
- » Foster, J.W. (1991). *Salmonella* acid shock proteins are required for the adaptive acid tolerance response. *Journal of bacteriology* **173**, 6896-6902.
- » Furter, M., Sellin, M.E., Hansson, G.C., Hardt, W.D. (2019). Mucus Architecture and Near-Surface Swimming Affect Distinct *Salmonella* Typhimurium Infection Patterns along the Murine Intestinal Tract. *Cell Reports* **27**, 2665-2678.
- » Gagnon, M., Zihler Berner, A., Chervet, N., Chassard, C., Lacroix, C. (2013). Comparison of the Caco-2, HT-29 and the mucus-secreting HT29-MTX intestinal cell models to investigate *Salmonella* adhesion and invasion. *Journal of Microbiological Methods* **94**, 274-279.
- » Galán, J.E. and Curtiss, R., 3rd (1989). Cloning and molecular characterization of genes whose products allow *Salmonella* Typhimurium to penetrate tissue culture cells. *Proceedings of the National Academy of Sciences of the United States of America* **86**, 6383-6387.
- » Garai, P., Gnanadhas, D.P. and Chakravortty, D. (2012). *Salmonella enterica* serovars Typhimurium and Typhi as model organisms: revealing paradigm of host-pathogen interactions. *Virulence* **3**, 377-388.
- » Garrido, D., Kim, J.H., German, J.B., Raybould, H.E., Mills, D.A. (2011). Oligosaccharide binding proteins from *Bifidobacterium longum* subsp. infantis reveal a preference for host glycans. *PLoS One* **6**(3), e17315.
- » Gerlach, R.G. and Hensel, M. (2007a). Protein secretion systems and adhesins: The molecular armory of Gram-negative pathogens. *Int J Med Microbiol.* **297**, 401-415
- » Gerlach, R.G. and Hensel, M. (2007b). *Salmonella* pathogenicity islands in host specificity, host pathogen interactions and antibiotics resistance of *Salmonella enterica*. *Berliner und Münchener tierärztliche Wochenschrift* **120**, 317-327.
- » Gerlach, R.G., Jäckel, D., Geymeier, N. and Hensel, M. (2007c). *Salmonella* pathogenicity island 4-mediated adhesion is coregulated with invasion genes in *Salmonella enterica*. *Infect Immun* **75**, 4697-4709.
- » Gerlach, R.G., Jäckel, D., Stecher, B., Wagner, C., Lupas, A., Hardt, W.D. and Hensel, M. (2007d). *Salmonella* Pathogenicity Island
- » Gerlach, R.G., Claudio, N., Rohde, M., Jäckel, D., Wagner, C. and Hensel, M. (2008). Cooperation of *Salmonella* pathogenicity islands 1 and 4 is required to breach epithelial barriers. *Cellular microbiology* **10**, 2364-2376.

- » Gerlach, R.G., Jäckel, D., Hölzer, S.U. and Hensel, M. (2009). Rapid oligonucleotide-based recombining of the chromosome of *Salmonella enterica*. *Appl Environ Microbiol* **75**, 1575-1580.
- » Giammanco, G.M., Pignato, S., Mammina, C., Grimont, F., Grimont, P.A., Nastasi, A. and Giammanco, G. (2002). Persistent endemicity of *Salmonella bongori* 48:z35:- in Southern Italy: molecular characterization of Human, animal, and environmental isolates. *Journal of clinical microbiology* **40**, 3502-3505.
- » Goemaere, E.L., Cascales, E., Lloubès, R. (2007). Mutational Analyses Define Helix Organization and Key Residues of a Bacterial Membrane Energy-transducing Complex. *Journal of Molecular Biology* **9**, 1424-1436.
- » Grant, A.J., Restif, O., McKinley, T.J., Sheppard, M., Maskell, D.J., Mastroeni, P. (2008). Modelling within-Host Spatiotemporal Dynamics of Invasive Bacterial Disease. *PLoS Biol.* **6**(4), e74.
- » Griessl, M.H., Schmid, B., Kassler, K., Braunsmann, C., Ritter, R., Barlag, B., *et al.* (2013). Structural insight into the giant Ca(2+)-binding adhesion SiiE: Implications for the adhesion of *Salmonella enterica* to polarized epithelial cells. *Structure* **21**, 741-752.
- » Guibourdenche, M., Roggentin, P., Mikoleit, M., Fields, P.I., Bockemuhl, J., Grimont, P.A. and Weill, F.X. (2010). Supplement 2003-2007 (No. 47) to the White-Kauffmann-Le Minor scheme. *Research in microbiology* **161**, 26-29.
- » Guo, M., Huang, Z., Yang, J. (2018). Is there any crosstalk between the chemotaxis and virulence induction signaling in *Agrobacterium tumefaciens*? *Biotechnol Adv* **35**(4), 505-11.
- » Hansson, G.C. (2019). Mucus and mucins in diseases of the intestinal and respiratory tracts. *J Intern Med* **285**, 479- 490.
- » Hapfelmeier, S., Ehrbar, K., Stecher, B., Barthel, M., Kremer, M. and Hardt, W.D. (2004). Role of the *Salmonella* pathogenicity island 1 effector proteins SipA, SopB, SopE, and SopE2 in *Salmonella enterica* subspecies 1 serovar Typhimurium colitis in streptomycin-pretreated mice. *Infect Immun* **72**, 795-809.
- » Haraga, A., Ohlson, M.B. and Miller, S.I. (2008). *Salmonellae* interplay with host cells. *Nature reviews. Microbiology* **6**, 53-66.
- » Hase, K., Kawano, K., Nochi, T., Soares Pontes, G., Fukuda, S., Ebisawa, M., Kadokura, K., Tobe, T., Fujimura, Y., Kawano, S., Yabashi, A., Waguri, S., Nakato, G., Kimura, S., Murakami, T., Iimura, M., Hamura, K., Fukuoka, S., Lowe, A.W., Itoh, K., Kiyono, H., Ohno, H. (2009). Uptake through glycoprotein 2 of FimH1 bacteria by M cells initiates mucosal immune response. *Nature LETTERS* **462**, 226-231.
- » Hausmann, A. and Hardt, W.D. (2019). The Interplay between *Salmonella enterica* Serovar Typhimurium and the Intestinal Mucosa during Oral Infection. *Microbiol Spectrum* **7**(2).
- » Hazelbauer, G.L., Falke, J.J., Parkinson, J.S. (2008). Bacterial chemoreceptors: high-performance signaling in networked arrays. *Trends in Biochemical Sciences* **33**, 9-19.
- » Heinzen, R.A. and Hackstadt, T. (1997). The *Chlamydia trachomatis* Parasitophorous Vacuolar Membrane Is Not Passively Permeable to Low-Molecular-Weight Compounds. *INFECTION AND IMMUNITY* **65**, 1088-1094.
- » Helaine, S., Cheverton, A.M., Watson, K.G., Faure, L.M., Matthews, S.A., Holden, D.W. (2014). Internalization of *Salmonella* by Macrophages Induces Formation of Nonreplicating Persisters. *Science* **343**(6167), 204-208.
- » Hensel, M., Shea, J.E., Waterman, S.R., Mundy, R., Nikolaus, T., Banks, G., *et al.* (1998). Genes encoding putative effector proteins of the type III secretion system of *Salmonella* pathogenicity island 2 are required for bacterial virulence and proliferation in macrophages. *Molecular microbiology* **30**, 163174.
- » Hersh, D., Monack, D.M., Smith, M.R., Ghori, N., Falkow, S. and Zychlinsky, A. (1999). The *Salmonella* invasion SipB induces macrophage apoptosis by binding to caspase-1. *Proceedings of the National Academy of Sciences of the United States of America* **96**, 2396-2401.
- » Hoffmann, S., Schmidt, C., Walter, S., Bender, J.K. and Gerlach, R.G. (2017). Scarless deletion of up to seven methyl- accepting chemotaxis genes with an optimized method highlights key function of CheM in *Salmonella* Typhimurium. *PLoS One* **12**(2).
- » Hoffmann, S., Walter, S., Blume, A.K., Fuchs, S., Schmidt, C., Scholz, A. and Gerlach, R.G. (2018). High-Throughput Quantification of Bacterial-Cell Interactions Using Virtual Colony Counts. *Front. Cell. Infect. Microbiol.* **8**, 43.
- » Hoffmann, S., Gendera, K., Schmidt, S., Kirchwegger, P., Imhof, A., Bogdan, C., Muller, Y.A., Hensel, M. and Gerlach, R.G. (2021). A chemotactic sensor controls *Salmonella*-host cell interaction. *bioRxiv* preprint.
- » Holland, I.B., Schmitt, L. and Young, J. (2005). Type I protein secretion in bacteria, the ABC-transporter dependent pathway (review). *Molecular membrane biology* **22**, 29-39.
- » Hosking, E.R., Vogt, C., Bakker, E.P., Manson, M.D. (2006). The *Escherichia coli* MotAB Proton Channel Unplugged. *J. Mol. Biol.* **364**, 921-937.
- » Hoyer, L.L., Hamilton, A.C., Steenbergen, S.M., Vimr, E.R. (1992). Cloning, sequencing and distribution of the *Salmonella* Typhimurium LT2 sialidase gene, nanH, provides evidence for interspecies gene transfer. *Molecular Microbiology* **6**, 873-884.
- » Hughes, K.T. and Berg, H.C. (2017). The bacterium has landed: Mechanosensing mechanisms for surface recognition by bacteria allow biofilm formation. *Science* **358**, 446-447.
- » Ibarra, J.A. and Steele-Mortimer, O. (2009). *Salmonella* – the ultimate insider. *Salmonella* virulence factors that modulate intracellular survival. *Cellular microbiology* **11**, 1579-1586.
- » Janganan, T.K., Bavro, V.N., Zhang, L., Matak-Vinkovic, D., Barrera, N.P., Venien-Bryan, C., Robinson, C.V., Borges-Walmsley, M.I., Walmsley, A.R. (2011). Evidence for the Assembly of a Bacterial Tripartite Multidrug Pump with a Stoichiometry of 3:6:3. *The Journal of Biological Chemistry* **286**, 26900-26912.
- » Jepson, M.A. and Clark, M.A. (2001). The role of M cells in *Salmonella* infection. *Microbes and infection / Institut Pasteur* **3**, 1183-1190.
- » Johnson, R., Mylona, E., Frankel, G. (2018). Typhoidal *Salmonella*: Distinctive virulence factors and pathogenesis. *Cellular Microbiology* **20**, e12939.
- » Kell, D.B. and Young, M. (2000). Bacterial dormancy and culturability: the role of autocrine growth factors. *Current Opinion in Microbiology* **3**, 238-243.
- » Kentner, D., Thiem, S., Hildenbeutel, M., Sourjik, V. (2006). Determinants of chemoreceptor cluster formation in *Escherichia coli*. *Molecular Microbiology* **61**(2), 407-417.

- » Kirchweger, P., Weiler, S., Egerer-Sieber, C., Blasl, A.-T., Hoffmann, S., Schmidt, C., Sander, N., Merker, D., Gerlach, R.G., Hensel, M., Muller, Y.A. (2019). Structural and Functional Characterization of SiiA, an Auxiliary Protein From the SPI-4-encoded type I Secretion System From *Salmonella* Enterica. *Mol Microbiol* **112**(5), 1403-1422.
- » Kiss, T., Morgan, E. and Nagy, G. (2007). Contribution of SPI-4 genes to the virulence of *Salmonella* enterica. *FEMS Microbiol Lett.*
- » Knodler, L.A., Bestor, A., Ma, C., Hansen-Wester, I., Hensel, M., Vallance, B.A. and Steele-Mortimer, O. (2005). Cloning Vectors and Fluorescent Proteins Can Significantly Inhibit *Salmonella* enterica Virulence in Both Epithelial Cells and Macrophages: Implications for Bacterial Pathogenesis Studies. *Infect Immun* **3**, 7027-7031.
- » Kojima, S. and Blair, D.F. (2004). Solubilization and purification of the MotA/MotB complex of *Escherichia coli*. *Biochemistry* **43**, 26-34.
- » Kojima, S., Imada, K., Sakuma, M., Sudo, Y., Kojima, C., Minamino, T., Homma, M., Namba, K. (2009) Stator assembly and activation mechanism of the flagellar motor by the periplasmic region of MotB. *Molecular Microbiology* **73**, 710-718.
- » Kojima, S., Takao, M., Almira, G., Kawahara, I., Sakuma, M., Homma, M., Kojima, C. and Imada, K. (2018). The Helix Rearrangement in the Periplasmic Domain of the Flagellar Stator B Subunit Activates Peptidoglycan Binding and Ion Influx. *Structure* **26**, 590-598.
- » Kolodziej, A.F., Tan, T., Koshland D.E., Jr (1996). Producing positive, negative, and no cooperativity by mutations at a single residue located at the subunit interface in the aspartate receptor of *Salmonella typhimurium*. *Biochemistry*. **35**, 14782-92.
- » Kondoh, H., Ball, C.B., Adler, J. (1979). Identification of a methyl-accepting chemotaxis protein for the ribose and galactose chemoreceptors of *Escherichia coli*. *PNAS* **76**, 260-264.
- » König, J., Wells, J., Cani, P.D., García-Ródenas, C.L., MacDonald, T., Mercenier, A., Whyte, J., Freddy Troost, F., Brummer, R.J. (2016). Human Intestinal Barrier Function in Health and Disease. *Clin Transl Gastroenterol.* **7**(10), e196.
- » Kraehenbuhl, J.P. and Neutra, M.R. (2000). Epithelial M cells: differentiation and function. *Annual review of cell and developmental biology* **16**, 301-332.
- » Lara-Tejero, M., Kato, J., Wagner, S., Liu, X. and Galan, J.E. (2011). A sorting platform determines the order of protein secretion in bacterial type III systems. *Science* **331**, 1188-1191.
- » Latasa, C., Roux, A., Toledo-Arana, A., Ghigo, J., Gamazo, C., Penadés, J.R., Lasa, I. (2005). BapA, a large secreted protein required for biofilm formation and host colonization of *Salmonella* enterica serovar Enteritidis. *Molecular Microbiology* **56**, 1322-1339.
- » Lazova, M.D., Butler, M.T., Shimizu, T.S., Harshey, R.M. (2012). *Salmonella* chemoreceptors McpB and McpC mediate a repellent response to L-cystine: a potential mechanism to avoid oxidative conditions. *Molecular Microbiology* **84**, 697-711.
- » Lele, P.P., Hosu, B.G., Berg, H.C. (2013). Dynamics of mechanosensing in the bacterial flagellar motor. *PNAS* **110**, 11839-11844.
- » Li, X., Bleumink-Pluym, N.M.C., Luijckx, Y.M.C.A., Wubbolts, R.W., van Putten, J.P.M., Strijbis, K. (2019). MUC1 is a receptor for the *Salmonella* SiiE adhesin that enables apical invasion into enterocytes. *PLoS Pathogen* **15**(2).
- » Lievin-Le Moal, V. and Servin, A.L. (2006). The front line of enteric host defense against unwelcome intrusion of harmful microorganisms: mucins, antimicrobial peptides, and microbiota. *Clinical microbiology reviews* **19**, 315-337.
- » Lifscis, M.R., Lancy, E.D., Maurer, R. (1992). DNA Replication Defect in *Salmonella* Typhimurium Mutants Lacking the Editing (ϵ) Subunit of DNA Polymerase III. *Journal of Bacteriology* **174**, 6965-6973.
- » Lim, B.K. and Thong, K.L. (2009). Application of PCR-based serogrouping of selected *Salmonella* serotypes in Malaysia. *Journal of infection in developing countries* **3**, 420-428.
- » Liu, Y., Zhang, F., Zhou, X., Xu, L., Zhang, L., Shi, X. (2017). Comprehensive Analysis Reveals Two Distinct Evolution Patterns of *Salmonella* Flagellin Gene Clusters. *Front Microbiol.* **8**, 2604.
- » Lloubès, R., Cascales, E., Walburger, A., Bouveret, E., Lazdunski, C., Bernadac, A., Journet, L. (2001). The Tol-Pal Proteins of the *Escherichia coli* Cell Envelope: An Energized System Required for Outer Membrane Integrity? *Res Microbiol* **152**(6), 523-9.
- » Lorkowski, M., Felipe-López, A., Danzer, C.A., Hansmeier, N., Hensel, M. (2014). *Salmonella* enterica Invasion of Polarized Epithelial Cells Is a highly Cooperative Effort. *Infection and Immunity* **82**(6), 2657-2667.
- » Lucchini, S., Rowley, G., Goldberg, M.D., Hurd, D., Harrison, M. and Hinton, J.C. (2006). H-NS mediates the silencing of laterally acquired genes in bacteria. *PLoS pathogens* **2**, e81.
- » Maier, L., Vyas, R., Cordova, C.D., Lindsay, H., Schmidt, T.S.B., Brugiroux, S., Periaswamy, B., Bauer, R., Sturm, A., Schreiber, F., von Mering, C., Robinson M.D., Stecher, B., Hardt, W.D. (2013). Microbiota-Derived Hydrogen Fuels *Salmonella* Typhimurium Invasion of the Gut Ecosystem. *Cell Host & Microbe* **14**, 641-651.
- » Main-Hester, K.L., Colpitts, K.M., Thomas, G.A., Fang, F.C. and Libby, S.J. (2008). Coordinate regulation of *Salmonella* pathogenicity island 1 (SPI-1) and SPI-4 in *Salmonella* enterica serovar Typhimurium. *Infect Immun* **76**, 1024-1035.
- » Majowicz, S.E., Musto, J., Scallan, E., Angulo, F.J., Kirk, M., O'Brien, S.J., Jones, T.F., Fazil, A., Hoekstra R.M. (2010). The Global Burden of Nontyphoidal *Salmonella* Gastroenteritis. *Clinical Infectious Diseases* **50**, 882-889.
- » Männe, C., Takaya, A., Yamasaki, Y., Mursell, M., Hojyo, S., Wu, T.-Y., Sarkander, J., McGrath, M.A., Cornelis, R., Hahne, S., Cheng, Q., Kawamoto, T., Hiepe, F., Kaufmann, S.H.E., Yamamoto, T., Radbruch, A. and Tokoyod, K. (2019). *Salmonella* SiiE prevents an efficient humoral immune memory by interfering with IgG⁺ plasma cell persistence in the bone marrow. *PNAS* **116**, 7425-7430.
- » Marcus, S.L., Brumell, J.H., Pfeifer, C.G. and Finlay, B.B. (2000). *Salmonella* pathogenicity islands: big virulence in small packages. *Microbes and infection / Institut Pasteur* **2**, 145-156.
- » Martens-Habbena, W. and Sass, H. (2006). Sensitive Determination of Microbial Growth by Nucleic Acid Staining in Aqueous Suspension. *Applied and Environmental Microbiology* **72**, 87-95.
- » Martínez-Gil, M., Ramos-González, M.I., Espinosa-Urgel, M. (2014). Roles of Cyclic Di-GMP and the Gac System in Transcriptional Control of the Genes Coding for the *Pseudomonas putida* Adhesins LapA and LapF. *Journal of Bacteriology* **196**(8), 1484-1495.
- » Masi, M. and Wandersman, C. (2010). Multiple Signals Direct the Assembly and Function of a type I Secretion System. *J Bacteriol* **192**(15), 3861-9.

- » Matilla, M.A., Krell, T. (2018). The effect of bacterial chemotaxis on host infection and pathogenicity. *FEMS Microbiol Rev* **42**(1).
- » McClelland, M., Sanderson, K.E., Spieth, J., Clifton, S.W., Latreille, P., Courtney, L., *et al.* (2001). Complete genome sequence of *Salmonella enterica* serovar Typhimurium LT2. *Nature* **413**, 852-856.
- » McCormick, B.A., Hofman, P.M., Kim, J., Carnes, D.K., Miller, S.I. and Madara, J.L. (1995). Surface attachment of *Salmonella* Typhimurium to intestinal epithelia imprints the subepithelial matrix with gradients chemotactic for neutrophils. *The Journal of cell biology* **131**, 1599-1608.
- » McGhie, E.J., Brawn, L.C., Hume, P.J., Humphreys, D. and Koronakis, V. (2009). *Salmonella* takes control: effector-driven manipulation of the host. *Current opinion in microbiology* **12**, 117-124.
- » McLaughlin, H.P., Caly, D.L., McCarthy, Y., Ryan, R.P., Dow, J.M. (2012). An Orphan Chemotaxis Sensor Regulates Virulence and Antibiotic Tolerance in the Human Pathogen *Pseudomonas aeruginosa*. *PLoS ONE* **7**(8).
- » Minamino, T., Imada, K., Namba, K. (2008). Molecular Motors of the Bacterial Flagella. *Current Opinion in Structural Biology* **18**(6), 693-701.
- » Misselwitz, B., Kreibich, S.K., Rout, S., Stecher, B., Periaswamy, B., Hardt, W.D. (2010). *Salmonella enterica* Serovar Typhimurium Binds to HeLa Cells via Fim-Mediated Reversible Adhesion and Irreversible type Three Secretion System 1-Mediated Docking. *Infection and Immunity* **79**, 330-341.
- » Monack, D.M., Hersh, D., Ghori, N., Bouley, D., Zychlinsky, A. and Falkow, S. (2000). *Salmonella* exploits caspase-1 to colonize Peyer's patches in a murine typhoid model. *The Journal of experimental medicine* **192**, 249-258.
- » Monack, D.M., Detweiler, C.S., Falkow, S. (2001). *Salmonella* pathogenicity island 2-dependent macrophage death is mediated in part by the host cysteine protease caspase-1. *Cellular Microbiology* **3**, 825-837
- » Morgan, E., Campbell, J.D., Rowe, S.C., Bispham, J., Stevens, M.P., Bowen, A.J., *et al.* (2004). Identification of host-specific colonization factors of *Salmonella enterica* serovar Typhimurium. *Molecular microbiology* **54**, 994-1010.
- » Morgan, E., Bowen, A.J., Carnell, S.C., Wallis, T.S., Stevens, M.P. (2007). SiiE Is Secreted by the *Salmonella enterica* Serovar Typhimurium Pathogenicity Island 4-Encoded Secretion System and Contributes to Intestinal Colonization in Cattle. *Infection and Immunity* **75**, 1524-1533.
- » Morimoto, Y.V., Che, Y.S., Minamino, T. and Namba, K. (2010). Proton-conductivity assay of plugged and unplugged MotA/Bp roton channel by cytoplasmic pHluorin expressed in *Salmonella*. *FEBS Lett* **584**, 1268-1272.
- » Moussatova, A., Kandt, C., O'Mara, M.L. and Tieleman, D.P. (2008). ATP-binding cassette transporters in *Escherichia coli*. *Biochimica et biophysica acta* **1778**, 1757-1771.
- » Naghili, H., Tajik, H., Mardani, K., Rouhani, S.M.R., Ehsani, A., Zare, P. (2013). Validation of drop plate technique for bacterial enumeration by parametric and nonparametric tests. *Veterinary Research Forum* **4**, 179-183.
- » Nakamura, S., Kami-ike N., Yokota, J.P., Kudo, S., Minamino, T. and Namba, K. (2009). Effect of intracellular pH on the torque-speed relationship of bacterial proton-driven flagellar motor. *Journal of molecular biology* **386**, 332-338.
- » Navarre, W.W., Porwollik, S., Wang, Y., McClelland, M., Rosen, H., Libby, S.J. and Fang, F.C. (2006). Selective silencing of foreign DNA with low GC content by the H-NS protein in *Salmonella*. *Science* **313**, 236-238.
- » Neutra, M.R., Mantis, N.J. and Kraehenbuhl, J.P. (2001). Collaboration of epithelial cells with organized mucosal lymphoid tissues. *Nature immunology* **2**, 1004-1009.
- » Newell, P.D., Boyd, C.D., Sondermann, H. and O'Toole, G.A. (2011). A c-di-GMP effector system controls cell adhesion by inside-out signaling and surface protein cleavage. *PLoS biology* **9**, e1000587.
- » Nguyen, B.D., Cuenca V., M., Hartl, J., Gul, E., Bauer, R., Meile, S., Ruthi, J., Margot, C., Heeb, L., Besser, F., Pérez Escriba, P., Fetz, C., Furter, M., Laganenka, L., Keller, P., Fuchs, L., Christen, M., Porwollik, S., McClelland, M., Vorholt, J.A., Sauer, U., Sunagawa, S., Christen, B. and Hardt, W.-D. (2020). Import of Aspartate and Malate by DcuABC Drives H₂/Fumarate Respiration to Promote Initial *Salmonella* Gut-Lumen Colonization in Mice. *Cell Host & Microbe* **27**, 1-15.
- » Nieto, J.M., Bailey, M.J.A., Hughes, C., Koronakis, V. (1996). Suppression of transcription polarity in the *Escherichia coli* haemolysin operon by a short upstream element shared by polysaccharide and DNA transfer determinants. *Molecular Microbiology* **19**, 705-713.
- » Noinaj, N., Guillier, M., Barnard, T.J., Buchanan, S.K. (2011). TonB-dependent transporters: regulation, structure, and function. *Annu Rev Microbiol* **64**, 43-60.
- » O'Toole, G.A. and Wong, G.C.L. (2016). Sensational biofilms: surface sensing in bacteria. *Current Opinion in Microbiology* **30**, 139-146.
- » Ochman, H. and Groisman, E.A. (1996). Distribution of pathogenicity islands in *Salmonella* spp. *Infect Immun* **64**, 5410-5412.
- » Ollis, A.A., Manning, M., Held, K.G., Postle, K. (2009). Cytoplasmic membrane protonmotive force energizes periplasmic interactions between ExbD and TonB. *Molecular Microbiology* **73**(3), 466-481.
- » van Ooij, C., Apodaca, G., Engel, J. (1997). Characterization of the *Chlamydia trachomatis* Vacuole and Its Interaction with the Host Endocytic Pathway in HeLa Cells. *Infection and Immunity* **65**, 758-766.
- » Ouwerkerk, J.P., de Vos, W.M., Belzer, C. (2013). Glycobiome: Bacteria and mucus at the epithelial interface. *Best Practice & Research Clinical Gastroenterology* **27**, 25-28.
- » Ovesen, L., Bendtsen, F., Tage-Jensen, U., Pedersen, N.T., Gram, B.R., Rune, S.J. (1986). Intraluminal pH in the Stomach, Duodenum, and Proximal Jejunum in Normal Subjects and Patients With Exocrine Pancreatic Insufficiency. *Gastroenterology* **90**, 958-62.
- » Park, H., Im, W., Seok, C. (2011). Transmembrane Signaling of Chemotaxis Receptor Tar: Insights from Molecular Dynamics Simulation Studies. *Biophysical Journal* **100**(12), 2955-2963.
- » Parkinson, J.S. (2010). Signaling Mechanisms of HAMP Domains in Chemoreceptors and Sensor Kinases. *Annual Review of Microbiology* **64**, 101-122.
- » Parkinson, J.S., Hazelbauer, G.L., Falke, J.J. (2015). Signaling and sensory adaptation in *Escherichia coli* chemoreceptors: 2015 update. *Trends Microbiol* **23**(5), 257-66.

- » Pérez-Mendoza, D., Coulthurst, S.J., Sanjuán, J., Salmond, G.P.C. (2011). N-Acetylglucosamine-dependent biofilm formation in *Pectobacterium atrosepticum* is cryptic and activated by elevated c-di-GMP levels. *Microbiology* **157**(12).
- » Peters, B., Stein, J., Klingl, S., Sander, N., Sandmann, A., Taccardi, N., Sticht, H., Gerlach, R.G., Müller, Y.A., Hensel, M. (2017). Structural and functional dissection reveals distinct roles of Ca²⁺-binding sites in the giant adhesin SiiE of *Salmonella enterica*. *PLoS Pathogens* **13**, e1006418.
- » Png, C.W., Lindén, S.K., Gilshenan, K.S. Zoetendal, E.G., McSweeney, C.S., Sly, L.L., McGuckin, M.A., Florin, T.H.J. (2010). Mucolytic Bacteria With Increased Prevalence in IBD Mucosa Augment In Vitro Utilization of Mucin by Other Bacteria. *American Journal of Gastroenterology* **105**, 2420-2428.
- » Raffatellu, M., Chessa, D., Wilson, R.P., Tukel, C., Akcelik, M. and Baumler, A.J. (2006). Capsule-mediated immune evasion: a new hypothesis explaining aspects of typhoid fever pathogenesis. *Infect Immun* **74**, 19-27.
- » Raffatellu, M., Wilson, R. P., Winter, S. E., Bäumlner, A.J. (2008). Clinical pathogenesis of typhoid fever. *J Infect Developing Countries* **2**(4), 260-266
- » Ramachandran, V.K., Shearer, N., Jacob, J.J., Sharma, C.M. and Thompson, A. (2012). The architecture and ppGpp-dependent expression of the primary transcriptome of *Salmonella* Typhimurium during invasion gene expression. *BMC genomics* **13**, 25.
- » Ramsden, A.E., Holden, D.W. and Mota, L.J. (2007). Membrane dynamics and spatial distribution of *Salmonella*-containing vacuoles. *Trends in microbiology* **15**, 516-524.
- » Rescigno, M., Urbano, M., Valzasina, B., Francolini, M., Rotta, G., Bonasio, R., *et al.* (2001). Dendritic cells express tight junction proteins and penetrate gut epithelial monolayers to sample bacteria. *Nature immunology* **2**, 361-367.
- » Rivera-Chávez, F., Winter, S.E., Lopez, C.A., Xavier, M.N., Winter, M.G., Nuccio, S.P., Russell, J.M., Laughlin, R.C., Lawhon, S.D., Sterzenbach, T., Bevins, C.L., Tsolis, R.M., Harshey, R., Adams, L.G., Bäumlner, A.J. (2013). *Salmonella* uses energy taxis to benefit from intestinal inflammation. *PLoS Pathogens* **9**(4), e1003267.
- » Rivera-Chávez, F., Lopez, C.A., Zhang, L.F., García-Pastor, L., Chávez-Arroyo, A., Lokken, K.L., Tsolis, R.M. Winter, S.E., Bäumlner, A.J. (2016). Energy Taxis toward Host-Derived Nitrate Supports a *Salmonella* Pathogenicity Island 1-Independent Mechanism of Invasion. *mBio* **7**(4).
- » Rosselin, M., Abed, N., Virlogeux-Payant, I., Bottreau, E., Sizaret, P.Y., Philippe Velge, P., Wiedemann, A. (2011). Heterogeneity of type III secretion system (T3SS)-1-independent entry mechanisms used by *Salmonella* Enteritidis to invade different cell types. *Microbiology* **157**, 839-847.
- » Rossez, Y., Wolfson, E.B., Holmes, A., Gally, D.L., Holden, N.J. (2015). Bacterial Flagella: Twist and Stick, or Dodge across the Kingdoms. *PLoS Pathogens* **11**(1).
- » Roujeinikova, A. (2008). Crystal structure of the cell wall anchor domain of MotB, a stator component of the bacterial flagellar motor: Implications for peptidoglycan recognition. *Proceedings of the National Academy of Sciences of the United States of America* **105**, 10348-10353.
- » Sabbagh, S.C., Forest, C.G., Lepage, C., Leclerc, J.M. and Daigle, F. (2010). So similar, yet so different: uncovering distinctive features in the genomes of *Salmonella enterica* serovars Typhimurium and Typhi. *FEMS microbiology letters* **305**, 1-13.
- » Saini, S. and Rao, C.V. (2010). SprB is the molecular link between *Salmonella* pathogenicity island 1 (SPI-1) and SPI-4. *Journal of bacteriology* **192**, 2459-2462.
- » Sansonetti, P.J. (2004). War and peace at mucosal surfaces. *Nature reviews* **4**, 953-964.
- » Santos, R.L., Raffatellu, M., Bevins, C.L., Adams, L.G., Tukel, C., Tsolis, R.M. and Bäumlner, A.J. (2009). Life in the inflamed intestine, *Salmonella* style. *Trends in microbiology* **17**, 498-506.
- » Sarshar, M., Scribano, D., Tranquilli, G., Pietro, M., Filardo, S., Zagaglia, C., Sessa, R., Palamara, A.T., Ambrosi, C. (2019). A simple, fast and reliable scan-based technique as a novel approach to quantify intracellular bacteria. *BMC Microbiology* **19**, 252.
- » Satchell, K.J.F. (2011). Structure and Function of MARTX Toxins and Other Large Repetitive RTX Proteins. *Annual Review of Microbiology* **65**, 71-90.
- » Schmidt, H. and Hensel, M. (2004). Pathogenicity islands in bacterial pathogenesis. *Clinical microbiology reviews* **17**, 14-56.
- » Siebers, A. and Finlay, B.B. (1996). M cells and the pathogenesis of mucosal and systemic infections. *Trends in microbiology* **4**, 22-29.
- » Smith, T.J., Font, M.E., Kelly, C.M., Sondermann, H., O'Toole G.A. (2018). An N-Terminal Retention Module Anchors the Giant Adhesin LapA of *Pseudomonas fluorescens* at the Cell Surface: a Novel Subfamily of type I Secretion Systems. *J Bacteriol.* **200**(8).
- » Sourjik, V. and Berg, H.C. (2000). Localization of components of the chemotaxis machinery of *Escherichia coli* using fluorescent protein fusions. *Molecular microbiology* **37**, 740-751.
- » Sourjik, V. and Berg, H.C. (2002). Receptor sensitivity in bacterial chemotaxis. *Proceedings of the National Academy of Sciences of the United States of America* **99**, 123-127.
- » Sourjik, V. and Berg, H.C. (2004). Functional interactions between receptors in bacterial chemotaxis. *Nature* **428**, 437-441.
- » Sourjik, V. (2004). Receptor clustering and signal processing in *E. coli* chemotaxis. *TRENDS in Microbiology* **12**, 569-576.
- » Stecher, B., Robbani, R., Walker, A.W., Westendorf, A.M., Barthel, M., Kremer, M., *et al.* (2007). *Salmonella enterica* serovar Typhimurium exploits inflammation to compete with the intestinal microbiota. *PLoS biology* **5**, 2177-2189.
- » Stecher, B., Hapfelmeier, S., Müller, C., Kremer, M., Stallmach, T. and Hardt, W.D. (2004). Flagella and chemotaxis are required for efficient induction of *Salmonella enterica* serovar Typhimurium colitis in streptomycin-pretreated mice. *Infect Immun* **72**, 4138-4150.
- » Sukomon, N., Widom, J., Borbat, P.P., Freed, J.H., Crane, B.R. (2017). Stability and Conformation of a Chemoreceptor HAMP Domain Chimera Correlates with Signaling Properties. *Biophysical Journal* **112**(7), 1383-1395.
- » Suwandi, A., Galeev, A., Riedel, R., Sharma, S., Seeger, K., Sterzenbach, T., García Pastor, L., Boyle, E.C., Gal-Mor, O., Hensel, M., Casadesús, J., Baines, J.F., Grassl, G.A. (2019). Std fimbriae-fucose interaction increases *Salmonella*-induced intestinal inflammation and prolongs colonization. *PLoS Pathogens* **15**(7).
- » Takekawa, N., Terahara, N., Kato, T., Gohara, M., Mayanagi, K., Hijikata, A., Onoue, Y., Kojima, S., Shirai, T., Namba, K., Homma, M. (2016). The tetrameric MotA complex as the core of the flagellar motor stator from hyperthermophilic bacterium. *Scientific Reports* **6**, 31526.

- » Terashima, H., Kojima, S., Homma, M. (2008). Chapter 2 Flagellar Motility in Bacteria: Structure and Function of Flagellar Motor. *International Review of Cell and Molecular Biology* **270**, 39-85.
- » Terashima, H., Kawamoto, A., Morimoto, Y.V., Imada, K., Minamino, T. (2017). Structural differences in the bacterial flagellar motor among bacterial species. *Biophysics and Physicobiology* **14**, 191-198.
- » Thijs, I.M., De Keersmaecker, S.C., Fadda, A., Engelen, K., Zhao, H., McClelland, M., et al. (2007). Delineation of the Salmonella Typhimurium HilA regulon through genome-wide location and transcript analysis. *Journal of bacteriology*.
- » Thomas, S., Holland, B.I., Schmitt L. (2013). The type I secretion pathway – The hemolysin system and beyond. *Biochimica et Biophysica Acta*
- » Thormann, K.M. and Paulick, A. (2010). Tuning the Flagellar Motor. *Microbiology* **156**(5), 1275-1283.
- » Tipping, M.J., Delalez, N.J., Lim, R., Berry, R.M., Armitage, J.P. (2013). Load-Dependent Assembly of the Bacterial Flagellar Motor. *mBio* **4**(4), e00551-13.
- » Toker, A. and Cantley, L.C. (1997). Signalling through the lipid products of phosphoinositide-3-OH kinase. *Nature* **387**, 673-676.
- » Trépoût, S., Taveau, J.C., Benabdelhak, H., Granier, T., Ducruix, A., Frangakis, A.S., Lamberta, O. (2010). Structure of reconstituted bacterial membrane efflux pump by cryo-electron tomography. *Biochimica et Biophysica Acta (BBA) – Biomembranes* **1798**, 1953-1960.
- » Tseng, T.T., Tyler, B.M., Setubal, J.C. (2009). Protein secretion systems in bacterial-host associations, and their description in the Gene Ontology. *BMC Microbiology* **9**.
- » Turner, J.R. (2009). Intestinal mucosal barrier function in health and disease. *Nature reviews* **9**, 799-809.
- » Velge, P., Wiedemann, A., Rosselin, M., Abed, N., Boumart, Z., Chausse, A.M., et al. (2012). Multiplicity of Salmonella entry mechanisms, a new paradigm for Salmonella pathogenesis. *MicrobiologyOpen* **1**, 243258.
- » Verma, R.K., Samal, B., Chatterjee, S. (2019). Xanthomonas oryzae pv. oryzae chemotaxis components and chemoreceptor Mcp2 are involved in the sensing of constituents of xylem sap and contribute to the regulation of virulence-associated functions and entry into rice. *Molecular Plant Pathology* **19**(11), 2397–2415.
- » Vimal, D., Khullar, M., Gupta, S., Ganguly, N. (2000). Intestinal mucins: the binding sites for salmonella typhimurium. *Mol Cell Biochem* **204**, 107–117.
- » Wagner, C., Polke, M., Gerlach, R.G., Linke, D., Stierhof, Y.D., Schwarz, H. and Hensel, M. (2011). Functional dissection of SiiE, a giant non-fimbrial adhesin of Salmonella enterica. *Cellular microbiology* **13**, 1286-1301.
- » Wagner, C., Barlag, B., Gerlach, R.G., Deiwick, J., Hensel, M. (2014). The Salmonella enterica giant adhesin SiiE binds to polarized epithelial cells in a lectin-like manner. *Cellular Microbiology* **16**, 962-975.
- » Welch, M., Oosawa, K., Aizawa, S., Eisenbach, M. (1993). Phosphorylation-dependent binding of a signal molecule to the flagellar switch of bacteria. *PNAS* **90**, 8787-8791.
- » Wille, T., Wagner, C., Mittelstädt, W., Blank, K., Sommer, E., Malengo, G., Döhler, D., Lange, A., Sourjik, V., Hensel, M., Gerlach, R.G. (2014). SiiA and SiiB are novel type I secretion system subunits controlling SPI-4-mediated adhesion of Salmonella enterica. *Cellular Microbiology* **16**, 161-178.
- » Wilson, R.P., Raffatellu, M., Chessa, D., Winter, S.E., Tükel, Ç., Bäumlér, A.J. (2007). The Vi-capsule prevents Toll-like receptor 4 recognition of Salmonella. *Cellular Microbiology* **10**, 876-890.
- » Wilson, R.P., Winter, S.E., Spees, A.M., Winter, M.A., Nishimori, J.H., Sanchez, J.F., Nuccio, S.P., Crawford, R.W., Tükel, C., Bäumlér, A.J. (2010) The Vi Capsular Polysaccharide Prevents Complement Receptor 3-Mediated Clearance of Salmonella enterica Serotype Typhi. *Infection and Immunity* **79**, 830-837.
- » Wojdyla, J.A., Cutts, E., Kaminska, R., Papadakos, G., Hopper, J.T.S., Stansfeld, P.J., Staunton, D., Robinson, C.V., Kleanthous, C. (2015) Structure and Function of the Escherichia coli Tol-Pal Stator Protein TolR. *Journal of Biological Chemistry* **290**, 26675-26687.
- » Wolf, J.L. and Bye, W.A. (1984). The membranous epithelial (M) cell and the mucosal immune system. *Annual review of medicine* **35**, 95-112.
- » Wong, K.K., McClelland, M., Stillwell, L.C., Sisk, E.C., Thurston, S.J. and Saffer, J.D. (1998). Identification and sequence analysis of a 27-kilobase chromosomal fragment containing a Salmonella pathogenicity island located at 92 minutes on the chromosome map of Salmonella enterica serovar Typhimurium LT2. *Infect Immun* **66**, 3365-3371.
- » Xu, X. and Hensel, M. (2011). Systematic analysis of the SsrAB virulon of Salmonella enterica. *Infect Immun* **78**, 49-58.
- » Yamamoto, K. and Imea, Y. (1993). Cloning and characterization of the Salmonella typhimurium-specific chemoreceptor Tcp for taxis to citrate and from phenol. *Proc. Natl. Acad. Sci. USA* **90**, 217-21.
- » Yonekura, K., Maki-Yonekura, S., Homma, M. (2011). Structure of the Flagellar Motor Protein Complex PomAB: Implications for the Torque-Generating Conformation. *Journal of Bacteriology* **193**, 3863-3870.
- » Zhai, Y.F., Heijne, W., Saier Jr., M.H. (2003). Molecular modeling of the bacterial outer membrane receptor energizer, ExbBD/TonB, based on homology with the flagellar motor, MotAB. *Biochimica et Biophysica Acta* **1614**, 201-210.
- » Zhang, S., Kingsley, R.A., Santos, R.L., Andrews-Polymeris, H., Raffatellu, M., Figueiredo, J., et al. (2003). Molecular pathogenesis of Salmonella enterica serotype Typhimurium-induced diarrhea. *Infect Immun* **71**, 1-12.
- » Zhang, X.Y.-Z., Goemaere, E.L., Seddiki, N., Célia, H., Gavioli, M., Cascales, E., Lloubes, R. (2011). Mapping the Interactions between Escherichia coli TolQ Transmembrane Segments. *The Journal of Biological Chemistry* **286**, 11756–11764.
- » Zhao, L., Ezak, T., Li, Z.Y., Kawamura, Y., Hirose, K. and Watanabe, H. (2001). Vi-Suppressed wild strain Salmonella Typhi cultured in high osmolarity is hyperinvasive toward epithelial cells and destructive of Peyer's patches. *Microbiology and immunology* **45**, 149-158.
- » Zhou, J., Lloyd, S.A., Blair, D.F. (1998). Electrostatic interactions between rotor and stator in the bacterial flagellar motor. *Proc. Natl. Acad. Sci. USA* **95**, 6436–6441.
- » Zhu, S., Kojima, S., Homma, M. (2013). Structure, gene regulation and environmental response of flagella in Vibrio. *Front Microbiol* **4**.
- » Zhua, S., Takao, M., Lia, N., Sakuma, M., Nishino, Y., Homma, M., Kojima, S., Imada, K. (2014). Conformational change in the periplasmic region of the flagellar stator coupled with the assembly around the rotor. *PNAS* **111**, 13523-13528.

Units

Abbreviation	Term
°C	degree Celsius
A	ampere
AS	amino acids
bar	bar
bp	base pair
Da	dalton
g	gram
h	hours
l	liter
m	meter
M	molar (mol/l)
min	minutes
mol	$6,022 \times 10^{23}$ particles
sek	sekunds
V	volt

Unit Prefixes

Abbreviation	Physical Term	Powers of Ten
M	mega	10^6
k	kilo	10^3
m	milli	10^{-3}
μ	micro	10^{-6}
n	nano	10^{-9}
p	pico	10^{-12}
f	femto	10^{-15}

VI. LIST OF UNITS/ PREFIXES/ ABBREVIATIONS

Abbreviation	Term	Abbreviation	Term
% (v/v)	volume percent	MEM	minimum essential medium
% (w/v)	mass fraction	MFP	membrane fusion protein
ABC	ATP binding cassette	mLN	mesenteric lymph nodes
<i>aph</i>	aminoglycoside phosphotransferase gene	MOI	multiplicity of infection
ATP	Adenosin-5' -triphosphate	M-cells	Microfold-cells
ATR	acid tolerance respons	OD _x	Optical density at a wavelength of x [nm]
att	attachment	OMP	outer membrane protein
B2H	Bacterial Two-Hybrid	ops	operon polarity suppressor
CAP	Catabolite activator protein	ORF	open reading frame
DC	dendritic cell	PAI	pathogenicity island
ddH ₂ O	double-distilled water	PAP	periplasmic adaptor protein
DMEM	dulbecco's modified eagle medium	PBS	phosphate buffered saline
DNA	deoxyribonucleid acid	PCA	protein complementation assay
dNTP	deoxynucleoside triphosphate	PCR	polymerase-chain-reaction
<i>E.</i>	<i>Escherichia</i>	PG	peptidoglycan
EEA	early endosome antigen	PMF	proton motive force
EDTA	ethylenediaminetetraacetic acid	PMN	polymorphonuclear neutrophil
EGTA	ethylene glycol-bis(2-aminoethylether)-N,N,N',N'-tetraacetic acid	P _{<i>siiA</i>}	SPI-4 promotor
ELISA	enzyme-linked immunosorbent assay	RBS	ribosomal binding site
<i>et al.</i>	lat. <i>et alii</i> , and others	RHS	reticulohistiocytic system
FAE	follicle associated epithelium	RTX	repeats in toxin
FRT	flippase recognition target sites	<i>S.</i>	<i>Salmonella</i>
GEF	guanine nucleotide exchange factor	<i>sif</i>	<i>Salmonella induced filament</i>
HeLa	„Henrietta Lacks“	<i>sii</i>	<i>Salmonella intestinal infection</i>
Ig	immune globuli	SCV	<i>Salmonella</i> -containing vacuole
IL	interleukin	SPI	<i>Salmonella</i> pathogenicity island
IM	inner membrane	<i>spp.</i>	species
Int	phage-encoded integrase	T1SS	type-I secretion system
KbE	colony forming unit	T2SS	type -II secretion system
Km	kanamycin monosulfate	T3SS	type -III secretion system
Km ^R	kanamycin monosulfate resistant	T4SS	type -IV secretion system
LAMP	lysosomal-associated membrane protein	T5SS	type -V secretion system
LB	lysogeny broth	TJ	tight junctions
log	Logarithm	TLR	toll-like receptor
MALT	mucosa-associated lymphoid tissue	TMD	transmembrane domain
MCP	Methyl-accepting chemotaxis protein	VCC	virtual colony count
MDCK	Madin-Darby canine kidney	WASP	Wiskott-Aldrich Syndrome protein
ME	Mosaic element	WT	wildtype
MeAsp	α -methylaspartate		

VII. CURRICULUM VITAE

Persönliche Daten

Stefanie Hoffmann

geboren am 15.05.1992 in Blankenburg (Harz)

Hochschulausbildung

10/2010 – 05/2015

Studium „Biochemie“

an der Martin-Luther-Universität Halle-Wittenberg

Master-Studiengang:

Vertiefungsthemen: Nukleinsäurebiochemie, Zellbiochemie und Virologie,
Pflanzenbiochemie

Abschluss: Master of Science,
Ø 1,7

Bachelor-Studiengang:

Vertiefungsthemen: Molekularbiologie und Gentechnik, Technische Biochemie,
Pflanzenbiochemie

Abschluss: Bachelor of Science,
Ø 2,8

Schulausbildung

08/2004 – 06/2010

Gerhart-Hauptmann-Gymnasium, Wernigerode

Abitur: Ø 1,8

Bachelorarbeit, Masterarbeit und berufliche Erfahrungen

05/2015 – 01/2019

Doktorand am Robert Koch-Institut,
Standort Wernigerode

Doktorarbeit

„Strukturelle und funktionelle Analyse des von *Salmonella*
Pathogenitätsinsel 4 kodierten Typ 1 Sekretionssystems und
dessen Interaktion mit Methyl-akzeptierenden Chemotaxisproteinen“

Betreuer: Herr Dr. Roman G. Gerlach

04/2014 – 05/2015

Masterarbeit

„Serovar-spezifische Expression von SPI-4 und
deren Einfluss auf die Virulenz von *Salmonella*“

Betreuer: Herr Dr. Roman G. Gerlach

01/2014 – 04/2014

Bachelorarbeit

„*Gaussia* Luziferase – basierte Transposon – Mutagenese
zur Identifizierung unbekannter *Salmonella* Proteine mit
C-terminalem Sekretionssignal“

Betreuer: Herr Dr. Roman G. Gerlach

Teilnahme an Tagungen

- 10/2018 **Salmonella Meeting** (Dorfweil-Schmitten)
Vortrag: „A chemotactic sensor controls *Salmonella* Pathogenicity Island 4 function“
- 06/2018 **Fachgruppentreffen „Mikrobielle Pathogenität“** (Bad Urach)
Vortrag: „A chemotactic sensor controls *Salmonella* Pathogenicity Island 4 function“
- 11/2017 **Salmonella Meeting** (Freiburg)
Vortrag: „A chemotactic sensor controls *Salmonella* Pathogenicity Island 4 function“
- 03/2017 **DGHM** (Würzburg)
Poster: „Interplay between chemotaxis protein CheM and SPI-4 components modulates function of the SPI-4 encoded adhesin SiiE“
- 08/2016 **ASM Salmonella-Konferenz** (Potsdam)
Vortrag: „Interplay between chemotaxis protein CheM and SPI-4 components modulates function of the adhesin SiiE“
- 06/2016 **Fachgruppentreffen „Mikrobielle Pathogenität“** (Bad Urach)
Vortrag: „Interplay between chemotaxis protein CheM and SPI-4 components modulates function of the adhesin SiiE“
- 10/2015 **SFB796 Meeting** (Erlangen)
Vortrag/Poster: „Elevated activity of *Salmonella* Pathogenicity Islands (SPI) 1 and 4 in *Salmonella* Dublin results in increased virulence“
- 09/2015 **DGHM** (Münster)
Poster: „Elevated activity of *Salmonella* Pathogenicity Islands (SPI) 1 and 4 in *Salmonella* Dublin results in increased virulence“
- 09/2015 **Salmonella Meeting** (Dorfweil-Schmitten)
Poster: „Elevated activity of *Salmonella* Pathogenicity Islands (SPI) 1 and 4 in *Salmonella* Dublin results in increased virulence“

VIII. LIST OF PUBLICATIONS

Scarless deletion of up to seven methyl- accepting chemotaxis genes with an optimized method highlights key function of CheM in *Salmonella* Typhimurium.

Hoffmann, S., Schmidt, C., Walter, S., Bender, J.K. and Gerlach, R.G.

PloS One. 2017 Feb 17; 12(2): e0172630. doi:10.1371/journal.pone.0172630.

High-Throughput Quantification of Bacterial-Cell Interactions Using Virtual Colony Counts.

Hoffmann, S., Walter, S., Blume, A.K., Fuchs, S., Schmidt, C., Scholz, A. and Gerlach, R.G.

Frontiers in Cellular and Infection Microbiology. 2018 Feb 15; 8:43. doi: 10.3389/fcimb.2018.00043.

Structural and functional characterization of SiiA, an auxiliary protein from the SPI-4-encoded type I secretion system from *Salmonella enterica*.

Kirchwegger, P., Weiler, S., Egerer-Sieber, C., Blasl, A.-T., Hoffmann, S., Schmidt, C., Sander, N., Merker, D., Gerlach, R.G., Hensel, M., Muller, Y.A.

Molecular Microbiology. 2019 Sep 17; 112(5): 1403–1422. doi:10.1111/mmi.14368.

A chemotactic sensor controls *Salmonella*-host cell interaction.

Hoffmann, S., Gendera, K., Schmidt, S., Kirchwegger, P., Imhof, A., Bogdan, C., Muller, Y.A., Hensel, M. and Gerlach, R.G.

bioRxiv preprint. 2021 May 15; doi: <https://doi.org/10.1101/2021.05.14.443827>

IX. DANKSAGUNG

Mein besonderer Dank gilt meinem Mentor Dr. Roman Gerlach für die Bereitstellung des Themas sowie der Möglichkeit die hier vorliegende Arbeit in seiner Arbeitsgruppe anfertigen zu können. Danke für die allzeit geöffnete Bürotür und die Möglichkeit Probleme offen zu diskutieren, für die unermüdliche Korrektur dieser Arbeit und die sehr schöne Zeit inner- und außerhalb des Labors.

Bei Prof. Dr. Michael Hensel bedanke ich mich ganz herzlich für die Betreuung der Arbeit innerhalb der Universität, der Hilfe bei allen Formalitäten sowie für die Erstellung des Erstgutachtens dieser Arbeit.

Mein dritter Dank gilt Prof. Dr. Guntram Grassl für die Erstellung des Zweitgutachtens, sowie Prof. Dr. Christian Kost und Dr. Jörg Deiwick für die Bereitschaft Teil meiner Prüfungskommission zu sein.

Allen Co-Autoren und Kooperationspartnern in Erlangen und Osnabrück danke ich für die gute Zusammenarbeit.

Steffi, meiner „Berliner Schnauze“, danke ich für so manch einen Lacher der den einen oder anderen Tag gerettet hat. Vielen Dank für viele schöne Kaffeepausen und die Versüßung meiner Freizeit. Du bist die Beste. Unsere gemeinsamen Abende auf dem Sofa oder bei Bohne fehlen mir schon jetzt unglaublich.

Ein großes Dankeschön geht auch an Christiane für die tatkräftige Unterstützung und super Arbeitsatmosphäre im Labor und natürlich für die ganzen tollen, selbst genähten Geschenke.

Jenny, Franzi, Kathleen, Bernd und allen anderen Kollegen, die nicht nur das, sondern auch gute Freunde geworden sind, danke ich für wundervolle Stunden in der Freizeit und jegliche Hilfe im Labor, sowie Anregungen zu diversen Experimenten. Ihr habt die Doktorandenzeit für mich unvergesslich gemacht.

Großer Dank gilt auch meiner guten Freundin Anne, die mich während des Studiums und auch in meiner Freizeit immer zum Lachen gebracht hat, egal in welcher Situation und die sich meine Probleme ohne zu Klagen anhörte.

Bei Julia bedanke ich mich für die Unterstützung, gerade zum Ende der praktischen Arbeit. Du hast mir durch ein neues Hobby einen perfekten Ausgleich zum stressigen Laboralltag geliefert und mich auch bei vielen privaten Problemen super unterstützt.

Zu guter Letzt bedanke ich mich bei meinen Eltern und meiner Schwester, ohne die das Studium an sich niemals möglich gewesen wäre. Sie haben immer zu mir gehalten und mich auf meinem Weg mit all ihrer Liebe und ihrem Vertrauen unterstützt und mir so zu jeder Zeit das Gefühl gegeben, das Richtige zu tun.

X. ERKLÄRUNG ÜBER DIE EIGENSTÄNDIGKEIT DER ERBRACHTEN WISSENSCHAFTLICHEN LEISTUNG

Ich erkläre hiermit, dass ich die vorliegende Arbeit ohne unzulässige Hilfe Dritter und ohne Benutzung anderer als der angegebenen Hilfsmittel angefertigt habe. Die aus anderen Quellen direkt oder indirekt übernommenen Daten und Konzepte sind unter Angabe der Quelle gekennzeichnet.

Bei der Auswahl und Auswertung haben mir die in jeder Veröffentlichung unter „Author Contributions“ aufgeführten Personen in der jeweils beschriebenen Weise unentgeltlich geholfen. Weitere Personen waren an der inhaltlichen und materiellen Erstellung der vorliegenden Arbeit nicht beteiligt. Insbesondere habe ich hierfür nicht die entgeltliche Hilfe von Vermittlungs- bzw. Beratungsassistenten (Promotionsberater oder andere Personen) in Anspruch genommen. Niemand hat von mir unmittelbar oder mittelbar geldwerte Leistungen für Arbeiten erhalten, die im Zusammenhang mit dem Inhalt der vorgelegten Dissertation stehen.

Die Arbeit wurde bisher weder im In- noch im Ausland in gleicher oder ähnlicher Form einer anderen Prüfungsbehörde vorgelegt.

(Ort, Datum)

(Unterschrift)

XI. SUPPLEMENTS ON DVD



